LUMINESCENT TRANSITION METAL COMPLEXES OF 2-(2'-PYRIDYL)BENZIMIDAZOLYL AND 2-(2'-PYRIDYL)INDOLYL BASED LIGANDS AND THEIR APPLICATIONS

by

Theresa Michelle M^{c}Cormick

A thesis submitted to the Department of Chemistry

In conformity with the requirements for

the degree of Doctor of Philosophy

Queen's University

Kingston, Ontario, Canada

(September, 2008)

Abstract

The objective of this thesis is to examine the photophysical and structural properties of Cu(I) complexes of 2-(2'-pyridyl)benzimidazolyl based ligands and Cu(I), Pd(II) and Pt(II) complexes of 2-(2'-pyridyl)indolyl based ligands, for possible use as phosphorescent emitters in OLEDs. The discovery of the atropisomeric 3,3'-bis(2-(2'-pyridyl)indolyl based ligands led to the examination of C-C coupling reactions and the investigation of the new chiral ligands with transition metal ions.

Cu(I) complexes of 2-(2'pyridyl)benzimidazolyl-benzene with varying phosphine ligands were prepared. The structures were studied with X-ray crystallography and NMR. Experimental and computational results established that steric and electronic properties of the phosphine ligands influence the photophysical properties of the Cu(I) complexes. Polynuclear Cu(I) complexes with 2-(2'-pyridyl)benzimidazolyl based ligands and two PPh_3 ancillary ligands were synthesized, the photoluminescent and electroluminescent properties were examined.

A series of 2-(2'-pyridyl)indolyl based ligands; 2-(2'-pyridyl)indolyl-benzene (pib), 1,4-bis[2-(2'-pyridyl)indolyl]benzene (bib) and 1,3,5-tris[2-(2'-pyridyl)indolyl]benzene) (tib) and the corresponding C-C coupled dimers bis[3,3'(2-(2'-pyridyl)indolyl-benzene)] (bpib), bis[3,3'(1,4-bis[2-(2'-pyridyl)indolyl]benzene (bbib) and bis[3,3'(1,3,5-tris[2-(2'-pyridyl)indolyl]benzene)] (btib) were synthesized in a one-pot reaction with the formation of both C-N and C-C bonds. The photophysical properties of these new molecules were investigated. The dimers display intramolecular

exciplex formation. The rotation barrier around the C-C bond in the 3 position of the bis-indole was calculated using DFT which support that bpib is an atropisomeric ligand.

Cu(I), Pd(II) and Pt(II) complexes were synthesized with pib and bpib. $[Cu(pib)(PPh_3)_2]^+$ contains a three-coordinate Cu(I) ion and doesn't display MLCT but rather $^3\pi$-$^1\pi$ phosphorescence. In Pd(pib)(acac) and Pt(pib)(DMSO)Cl the pib ligand forms C,N chelated neutral complexes that display red emission in frozen solution and in solid state. The X-ray crystal structure for $[Cu(bpib)_2]^+$ revealed a homo-chiral crystal and for $Pd(bpib)Cl_2$ and $Pt(bpib)Cl_2$ show a trans-chelating geometry around the metal centre. Frozen solutions of $[Cu(bpib)_2]^+$ and $Pd(bpib)Cl_2$ display MCLT phosphorescence.

Finally the atropisomeric ligands bpib and bbib were examined as sensors to determine the enantiomeric excess of Zn(2-bromo-3-methylbutyrate)$_2$ by CD spectroscopy. CD and fluorescent titration experiments verified that these ligands have selective interactions with different Zn(II) carboxylates. DFT computations showed that diastereomeric excess caused by chiral discrimination leads to the CD spectral-response of the atropisomeric ligands toward chiral Zn(II) carboxylates.

Acknowledgements

I would like to express my gratitude to my supervisor, Dr. Suning Wang for her patience and guidance throughout this work. Under her guidance this work has molded into what is presented in this thesis, and I have developed into the chemist that I am. Dr. Wang always encouraged me to strive for more, and I would not be where I am without that. Her guidance will stay with me as I pursue a career in chemistry.

I am thankful to the many wonderful professors and staff at Queen's University who taught me courses during both my undergraduate and graduate studies and who were always available and supported me both academically and personally. Especially to my supervisory committee members Dr. Phillip Jessop and Dr. David Zechel who have provided guidance during my studies. Also thanks to Dr. Rui-Yao Wang for his help with X-ray crystallography, Dr. Francoise Sauriol for her help with NMR and Harmut Schmider for his help with hpcvl.

My studies have been enriched by the interactions with the past and present members of the Wang group. Thanks to Corey Seward for introducing me to the Wang group and for encouraging me to pursue graduate studies. Thanks to Dr. Wen-Li Jai for his patience in teaching me many synthetic chemistry techniques during my undergraduate work, the skills he taught me have been the foundation of my success. Thanks to Wade White, Shubin Zhao, Sanela Martic, Yingli Rao, Hazem Amarne, Yasmin Jessa, Dr. Junghyun Lee, Dr. Liu, Dr. Yi Sun, Dr. Yi Cui and Dr. Dongren Bai for their guidance in the lab and their companionship and support. Thanks to the many undergraduates who have come through the lab, John Li, Nicole Ross, Brian Ross,

Guohui (Joy) Liu, Elizabeth Wong, Peng Jia, Philip Wucher and Zac Hudson for always reminding me where I started and how much I still need to learn and especially Julian Morey for his help with some of the work presented in this thesis.

Also my experience would not have been what it was without the many friends I have made in the chemistry department; too many people have come and gone to mention them all, but a special thanks to Christa Huntley for being a constant shoulder to lean on. Sanela Martic for being both an indispensible aid in the lab, but also a friend. Also thanks to Dr. Jeff Roberts, Dr. Matt Thompson and Dr. Jason Vlahakis for giving me advice and encouragement as I prepare to move forward in my chemistry career.

My graduate studies would not have been possible without the funding I received from Queen's University and especially from NSERC. I was honored with both a Canadian Graduate Scholarship, and also an NSERC PDF. I am grateful for this funding that has allowed me some freedom and extra time in directing my research.

I also would not have been able to maintain my sanity without support from friends and family outside of the chemistry department. Thanks to Katie Top, Rebecca McWatters and Graeme Mask for always being able to provide me with some perspective. The encouragement and support provided by my boyfriend Omar El Akkad was truly indispensable, he always believed in me. I would also like to thank my parents for raising me to never set limits on what I can accomplish; I would not be here if it wasn't for their belief in me, in what I am doing and what I will do in the future. Also thanks to Tim, Lyn and Andrew for keeping me grounded and to the rest of my family whose pride has always given me strength.

Statement of Originality

I hereby certify that all of the work described within this thesis is the original work of the author carried out under the guidance and supervision of Prof. Suning Wang with the following exceptions. Dr. Wen-Li Jia synthesized the phosphine ligands DPPMB and DPEphos in Chapter 2 also the ligands presented in Chapter 3 and complexes **3.1** and **3.4**, which he also partially characterized. From Chapter 4, the ligand tib was first synthesized by Qinde Liu, and the X-ray structure was solved by him. The reaction of 2-phenylindole with bromo-benzene was performed by Julian Morey (as indicated in the text). Any published (or unpublished) ideas and/or techniques from the work of others are fully acknowledged in accordance with the standard referencing practices.

(Theresa Michelle McCormick)

(September, 2008)

Table of Contents

List of Tables

List of Figures

List of Symbols and Abbreviations

1,3-bmb	1,3-bis[2-(2'-pyridyl)benzimidazolyl]benzene
1,4-bmb	1,4-bis[2-(2'-pyridyl)benzimidazolyl]benzene
A	ampere, absorbance
Å	angstrom
Anal	analysis
B3LYP	Becke 3-Parameter Exchange, Lee, Yang and Parr
bib	1,4-bis[2-(2'pyridyl)indolyl] benzene
bbib	bis[3,3'(1,4-bis[2-(2'-pyridyl)indolyl]benzene)]
BINAP	2,2'-bis(diphenylphosphino)-1,1'-binaphthyl
BINOL	1,1-bi-2-napthol
bpib	bis[3,3'(2-(2'-pyridyl)indolyl benzene)]
btib	bis[3,3'(1,3,5 – tris[2-(2'-pyridyl)indolyl]benzene)]
bmbp	4,4'-bis[2-(2'-pyridyl)benzimidazolyl]benzenebiphenyl
c	concentration
Calcd	calculated
cm	centimetres

cd	candela
CD	circular dichroism
CH_3CN	acetonitrile
CH_2Cl_2	dichloromethane
COSY	correlation spectroscopy
CV	cyclic voltametry
d	doublet
dd	doublet of doublets
ddd	doublet of doublet of doublets
DCM	4-(dicyanomethylene)-2-methyl-6-[4-(dimethylaminostyryl)-4H- pyran]
DFT	density functional theory
DMF	dimethylformamide
DMSO	dimethylsulfoxide
DNA	deoxyribonucleic acid
DPEphos	bis[2-(diphenylphosphino)phenyl]ether
DPPE	1,2-bis(diphenylphosphino)ethane
DPPMB	bis(diphenylphosphinomethyl)diphenylborate

ECD	electronic circular dichroism
ee	enantiomeric excess
EIPL	electron injection and protection layer
EL	electroluminescent
EML	emitting layer
ETM	electron transport material
eV	electron volt
F-TBB	1,3,5-tris(4’-fluorobiphnenyl-4-yl)benzene
Hz	hertz
HOMO	highest occupied molecular orbital
HPLC	high pressure liquid chromatography
HRMS	high resolution mass spectrometry
HTL	hole injection and transport layer
HTM	hole transport material
ISC	intersystem crossing
ITO	indium tin oxide
J	coupling constant, current density

K	kelvin
kV	kilovolts
l	path length
L	liter, luminance
LLCT	ligand to ligand charge transfer
LMCT	ligand to metal charge transfer
LUMO	lowest unoccupied molecular orbital
m	meter, multiplet
M	molar
mA	milliampere
MC	metal centred
mg	milligram
MHz	megahertz
mL	millilitre
MLCT	metal to ligand charge transfer
^{3}MLCT	triplet metal to ligand charge transfer
mmol	millimole

MO	molecular orbital
mol	mole
m. p.	melting point
mw	milliwatts
NPB	N,N’-diphenyl-N,N’-bis(1-naphthalenyl)-1,1’-biphenyl-4,4’- diamine
nm	nanometers
NMR	nuclear magnetic resonance
NRC	National Research Council
OLED	organic light emitting diode
pbb	2-(2’-pyridyl)benzimidazolyl benzene
PC	personal computer
pib	2-(2’-pyridyl)indolyl benzene
PIFA	phenyliodine bis(trifluoroacetate)
PMMA	poly(methyl methacrylate)
ppb	2-(2’-pyridyl)benzimidazolyl benzene
PPh_3	triphenylphosphine
ppy	2-phenylpyridine

PVK	polyvinyl carbazole
py	pyridine
q	8-hydroxyquinolate
RHF	restricted Hartree-Fock
Rt	room temperature
s	seconds
S_0	singlet ground state
S_1	singlet excited state
SOC	spin orbit coupling
spec	spectrometry
t	triplet
T_1	triplet excited state
TAB	tris(N-7-azaindolyl)benzene
T_g	glass transition temperature
TBAP	tetrabutylammonium hexafluorophosphate
TBPI	1,3,5-tris(N-phenyl-benzimidazol-2-yl)benzene
TD-DFT	time-dependent density functional theory

TDAT	2,4,6-tris(dipyridylamino)-1,3,5-triazine
tfa	trifluoroacetate
TGA	thermogravimetric analysis
THF	tetrahydrofuran
tib	1,3,5-tris[2-(2'-pyridyl)indolyl] benzene
TLC	thin layer chromatography
tmb	1,3,5-tris[2-(2'-pyridyl)benzimidazolyl]benzene
TMSBr	bromotrimethylsilane
UV	ultraviolet
UV-Vis	ultraviolet-visible
V	volts
δ	chemical shift
μs	microsecond
λ	wavelength
φ	quantum yield
τ	lifetime

Chapter 1
Introduction

Luminescent molecules are of great interest to several areas of research such as non-linear optics,[1, 2] fluorescent sensing[3-5] and display technologies.[6, 7] Luminescence can be either from fluorescence or phosphorescence with phosphorescence often being displayed from luminescent heavy metal complexes. For use in organic light emitting diode (OLED) display technology, phosphorescent emitters have the advantage of increased theoretical device quantum efficiency.[8, 9] A variety of metal complexes have been shown to be efficient emitters in OLED devices because the metal centre allows for access to the triplet phosphorescent state. Much of the work has focused on metal ions such as Ru(II)[10, 11] and Ir(III)[12] although recent reports have shown that the much more inexpensive metal ion Cu(I) can also be used.[13] Most of the luminescent Cu(I) complexes have ligands based on 1,10-phenanthroline derivatives and suffer from low quantum efficiency and instability thus more research needs to be done to overcome these problems to make Cu(I) complexes competitive with the heavy metal emitters for use in OLED display applications.[13-18]

Many phosphorescent metal-complexes are based on the bipyridine N,N' chelating ligand. However, it has been shown that other N,N' chelating ligands are useful in complexes for OLED devices. The neutral ligand 2-(2-pyridyl)benzimidazole (an example shown in Figure 1.1) has been shown to coordinate to metals such as Ru(II)[11, 19] and Pt(II),[20-22] but investigations into Cu(I) complexes of this ligand have

previously been unreported. Cu(I) complexes are often stabilized by ancillary phosphine ligands; preliminary studies have shown that the phosphine ligands affect the emission wavelength as well as decay lifetimes.[17, 18, 23] Although it is well known that Cu(I) can adopt many coordination geometries, the emission properties of Cu(I) with coordination number other than four have only recently been reported.[24-26] Our group has reported luminescent compounds based on the anionic ligand 2-(2'-pyridyl)indole.[27, 28] If the indole nitrogen is protected, this ligand acts as a neutral monodentate ligand, coordinating through the pyridyl nitrogen, allowing three coordinate Cu(I) compounds to be synthesized.[29] Examining the effect of the nitrogen based ligands, the phosphine ligands and coordination geometry on the luminescent properties of Cu(I) complexes will aid in the understanding of the optimum conditions required for developing a copper based OLED material.

While synthesizing the phenyl protected 2-(2'-pyridyl)indolyl benzene ligand, a side product was isolated and found to be the C-C bonded homo-coupled dimer of 2-(2'-pyridyl)indolyl benzene (shown in Figure 1.1). This new ligand was found not only to be chiral but also to act as a N,N-chelating ligand to transition metal centres and as a chiral sensor for Zn(II) carboxylates. This discovery was unexpected but yielded some interesting results. This ligand was formed in a one pot reaction where both C-C and C-N coupling occurred. Further investigation into this reaction was carried out and a brief background of some C-C bond forming reactions is presented in this chapter, as well as some background in chiral sensing.

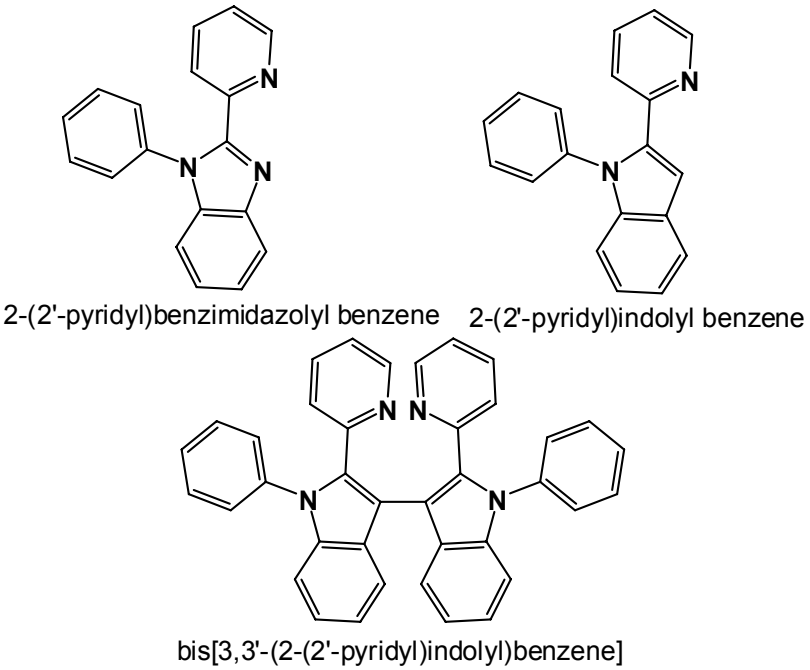

Figure 1.1 Structure of some ligands – pbb, pib and bpib – presented in this thesis.

1.1 Luminescence

1.1.1 Principles of Luminescence

Luminescence is the generation of light by an electronic transition from an excited state to the ground state. It is often categorized by how the molecule is excited, as well as the path the electron takes back to the ground state. When a molecule absorbs a photon of light that results in luminescence, it is called photoluminescence. An excited molecule can return to the ground state through non-radiative decay, where the molecule relaxes through a series of vibrational modes, and no light is generated. However, if the relaxation process is radiative, that is it produces light, it can either come from a singlet

excited state (S_1) and is called fluorescence or from a triplet excited state (T_1) and is called phosphorescence.[8]

The transition from the excited S_1 state to the singlet ground state S_0 is a spin allowed transition and occurs quickly with excited state lifetimes on the nano-second, or less, time scale. For phosphorescence, the excitation is still from S_0 to S_1 but intersystem crossing allows access to a lower energy triplet excited state T_1, as shown in the Jablonski diagram in Figure 1.2. Relaxation from T_1 to S_0 is spin forbidden, resulting in the excited state having lifetimes ranging from a microsecond to milliseconds. Although it is a spin forbidden transition, when a heavy metal is present in the molecule, spin-orbit coupling allows mixing of the states, which increases the likelihood of intersystem crossing to the triplet state. This also decreases the excited state lifetime, thus the non-radiative decay. Fluorescence and phosphorescence are often differentiated by measuring their decay lifetimes.[8]

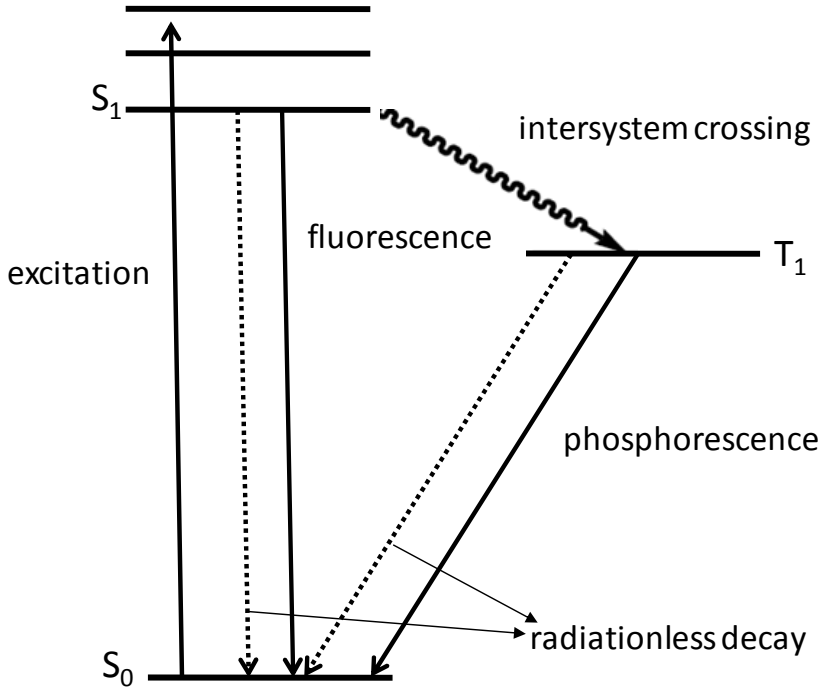

Figure 1.2 Jablonski diagram showing transitions from ground state to excited state and both phosphorescent and fluorescent emission.

Electroluminescence (EL) is another type of luminescence where the light is still generated by transitions from an excited state (S_1 or T_1) to the ground state (S_0), but the excitation process is different from that of photoluminescence.[30] As shown in Figure 1.3, in an EL device, electrons are injected from the cathode to the lowest unoccupied molecular orbital (LUMO) of the emitter, and holes (a positive charge created when an electron is removed from a molecule) are injected into the highest occupied molecular orbital (HOMO) at the anode. The recombination of the holes and electrons in the emitter results in generation of light. The light emitted from a molecule acting as an emitter in an electroluminescent device is often similar in wavelength to that seen for the

photoluminescence of the same molecule. In 1963, Pope and coworkers observed emission from an organic electroluminescent cell when an anthracene crystal was exposed to a large electric potential of 400 V.[31] It was later observed that by using different layers for electron transport, emission and hole transport efficient light emitting devices or OLEDs could be made.[32]

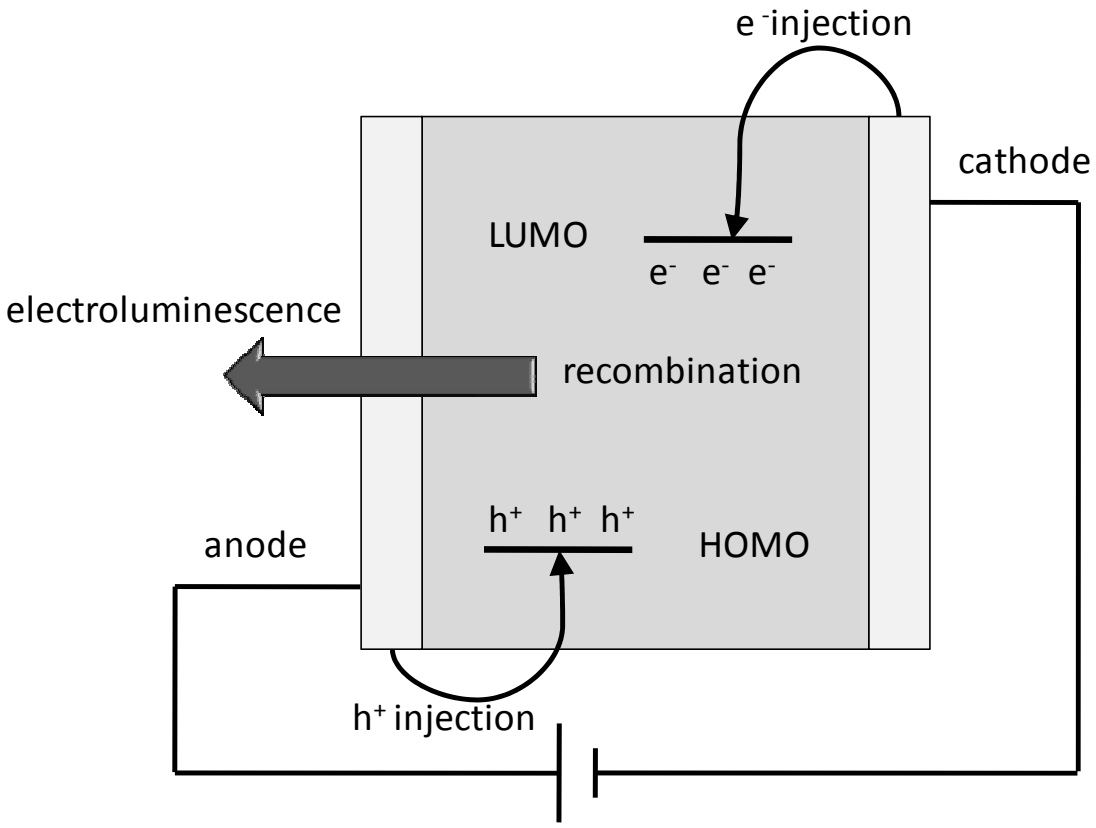

Figure 1.3 General structure of an electroluminescent device.

1.1.2 Organic Light Emitting Diodes (OLEDs)

1.1.2.1 Multilayer Design

Most OLEDs contain a structure similar to the multilayered device shown in Figure 1.4. Each layer is usually only 1 nm–100 nm thick and can be made by a solution process such as spin coating or by vacuum deposition. The holes are injected by the anode which is usually indium tin oxide (ITO), a composition of approximately 20% SnO_2 and 80% In_2O_3. ITO is chosen because of its high work function and transparency to visible light. Next to the anode is the hole injection and transport layer (HTL) that allows for transport of the hole into the emitting layer (EML). The HTL is often made with aromatic amines such as N,N'-diphenyl-N,N'-bis(1-naphthalenyl)-1,1'-biphenyl-4,4'-diamine (NPB, Figure 1.5)[33] and should have a HOMO level that matches the work function of the anode. On the other side of the device, the cathode (which needs a low work function and is often Mg-Ag 10:1 or LiF/Al) injects electrons into the electron transport layer (ETL). The ETL allows for efficient transport of electrons to the emitting layer, and also blocks the holes. The LUMO level of the ETL should be close to or lower than that of the emitter material. The most common ETL material is 8-hydroxyquinoline aluminum (Alq_3) shown in Figure 1.5, that was the first molecule for use in an efficient OLED, used as the emitter and as on ETL.[32] The electrons recombine with the holes in the EML and emit light. Organic molecules, such as the blue emitting 2,2'-bistriphenylenyl (BTP) (Figure 1.5) can be used at emitting layers; metal containing complexes can also be used, and this work will focus on these complexes as emitters.

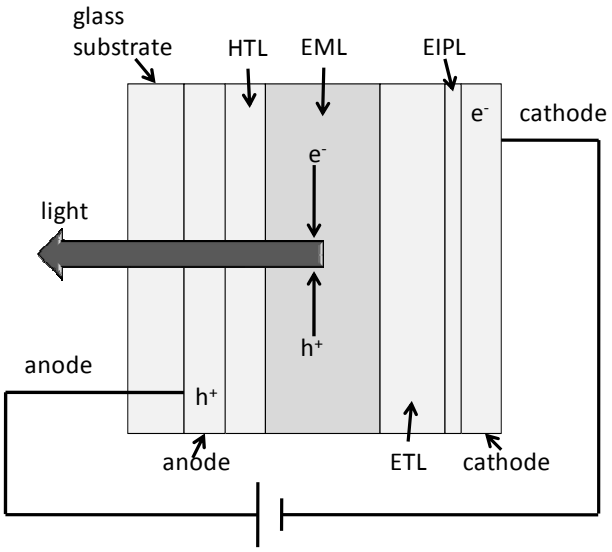

Figure 1.4 Multilayer structure of OLEDs – HTL is the hole transport layer, EML is the emitting layer, ETL is the electron transport layer and EIPL is the electron injection and protection layer.

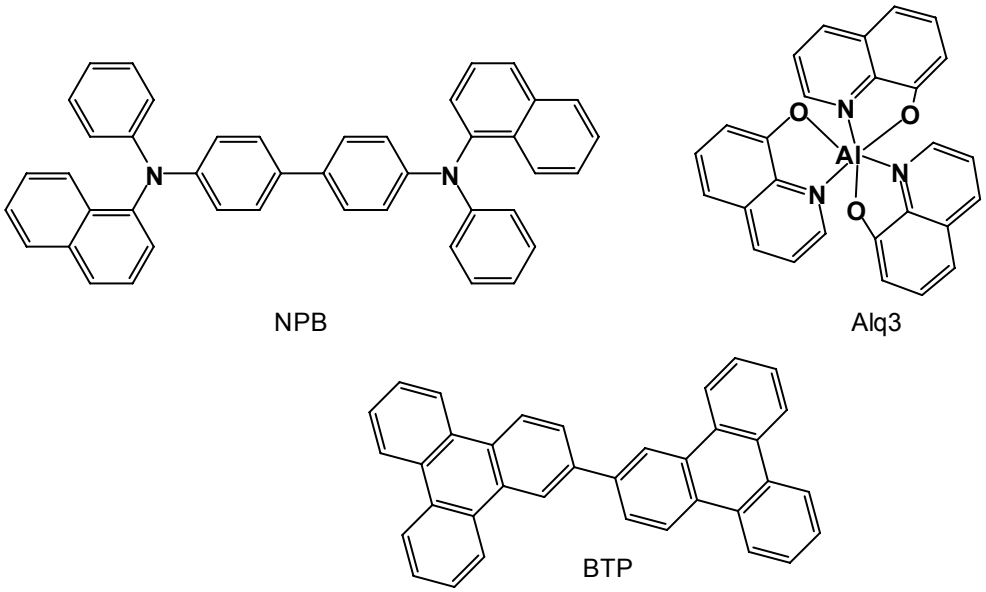

Figure 1.5 Structure of a common hole transport material NPB, a common electron transport material Alq_3 and a poly-aromatic blue emitter BTP.

1.1.2.2 Light Emission in OLEDs

In an electroluminescent device, the electrons migrate toward the anode, but at some point meet a hole, thus creating an exciton. The exciton consists of four states, one singlet and three triplet states that appear as four quasi-degenerate states at large hole-electron separation distances. Statistically, all four states will be populated with equal probability. When the hole and the electron are on the same molecule, the states are no longer degenerate, and a 1:3 ratio of singlet to triplets is seen. In organic molecules where the spin orbit coupling (SOC) is small, emission is usually observed by recombination of the electrons in the singlet excited state with the holes, and the exciton in the triplet state return to the ground state through non-radiative decay pathways. Thus, only 25% of the injected electrons result in emitted light in fluorescent molecules. However, if the SOC is large, the exciton of the singlet state will experience intersystem crossing to the triplet state, and emission from all excitons in the triplet state may occur. Hence, 100% efficiency may be obtained, compared with only 25% when the SOC is small.[8, 34] Molecules containing heavy metals display phosphorescent emission from the triplet state because of the presence of strong SOC and for this reason much research into emitters containing metals has been done.

1.1.2.3 Properties of Emitting Layers

A good EML must have many optimized properties including high emission quantum efficiency, good processability and high stability. It has already been discussed that high quantum efficiency can be achieved by gaining access to the triplet state. It is also

desirable to have the ability to easily tune the colour of emission, because full colour displays need red, green and blue emitters.[35] Although much work has been done in achieving a full colour display, work still needs to be done on colour purity and device stability. Early red emitters used organic dopants such as 4-(dicyanomethylene)-2-methyl-6-[4-(dimethylaminostyryl)-4H-pyran] (DCM) displayed in Figure 1.6.[36] $Ru(bpy)_3^{+2}$ (bpy = 2,2' bipyridine) type complexes have also been shown to be useful phosphorescent red emitters.[10, 11] The commonly used hole transport layer Alq_3 (Figure 1.5) is also a good green emitter. Blue emitters have been more difficult to achieve due to the poor device stability of such large-band gap materials. Some examples of compounds explored as blue emitters include extensively conjugated poly-aromatic molecules (*e.*g. BTP, Figure 1.5), three and four coordinate organo-boron compounds[37-39] and Ir(III) complexes. In fact Ir(III) based emitters such as those shown in Figure 1.7, have demonstrated colour tunability from the UV to the near infrared.[40, 41]

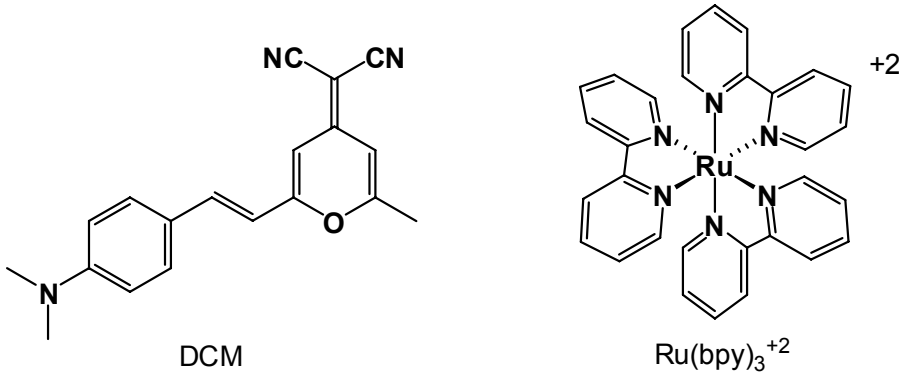

Figure 1.6 The organic red emitter DCM and the Ru(II) based red emitter $Ru(bpy)_3^{+2}$.

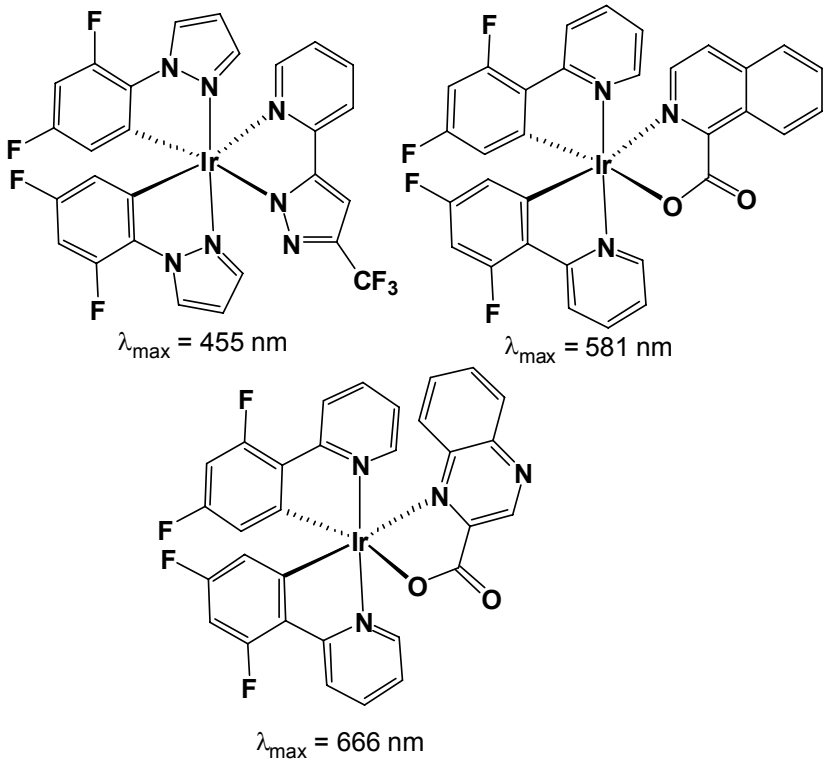

Figure 1.7 Three Ir(III) complexes displaying the large colour tuning possible by varying the ligands.

Good processability can be achieved by making neutral molecules that can be sublimed so that they can easily be processed in OLED fabrication through vapour deposition. Molecules can also be deposited by spin coating for device fabrication. For both methods a uniform amorphous film is usually desired during layer deposition. This can be achieved through the use of molecules with high glass transition temperatures, such as star burst shaped molecules.[42, 43]

1.2 Phosphorescent Emitters

1.2.1 Emission from Metal Complexes

The emission from metal complexes can be from several different excited states, depending on the metal and the ligands used. Transitions are generally considered to be between HOMO to LUMO energy levels, and as such, the electronic distribution and energy of the HOMO and LUMO determine the type of emission seen. Many phosphorescent emitters rely on MLCT transitions where the HOMO is on the metal centre, and the LUMO is on the ligand.[44] It is also possible to have a ligand based emission, where the proximity of the metal centre allows access to a $^3\pi$ excited state that is localized on the ligand. This emission is $^3\pi$-$^1\pi$ in character. The energies of both the excited state $^3\pi$ and ground state $^1\pi$ are perturbed by coordination of the ligand to the metal centre, often leading to a red shift in the emission energy compared to that observed for the free ligand.[8]

Metal centered emission are also seen for some transition metal complexes, and are often the site of emission for lanthanide complexes, displaying forbidden f-f* transitions. Some examples are Eu(III) and Tb(III) emitters, which need ligand sensitizers to achieve emission from the f-f* transition.[44, 45] The ligands are excited and the energy is transferred to the metal centre that displays the emission. A ligand commonly used for europium complexes for EL is tris(thienyltrifluoroacetono) (TTA); an anionic ligand. Neutral ligands such as 1,10-phenanthroline with well matched triplet energy levels increase the observed luminescence and lead to mixed ligand complexes;

examples of complexes made with these ligands are shown in Figure 1.8.[45] Often d* states are prone to non-radiative decay and as such, access to them can be undesired since it can lead to thermal emission quenching. Another possibility is a LMCT (ligand to metal charge transfer) where the HOMO is centered on the ligand and the LUMO is an empty d orbital on the metal. The ordering of the excited states in a transition metal complex can be sensitive to both the metal and the ligands. It has been found that altering the oxidation state, geometry, or type of metal used in complex can alter the emission observed. Similarly, changing the π ligand or ancillary ligands on the complex can also be used to tune the emission properties.[44] Each metal has its own benefits and drawbacks for OLED applications and the most common are mentioned here.

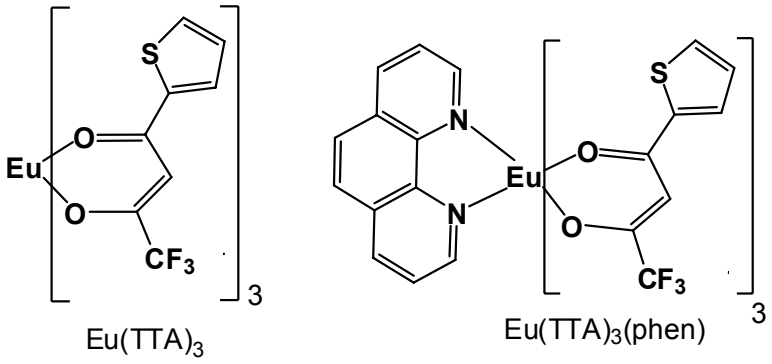

Figure 1.8 Structures of europium based emitters: $Eu(TTA)_3$ and $Eu(TTA)_3(phen)$.

1.2.2 Phosphorescent Transition Metal Complexes

1.2.2.1 Ruthenium(II) Phosphorescent Complexes

The compound $[Ru(bpy)_3]^{2+}$ (bpy = 2,2'-bipyridyne) (Figure 1.6) and its derivatives are among some of the most studied phosphorescent molecules of the last 30 years due to a

combination of their chemical stability, redox properties, excited state and phosphorescent emission.[10, 44] Ru(II) complexes often display MLCT emission at room temperature in fluid solution. The lowest ^{3}MLCT state of $[Ru(bpy)_3]^{2+}$ is long lived (τ = ~5 μs) and as such has found utility in energy transfer reactions.[12] Although emission is observed from the MLCT state, the non-emissive MC (metal centered) levels are thermally accessible, as such, quantum yields for most Ru(II) based complexes are less than 0.1.[12] The use of a tetradentate bis-1,10-phenanthroline ligand was found to increase quantum yields to ~0.30 attributed to the rigidity of the molecules.[46] However, emission tuning has been largely unsuccessful for Ru(II) complexes and emission wavelengths are generally restricted to the orange-red region of the spectrum.[44]

1.2.2.2 Iridium(III) Phosphorescent Complexes

It was later found that bipyridyl based complexes of Ir(III) are also luminescent and the non-emissive MC state is less thermally available, increasing the phosphorescent quantum yields. It was soon discovered that cyclometallated Ir(III) complexes, with ligands like phenylpyridine are useful in OLED fabrication as they are neutral species and are easily processed in device fabrication. Ir(III) complexes have also shown great tunability with emissions ranging from red to blue and the emission can originate from ^{3}LC or ^{3}MLCT depending on the ligands.[12, 47] Adachi and coworkers reported a red phosphorescent Ir(III) complex made with the ligand *bis*(2-(2'-benzo[4,5-α]thienyl) pyridinato-N,C$^{3'}$(btp) and an ancillary acetyl-acetonate ligand (acac) ($Ir(btp)_2(acac)$) as shown in Figure 1.9. An electroluminescent device was made with $Ir(btp)_2(acac)$ that

displayed a λ_{max} = 616 nm and a high external device quantum efficiency of ~7.0 %.[48] To go from red emission to blue the emission energy gap must increase. To do this, many have focused on decreasing the HOMO energy while keeping the LUMO energy relatively unchanged. This can be achieved in a couple of different ways; one is by the addition of electron withdrawing groups to the phenyl ring of the cyclometallated ligand altering the LC emission.[49, 50] An example is shown in Figure 1.9 where 2-(4,6-difluorophenyl)pyridyl Ir(III) complex emits at 450 nm in frozen solution.[51] An alternate approach uses ancillary ligands to lower the metal based HOMO energy of biscyclometallated derivatives by perturbation of the energy level of the metal altering MLCT emission.[41, 49]

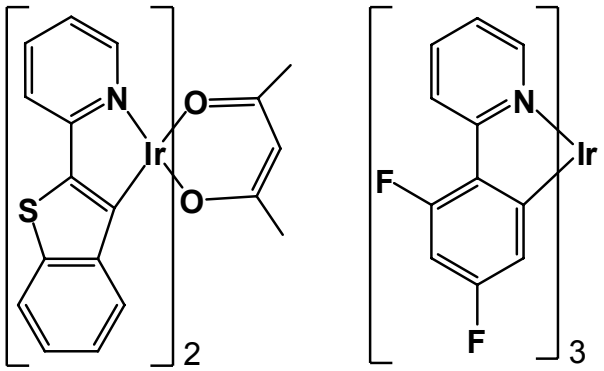

Figure 1.9 Structure of red emitting $Ir(btp)_2(acac)$ (left) and blue emitting $Ir(F_2ppy)_3$ (right).

1.2.2.3 Platinum and Palladium Phosphorescent Emitters

Fewer d^8 metal complexes are known to be emissive in fluid solution at room-temperature compared to Ru(II) and Ir(III), however phosphorescence from many Pt(II) complexes is

observed. The heavy Pt(II) metal ion exerts strong spin–orbit coupling in these complexes promoting efficient mixing of singlet and triplet states enhancing phosphorescence emission and shortening the emission lifetimes. The heavy atom effect exerted by a Pd(II) metal centre is much weaker making the MC states more accessible and consequently phosphorescence from palladium(II) complexes are rare when compared with analogous Pt(II) complexes.[44]

The square planar geometry of Pd(II) and Pt(II) complexes can lead to some properties that are not seen for the octahedral d^6 complexes such as axial intermolecular interactions. The flat nature of the complexes can allow for both metal-metal interactions, as well as intermolecular π stacking. The emission properties of a large variety of Pt(II) complexes have been studied where the Pt(II) contains N,N' chelate and two ancillary ligands,[47] or N,N,N chelate by terpyridyl based ligands.[52] The photophysical properties have been shown to be influenced by the fourth ligand as well as substituents on the tpy ligand (Figure 1.10).[53]

Emission from simple mononuclear Pt(II) bipyridine or terpyridine complexes is rarely observed because of the presence of low lying metal-centred excited states providing non-radiative deactivation pathways through molecular distortion. To obtain significant room temperature luminescence, ligands with low-lying excited state orbitals and/or a strong electron donating ability can be used. The strong ligand field associated with such ligands raises the energy of the metal d–d states, removing the deactivation

pathway.[44, 54] Cyclometallating ligands are known strong field ligands because of the anionic carbon.

Cyclometallation is when a polydentate ligand binds to a metal centre through a covalent metal-carbon bond, with the remaining bonds being coordination bonds often from heteroatoms such as nitrogen. The most common cyclometallating ligand is 2-phenylpyridine (ppy) that can form a five membered C,N chelate to many second and third row metals ions. These ligands offer a very strong ligand field caused by the strong σ donor of the C^- and the good π acceptor in the pyridyl group. As a result, the MC state is raised, eliminating the thermal deactivation pathway. Also tridentate cyclometallating ligands can be used that can coordinate in a variety of ways as shown in Figure 1.10. Thus, many cyclometallated Pt(II) complexes are luminescent under ambient conditions with excited states having the ^{3}MLCT character.[55, 56] This has led to interest in using these complexes as triplet emitters in OLEDs.[57]

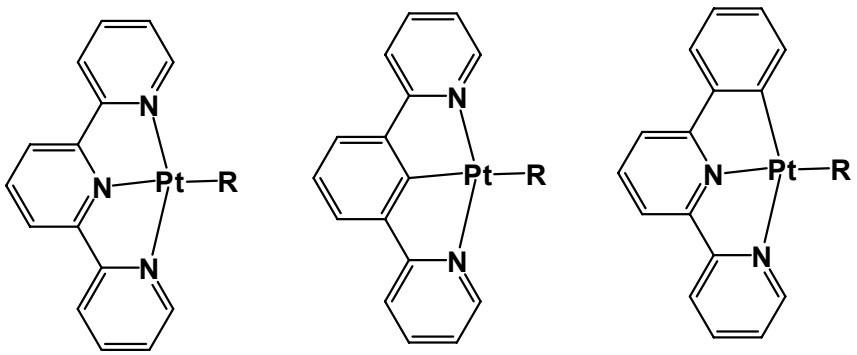

Pt(tpy) tridentate cyclometalating ligands

Figure 1.10 Tridentate Pt(II) complexes with either two or three pyridyl donors.

Work from our group has shown that the 2-(2'-pyridyl)benzimidazolyl group forms a five-membered chelate ring with a metal centre resulting in a relatively rigid chelate to the complex, as shown in Figure 1.11. It was found that 2-(2'-pyridyl)benzimidazolyl Pt(II) complexes display orange-red phosphorescent emission. Although most Pt(II) complexes do not emit in solution at ambient temperature, they do often emit in the solid state at ambient temperature, which renders them potentially useful as phosphorescent emitters for OLEDs.[20] This indicates the importance of examining a variety of ligands to optimize OLED materials.

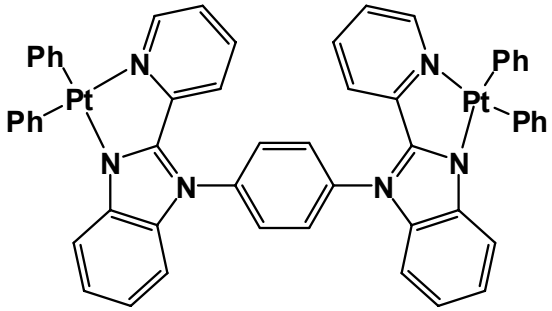

Figure 1.11 Structure of one of the 2-(2'-pyridyl)benzimidazolyl Pt(II) complexes reported.

1.2.3 Copper Complexes

1.2.3.1 Overview of Copper

Copper complexes for OLED devices are an example of a luminescent metal complex made with a relatively inexpensive, abundant metal.[58] The abundance of copper results in it having a low cost and it is generally not harmful to the environment, making copper complexes desirable for OLED applications. Copper has two common oxidation states:

+1 and +2. Cu(II) often displays d-d metal centered transitions which cause absorption bands in the visible region of the spectrum. The lowest electronic states are short lived and non-emissive due to non-radiative decay and as such have no interesting luminescent properties.[13] Conversely, Cu(I) complexes have demonstrated rich photophysical chemistry.

Cu(I) favours a tetrahedral geometry because of the full d shell with a d^{10} configuration. Complexes of the type $[Cu(NN)_2]^+$ and heteroleptic complexes $[Cu(NN)(PP)]^+$ are known to be luminescent, where NN is typically 1,10-phenanthroline or its derivatives and PP is either two monodentate phosphine ligands or a diphosphine ligand, as shown in Figure 1.12. Luminescence has also been observed for Cu(I) cluster compounds but these will not be discussed here.[13] Often the luminescence from tetrahedral Cu(I) complexes originates from MLCT states much like Ru(II) and Pd(II) complexes.

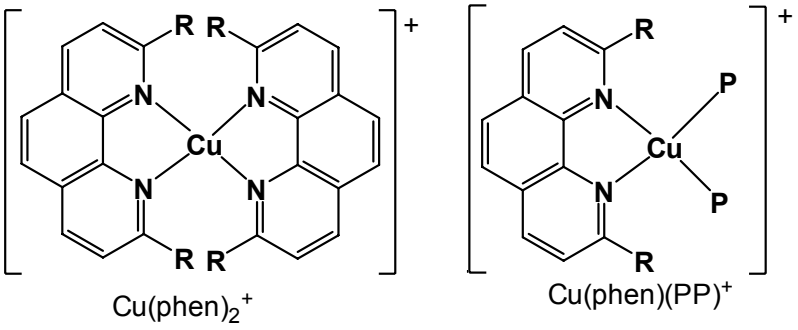

Figure 1.12 General structure of $Cu(phen)_2^+$ and heteroleptic $Cu(phen)(PP)^+$ where PP is either two phosphine ligands or one chelating diphosphine ligand.

1.2.3.2 Cu(I)-Bis(1,10-phenanthroline) Complexes

The ground state geometry of $[Cu(phen)_2]^+$ (where phen = 1,10-phenanthroline and its derivatives) is a distorted tetrahedron. By varying the substituents in the 2 and 9 position of the phen ligand it was shown that the steric bulk of the ligands influence the geometry around the Cu(I) centre as well as electronic factors, as observed in the tuning of the absorption spectra.[59, 60]

The absorption spectrum of $[Cu(phen)_2]^+$ displays ligand centered π-π transitions in the UV region and MLCT transitions in the visible region of the spectrum. Upon excitation, the lowest MLCT bands become populated and the Cu(I) changes the formal oxidation state from Cu(I) to Cu(II).[61] With this the geometry changes to a flattened tetrahedral, closer to the square planar geometry common for Cu(II). This allows for a fifth coordination site to become available to nucleophilic species such as solvent molecules that can quench the emission.[15, 62] It was discovered that the excited state lifetimes of the Cu(I) complexes in CH_2Cl_2 are dependent on the degree of excited state distortion and protection of the metal centre towards exciplex quenching by deactivation by a solvent molecule, or other ligand coordinated at the fifth site.[15]

1.2.3.3 Heteroleptic Cu(I) Complexes

Heteroleptic complexes $[Cu(NN)(PP)]^+$ with phosphines replacing one of the NN ligands improve emission properties by stabilizing the Cu(I). The ancillary phosphine ligands are not involved in the electronic transition in emission but they do play a key role in stabilizing the Cu(I) centre and do impact the photophysical properties of the

complex.[17, 18] The emission spectrum of $[Cu(dbp)(DPEphos)]^+$ (dbp = 2,9-butyl,-1,10-phenanthroline and DPEphos = bis[2-(diphenylphosphino)phenyl] ether) is reported to have a blue-shifted emission compared to $[Cu(phen)_2]^+$.[18, 63] The effect of the phosphines on Cu(I) disfavours electron donation to the NN chelate and as such causes the observed blue shift in the MLCT emission.[17] It was also found that the phosphine ligand itself influences the emission properties. $[Cu(phen)(DPEphos)]^+$ has an emission quantum yield of ~0.15 and a decay lifetime of ~15 μs. The replacement of DPEphos by two PPh_3 ligands results in a weaker, red shifted emission.[18] This is partially attributed to the geometric rigidity of the ancillary DPEphos ligand.

1.2.3.4 Cu(I) Complexes in OLEDs

Interest in using Cu(I) in OLEDs is driven in part by its relatively low cost and abundance when compared to other metals used as phosphorescent emitters. The cost of the materials becomes particularly important for mass production. Several OLED devices have been made using Cu(I) emitters. A phenanthroline-based green emitting OLED was prepared using Cu(I) complex, $[Cu(dnpb)(DPEphos)]BF_4$; dnpb = 2,9-di-*n*-butyl-1,10-phenanthroline (shown in Figure 1.13), as the emitting layer. The device was reported to have a current efficiency of 10.5 cd/A and a peak brightness of 1663 cd/m^2.[23] A highly efficient device was made with $[Cu(DPEphos)(Dicnq)]BF_4$ (Dicnq=6,7-Dicyanodipyrido(2,2-*d*:2',3'-*f*) quinoxaline also shown in Figure 1.13, with a maximum current efficiency of 11.3 cd/A, a peak brightness of 2322 cd/m^2 and a turn on voltage of 4 V with λ_{max} = 572 nm.[64] Although these devices may compete with some Ir(III)

complexes, further efforts are needed to increase the device efficiency and stability to fully utilize the low cost and low environmental impact of copper materials.

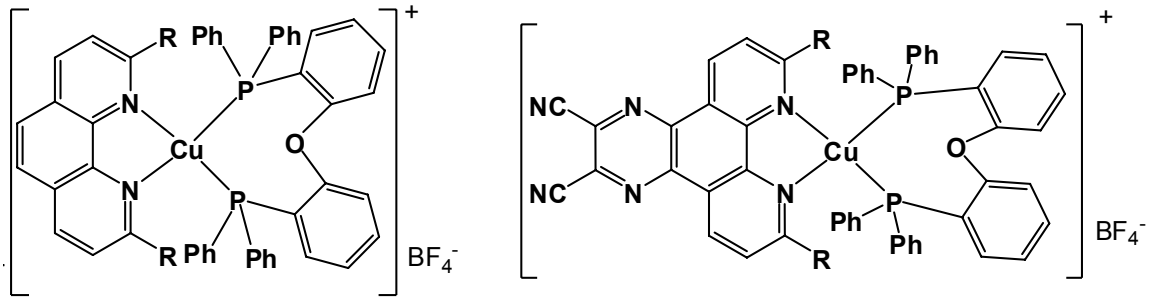

Figure 1.13 Structure of Cu(I) complexes used in OLED devices.

1.2.4 Ligand Selection

From the sensitivity of emission colour and excited state lifetimes of previous Cu(I) complexes to small changes in electronic structure, it is clearly important to study a variety of ligands in order to optimize emission and understand the luminescence. As previously mentioned, 2-(2'-pyridyl)benzimidazole has recently been shown to act as an N,N'-chelate with Pt(II),[20] Pd(II)[65] and Ru(III),[19] as well as with other transition metals. By functionalizing the NH nitrogen with a phenyl group, a variety of linear and molecular star shape ligands have been made by our group as shown in Figure 1.14.[11, 20]

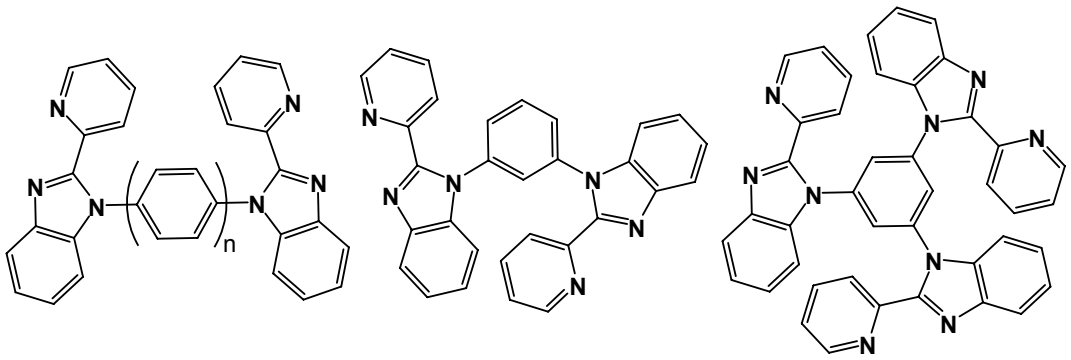

Figure 1.14 Structures of linear and star shaped 2-(2'-pyridyl)benzimidazolyl ligand.

Work by our group has also shown that diphenylborates coordinated to 2-(2'-pyridyl)benzimidazolyl derivative ligands can act as blue to green luminescent materials, and it was shown that the colour could be tuned by varying substituents in the 5-position of the benzimidazolyl ligand.[27] Our group has also shown that Ru(II) complexes of the 2-(2'-pyridyl)benzimidazolyl ligands in Figure 1.14 can be used as the emitting layer in OLED devices. The devices displayed the typical MLCT based red phosphorescence of Ru(II) complexes and when compared to identical devices using $[Ru(bpy)_3][PF_6]_2$ as the emitter, the devices constructed from the 2-(2'-pyridyl)benzimidazolyl derivatives were generally brighter and more efficient than their $[Ru(bpy)_3](PF_6)_2$ analogues. Although no devices have been made with the Pt(II) complexes of 2-(2'-pyridyl)benzimidazolyl ligands, they do show red-orange emission in the solid state at room temperature.[20] Copper (I) complexes have recently been reported in literature where deprotonated 2-(2'-pyridyl)benzimidazole is coordinated to Cu(I) and forms coordination polymer with cyanide. These polymers displayed solid state emission ranging from 575 – 640 nm.[66]

These examples support that 2-(2'-pyridyl)benzimidazolyl ligands can be used for achieving phosphorescent materials.

The ligand 2-(2'-pyridyl)indole (pyin) differs in structure to 2-(2'-pyridyl)benzimidazole by a nitrogen in the five membered ring as shown in Figure 1.15. It has been shown that pyin is a blue emitting N,N' chelate ligand when deprotonated.[28] Complexes of pyin with boron,[27] palladium(II) and platinum(II) have been made.[67] The ligand acts as an anionic N,N' chelating ligand. When the nitrogen was protected by a methyl group, Thummel *et al.* found that it could act as an anionic C,N chelate to certain metal centres.[68, 69] It is postulated that it can also act as a monodentate ligand to other metals ions such as Cu(I).

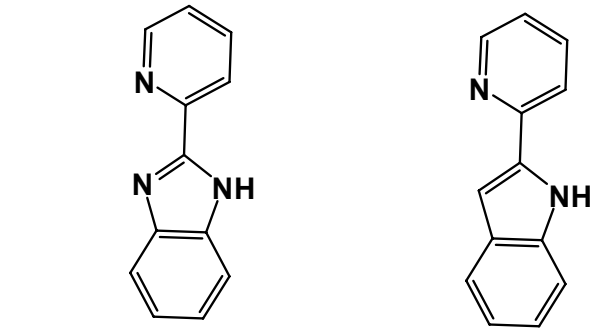

2-(2'-pyridyl)benzimidazole 2-(2'-pyridyl)indole

Figure 1.15 Structure of ligands 2-2'-pyridyl)benzimidazole and 2-(2'-pyridyl)indole.

1.3 C-C Coupling Reactions

Carbon-carbon bond forming reactions are indispensible to synthetic chemists. The ability to couple aryl groups is of primary importance in pharmaceuticals as many biologically active molecules are poly heterocyclic aryls. Many common catalysts for C-

C coupling reactions are based on transition metal complexes such as palladium and copper.[70] In fact, Pd-catalyzed cross coupling of organometallic nucleophiles with aryl halides has become the most commonly used method for biaryl synthesis. Two common reactions that employ Pd catalysts are the Heck reaction[71] and Suzuki-Miyaura[72, 73] coupling shown in Figure 1.16.[74]

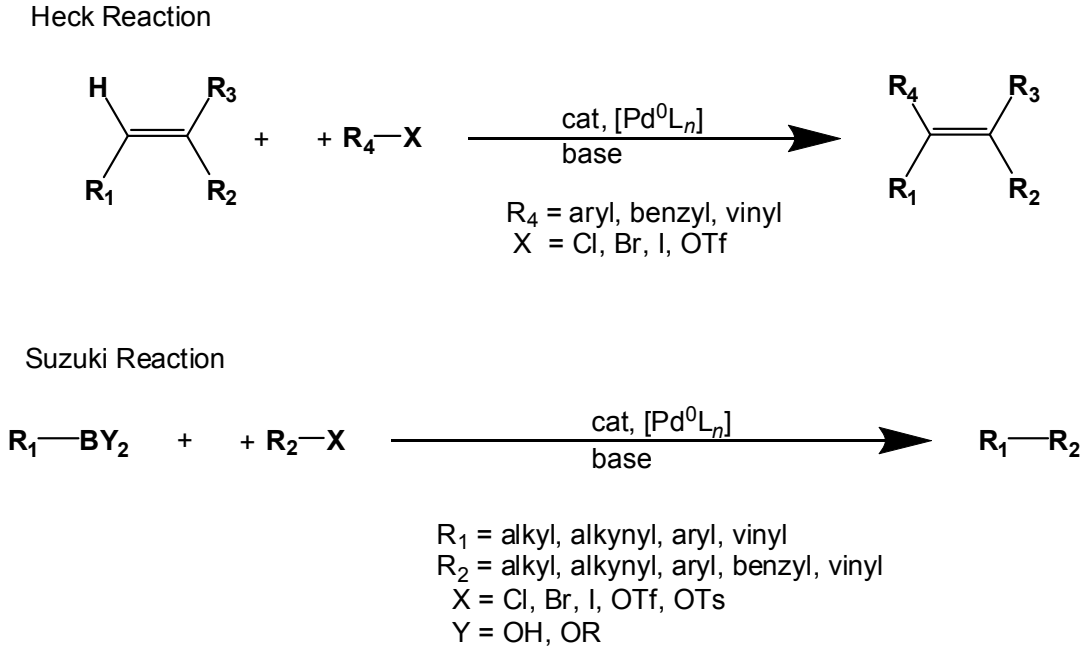

Figure 1.16 General reaction schemes of palladium catalyzed Heck and Suzuki-Miyaura reactions.

In the Heck reaction, an aryl halide couples with an olefin to form a new C-C bond. Similarly in the Suzuki-Miyaura cross coupling reaction again an aryl halide is one of the coupling partners, which couples with a boronic acid. In both cases it is required to have pre-functionalized coupling partners; a fundamental drawback common

to almost all catalytic couplings between aryl nucleophiles and electrophiles. The Suzuki-Miyaura reaction requires stoichiometric amounts of a boronic acid, which must generally be prepared from precursors under anaerobic conditions.[75] When both arene components must be prepared prior to cross-coupling to install the organometallic and halide moieties, large amounts of waste can be generated preceding the biaryl formation.[76] Recently, efforts to discover direct arylation reactions have attracted much attention. In direct arylation reactions, pre-formation of the organometallic species or even the halogenated species is not required, reducing the number of steps required, as well as the amount of waste produced in the reaction. A few examples of such reactions are presented here.

1.3.1.1 Direct Arylation Reactions

Aryl halides are capable of coupling directly with aromatic and heteroaromatic compounds through cleavage of unactivated C-H bonds with the advantage of being carried out without stoichiometric metallation of the coupling partner.[77] Most coupling reactions are of the type shown in Figure 1.17 A where both aryls are preactivated, usually as an aryl halide and an organometallic species. However, recent work has shown that coupling reactions can occur with either one or both coupling partners being unfunctionalized as shown in Figure 1.17 B-D.

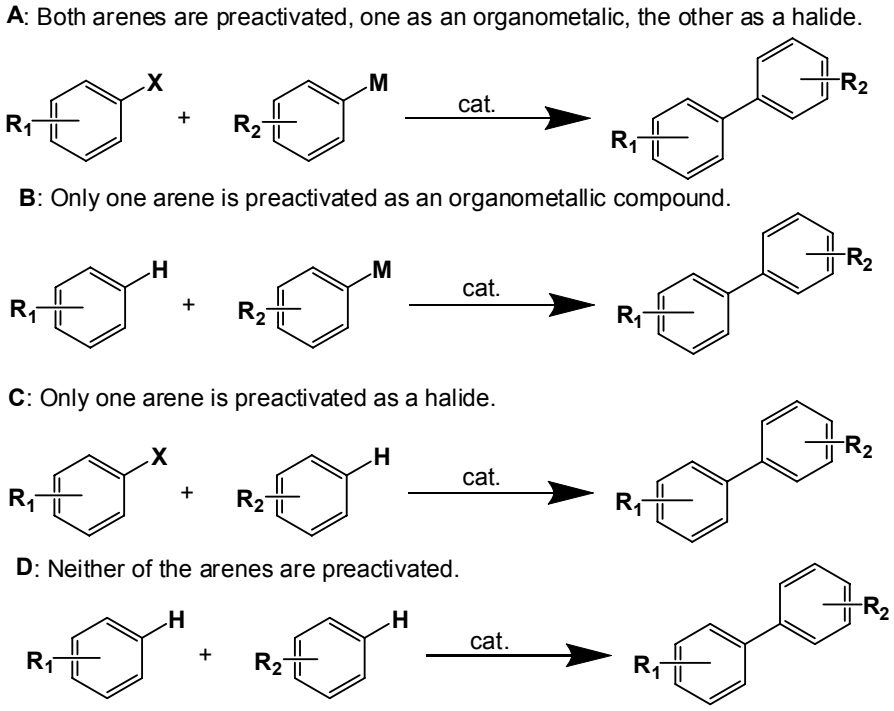

Figure 1.17 Reaction schemes showing different number of preactivated coupling partners.

The arylation of 1-methylimidazole is given as an example of a reaction where only one coupling partner is preactivated (Figure 1.18). In this example, the reaction of the azole compound occurs preferentially at the most electron-rich 5-position, indicating that the coupling involves electrophilic attack of the aryl-palladium species on the azole. However, as shown in the reaction scheme the electron-poor 2-position can also be arylated to get a minor biaryl product, suggesting that another mechanism intervenes.[77] In this example, halogenation of the arene is still required. However, recently, work has been done to establish biaryl coupling conditions where neither coupling partner is pre-functionalized.[76, 78, 79]

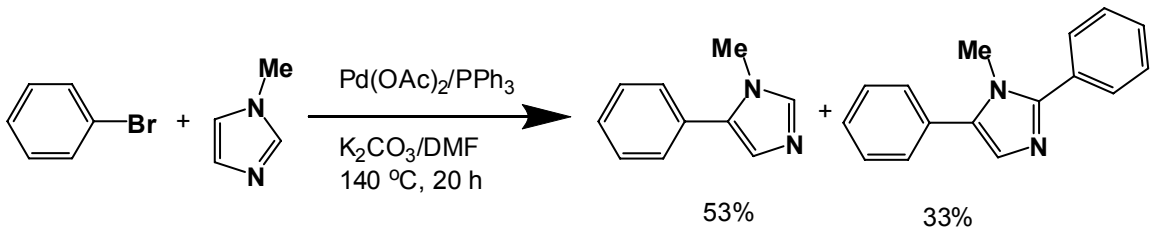

Figure 1.18 The arylation of 1-methylimidazole displaying direct arylation with only one preactivated coupling partner.

Catalytic arene cross-coupling that does not involve any substrate preactivation, as shown in Figure 1.17D, presents several new challenges. In addition to issues of reactivity and regioselectivity, the generation of unwanted arene homo-coupling products must also be avoided. To do this the catalyst must selectively react with one arene in one step of the catalytic cycle and then invert its selectivity in the other step to react selectively with the other arene. This was demonstrated by Stuart and coworkers when N-acetylindoles were cross-coupled with benzene. The reaction is illustrated in Figure 1.19 with the major product shown. The 2-substituted and 2,3'-disubstituted indolyl products were also observed, but there was no homo-coupling.[78] It is generally accepted that in direct arylation reactions, the π-electron rich substrates react through an electrophilic palladation step and that the arylations are facilitated by the highly nucleophilic nature of the arenes used in the coupling. It has also been shown that direct arylation can also be catalyzed by copper. Development of copper catalysts is driven by similar desires propelling the search for copper emitting materials in OLEDs: cost and availability of the copper when compared to palladium.[79]

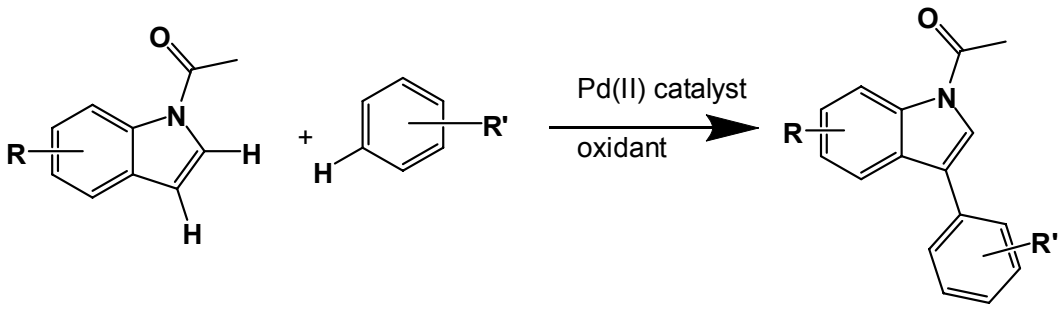

Figure 1.19 N-acetylindoles are cross coupled with benzene with no preactivation required.

1.3.2 Cu(I) Catalyzed Reactions

Copper catalyzed direct arylation of benzoxazole by aryliodide, as shown in Figure 1.20, has recently been reported. It was also noted that in addition to arylation of the electron-rich five-membered heterocycles shown in Figure 1.20, electron-poor pyridine oxides could also be arylated. [80] Li and coworkers have also demonstrated copper catalyzed C-C coupling on sp^2 carbons with the aid of an oxidant.[81-83]

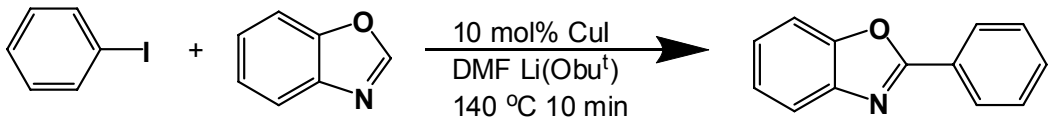

Figure 1.20 Copper catalyzed direct arylation of benzoxyazole by phenyl iodide.

Homo-coupling of aryls with no preactivation, catalyzed by copper, has also been established. Mulrooney *et al*. have demonstrated that when the copper catalyst is derived from a chiral diamine, it can be used to construct a range of symmetrical and

asymmetrical 3,3'-BINOL compounds as shown in Figure 1.21.[84, 85] In this reaction, the first step is believed to be ligand exchange between the amine coordinated to the copper catalyst and the substrate to release water, followed by the formation of a complex where the amine and substrate are both coordinated to the copper catalyst. Subsequent one electron transfer, from the metal centre to the ligand, gives rise to a carbon-centered radical on the substrate, reducing the copper centre from Cu(II) to Cu(I). In the last step of the catalytic cycle the product is released after radical-radical coupling as shown in Figure 1.22.[84, 85]

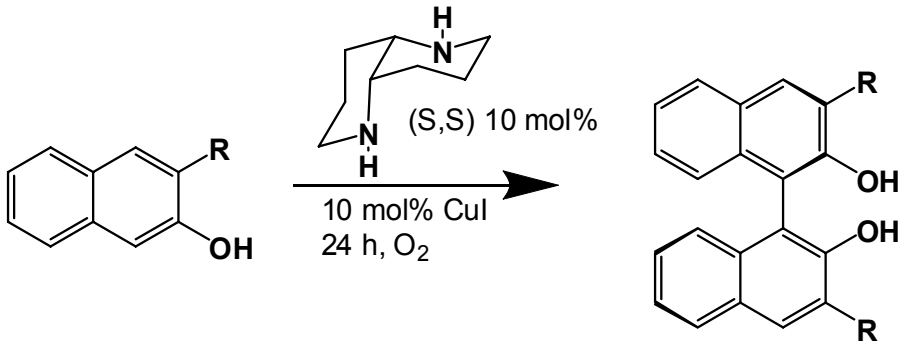

Figure 1.21 Asymmetric copper catalyzed homo-coupling of naphthol derivatives.

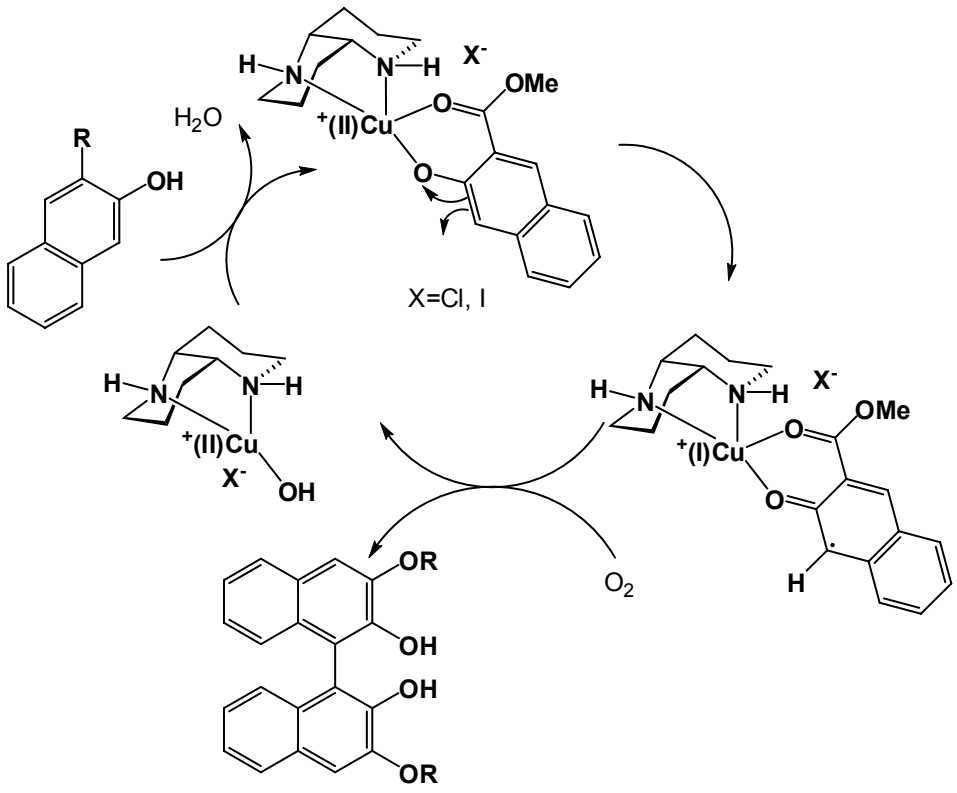

Figure 1.22 Catalytic cycle of the homo-coupling of naphthol derivatives.

It is worth noting that oxidative homo-coupling of heterocycles in the absence of a metal catalyst is also known. Dohi and coworkers displayed a synthetic method using a hypervalent iodine(III) reagent phenyliodine bis(trifluoroacetate) (PIFA) with bromotrimethylsilane (TMSBr), which provides the facile and selective construction of 2,2'-bipyrroles and even 2,3'-bipyrrole. PIFA is a safe and useful oxidant having reactivities similar to those of highly toxic heavy metal oxidizers. The reaction shown is presumed to undergo a one-electron oxidation by PIFA-TMSBr yielding pyrrole cation radical. The radical then reacts with another pyrrole to give the bipyrroles after further one-electron oxidation followed by deprotonation.[86]

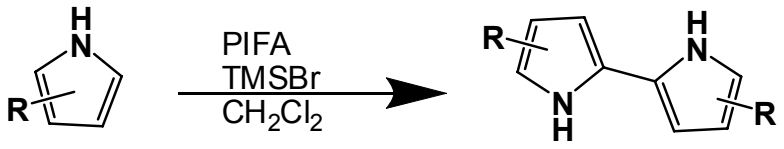

Figure 1.23 Homo coupling of pyrole with no metal catalyst and no preactivation.

1.4 Chiral Recognition and Sensing

Chiral recognition is one of the most fundamental processes in living systems and as such the design and understanding of artificial chiral receptors is of great interest.[87-89] In addition, understanding the mechanisms of chiral recognition can provide insight into catalytic design for asymmetric catalysis, not to mention the utility of developing a sensor capable of determining enantiomeric excess (ee) and absolute configuration of a chiral target.[90-92] Asymmetric synthesis is an important area of research and asymmetric catalysis has allowed many reactions with high enantiomeric excess (ee) to be established. One of the difficulties in this field is the rapid and efficient determination of ee and absolute configuration. This is necessary for many applications, especially in pharmaceuticals where often only one enantiomer is beneficial, and the other may be harmful. Commonly used chiral detection methods include creating diastereomers that can be detected by methods such as NMR. However for NMR to be used the conditions must be optimized as to provide enough separation of the chemical shifts to allow for reliable integration of the peaks, and prevent racemization of both the target molecule and the chiral derivatizing reagent.[93] Chiral HLPC is also commonly used, but it can be difficult to achieve optimal conditions that allow for complete separations of enantiomers

and often cannot provide insight into the absolute configuration. In chiral HPCL a chiral stationary phase discriminates between the enantiomers, however the columns can be quite costly and it may not be possible to find conditions that can separate the target molecules.[94]

1.4.1 Chiral Detection

The enantiomers of a chiral molecule both have the same physical properties with the exception of the direction they rotate plane-polarized light, or their specific rotation. Thus, determining an ee can be a difficult challenge, especially in the case of a novel molecule whose degree of optical rotation has not yet been established. The use of optical rotation is also sensitive to optical impurities and as a result it may not be a reliable method for determination of ee. The circular dichroism (CD) spectrum of a molecule is another method that can be used to determine ee. CD spectroscopy measures the difference in absorption of left vs. right handed polarised light with the magnitude of the absorption difference being a measure of the chirality.[95] In electronic circular dichroism (ECD) the absorptions are measured in the UV-Vis region (λ = ~190-900 nm) and are associated with electronic transitions between different molecular orbitals. When measured, the sample will give a positive or negative response, measured in ellipticity. The intensity of the spectrum depends on the sample's concentration (*c*) and path length (*l*), as well as the sample's internal chiroptical properties. The intensity of the CD signal is also dependent on the oscillator strength of the electronic transition (or the absorptivity of the corresponding UV-Vis band).[95] When using CD to determine

enantiomeric excess and for chiral sensing in general, a few different techniques are often employed, including induced chirality and chiral recognition.

1.4.2 Induced Chirality

Induced chirality occurs when an achiral host molecule interacts with a chiral guest molecule (or vice versa) and generates an overall chiral structure. Many supramolecular architectures display induced chirality. This can be used to sense the chirality of a target molecule that does not display an ECD spectrum when the supramolecular complex does. The CD spectra of enantiomers generated by the induced chirality are usually mirror images. This is because the complex formed with one enantiomer of the guest is usually the opposite enantiomer of the complex formed with the other enantiomer of the guest.

Incorporation of aromatic guests into cyclodextrins is an example of a chiral, transparent host (it does not have strong absorptions in the UV-Vis region) that forms a complex with an achiral chromophoric guest.[96, 97] More common is the case where an achiral chromophoric host such as calixerenes, porphyrins[98] or crown ethers forms a complex with a transparent chiral guest since many target molecules in asymmetric catalysis are not strong chromophores.[96]

It has been demonstrated that metallo-complexes of a bisporphyrin (shown in Figure 1.24), particularly Zn(II)[99, 100] and Mg(II) complexes, can be used for the stereochemistry assignment of enantiomeric amines, diamines, alcohols, amino alcohols, some amino acids and carboxylic acids.[100] The free bisporphyrin has also been shown to be able to sense chiral acids.[91, 101]

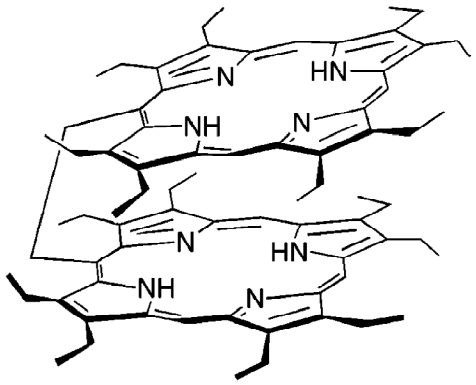

Figure 1.24 Structure of a free bisporphyrin used in induce chirality sensing that is often used with metal ions in the centre of the porphyrins.[101]

1.4.3 Chiral Recognition

Unlike induced chirality, for chiral recognition (or chiral discrimination) both the guest and the host are chiral. The resulting complex is also chiral, but if looking at one enantiomer of the host, the complexes made with the different enantiomers of the guest form diastereomers to each other. Thus, the physical properties of the complexes that can be observed through UV-Vis, luminescence, NMR, etc. are different and can be used to measure the chiral discrimination. Use of CD spectra for chiral recognition has also been reported, although the resulting spectra are often not mirror images when comparing the response to both enantiomers of a guest molecule.[90, 95, 102-106]

Supramolecular architectures such as porphyrins can be modified to be chiral hosts that show specific interactions with chiral guest molecules.[87, 98, 107] It has been shown that bisporphyrins connected through a chiral spacer, such as (*R*)-2,2'-dimethoxy-1,1'-binaphthyl, act as sensor for lysine derivatives.[91] Metal ions are important tools that

can promote assembly of supramolecular products. Similarly, metal centres can be used to facilitate chiral recognition. Kim *et al.* have shown that Zn(II) complex of (*N*,*N'*-bis(2-pyridylmethyl)-*N*,*N*'-dimethyl-*trans*-1,2-diaminocyclohexane) binds to the chiral vicinal diamines 1,2-diphenylethylenediamine stereoselectively (Figure 1.26).[102]

Metal-directed self-assembly of chiral molecular squares have also been reported for use in chiral sensing. The enantiomerically pure bridging ligand 4,4'-bis(pyridyl)-1,1'-bi-2-naphthol has been shown to form a molecular square with Re metal ions (Figure 1.25). The luminescence of the enantiopure molecular square was quenched by both enantiomers of 2-amino-1-propanol, but to significantly different degrees indicating chiral recognition.[108] Many other examples of enantiopure luminescent molecules that display differential luminescent quenching or enhancement to different enantiomers of target molecules have been reported.[105, 109] Even the emission of chiral lanthanide complexes can show differential quenching to chiral bio-molecules such as *c*-type cytochromes, vitamin B_{12},[110] and chiral amino alcohols.[111, 112]

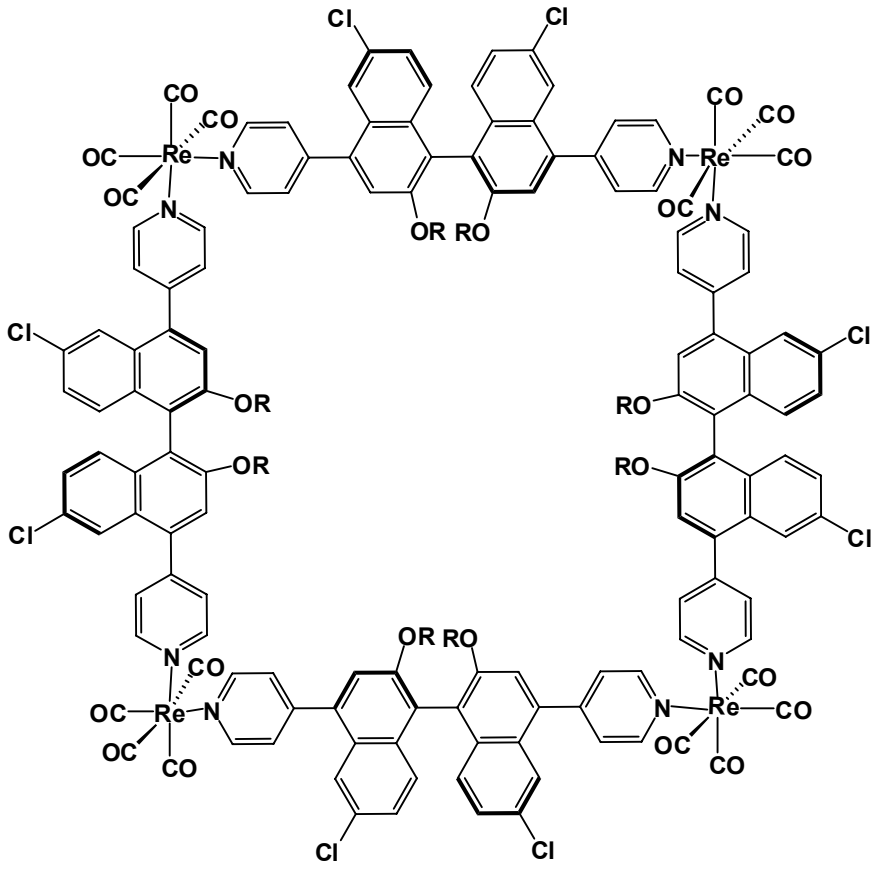

Figure 1.25 Structure of a self-assembled Re chiral molecular square.

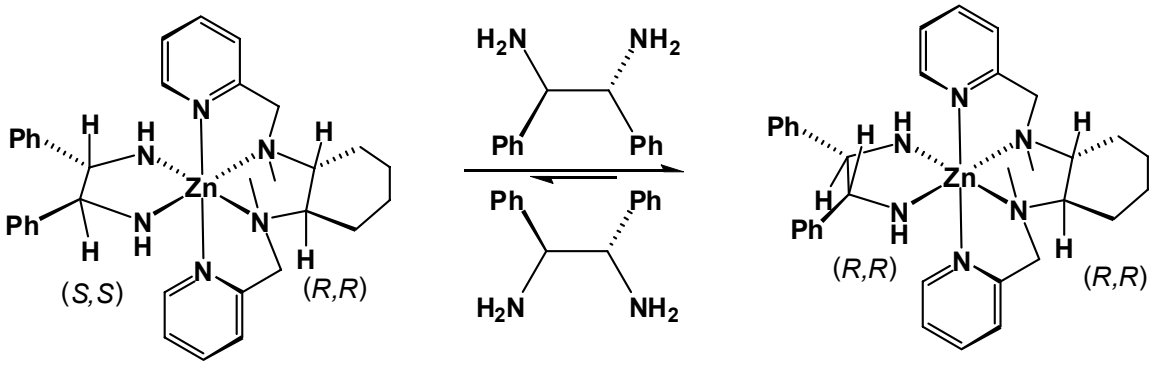

Figure 1.26 A scheme showing preferential formation of the (R,R)-(R,R) complex due to chiral discrimination.

1.5 Scope of Thesis

From the above introduction it is clear that transition metal complexes have a wide variety of uses in OLEDs, catalysis and sensors. The aim of this thesis is to investigate the structure and luminescent properties of Cu(I) complexes of 2-(2'-pyridyl)benzimidazolyl and 2-(2'-pyridyl)indolyl based complexes. In addition, Pd(II) and Pt(II) complexes of 2-(2'-pyridyl)indolyl based ligands will be examined. During the synthesis of the 2-(2'-pyridyl)indolyl benzene, a side product was isolated. The side product was found to be a chiral 2-(2'-pyridyl)indolyl based ligand, made by the formation of a new C-C bond in the 3 position of the indole. As a consequence this thesis also examines the C-C coupling reaction that led to the chiral side product as well as the photophysical properties of the new chiral ligands and their coordination complexes with Cu(I), Pd(II) and Pt(II).

In Chapter 2, the effects of ancillary phosphine ligands on the photophysical properties of copper(I) complexes of 2-(2'-pyridylbenzimidazole) benzene are examined. The effects of steric and electronic properties of the phosphine ligands on the luminescence of the Cu(I) complex are examined. In Chapter 3, polynuclear Cu(I) complexes based on bridging 2-(2'-pyridyl)benzimidazolyl derivative ligands are investigated and their photophysical properties are examined. In Chapter 4, the synthesis of new 2-(2'-pyridyl)indolyl based ligands is explored. During the synthesis of the 2-(2'-pyridyl)indolyl benzene (pib) based ligands a C-C bonded chiral dimer bis[3,3'-(2-(2'-pyridyl)indolyl)benzene] (bpib) was isolated. This was later expanded into a new class of

atropisomeric ligands. Chapter 4 examines the properties of both the monomer and dimer ligands and the homo-coupling reaction that took place. Chapter 5 presents the results of our investigation on Cu(I), Pd(II) and Pt(II) complexes of both the monomer ligand 2-(2'-pyridyl)indolyl benzene (pib) and the dimer ligand 3,3'-bis(2-(2'-pyridyl)indolyl benzene) (bpib) and their structures and luminescent properties. In Chapter 6, the use of the new atropisomeric ligands in sensing chiral of zinc carboxylates is described. The interaction of the atropisomeric ligands with Zn(II), Cd(II) and Hg(II) are examined to gain insight into the binding interactions. DFT calculations were also performed on the chiral Zn(II) complexes. Chapter 7 provides a general summary of the work in the thesis, with key conclusions and proposed future work.

1.6 References

(1) Cariati, E.; Pizzotti, M.; Roberto, D.; Tessore, F.; Ugo, R. *Coord. Chem. Rev.* **2006**, *250*, 1210.

(2) Klapshina, L. G.; Grigoryev, I. S.; Lopatina, T. I.; Semenov, V. V.; Domrachev, G. A.; Douglas, W. E.; Bushuk, B. A.; Bushuk, S. B.; Lukianov, A. Y.; Afanas'ev, A. V.; Benfield, R. E.; Korytine, A. I. *New J. Chem.* **2006**, *30*, 615.

(3) Domaille, D. W.; Que, E. L.; Chang, C. L. *Nat. Chem. Biol.* **2008**, *4*, 168.

(4) Burnworth, M.; Rowan, S. J.; Weder, C. *Chem. Eur. J.* **2007**, *13*, 7828.

(5) Knapton, D.; Burnworth, M.; Rowan, S. J.; Weder, C. *Angew. Chem. Int. Ed.* **2006**, *45*, 5825.

(6) Kalinowski, J. *Opt. Mater.* **2008**, *30*, 792.

(7) Ermakov, O. N.; Kaplunov, M. G.; Efimov, O. N.; Stakharny, S. A. *Proc. of SPIE* **2007**, *6636*, 1.

(8) Yersin, H., Ed.; In *Highly Efficient OLEDs with Phosphorescent Materials;* Wiley-VCH: Weinheim, Germany, 2008.

(9) Balzani, V.; Bergamini, G.; Campagna, S.; Puntoriero, F. *Top. Curr. Chem.* **2007**, *280*, 1.

(10) Campagna, S.; Puntoriero, F.; Nastasi, F.; Bergamini, G.; Balzani, V. *Top. Curr. Chem.* **2007**, *208*, 117.

(11) Jia, W. L.; Hu, Y. F.; Gao, J.; Wang, S. *Dalton Trans.* **2006**, 1721.

(12) Flamigni, L.; Barbier, A.; Sabatini, C.; Ventura, B.; Barigelletti, F. *Top. Curr. Chem.* **2007**, *281*, 143.

(13) Armaroli, N.; Gianluca, A.; Cardinali, F.; Listorti, A. *Top. Curr. Chem.* **2007**, *280*, 69.

(14) Horvath, O. *Coor. Chem. Rev.* **1994**, *135/136*, 303.

(15) Kirchhoff, J. R.; McMillin, D. R.; Robinson, W. R.; Powell, D. R.; McKenzie, A. T.; Chen, S. *Inorg. Chem.* **1985**, *24*, 3928.

(16) Eggleston, M. K.; McMillin, D. R.; Koenig, K. S.; Pallenberg, A. J. *Inorg. Chem.* **1997**, *36*, 172.

(17) Kuang, S. M.; Cuttell, D. G.; McMillin, D. R.; Fanwick, P. E.; Walton, R. A. *Inorg. Chem.* **2002**, *41*, 3313.

(18) Cuttell, D. G.; Kuang, S. M.; Fanwick, P. E.; McMillin, D. R.; Walton, R. A. *J. Am. Chem. Soc.* **2002**, 124, 6.

(19) Wang, B.; Liu, Y.; Li, B.; Yue, S.; Li, W. *J. Luminescence* **2008**, *128*, 341.

(20) Liu, Q. D.; Jia, W. L.; Wang, S. *Inorg. Chem.* **2005**, *44*, 1332.

(21) Chang, S.; Li, E. Y.; Chou, P.; Chi, Y. *Inorg. Chem.* **2007**, 7064.

(22) Chang, S.; Kavitha, J.; Li, S.; Hsu, C.; Chi, Y.; Yeh, Y.; Chou, P.; Lee, H.; Carty, A., J; Tao, Y.; Chien, C. *Inorg. Chem.* **2006**, 45, 137.

(23) Zhang, Q.; Zhou, Q.; Cheng, Y.; Wang, L.; Ma, D.; Jing, X.; Wang, F. *Adv. Mater.* **2004**, *16*, 432.

(24) Zhao, S.; Wang, R.; Wang, S. *Inorg. Chem.* **2006**, *45*, 5830.

(25) Li, D.; Li, R.; Qu, Z.; Feng, X.; Cai, J. *Inorg. Chem. Commun.* **2003**, *6*, 469.

(26) Omary, M. A.; Rawashdeh-Omary, M. A.; Diyabalanage, H. V. K.; Dias, H. V. R. *Inorg. Chem.* **2003**, *42*, 8612.

(27) Liu, Q.; Mudadu, M. S.; Schmider, H.; Thummel, R.; Tao, Y.; Wang, S. *Organometallics* **2002**, *21*, 4743.

(28) Liu, S.; Wu, Q.; Schmider, H. L.; Aziz, H.; Hu, N.; Popovic, Z.; Wang, S. *J. Am. Chem. Soc.* **2000**, *122*, 3671.

(29) Tollari, S.; Cenini, S.; Penoni, A.; Granata, G.; Palmisano, G.; Demartin, F. *J. Organomet. Chem.* **2000**, *608*, 34.

(30) Dodabalapur, A. *Solid State Commun.* **1997**, *102*, 259.

(31) Pope, M. *J. Chem. Phys.* **1963**, *38*, 2043.

(32) Tang, C. W.; VanSlyke, S. A. *Appl. Phys. Lett.* **1987**, *51*, 913.

(33) VanSlyke, S. A.; Chen, C. H.; Tang, C. W. *Appl. Phys. Lett.* **1996**, *69*, 2160.

(34) Yersin, H. *Top. Curr. Chem.* **2004**, *241*, 1.

(35) Yen, W. M. *Physics of the Solid State* **2005**, *47*, 1348.

(36) Chen, C. *Chem. Mater.* **2004**, *16*, 4389.

(37) Liang, F. S.; Cheng, G. P.; Su, G. P.; Ma, D. G.; Wang, L. X.; Jing, X. B.; Wang, F. S. *Synthetic Metals* **2003**, *137*, 1109.

(38) Jia, W. L.; Feng, X. D.; Bai, D. R.; Lu, Z. H.; Wang, S.; Vamvounis, G. *Chem. Mater.* **2005**, *17*, 164.

(39) Jia, W. L.; Moran, M. J.; Yuan, Y. -.; Lu, Z. H.; Wang, S. *J. Mater. Chem.* **2005**, *15*, 3326.

(40) Nazeeruddin, M. K.; Klein, C.; Grätzel, M.; Zuppiroli, L.; Berner, D. In *Molecular Engineering of Iridium Complexes and their Application in Organic Light Emitting Devices;* Yersin, H., Ed.; Highly Efficient OLEDs with Phosphorescent Materials; Wiley-VCH: Weinheim, Germany, 2008; 363.

(41) Li, J.; Djurovich, P. I.; Alleyne, B. D.; Yousufuddin, M.; Ho, N. N.; Thomas, J. C.; Peters, J. C.; Bau, R.; Thompson, M. E. *Inorg. Chem.* **2005**, *44*, 1713.

(42) Adachi, C.; Tsutsui, T.; Saito, S. *Appl. Phys. Lett.* **1990**, *56*, 799.

(43) Shirota, Y. *J. Mater. Chem.* **2000**, *10*, 1.

(44) Evans, R. C.; Douglas, P.; Winscom, C. J. *Coord. Chem. Rev.* **2006**, *250*, 2093.

(45) Bian, Z.; Huang, C. In *Progress in Electroluminescence Based on Lanthanide Complexes;* Yersin, H., Ed.; Highly efficient OLEDDs with Phosphorescent Materials; Wiley-VCH: Weinheim, Germany, 2008; 391.

(46) Goze, C.; Chambron, J.; Heitz, V.; Pomeranc, D.; Salom-Roig, X.; Sauvage, J.; Morales, A. F.; Barigelletti, F. *Eur. J. Inorg. Chem.* **2003**, *3752*, 3758.

(47) Ward, M. D. *Annu. Rep. Prog. Chem., Sect. A* **2006**, *102*, 584.

(48) Adachi, C.; Baldo, M. A.; Forrest, S. R.; Lamansky, S.; Thompson, M. E.; Kwong, R. C. *Appl. Phys. Lett.* **2001**, *78*, 1622.

(49) Sajoto, T.; Djurovich, P. I.; Tamayo, A.; Yousufuddin, M.; Bau, R.; Thompson, M. E.; Holmes, R. J.; Forrest, S. R. *Inorg. Chem.* **2005**, *44*, 7992.

(50) Ragni, R.; Plummer, E. A.; Brunner, K.; Hofstraat, J. W.; Babudri, F.; Farinola, G. M.; Naso, F.; De Cola, L. *J. Mater. Chem.* **2006**, *16*, 1161.

(51) Tamayo, A. B.; Alleyne, B. D.; Djurovich, P. I.; Lamansky, S.; Tsyba, I.; Ho, N. N.; Bau, R.; Thompson, M. E. *J. Am. Chem. Soc.* **2003**, *125*, 7377.

(52) Williams, J. A. G. *Top. Curr. Chem.* **2007**, *281*, 205.

(53) Yersin, H.; Donges, D. *Top. Curr. Chem.* **2001**, *214*, 81.

(54) Yang, Q. ; Wu, L.; Wu, Z.; Zhang, L.; Tung, C. *Inorg. Chem.* **2002**, *41*, 5653.

(55) Sandrini, D.; Maestri, M.; Balzani, V.; Chassot, L.; von Zelewsky, A. *J. Am. Chem. Soc.* **1987**, *109*, 3107.

(56) Liu, Q. D.; Thorn, L.; Kozin, I.; Song, D.; Seward, C. *J. Chem. Soc. Dalton. Trans.* **2002**, 3234.

(57) Kalinowski, J.; Cocchi, M.; Virgili, D.; Fattori, V.; Williams, J. A. G. *Adv. Mater.* **2007**, *19*, 4000.

(58) Barbieri, A.; Accorsi, G.; Armaroli, N. *Chem. Commun.* **2008**, 2185.

(59) Kovalevsky, A. Y.; Gembicky, M.; Coppens, P. *Inorg. Chem.* **2004**, *43*, 8282.

(60) Miller, M. T.; Gantzel, P. K.; Karpishin, T. P. *Angew. Chem. Int. Ed.* **1998**, *37*, 1556.

(61) Armaroli, N. *Chem. Soc. Rev.* **2001**, *30*, 113.

(62) Chen, L. X.; Jennings, G.; Liu, T.; Gosztola, D. J.; Hessler, J. P.; Scaltrito, D. V.; Meyer, G. J. *J. Am. Chem. Soc.* **2002**, *124*, 10861.

(63) Armaroli, N.; Accorsi, G.; Holler, M.; Moudam, O.; Nierengarten, J. ; Zhou, Z.; Wegh, R. T.; Welter, R. *Adv. Mater.* **2006**, *18*, 1313.

(64) Che, G.; Su, Z.; Li, W.; Chu, B.; Li, M.; Hu, Z.; Zhang, Z. *Appl. Phys. Lett.* **2006**, *89*, 103511.

(65) Ojwach, S.; Westman, G.; Darkwa, J. *Polyhedron* **2007**, *26*, 5544.

(66) Wang, H.; Li, M.; Shao, M.; He, X. *Polyhedron* **2007**, *26*, 5171.

(67) Cravotto, G.; Demartin, F.; Palmisano, G.; Penoni, Andrea Radice, Tiziano; Tollari, S. *J. Organomet. Chem.* **2005**, *690*, 2017.

(68) Wu, F.; Hardesty, J.; Thummel, R. P. *J. Org. Chem.* **1998**, *63*, 4055.

(69) Wu, F.; Chamchoumis, C. M.; Thummel, R. P. *Inorg. Chem.* **2000**, *39*, 584.

(70) Hassan, J.; Sévignon, M.; Gozzi, C.; Schulz, E.; Lemaire, M. *Chem. Rev.* **2002**, *102*, 1359.

(71) Heck, R. F.; Nolley, Jr., J. P. *J. Org. Chem.* **1972**, *37*, 2320.

(72) Miyaura, N.; Suzuki, A. *Chem. Rev.* **1995**, *95*, 2457.

(73) Miyaura, N.; Yamada, K.; Suzuki, A. *Tetrahedron Lett.* **1979**, *20*, 3437.

(74) Nicolaou, K. C.; Bulger, P. G.; Sarlah, D. *Angew. Chem. Int. Ed.* **2005**, *44*, 4442.

(75) Gooßen, L. J.; Deng, G.; Levy, L. M. *Science* **2006**, *313*, 662.

(76) Lafrance, M.; Lapointe, D.; Fagnou, K. *Tetrahedron* **2008**, *64*, 6015.

(77) Miura, M.; Nomura, M. *Top. Curr. Chem.* **2002**, *219*, 211.

(78) Stuart, D. R.; Fagnou, K. *Science* **2007**, *316*, 1172.

(79) Basle, O.; Li, C. *Green Chemistry* **2007**, *9*, 1047.

(80) Do, H.; Daugulis, O. *J. Am. Chem. Soc.* **2007**, *129*, 12404.

(81) Li, Z.; Li, C. J. *J. Am. Chem. Soc.* **2004**, *126*, 11810.

(82) Li, Z.; Li, C. J. *J. Am. Chem. Soc.* **2005**, *127*, 3672.

(83) Li, Z.; Li, C. J. *Eur. J. Org. Chem.* **2005**, *127*, 3173.

(84) Mulrooney, C. A.; Li, X.; DiVirgilio, E. S.; Kozlowski, M. C. *J. Am. Chem. Soc.* **2003**, *125*, 6856.

(85) Li, X. J.; Hewgley, B.; Mulrooney, C. A.; Yang, J.; Kozlowski, M. C. *J. Org. Chem.* **2003**, *68*, 5500.

(86) Dohi, T.; Morimoto, K.; Maruyama, A.; Kita, Y. *Org. Lett.* **2006**, *8*, 2007.

(87) Mateos-Timoneda, M. A.; Crego-Calama, M.; Reinhoudt, D. N. *Chem. Soc. Rev.* **2004**, *33*, 363.

(88) Dybtsev, N. N.; Nuzhdin, A. L.; Chun, H.; Bryliakov, K. P.; Talsi, E. P.; Fedin, V. P.; Kim, K. *Angew. Chem., Int. Ed.* **2006**, *45*, 916.

(89) Takeuchi, M.; Mizuno, T.; Shinkai, S.; Shirakami, S.; Itoh, T. *Tetrahedron: Asymmetry* **2000**, *11*, 3311.

(90) Chen, Z.; He, Y.; Hu, C.; Huang, X.; Hu, L. A. *J. Chem.* **2008**, *61*, 310.

(91) Hayashi, T.; Aya, T.; Nonoguchi, M.; Mitzutani, T.; Hiseda, Y.; Kitagawa, S.; Ogoshi, H. *Tetrahedron* **2002**, *58*, 2803.

(92) Gottarelli, G.; Lena, S.; Masiero, S.; Pieraccini, S.; Spada, G. P. *Chirality* **2008**, *20*, 471.

(93) Parker, D. *Chem*. *Rev.* **1991.** *91,* 1441.

(94) Pirkle, W. H.; Pochapsky T.C. *Chem. Rev*. **1989,** *89,* 347

(95)Hembury, G. A.; Borovkov, V. V.; Inoue, Y. *Chem. Rev.* **2008**, *108*, 1.

(96) Allenmark, S. *Chirality* **2003**, *15*, 409.

(97) Ikeda, H.; Li, Q.; Ueno, A. *Bioorg. & Med. Chem. Lett.* **2006**, *16*, 5420.

(98) Huang, X.; Nakanishi, K.; Berova, N. *Chirality* **2000**, *12*, 237.

(99) Kurtan, T.; Nasri, N.; Li, Y.; Huang, X.; Nakanishi, K.; Berova, N. *J. Am. Chem. Soc.* **2001**, *123*, 5962.

(100) Proni, G.; Pescitelli, G.; Huang, X.; Quraishi, N. Q.; Nakanishi, K.; Berova, N. *Chem. Commun.* **2002**, 1561.

(101) Bhyrappa, P.; Borokov, V. V.; Inoue, Y. *Org. Lett.* **2007**, *9*, 433.

(102) Kim, W.; So, S. M.; Chagal, L.; Lough, A. J.; Kim, B. M.; Chin, J. *J. Org. Chem* **2006**, 71, 8966.

(103) Maeda, K.; Morioka, K.; Yashima, E. *Macromolecules* **2007**, *40*, 1349.

(104) Li, W.; Jiang, D.; Suna, Y.; Aida, T. *J. Am. Chem. Soc.* **2005**, 7700.

(105) Lin, J.; Rajaram, A. R.; Pu, L. *Tetrahedron* **2004**, 11277.

(106) Pu, L. *Chem. Rev.* **2004**, *104*, 1687.

(107) Ishi-I, T.; Crego-Calama, M.; Timmerman, P.; Reinhoudt, D. N.; Shinkai, S. *Angew. Chem. Int. Ed.* **2002**, *41*, 1924.

(108) Lee, S. J.; Lin, W. B. *J. Am. Chem. Soc.* **2002**, *124*, 4554.

(109) Li, Z.; Pu, L. J. *Mater. Chem.* **2005**, *15*, 2860.

(110) Meskers, S. C. J.; Dekkers, H. P. J. M. J. *Phys. Chem. A* **2001**, *105*, 4589.

(111) Tsukube, H.; Hosokubo, M.; Wada, M.; Shinoda, S.; Tamiaki, H. *Inorg. Chem.* **2001**, *40*, 740.

(112) Tsukube, H.; Shinoda, S.; Tamiaki, H. *Coord. Chem. Rev.* **2002**, 226, 227.

Chapter 2
Phosphorescent Mononuclear Cu(I) 2-(2'-pyridylbenzimidazolyl)benzene Complexes with Various Ancillary Phosphine Ligands

2.1 Introduction

Phosphorescent metal complexes have been investigated for use in OLEDs because the metal ion allows access to the triplet excited state which can increase the quantum efficiency of the electroluminescent device. Earlier investigations focus mainly on Ir(III), Pt(II) and lanthanide complexes and many examples of devices made with complexes of these metals have been demonstrated.[1-10] Phosphorescent emitters based on complexes of inexpensive metal ions such as Cu(I) have not been extensively investigated. Recent work by Wang and coworkers has demonstrated that phosphorescent Cu(I) complexes are in general green emitters that contain a phenanthroline N,N-chelate (or its derivatives) and two ancillary phosphine ligands.[11-13] The ancillary phosphine ligands have been shown to play a key role in stabilizing the Cu(I) centre. Our group previously reported that 2-(2'-pyridyl)benzimidazolyl derivative ligands are blue emitters and are effective chelating ligands for metal ions such as Pt(II)[6] and Ru(III).[14] These complexes display red emission attributed to MLCT transitions.

Phosphorescent Cu(I) complexes based on a phenanthroline (and its derivatives) also display MLCT based emission. The ancillary phosphine donors, albeit not involved in the transition play a key role in stabilizing the Cu(I) centre and have a significant

impact on the photophysical properties of the complex.[11, 12] Further evidence for the role of the phosphine ligands came from a report by L. X. Wang and co-workers where they noted that the performance of [Cu(phen)(DPEphos)][BF_4] in OLEDs (DPEphos = bis[2-(diphenylphosphino)phenyl]ether, phen = 1,10-phenanthroline and derivatives) is much better than that of the analogous [Cu(phen)(PPh_3)$_2$][BF_4], because of the increased emission quantum efficiency and the shortened decay lifetime.[13] Clearly, the appropriate choice of the ancillary phosphine ligands is very important in optimizing the performance of the Cu(I) complexes as emitters. Although both phenanthroline and 2-(2'-pyridyl)benzimidazolyl are *N*,*N* chelate ligands, they have distinct geometric and electronic properties. As a result, the effects of the ancillary phosphine ligands on the properties of the corresponding Cu(I) complexes are not necessarily the same. Therefore, to establish the effects of the phosphine ligands on the properties 2-(2'-pyridyl)benzimidazolyl-based Cu(I) complexes, and hence to find a better phosphorescent Cu(I) emitter for OLEDs, it is necessary to examine the structures and photophysical properties of a series of Cu(I) 2-(2'-pyridyl)benzimidazolyl complexes involving different phosphine ancillary ligands. To simplify the investigation, a group of mononuclear Cu(I) complexes containing the 2-(2'-pyridyl)benzimidazolyl benzene (pbb) ligand with the common structure of [Cu(pbb)(P)$_2$]$^{+/0}$, as shown in Figure 2.1 were studied. The four different phosphine ligands used in the investigation are triphenylphosphine (PPh_3), bis(diphenylphosphino)ethane (dppe), bis[2-(diphenyl-phosphino)phenyl]ether (DPEphos), and bis(diphenylphosphinomethyl)-diphenylborate

(DPPMB) used to make complexes **2.1-2.4** respectively shown in Figure 2.2. The DPPMB ligand was included in the study because it is an anionic, chelating phosphine ligand that has been shown to stabilize Cu(I) complexes.[15] The Cu(I) complex will be neutral and neutral complexes are desirable for OLED applications because they can be sublimed in device fabrication. The syntheses, crystal structures, photophysical properties, and results of molecular orbital calculations of four new Cu(I) complexes that contain the common pbb chelate ligand and the four different phosphine ligands are presented. The goal of this investigation is to determine if the pbb ligand is capable of producing MLCT phosphorescent emission once bound to the Cu(I) centre, the efficiency of the emission and emission colour, for their potential use in OLEDs, and finally the effect of the phosphine ligand on these.

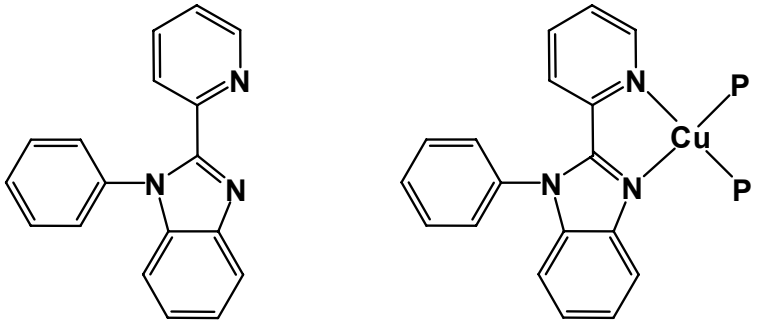

Figure 2.1 Structure of the ligand pbb and the general structure of the complexes with the formula $[Cu(pbb)(P_2)]^{0/+}$ where P_2 is $(PPh_3)_2$ (**2.1**), DPPE (**2.2**), DPEphos (**2.3**) and DPPMB (**2.4**).

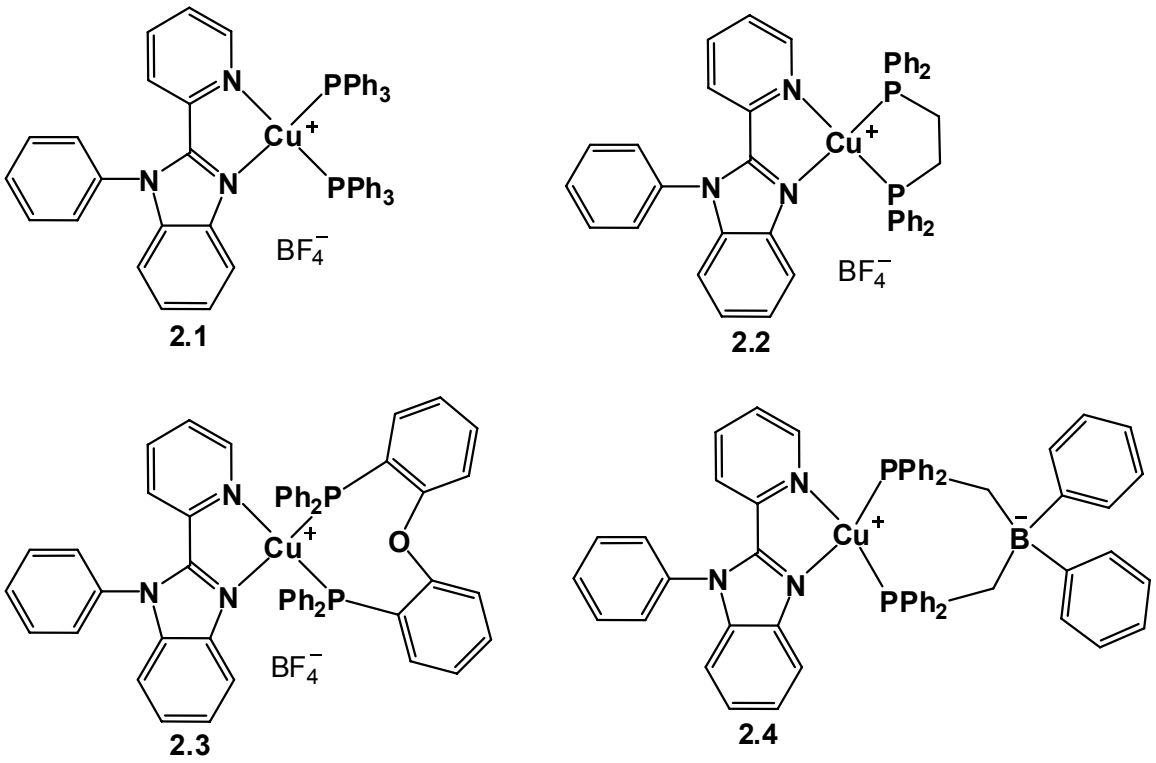

Figure 2.2 Structures of the phosphine ligands and the complexes **2.1-2.4.**

2.2 Experimental

2.2.1 General Considerations

All starting materials were purchased from Aldrich Chemical Co. and used without further purification. Solvents were freshly distilled over appropriate drying reagents under N_2 atmosphere. All experiments were carried out under a dry nitrogen atmosphere using standard Schlenk techniques or in the glove box unless otherwise stated. Thin layer chromatography (TLC) was carried out on silica gel. Flash chromatography was carried out on silica (silica gel 60, 70-230 mesh). ^{1}H and ^{31}P NMR spectra were recorded on a

Bruker Avance 300 MHz spectrometer. Excitation and emission spectra were recorded on a Photon Technologies International QuantaMaster model C-60 spectrometer. Emission lifetimes were measured on a Photon Technologies International Phosphorescent spectrometer (Time-Master C-631F) equipped with a xenon flash lamp and digital emission photon multiplier tube using a band pathway of 5 nm for excitation and 2 nm for emission. Elemental analyses were performed by Canadian Microanalytical Service Ltd., Delta, British Columbia, Canada. Cyclic voltammetry was performed using a BAS CV-50W analyzer with a scan rate of 500 mV s^{-1}. The electrolytic cell used was a conventional three-compartment cell, in which a Pt working electrode, a Pt auxiliary electrode, and a Ag/AgCl reference electrode were employed. The CV measurements were performed at room temperature using 0.10 M tetrabutylammonium hexafluorophosphate (TBAP) as the supporting electrolyte and CH_3CN as the solvent. The ferrocenium/ferrocene couple was used as the internal standard (E_0 = 0.45 V). The copper(I) complexes[16, 17] $[Cu(CH_3CN)_4][BF_4]$, $[Cu(CH_3CN)_2(PPh_3)_2][BF_4]$, and the phosphine ligands $[Ph_2B(CH_2PPh_2)_2]$-ASN (ASN = 5-azonia-spiro[4.4]nonane) DPPMB,[15, 18-20] and DPEphos[21] were synthesized according to literature procedures.

2.2.2 Synthesis of 2-(2-Pyridylbenzimidazolyl)benzene (pbb)

A mixture of bromobenzene (1.00 mL, 4.27 mmol), 2-(2'-pyridyl)benzimidazole (0.505 g, 2.6 mmol), copper(I) iodide (77 mg, 0.40 mmol), cesium carbonate (2.00 g, 6.15 mmol), and 1,10-phenanthroline (0.110 g, 0.61 mmol) was refluxed in 2 mL of DMF for 30 h. The product was purified by column chromatography (THF/hexanes/methanol,

1:1:0.05) and subsequent recrystallization from CH_2Cl_2 and hexanes (yield 78%). ^1H NMR in CD_2Cl_2 300 MHz (δ, ppm, 298 K): 8.36 (d, *J*=4.2 Hz, 1H), 8.21 (d, *J* = 8.1 Hz, 1H), 7.89-7.80 (m, 2H), 7.56-7.45 (m, 3H), 7.40-7.26 (m, 6H). Anal. Calcd for $C_{18}H_{13}N_3$: C, 79.68; H, 4.83; N, 15.49. Found: C, 80.00; H, 4.87; N, 15.38.

2.2.3 Synthesis of $[Cu(pbb)(PPh_3)_2][BF_4]$ (2.1)

To a solution of pbb (28 mg, 10 mmol) in CH_2Cl_2 (ca. 5 mL) was added a solution of $[Cu(CH_3CN)_2(PPh_3)_2][BF_4]$ (72 mg, 10 mmol) in CH_2Cl_2 (ca. 5 mL) at room temperature. The yellow solution was stirred for half an hour then layered with toluene (ca. 2 mL) and hexanes (ca. 2 mL). Diffusion of the layers and slow evaporation of the solvents afforded complex **2.1** after 1 week in 63% yield. ^1H NMR in CD_2Cl_2, 300 MHz (δ, ppm, 298 K): 8.38 (d, *J* = 4.8 Hz, 1H), 7.81-7.75 (m, 3H), 7.67 (d, *J* = 9.3 Hz, 1H), 7.44-7.32 (m, 12H), 7.27-7.20 (m, 24H), 7.01 (d, *J* = 8.1 Hz, 2H). $^{31}P\{^1H\}$ NMR in CD_2Cl_2 (δ, ppm, 298 K): 3.07. Anal. Calcd for $C_{54}H_{43}BCuF_4N_3P_2 \cdot 0.25CH_2Cl_2$: C, 67.42; H, 4.45; N, 4.35. Found: C, 67.28; H, 4.58; N, 4.55.

2.2.4 Synthesis of $[Cu(pbb)(dppe)][BF_4]$ (2.2)

A solution of $[Cu(CH_3CN)_4][BF_4]$ (82 mg, 0.26 mmol) and 1,2-bis(diphenylphosphenyl) ethane (dppe) (60 mg, 0.15 mmol) in CH_2Cl_2 (ca. 5 mL) was stirred for 1.5 h at room temperature. A solution of pbb (45 mg, 0.16 mmol) in CH_2Cl_2 (ca. 3 mL) was added, and the mixture was stirred for 1 h to obtain a dark yellow solution. The yellow solution was layered with toluene (ca. 2 mL). Diffusion of the layers and slow evaporation of the solvents afforded complex **2.2** after 3 days in 88% yield. ^1H NMR in CD_2Cl_2, 300 MHz

(δ, ppm, 298 K): 8.32 (d, *J* = 4.8 Hz, 1H), 7.84 (d, *J* = 4.2 Hz, 3H), 7.79 (d, *J* = 8.1 Hz, 1H), 7.67-7.65 (m, 2H), 7.50-7.42 (m, 12H), 7.39-7.34 (m, 10H), 7.30 (d, *J* = 5.4 Hz, 2H), 7.23 (d, *J* = 7.8 Hz, 2H), 2.76 (t, *J* = 6.0 Hz, 4H). $^{31}P\{^{1}H\}$ NMR in CD_2Cl_2 (δ, ppm, 298 K): -4.26. Anal. Calcd for $C_{44}H_{37}BCuF_4N_3P_2 \cdot 0.25CH_2Cl_2$: C, 63.17; H, 4.46; N, 4.99. Found: C, 63.18; H, 4.48; N, 5.04.

2.2.5 Synthesis of [Cu(pbb)(DPEphos)][BF_4] (2.3)

A solution of $[Cu(CH_3CN)_4][BF_4]$ (125 mg, 0.40 mmol) and bis[2-(diphenylphosphino)phenyl]ether (DPEphos) (215 mg, 0.40 mmol) in CH_2Cl_2 (ca. 5 mL) was stirred for 1.5 h. A solution of pbb (86 mg, 0.32 mmol) in CH_2Cl_2 (ca. 3 mL) was added, and the mixture was stirred for 1 h to obtain a dark yellow solution at room temperature. The yellow solution was layered with toluene (ca. 2 mL) and hexanes (ca. 2 mL). Diffusion of the layers and slow evaporation of the solvents afforded complex **2.3** after 3 days in 60% yield. ^{1}H NMR in CD_2Cl_2, 300 MHz (δ, ppm, 298 K): 8.36 (d, *J* = 4.8 Hz, 1H), 7.79 (dd, *J* = 5.1, 1.8 Hz, 3H), 7.61 (t, *J* = 8.0 Hz, 2H), 7.51 (d, *J* = 8.4 Hz, 1H), 7.46-7.43 (m, 2H), 7.38-7.31 (m, 7H), 7.28-7.14 (m, 15H), 7.09-6.99 (m, 8H), 6.97-6.90 (m, 2H). $^{31}P\{^{1}H\}$ NMR in CD_2Cl_2 (δ, ppm, 298 K): -10.56. Anal. Calcd for $C_{54}H_{41}BCuF_4N_3OP_2$: C, 67.54; H, 4.30; N, 4.38. Found: C, 67.50; H, 4.21; N, 4.26.

2.2.6 Synthesis of [Cu(pbb)(DPPMB)] (2.4)

A solution of $[Cu(CH_3CN)_4][BF_4]$ (36 mg, 0.11 mmol) and bis(diphenylphosphinomethyl) diphenyl borate ligand ($[Ph_2B(CH_2PPh_2)_2][ASN]$, = DPPMB) (66 mg, 0.10 mmol) in CH_2Cl_2 (ca. 5 mL) was stirred for 2 h at room temperature. A solution of pbb

(32 mg, 0.12 mmol) in CH_2Cl_2 (ca. 3 mL) was added, and the mixture was stirred for 1 h to obtain a deep red solution. The red solution was layered with toluene (ca. 2 mL) and hexanes (ca. 2 mL). Diffusion of the layers and slow evaporation of the solvents afforded complex **2.4** after 1 week in 72% yield. ^{1}H NMR in CD_2Cl_2 (δ, ppm, 298 K): 7.75 (t, J = 3.2 Hz, 3H), 7.57-7.54 (m, 2H), 7.49 (d, J = 7.8 Hz, 2H), 7.39- 7.25 (m, 10H), 7.17-7.12 (m, 10H), 7.10-6.96 (m, 10H), 6.90-6.89 (m, 5H), 6.67 (d, J = 8.7 Hz, 1H), 2.14 (d, J = 9.9 Hz, 4H). ^{31}P{^{1}H} NMR in CD_2Cl_2, 300 MHz (δ, ppm, 298 K): -4.00. Anal. Calcd for $C_{56}H_{47}BCuN_3P_2 \cdot 0.5CH_2Cl_2$: C, 73.42; H, 5.10; N, 4.47. Found: C, 72.85; H, 5.23; N, 4.63

2.2.7 Molecular Orbital Calculations

Ab initio molecular orbital calculations were performed for complexes **2.1**-**2.4**. The geometric parameters were taken from X-ray diffraction analysis and the energies were computed with the Gaussian suite of programs.[22] The calculations were performed with restricted density functional theory at the B3LYP/6-311++G** level of theory.

2.2.8 Quantum Yield Measurements.

The absolute photoluminescence quantum yields of Cu(I) complexes **2.1**-**2.4** doped in PMMA films (20% complex/80% PMMA by weight) were measured at ambient temperature using a commercial fluorimeter in combination with an integration sphere according to the literature procedure.[23] The measurements were performed at the Institute of Microstructural Science at NRC in Ottawa.

2.2.9 X-ray Crystallographic Analysis.

Single crystals of compounds **2.1**-**2.4** were obtained from the mixed solvent solution of toluene/ CH_2Cl_2/hexanes. Crystals were mounted on glass fibres for data collection. Data were collected on a Siemens P4 single-crystal X-ray diffractometer with a Smart CCD-1000 detector and graphite monochromated Mo Kα radiation, operating at 50 kV and 30 mA at 298 K for **2.2** and at 180 K for **2.1**, **2.3**, and **2.4**. No significant decay was observed for any sample. Data were processed on a PC using the Bruker SHELXTL software package10 (version 5.10)[24] and were corrected for Lorentz and polarization effects. Compounds **2.1**-**2.3** belong to the monoclinic space groups $P2_1$, $P2_1/n$, and *Cc*, respectively, determined by the systematic absences and the successful solution and refinements of the structures, whereas compound **2.4** belongs to the triclinic space group *P*-1. Solvent molecules were located in the crystal lattices for **2.2** and **2.4**. For **2.2**, each molecule co-crystallizes with 0.5 CH_2Cl_2 solvent molecules. For **2.4**, one disordered CH_2Cl_2 and 0.5 disordered toluene solvent molecules per molecule of **2.4** were located and were partially resolved and refined. The BF_4 anions in compounds **2.1**-**2.3** were also found to display some degree of disordering and were refined successfully. One of the phenyl groups of in **2.4** displays rotational disordering that was modeled and refined successfully. Most non-hydrogen atoms except the disordered ones in **2.1**-**2.4** were refined anisotropically. All hydrogen atoms except those on disordered carbon atoms were calculated, and their contributions were included in structural factor calculations. The crystallographic data are reported in Table 2.1 and selected bond lengths and angles are given in Table 2.2

Table 2.1 Crystallographic data for compounds **2.1-2.4.**

	2.1	**2.2**	**2.3**	**2.4**
formula	$C_{54}H_{43}N_3P_2F_4BCu$	$C_{44.5}H_{38}N_3F_4P_2BClCu$	$C_{54}H_{41}N_3F_4BP_2Cu$	$C_{64}H_{47}N_3BP_2Cu$
fw	946.2	862.52	960.18	994.345
space group	$P2_1$	$P2_1/n$	Cc	P-1
a, Å	9.961(2)	15.919(4)	9.2812(16)	13.261(3)
b, Å	18.067(3)	15.664(3)	20.546(3)	22.435(5)
c, Å	13.206(3)	17.884(4)	23.425(4)	17.237(4)
β, deg	102.720(3)	109.314(4)	90.608(3)	91.299(4)
V, Å^3	2318.4(8)	4208.6(16)	4466.7(13)	5127(2)
Z	2	4	4	4
D_{calc}, gcm^{-3}	1.355	1.361	1.428	1.288
μ, cm^{-1}	5.97	7.11	6.22	5.33
$2\theta_{max}$, deg	56.28	56.76	56.40	56.52
Reflns measd	14005	23568	12483	28507
Reflns used (R_{int})	7943 (0.0468)	9664 (0.0460)	8138 (0.0220)	11463 (0.0365)
no. of params	582	526	595	621
final *R* [I > 2σ(I)]				
R1[a]	0.0538	0.0810	0.0356	0.0672
*w*R2[b]	0.0996	0.1974	0.0770	0.1713
R (all data)				
R1[a]	0.1031	0.1649	0.0394	0.1113
*w*R2[b]	0.1156	0.2377	0.0780	0.1985
GOF on F^2	0.997	1.037	1.105	1.047

[a] $R1 = \Sigma[|F_o| - |F_c|]/\Sigma|F_o|$. [b] $wR2 = \{\Sigma[w(F_o^2 - F_c^2)]/ \Sigma(wF_o^2)\}^{1/2}$. $\omega = 1/[\sigma^2(F_o^2) + (0.075P)^2]$, where $P = [\max.(F_o^2,0) + 2F_c^2]/3$.

Table 2.2 Selected bond lengths (Å) and angles (°) of **2.1-2.4**.

		2.1	
Cu(1)-N(1)	2.091(4)	N(1)-Cu(1)-N(2)	78.62(16)
Cu(1)-N(2)	2.092(4)	N(1)-Cu(1)-P(3)	119.48(12)
Cu(1)-P(3)	2.2371(13)	N(2)-Cu(1)-P(3)	116.58(11)
Cu(1)-P(2)	2.2899(15)	N(1)-Cu(1)-P(2)	105.02(12)
		N(2)-Cu(1)-P(2)	103.20(12)
		P(3)-Cu(1)-P(2)	124.12(6)
		2.2	
Cu(1)-N(2)	2.009(5)	N(2)-Cu(1)-N(1)	80.1(2)
Cu(1)-N(1)	2.123(5)	N(2)-Cu(1)-P(2)	126.69(15)
Cu(1)-P(2)	2.2538(16)	N(1)-Cu(1)-P(2)	120.98(14)
Cu(1)-P(1)	2.2586(16)	N(2)-Cu(1)-P(1)	114.71(15)
		N(1)-Cu(1)-P(1)	126.32(14)
		P(2)-Cu(1)-P(1)	92.02(6)
		2.3	
Cu(1)-N(2)	2.053(2)	N(2)-Cu(1)-N(1)	78.87(9)
Cu(1)-N(1)	2.114(2)	N(2)-Cu(1)-P(2)	121.74(6)
Cu(1)-P(2)	2.2346(8)	N(1)-Cu(1)-P(2)	120.84(6)
Cu(1)-P(1)	2.2683(8)	N(2)-Cu(1)-P(1)	104.91(6)
		N(1)-Cu(1)-P(1)	112.12(6)
		P(2)-Cu(1)-P(1)	113.35(3)
		2.4	
Cu(1)-N(3)	2.016(3)	N(3)-Cu(1)-N(2)	78.72(12)
Cu(1)-N(2)	2.150(3)	N(3)-Cu(1)-P(1)	124.91(9)
Cu(1)-P(1)	2.2310(11)	N(2)-Cu(1)-P(1)	111.80(9)
Cu(1)-P(2)	2.2386(10)	N(3)-Cu(1)-P(2)	125.91(9)
		N(2)-Cu(1)-P(2)	109.19(9)
		P(1)-Cu(1)-P(2)	102.24(4)

2.3 Results and Discussion

2.3.1 Synthesis and Characterization

The new *N*,*N*-chelate ligand, pbb, was synthesized by the reaction of 2-(2`-pyridyl)benzimidazole with bromobenzene using a modified Ullmann condensation procedure[25] where CuI and 1,10-phenanthroline were used as the catalysts and Cs_2CO_3 was used as the base. The ligand pbb was fully characterized by NMR spectroscopy and elemental analysis. Four different ancillary phosphine ligands, namely, PPh_3, dppe, DPEphos, and DPPMB, were used in the investigation. The bidentate chelate phosphine ligands DPEphos and DPPMB were synthesized by literature procedures.[15, 18-21] The choice of the three bidentate chelate phosphine ligands was based on the following considerations. First, the chelate phosphine ligands are known to provide better stability to the Cu(I) complex than the monodentate PPh_3 ligand as the PPh_3 has been shown to dissociate from the Cu(I) in solution for $[Cu(phen)(PPh_3)_2]^+$ complexes.[11, 12] Second, these three chelate phosphine ligands have distinct steric and electronic properties that offer an opportunity to examine the steric and electronic impacts of phosphine donors on the properties of the copper complexes. Third, it was shown previously that chelate phosphine ligands such as DPEphos can minimize emission quenching induced by solvent molecules or self-quenching, thus enhancing emission efficiency.[11-13] The anionic ligand DPPMB is unique among the four phosphine ligands that were studied because it allows the synthesis of a neutral Cu(I) complex instead of a salt, which is highly desirable if the Cu(I) complex were to be incorporated into OLEDs by a vacuum deposition

process. Furthermore, the negatively charged ligand DPPMB might enhance the electron density on the metal centre, thus having a significant impact on the MLCT state. In fact, the DPPMB ligand has been used successfully in many of transition metal complexes including Pt(II) and Cu(I), as reported by Peters and co-workers.[15, 18-20, 26]

Complex **2.1** was obtained by the reaction of $[Cu(CH_3CN)_2(PPh_3)_2][BF_4]$ with one equivalent of pbb under air. The syntheses of the Cu(I) complexes **2.2**-**2.4** were achieved by the reaction of $[Cu(CH_3CN)_4][BF_4]$ with pbb and the corresponding chelate phosphine ligand in a 1:1:1 ratio under a nitrogen atmosphere. Compounds **2.1**-**2.3** have a yellow colour and are stable in solution and in the solid state upon exposure to air. Compound **2.4** has a distinct red colour and decomposes gradually when exposed to air. The new complexes were fully characterized by NMR, elemental, and X-ray diffraction analyses.

The $^{31}P\{^{1}H\}$ NMR spectra for all four complexes were recorded and show that there is a considerable change in the ^{31}P chemical shifts for the four phosphine ligands in the complexes compared to those in the corresponding free ligands. Complex **2.1** has a peak at chemical shift 3.07 ppm. The dppe complex **2.2** and the DPEphos complex **2.3** have ^{31}P peaks at chemical shifts -4.26 ppm and -10.56 ppm, respectively, which are comparable to those of previously reported Cu(I) DPEphos and Cu(I) DPPE complexes.[11, 12] For complex **2.4**, the ^{31}P peak appears at -4.00 ppm, which is within the normal expected range for the DPPMB ligand.[15, 18-20, 26] The absence of free phosphines peaks indicates that there is not significant dissociation of the ancillary ligand in solution.

2.3.2 Crystal Structure

The crystal structures of the Cu(I) complexes **2.1**-**2.4** were determined and are shown in Figure 2.3 - Figure 2.6, respectively. The selected bond lengths and angles for complexes **2.1**-**2.4** are listed in Table 2.2. For complexes **2.1-2.3**, the BF_4^- anion is omitted for clarity. The Cu(I) centre in all four complexes has a distorted tetrahedral geometry. The dihedral angles between the N-Cu-N plane and the P-Cu-P plane for the four complexes are 90.2°, 81.9°, 94.4°, and 86.8°, respectively. The Cu-N (pyridyl) bond lengths for the pyridyl bond [avg 2.119(4) Å] are greater than the Cu-N (imidazolyl) bond lengths [avg 2.042(4) Å], indicating a stronger bond for the imidazolyl nitrogen because the imidazolyl nitrogen atom is a stronger donor than that of the pyridyl ring. The Cu-N bond lengths observed in **2.1**-**2.4** are similar to those in $[Cu(phen)(PPh_3)_2]NO_3$ (2.075 Å) and $[Cu(dmp)(PPh_3)_2]NO_3$ (dmp = 2,9-dimethyl-1,10-phenanthroline) (2.117 Å).[27] The Cu-P bond lengths for all four complexes are similar.

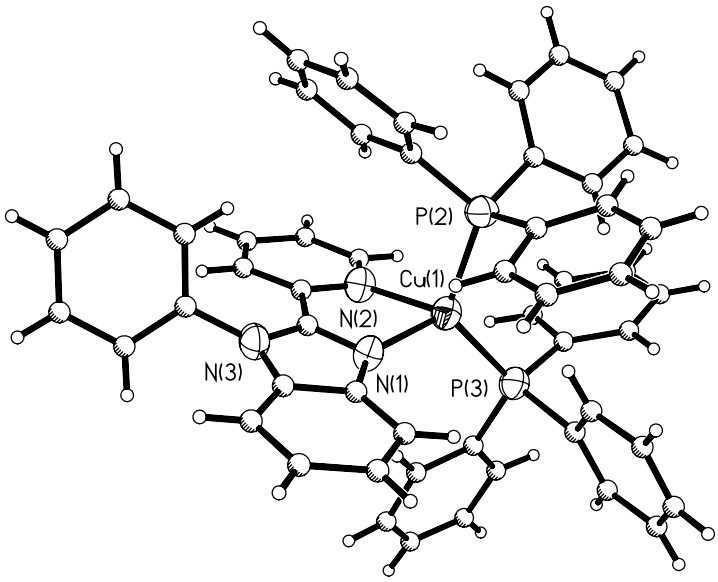

Figure 2.3 Structure of **2.1** with thermal ellipsoids and labelling schemes. The BF_4^- anion is omitted. Carbon atoms are shown as ideal spheres.

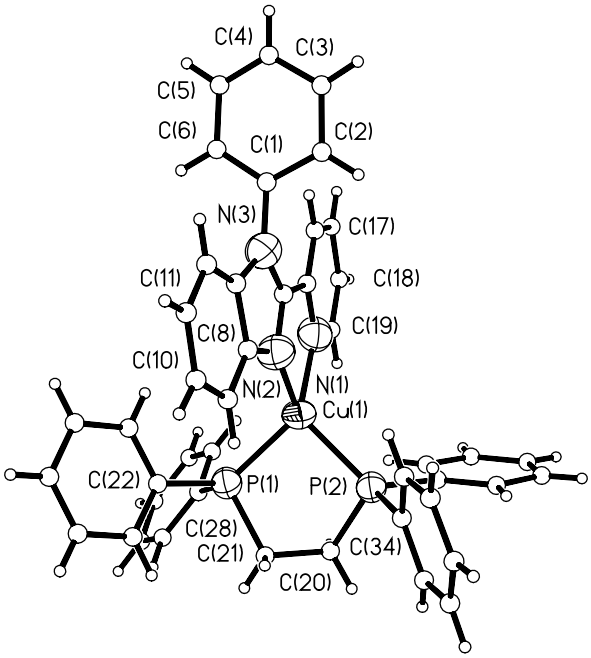

Figure 2.4 Structure of **2.2** are shown with thermal ellipsoids and labelling schemes. The BF_4^- anion is omitted. Carbon atoms are shown as ideal spheres.

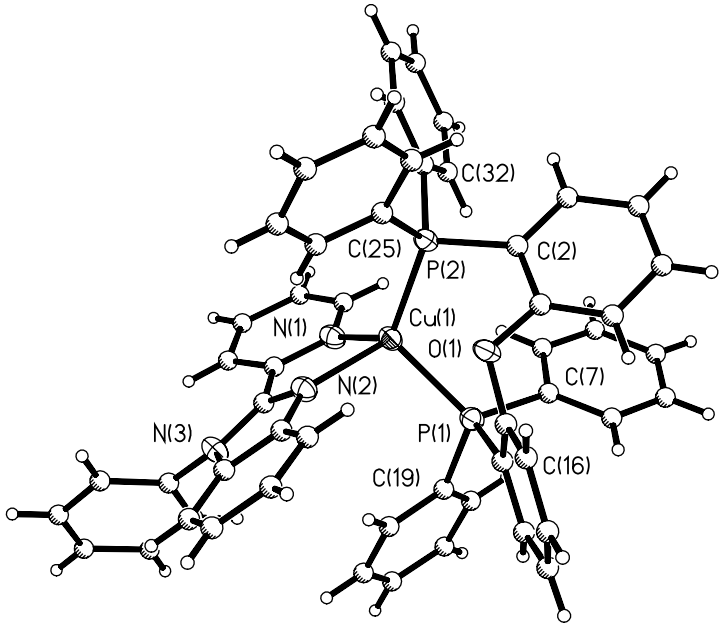

Figure 2.5 Structure of **2.2** are shown with thermal ellipsoids and labelling schemes. The BF_4^- anion is omitted. Carbon atoms are shown as ideal spheres.

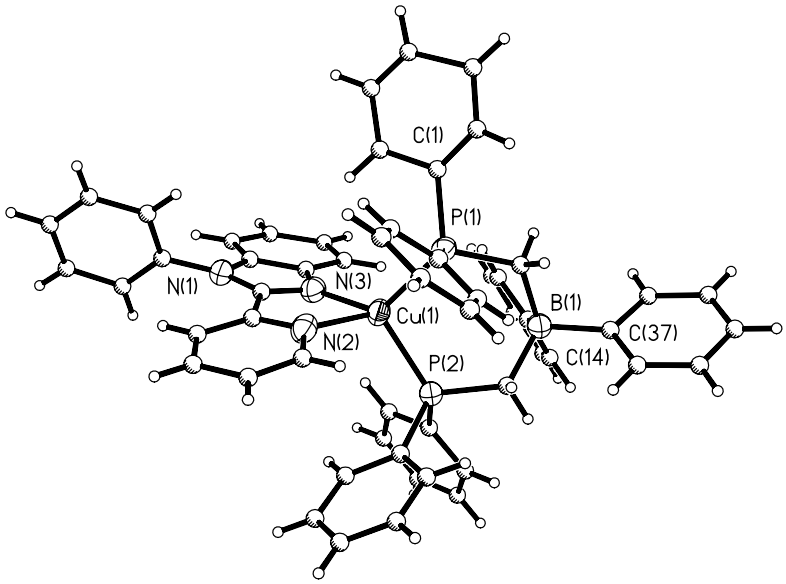

Figure 2.6 Structure of **2.4** with thermal ellipsoids and labelling schemes. For the disordered phenyl ring only one set of the disordered atoms (C(2A) and C(3A)) are shown. All carbon atoms are shown as ideal spheres.

The N-Cu-N bond angles are similar for complexes **2.1**, **2.3**, and **2.4** (78.6-78.8°) with little variation. The N-Cu-N bond angle of **2.2** is somewhat greater, 80.1°, clearly due to the reduced steric congestion. In contrast, however, the P-Cu-P angles vary dramatically from 92.02(6)° for complex **2.2** to 124.12(6)° for complex **2.1** as shown in Table 2.2. Previously, it was observed that the P-Cu-P angle is 115.85(9)° for $[Cu(phen)(PPh_3)_2]NO_3$ and 122.7(1)° for the more sterically crowded complex $[Cu(dmp)(PPh_3)_2]NO_3$; the latter is similar to that of **2.1**.[27] The fact that the dppe complex **2.2** has the smallest P-Cu-P angle is an indication that the dppe ligand is the least crowded. The DPEphos natural bite angle was calculated by Kranenburg et al. to be 102.2°, with a flexibility range from 86° to 120°.[21] $[Cu(dmp)(DPEphos)]^+$ has a P-Cu-P angle of 116.44°, which is slightly larger than that found in complex **2.3** (113.35°).[21] One notable feature of the *N*,*N*-chelate ligand pbb in complexes **2.1**-**2.4** is that the phenyl ring and the 2-(2'-pyridyl)benzimidazolyl unit in pbb are not coplanar, but have a dihedral angle of 67.5°, 84.1°, 62.4°, and 65.5°, respectively, which is clearly caused by the nonbonding interactions between the ortho hydrogen atoms of the phenyl ring and the pyridyl ring. The oxygen atom of the DPEphos ligand in **2.3** is at a distance of 3.16 Å from the Cu(1) centre and opposite that of N(1) [N(1)-Cu(1)-O(1)) 176.8°]. Similar Cu-O separations have also been reported in DPEphos Cu(I) complexes that contain 1,10-phenanthroline and derivative ligands.[11, 12]

Analysis of the crystal structure packing reveals some weak π-π intermolecular interactions. Complex **2.1** show face to face interactions with half overlap of two of the

phenyl rings on the phosphine ligands with a distance of 3.889 Å. Complex **2.3** also displays a face to face type intermolecular interaction with a distance of 3.340 Å between the phenyl rings on the phosphines. Complexes **2.2** and **2.4** display edge to face π-π intermolecular interactions. For complex **2.2** there is a separation distance of 4.017 Å between phenyl rings on the phosphines on neighbouring molecules. However, for **2.4** the intermolecular interaction is between the phenyl ring on the pbb ligand on one molecule and a phenyl ring on the phosphine part of the other molecule with a separation distance of 4.075 Å.

2.3.3 UV-Vis Absorption Spectra

In CH_2Cl_2, the free ligand pbb shows two absorption peaks at $\lambda_{max} \approx 240$ and 300 nm attributed to π-π* transitions centered on the 2-(2'-pyridyl)benzimidazolyl. As shown in Figure 2.7 and in Table 2.3, in CH_2Cl_2, complexes **2.1-2.4** have multiple absorption peaks in the 200-320 nm region that can be attributed to both the pbb and phosphine ligands. In addition, a low-energy and broad absorption band is observed for all complexes, which is characteristic of metal-to-ligand charge-transfer (MLCT) transitions. For complex **2.1**, this MLCT absorption band appears at λ_{max} = 370 nm. For complexes **2.2**-**2.4**, this MLCT band shifts to lower energy with λ_{max}= 420 nm for **2.2**, 400 nm for **2.3**, and 485 nm for **2.4**. This dramatic variation of the MLCT band supports the conclusion that the ancillary phosphine ligands significantly perturb the MLCT state of the copper complexes. The trend of the MLCT band observed for complexes **2.1**-**2.3** is consistent with that observed for the $[Cu(phen)(PP)]^+$ and $[Cu(dmp)(PP)]^+$ complexes where (PP) =

2PPh_3, dppe, and DPEphos.[11, 12] The energy of the MLCT band of **2.4** is dramatically lower than those of **2.1**-**2.3**, which is clearly responsible for the distinct red colour of complex **2.4**. The optical band gap using the edge of the lowest-energy absorption band was determined to be 2.80, 2.50, 2.60, and 2.10 eV for complexes **2.1**-**2.4**, respectively. Sakaki et al. reported a series of $[Cu(dmp)L_2]^+$ complexes with L = $PPh_n(C_6H_4OMe\text{-}p)_{3-n}$ where the phosphine ligands have a similar cone angle but different electron donating capabilities because of the variation in the number of methoxy-substituted phenyl groups.[28] It was observed that the MLCT band of the $[Cu(dmp)L_2]^+$ complex shifts to somewhat longer wavelengths with increasing electron donating character of the phosphine.[28] Therefore, judging from the MLCT energy, the electron-donating capabilities of the ancillary phosphine ligands appear to increase in the order DPPMB > dppe > DPEphos > PPh_3. It is not surprising that the anionic ligand DPPMB in **2.4** is the strongest electron donor, as a formally negative charge on the ligand is anticipated to increase the electron density on the metal centre.[18-20] It has been noted by McMillin and co-workers that a wider P-Cu-P bite angle can decrease the d-σ* interactions and enhance the energy required for MLCT excitation.[11, 12] The P-Cu-P angle, therefore, might also play a role in the observed band gap variation of compounds **2.1**-**2.4**. In fact, the P-Cu-P bond angles of **2.1**-**2.3** follow the order of **2.1** (124.12°) > **2.3** (113.35°) > **2.2** (92.02°), which is the same order as the MLCT energies (372, 396, and 422 nm, respectively), consistent with the observations of McMillin *et al.*[11, 12] Therefore, it can be concluded that for complexes **2.1**-**2.3**, steric factors play a key role in the electronic properties of the

complex. However, for complex **2.4**, which has a P-Cu-P bond angle (102.24°) much greater than that of **2.2** but a MLCT energy (484 nm) much less than that of **2.2**, electronic factors clearly dominate. The MLCT bands of **2.1**-**2.4** shift somewhat toward shorter wavelengths in polar solvents such as CH_3OH and DMF which is consistent with the behaviour of Cu(I) phenanthroline complexes.[11, 12] An example of solvent dependent absorption spectrum is shown in Figure 2.8 for complex **2.3**. The dependence of this absorption peak on solvent polarity supports that this is a charge transfer band.

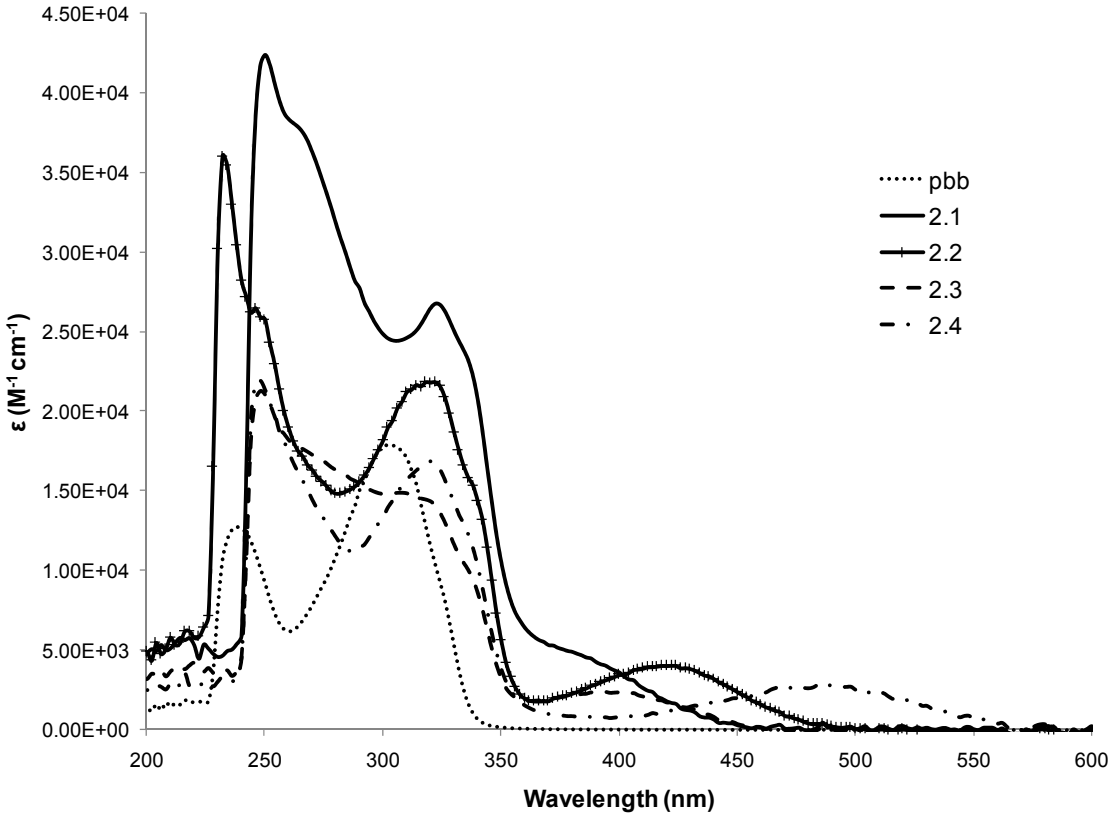

Figure 2.7 UV-Vis spectra of pbb and complexes **2.1-2.4** in CH_2Cl_2 at rt.

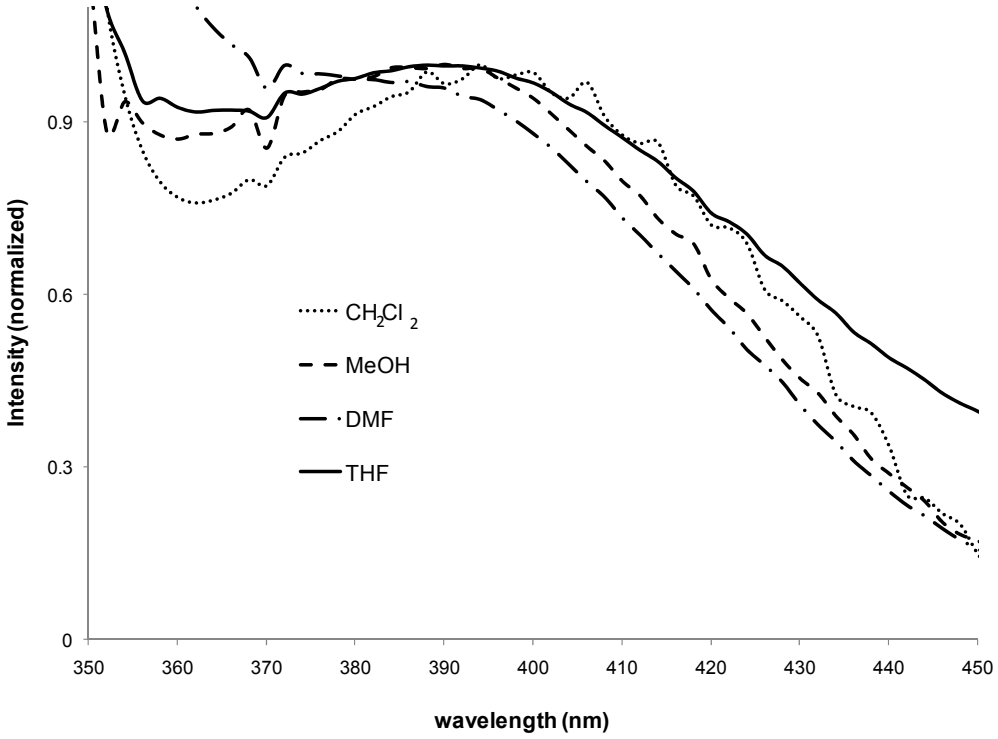

Figure 2.8 Effect of solvent on the MLCT absorption band of complex **2.3.**

Table 2.3 Absorption and luminescent data for **2.1-2.2.**

compd	Absorption[a] λ_{max}, nm (ε, $M^{-1}cm^{-1}$)	Emission, λ_{max}, nm in CH_2Cl_2[a] 77 K	in PMMA[b] 77 K	In PMMA[b] rt	Φ[c]	τ(μs) in CH_2Cl_2[a] 77 K	in PMMA[b] 77 K
2.1	236 (34600) 248 (28034) 324 (16991) 372 (3452)	553	561	536	13	296(6) 115(5)	353(1)
2.2	232 (36028) 246 (26503) 318 (21854) 422 (34916)	586	597	545	<1	291(8) 106(4)	503(6) 126(3)
2.3	236 (34916) 246 (29064) 318 (21565) 396 (4014)	564	557	537	1.04	247(6) 106(6)	322(4) 122(3)
2.4	236 (32908) 316 (16507) 484 (1579)	587	603	593	<1	315(3) 111(3)	228.8(7)
pbb	238 (12741) 302 (17893)	382	380	394		311(2)[d]	

[a] [c]≈ 10^{-5} M. [b] 20 wt % in PMMA, rt. [d] For the phosphorescent band with λ_{max} = 525 nm

2.3.4 Cyclovoltametry

In an CH_3CN solution, complexes **2.1**-**2.4** display an irreversible oxidation peak at ~1.80 V (**2.1**), 1.50 V (**2.2**), 1.60 V (**2.3**), and 0.60 V (**2.4**), which can be attributed to the oxidation of Cu(I) to Cu(II). The exceptionally low oxidation potential displayed by compound **2.4** indicates that it has a relatively high HOMO level, which is most likely due to the presence of the anionic DPPMB chelate ligand, which increases the electron density on the copper centre, thus destabilizing the HOMO level. The first reduction peaks for the four complexes were observed at -1.52 V (**2.1**), -1.60 V (**2.2**), -1.60 V (**2.3**), and -1.75 V (**2.4**), that are attributed to the reduction of the *N*,*N*-chelate ligand. Using the reduction and oxidation potentials, the electrochemical band gaps for complexes **2.1**-**2.4** were estimated to be 3.36 eV, 3.10 eV, 3.20 eV, and 2.35 eV, respectively. Although the values of the electrochemical band gaps deviate considerably from those of the optical band gaps, the general trends revealed by the electrochemical and optical band gaps are consistent, compound **2.1** has the largest and compound **2.4** the smallest HOMO-LUMO energy gap.

2.3.5 Ab Initio Molecular Orbital Calculations

To further understand the variation of the electronic properties of compounds **2.1**-**2.4**, ab initio molecular orbital calculations were performed for all four complexes using the Gaussian suite of programs (Gaussian 03)[22] and geometric parameters obtained from single-crystal X-ray diffraction analysis. The molecular orbital surfaces generated by Gaussian 03 for all four molecules show that the HOMO is indeed dominated by the d

orbital of the copper(I) ion, but significant contributions from the phosphine ligands and a small contribution from the pbb ligand are also evident. The LUMO is almost entirely made up of atomic orbitals of the pbb ligand. The LUMO and HOMO diagrams for compounds **2.1, 2.2, 2.3** and **2.4** are shown in Figure 2.9. A larger view of the least sterically crowded complex **2.2** is shown in Figure 2.10. The MO calculation results confirmed that the lowest electronic transition in complexes **2.1**-**2.4** is indeed MLCT in nature, but with considerable contribution from the phosphine ligands (i.e., phosphine ligand to pbb charge transfer). The HOMO and LUMO energies, the band gaps, and the optical and electrochemical band gaps are summarized in Table 2.4. The variations among complexes **2.1**-**2.3** in both the HOMO energy (from -0.29424 to -2.8628 Hartree) and the LUMO energy (from -0.17577 to -0.16716 Hartree) are small. In contrast, the HOMO (-0.18349 Hartree) and LUMO (-0.09006 Hartree) energy levels of complex **2.4** are substantially higher than those of **2.1**-**2.3**. The HOMO-LUMO band gaps obtained from Gaussian 03 MO calculations were 3.37, 3.01, 3.28, and 2.54 eV, respectively, for complexes **2.1**-**2.4**. The band gap trend obtained from the MO calculations is consistent with the electrochemical and UV-Vis data. The MO results support the conclusion that the anionic DPPMB ligand destabilizes both the HOMO and the LUMO levels in complex **2.4** by increasing the electron density on the metal centre. However, because the destabilization of the HOMO level is much more pronounced than that of the LUMO level, the net result is an overall decrease of the band gap in **2.4** compared to those in **2.1**-**2.3**.

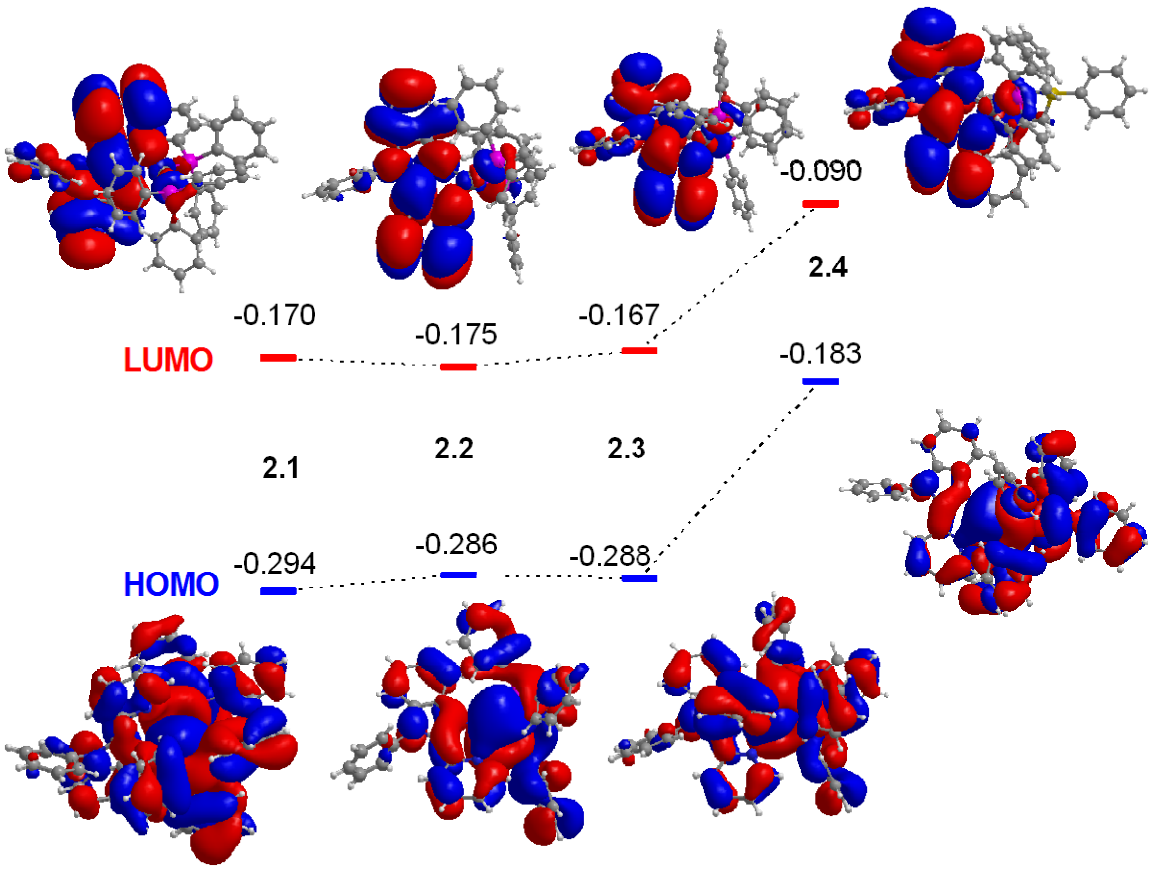

Figure 2.9 HOMO and LUMO diagrams for compounds **2.1-2.4** where the calculated energy levels are shown in Hartree.

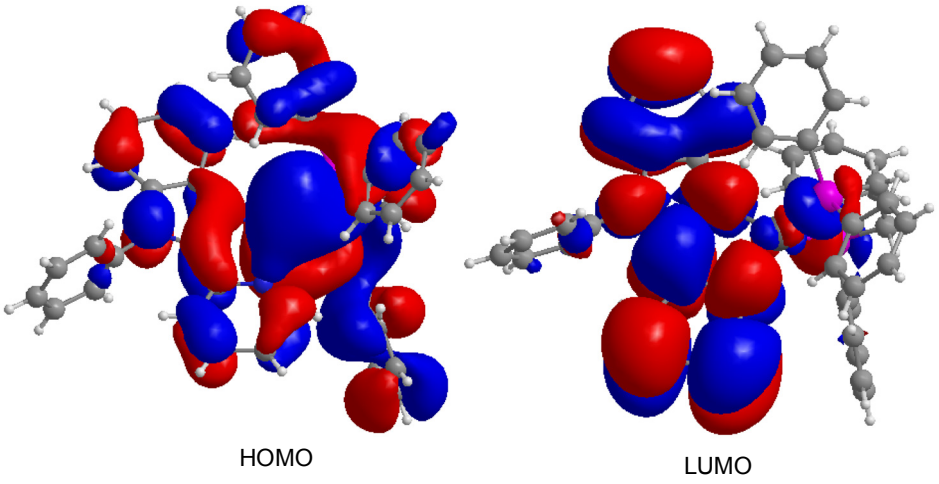

Figure 2.10 Enlarged view of HOMO and LUMO for **2.2**.

Table 2.4 Calculated and experimental HOMO and LUMO energies and bandgaps for **2.1**-**2.4.**

	MO data			Experimental data			
Complex	HOMO (eV)	LUMO (eV)	Gap (eV)	Optical band gap (eV)	E_{ox} (V)	E_{red} (V)	Electrochemical band gap (eV)
2.1	-8.01	-4.64	3.37	2.79	1.80	-1.52	3.32
2.2	-7.79	-4.78	3.01	2.50	1.50	-1.60	3.10
2.3	-7.83	-4.59	3.28	2.58	1.60	-1.60	3.20
2.4	-4.55	-2.45	2.54	2.10	0.60	-1.75	2.35

2.3.6 Luminescent Properties

The free ligand pbb emits a purple colour when irradiated with UV light with λ_{max} = 380 nm at room temperature in CH_2Cl_2, which is attributed to the fluorescent emission of the singlet state. In contrast, complexes **2.1**-**2.4** all emit in the yellow-orange region with a broad emission band and λ_{max} at 553, 586, 564, and 587 nm, respectively, when excited by the MLCT energy (77 K in CH_2Cl_2), as shown in Figure 2.11. At ambient temperature, complexes **2.1**-**2.4** do not display any detectable emission in solution due to solvent quenching consistent with previous reports for less sterically crowded Cu(I) phenanthroline derivative complexes.[27]

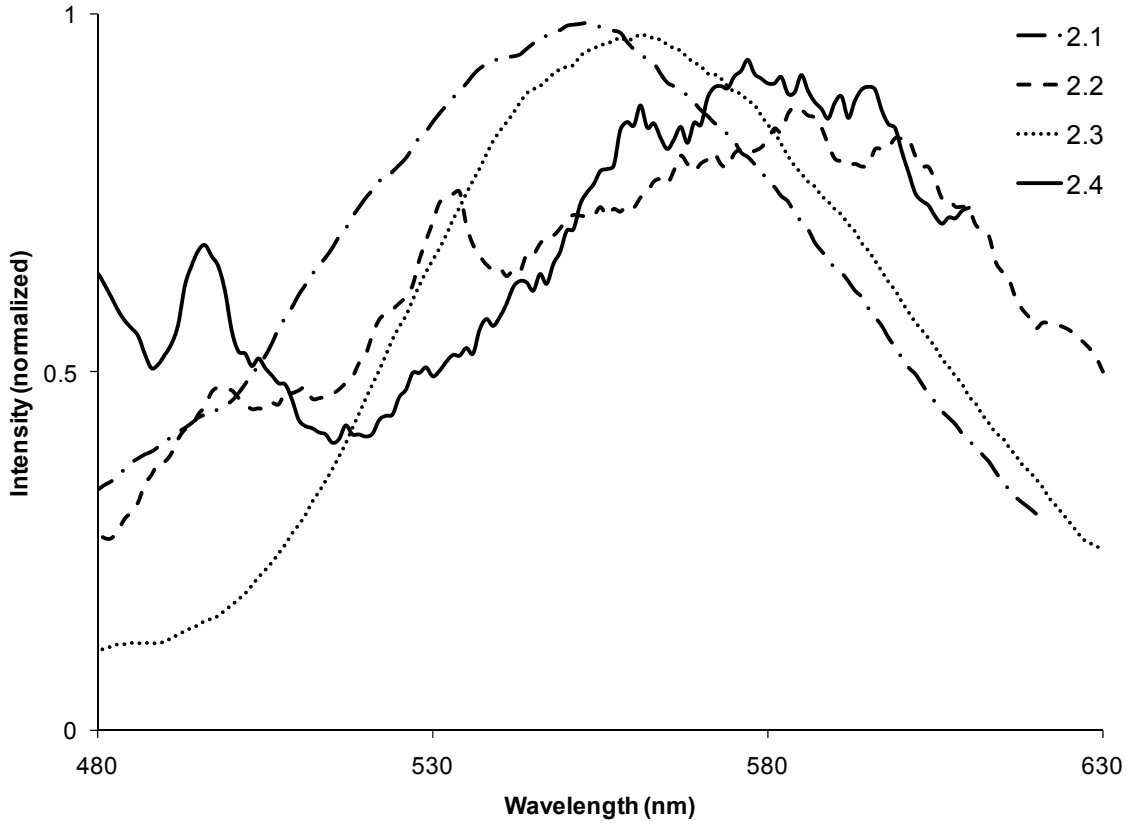

Figure 2.11 Emission spectra of **2.1**-**2.4** in CH_2Cl_2 at 77 K.

The emission energy appears to follow the same trend as the absorption energy, with complex **2.1** having the highest emission energy. The exception is complex **2.2**, which has emission energy similar to that of **2.4** in solution. This anomaly could be attributed to the fact that **2.2** is the least sterically crowded molecule, and hence the most susceptible to structural relaxation, resulting in a relatively low emission energy in solution.[29] The emission bands of **2.1**-**2.4** shift toward shorter wavelength in polar solvents such as DMF at 77 K as shown in Figure 2.12. For example, the emission

wavelength of **2.3** in CH_2Cl_2 is at 564 nm, which shifts to 540 nm in DMF. Interestingly, however, in THF, which is a slightly less polar solvent than CH_2Cl_2, the emission band of **2.3** also shifts to a shorter wavelength, 544 nm. The polarity of the solvent molecules appears not to be the only factor that is responsible for the emission energy shift.

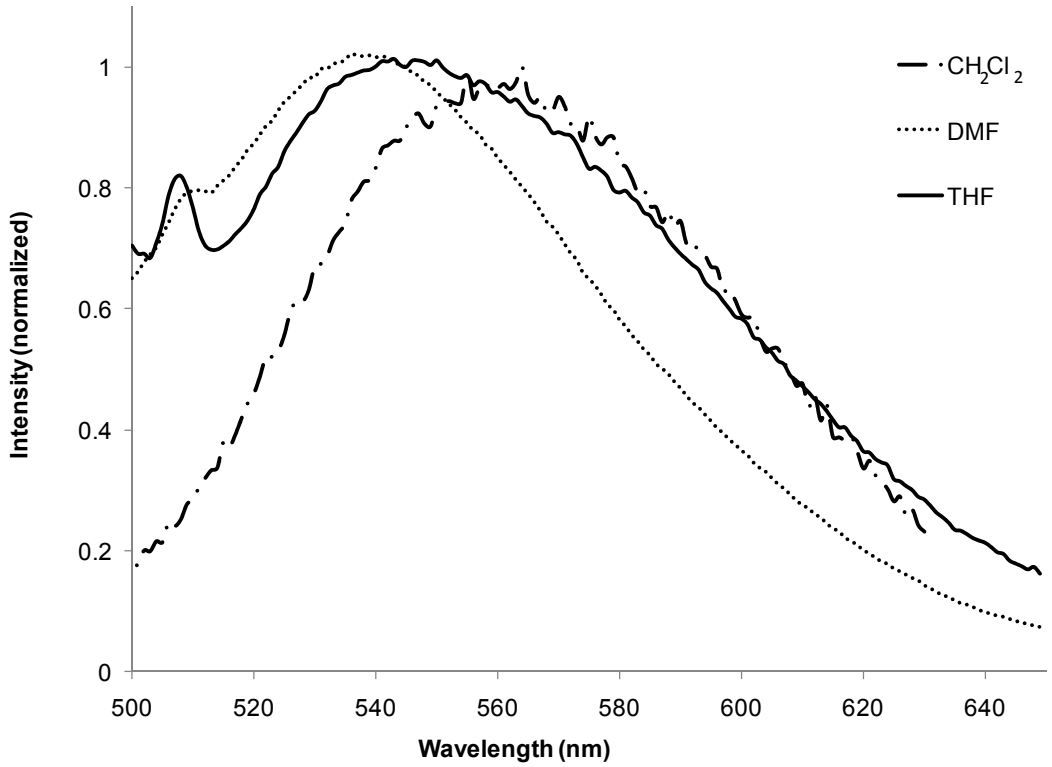

Figure 2.12 Emission of **2.3** in CH_2Cl_2, DMF and THF at 77 K.

Although complexes **2.1**-**2.4** are not emissive in solution at ambient temperature, they do emit when doped into PMMA polymer as shown by Figure 2.13. The emission peak in PMMA at ambient temperature is considerably blue shifted, compared to that at

77 K in CH_2Cl_2, which can be attributed to the increased contribution of emission from the singlet MLCT state and the pbb ligand's triplet emission (λ_{max} = 525 nm). The emission data for complexes **2.1-2.4** are provided in Table 2.3. Complex **2.4** is unique because it is a charge-neutral molecule and consistently displays a red-orange emission colour in solution and in PMMA (Figure 2.13). Compounds **2.1**-**2.4** do not emit as pure solids at ambient temperature, but the emission spectra of **2.1**-**2.4** as pure solids at 77 K are similar to those in PMMA matrix.

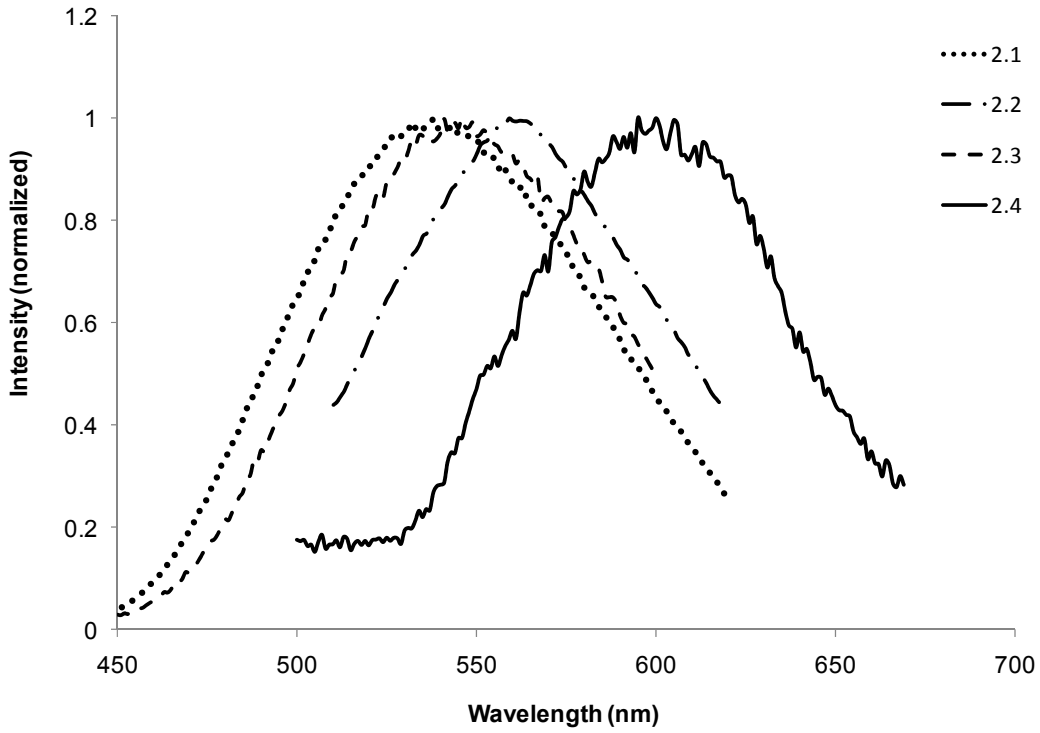

Figure 2.13 Emission spectra of **2.1**-**2.4** in PMMA films (20% wt) at rt.

The decay lifetimes at 77 K in frozen solution or in PMMA matrix were determined for all four complexes by using a time-resolved phosphorescence

spectrometer. When fitted with a single decay component, some deviation from the experimental data was observed for most of the complexes. As a result, two components were used in fitting the decay curve, producing a good fit. As shown in Table 2.3, complexes **2.1**-**2.4** display remarkably long decay lifetimes (the longer lifetime is the dominating component for all complexes). These long decay lifetimes confirmed that the observed MLCT emission is from the triplet state. The variation of the phosphine ligands appears to have no dramatic impact on the decay lifetime. The long decay lifetimes of **2.1**-**2.4** are in sharp contrast to those of Cu(I) complexes of phenanthroline and derivative ligands, which were reported to have much shorter decay life times (<50 μs).[11-13] It is likely that the partial involvement of the phosphine ligands in the charge-transfer process that leads to a partial ligand-to-ligand charge-transfer character in the lowest electronic transition might play a role in the exceptionally long decay lifetimes of **2.1**-**2.4**. The lack of emission by complexes **2.1**-**2.4** in solution at ambient temperature could be explained by their long decay lifetimes, which make them highly susceptible to solvent-induced thermal quenching. Attempts were made to measure the quantum yields of complexes **2.1**-**2.4** in PMMA by using integration sphere methods. The quantum yields of complexes **2.1**-**2.4** are included in Table 3. Unlike the Cu(I) phen or dmp complexes where the chelate phosphine ligands such as DPEphos were found to increase quantum efficiency, compared to PPh_3,[11, 12] the DPEphos complex **2.3** has a much lower quantum efficiency compared to the PPh_3 complex. In fact the simple PPh_3 has the highest emission efficiency which makes it a potential candidate for OLED applications.

2.4 Conclusion

The investigation of the four new Cu(I) complexes based on the pbb chromophore and four different ancillary phosphine ligands leads to the following conclusions: (1) Sterically, the DPPE ligand is the least demanding and PPh_3 is the most demanding, which results in considerable variations in P-Cu-P bond angles in the four complexes, but little impact on Cu-P and Cu-N bond lengths and the N-Cu-N bond angles. (2) Both steric and electronic properties of the phosphine ligands have an impact on the electronic properties of the copper complexes. For the neutral phosphine ligands PPh_3, DPEphos, and dppe, steric factors appear to play a key role in the variation of the electronic properties of complexes **2.1**-**2.3**. In contrast, for the anionic ligand DPPMB, electronic factors appear to be dominant, which results in complex **2.4** having the smallest HOMO-LUMO energy gap. (3) All four complexes display characteristic MLCT emissions with significant contributions from the phosphine ligands, which is clearly phosphorescent in nature, as evidenced by their exceptionally long decay lifetimes. The long decay lifetimes might hinder the use of the new complexes as phosphorescent emitters in OLEDs, but might be very desirable for using these molecules in photochemistry. (4) Among complexes **2.1**-**2.4**, **2.4** is a unique molecule because it displays a red colour and is a neutral molecule. In principle, compound **2.4** could be incorporated into OLEDs by a vacuum deposition process. However, its poor stability along with the long decay lifetime preclude its use in OLEDs. (5) The impact of the phosphine ligands, PPh_3, dppe, and DPEphos, on the electronic properties of the 2-(2'-pyridyl)benzimidazolyl-based Cu(I) complexes is parallel to that observed for the phenanthroline-based Cu(I) complexes. The

major difference between the two systems is the decay lifetime: the 2-(2'-pyridyl)benzimidazolyl-based complexes have a much longer decay lifetime than the phen-based Cu(I) complexes. The participation of the phosphine ligands in the charge-transfer process might be partially responsible for the observed long decay lifetimes of complexes **2.1**-**2.4**. Furthermore, unlike the phenanthroline-based Cu(I) complexes, where the chelate phosphine ligands such as DPEphos are known to substantially increase the emission quantum efficiency, compared to the PPh_3 ligand, the chelate phosphine ligands for the 2-(2'-pyridyl)benzimidazolyl-based Cu(I) complexes appear to dramatically decrease the emission quantum efficiency.

2.5 References

(1) Shen, Z.; Burrows, P. E.; Bulovic, V.; Borrest, S. R.; Thompson, M. *Science* **1997**, *276*, 2009.

(2) Baldo, M. A.; Lamansky, S.; Burrows, P.; Thompson, M. E. *Appl. Phys. Lett.* **1999**, *75*, 5.

(3) Kwong, R. C.; Sibley, S.; Dubovoy, T.; Baldo, M.; Forrest, S. R.; Thompson, M. E. *Chem. Mater.* **1999**, *11*, 3709.

(4) Adachi, C.; Baldo, M. A.; Forrest, S. R.; Thompson, M. E. *Appl. Phys. Lett.* **2000**, *77*, 904.

(5) Lamansky, S.; Djurovich, P.; Murphy, D.; Abdel-Razzaq, F.; Lee, H. E.; Adachi, C.; Burrows, P. E.; Forrest, S. R.; Thompson, M. E. *J. Am. Chem. Soc.* **2001**, *123*, 4304.

(6) Liu, Q. D.; Thorn, L.; Kozin, I.; Song, D.; Seward, C. *J. Chem. Soc. Dalton. Trans.* **2002**, 3234.

(7) Lu, W.; Mi, B. X.; Chan, M. C. W.; Hui, Z.; Zhu, N.; Lee, S. T.; Che, C. M. *Chem. Commun.* **2002**, 206.

(8) Rudmann, H.; Shimada, S.; Rubner, M. F. *J. Am. Chem. Soc.* **2002**, *124*, 4918.

(9) Bernhard, S.; Barron, J. A.; Houston, P. L.; Abruna, H. D.; Ruglovksy, J. L.; Gao, X.; Malliaras, G. G. *J. Am. Chem. Soc.* **2002**, *124*, 13624.

(10) Buda, M.; Kalyzuzhny, G.; Bard, A. *J. Am. Chem. Soc.* **2002**, *124*, 6090.

(11) Cuttell, D. G.; Kuang, S. M.; Fanwick, P. E.; McMillin, D. R.; Walton, R. A. *J. Am. Chem. Soc.* **2002**, *124*, 6.

(12) Kuang, S. M.; Cuttell, D. G.; McMillin, D. R.; Fanwick, P. E.; Walton, R. A. *Inorg. Chem.* **2002**, *41*, 3313.

(13) Zhang, Q.; Zhou, Q.; Cheng, Y.; Wang, L.; Ma, D.; Jing, X.; Wang, F. *Adv. Mater.* **2004**, *16*, 432.

(14) Jia, W. L.; Hu, Y. F.; Gao, J.; Wang, S. *Dalton Trans.* **2006**, 1721.

(15) Thomas, J. C.; Peters, J. C. *Polyhedron* **2004**, *23*, 2901.

(16) Kubas, G. J. *Inorg. Synth.* **1979**, *19*, 90.

(17) Diez, J.; Falagan, S.; Gamasa, P.; Gimeno, J. *Polyhedron* **1988**, *7*, 37.

(18) Thomas, J. C.; Peters, J. C. *J. Am. Chem. Soc.* **2003**, *125*, 8870.

(19) Thomas, J. C.; Peters, J. C. *Inorg. Chem.* **2003**, *42*, 5055.

(20) Thomas, J. C.; Peters, J. C. *J. Am. Chem. Soc.* **2001**, *123*, 5100.

(21) Kranenburg, M.; van der Burgt, Y. E.; Kamer, P. C. J.; van Leeuwen, P. W. N. M. *Organometallics* **1995**, *14*, 3081.

(22) Gaussian 03, Revision C.02, Frisch, M. J.; Trucks, G. W.; Schlegel, H. B.; Scuseria, G. E.; Robb, M. A.; Cheeseman, J. R.; Montgomery, Jr., J. A.; Vreven, T.; Kudin, K. N.; Burant, J. C.; Millam, J. M.; Iyengar, S. S.; Tomasi, J.; Barone, V.; Mennucci, B.; Cossi, M.; Scalmani, G.; Rega, N.; Petersson, G. A.; Nakatsuji, H.; Hada, M.; Ehara, M.; Toyota, K.; Fukuda, R.; Hasegawa, J.; Ishida, M.; Nakajima, T.; Honda, Y.; Kitao, O.; Nakai, H.; Klene, M.; Li, X.; Knox, J. E.; Hratchian, H. P.; Cross, J. B.; Bakken, V.; Adamo, C.; Jaramillo, J.; Gomperts, R.; Stratmann, R. E.; Yazyev, O.; Austin, A. J.; Cammi, R.; Pomelli, C.; Ochterski, J. W.; Ayala, P. Y.; Morokuma, K.; Voth, G. A.; Salvador, P.; Dannenberg, J. J.; Zakrzewski, V. G.; Dapprich, S.; Daniels, A. D.; Strain, M. C.; Farkas, O.; Malick, D. K.; Rabuck, A. D.; Raghavachari, K.; Foresman, J. B.; Ortiz, J. V.; Cui, Q.; Baboul, A. G.; Clifford, S.; Cioslowski, J.; Stefanov, B. B.; Liu, G.; Liashenko, A.; Piskorz, P.; Komaromi, I.; Martin, R. L.; Fox, D. J.; Keith, T.; Al-Laham, M. A.; Peng, C. Y.; Nanayakkara, A.; Challacombe, M.; Gill, P. M. W.; Johnson, B.; Chen, W.; Wong, M. W.; Gonzalez, C.; and Pople, J. A.; Gaussian, Inc., Wallingford CT, 2004.

(23) Palsson, L.; Monk, A. P. *Adv. Mater.* **2002**, *14,* 757.

(24) Bruker Analytical X-ray Systems **1999**, *5.10*.

(25) Liu, Q. D.; Jia, W. L.; Wang, S. *Inorg. Chem.* **2005**, *44*, 1332.

(26) Mankad, N. P.; Peters, J. C. *Chem. Commun.* **2008**, 1061.

(27) Kirchhoff, J. R.; McMillin, D. R.; Robinson, W. R.; Powell, D. R.; McKenzie, A. T.; Chen, S. *Inorg. Chem.* **1985**, *24*, 3928.

(28) Sakaki, S.; Mizutani, H.; Kase, Y.; Inokuchi, K.; Arai, T.; Hamada, T. *J. Chem Soc., Dalton Trans.* **1996**, 1909.

(29) Eggleston, M. K.; McMillin, D. R.; Koenig, K. S.; Pallenberg, A. J. *Inorg. Chem.* **1997**, *36*, 172.

Chapter 3

Phosphorescent Polynuclear Cu(I) Compounds Based on Linear and Star-Shaped 2-(2'-Pyridyl)benzimidazolyl Derivative Ligands

3.1 Introduction

Extensive research efforts have been centered on phosphorescent Cu(I) complexes based on phenanthroline and its derivative ligands because of their potential applications in photochemistry and organic light-emitting diodes.[1-10] Many Cu(I) complexes based on polypyridyl chelate ligands have also been investigated.[3-9] Except for the phenanthroline based Cu(I) complexes, phosphorescent Cu(I) compounds that are useful in electroluminescent (EL) devices remain scarce. The investigation focuses on new dinuclear and trinuclear Cu(I) complexes based on 2-(2'-pyridyl)benzimidazolyl aryl derivative ligands. In Chapter 2 it was shown that 2-(2'-pyridylbenzimidazolyl)benzene (pbb) Cu(I) complexes display MLCT based emission.

In Chapter 2 a series of complexes with varying ancillary phosphine ligands was presented and it was found that these complexes although displaying phosphorescent based emission were not suitable for efficient electroluminescent devices.[11] Stable red phosphorescent polynuclear Pt(II) complexes based on this class of ligands have previously been reported.[12] It has been demonstrated that one of the key factors to obtain stable OLEDs is the ability to form uniform films while depositing the layers of the OLED devices.[13] Starburst and long linear-shaped organic compounds with large conjugation systems have been found to often possess relatively high glass transition

temperature (*T*g) and very good film-forming properties.[14] The goal of the investigation is to determine if polynuclear 2-(2'-pyridyl)benzimidazolyl ligands shown in Figure 3.1 would display emission once they are bound to multiple Cu(I) centres (Figure 3.2). The photophysical properties of the mononuclear complexes presented in Chapter 2 are compared to the photophysical properties when several Cu(I) centres are coordinated to same ligand. The effect of the size and shape of the complexes on the photophysical and electroluminescent properties will be examined. The results of the investigation including syntheses, structural characterization, luminescent and electroluminescent properties of four new polynuclear Cu(I) complexes are presented herein.

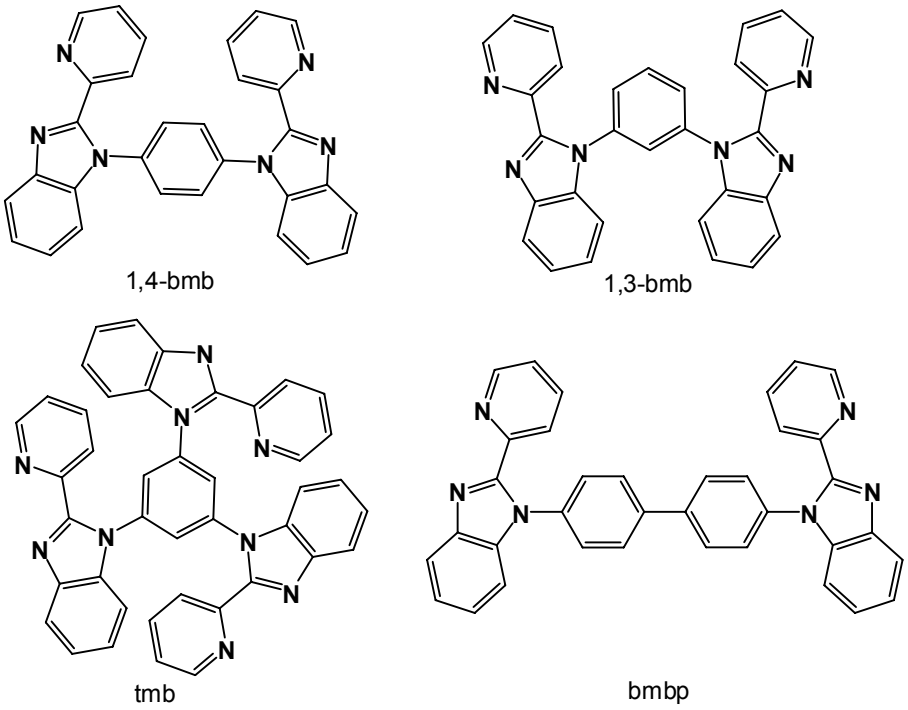

Figure 3.1 Structure of ligands 1,4-bmb, 1,3-bmb, tmb and bmpb used to make complexes **3.1-3.4** respectively.

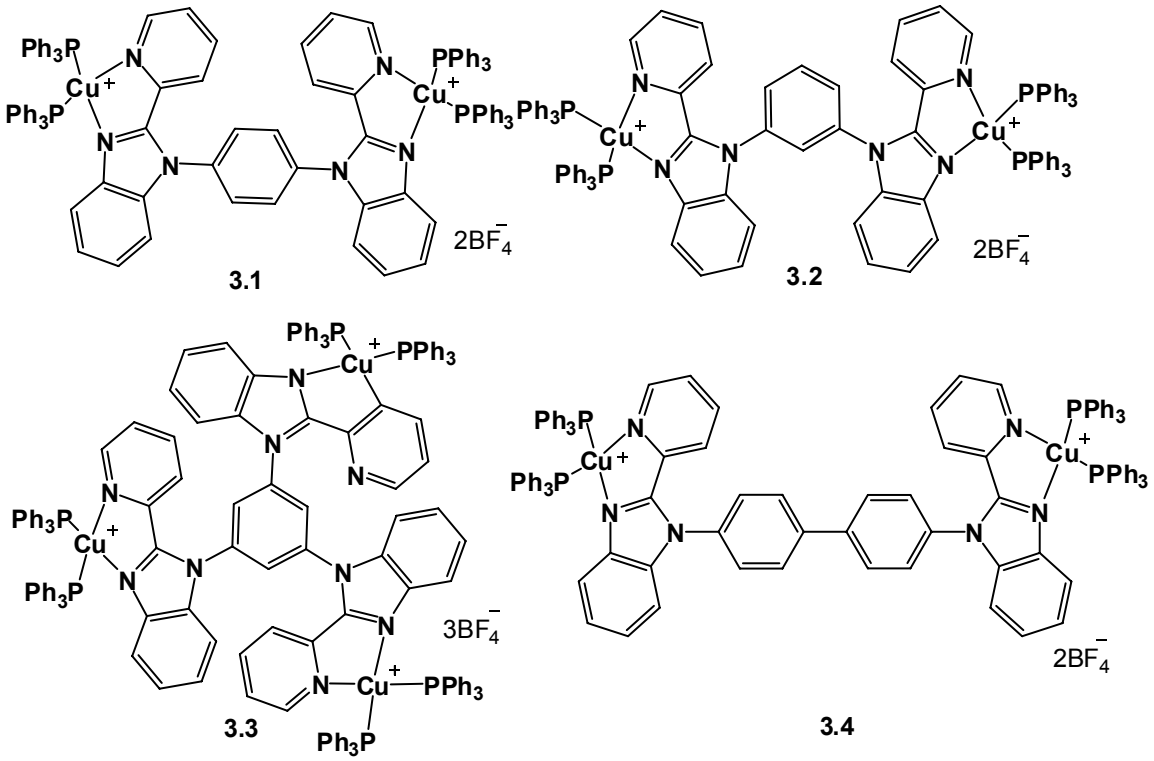

Figure 3.2 Diagram illustrating complexes **3.1-3.4**.

3.2 Experimental

3.2.1 General Considerations

All starting materials were purchased from Aldrich Chemical Company and used without further purification. Solvents were freshly distilled over appropriate drying reagents. All experiments were carried out under a dry nitrogen atmosphere using standard Schlenk techniques unless otherwise stated. Flash chromatography was carried out on silica (silica gel 60, 70-230 mesh). $^{13}P\{^{1}H\}$ NMR spectra were recorded on a Bruker Avance 400 or 500 MHz spectrometers as stated. Variable temperature ^{1}H NMR spectra for **3.1 –3.4** were recorded on a Bruker Avance 500 MHz spectrometer. Excitation and emission

spectra were recorded on a Photon Technologies International QuantaMaster Model C-60 spectrometer. Emission lifetime was measured on a Photon Technologies International Phosphorescent spectrometer, Time-master C-631F equipped with a Xenon flash lamp and digital emission photon multiplier tube using band pathway of 5 nm for excitation and 2 nm for emission. Elemental analyses were performed by Canadian Microanalytical Service Ltd., Delta, British Columbia, Canada. Cyclic voltammetry was performed using a BAS CV-50W analyzer with a scan rate of 500 mV s^{-1}. The electrolytic cell used was a conventional three compartments cell, in which a Pt working electrode, a Pt auxiliary electrode, and Ag/AgCl reference electrode were employed. The CV measurements were performed at room temperature using 0.10 M tetrabutylammonium hexafluorophosphate (TBAP) as the supporting electrolyte and CH_3CN as the solvent. The ferrocenium/ferrocene couple was used as the internal standard (E_o = 0.53 V). Copper(I) complexes, $[Cu(CH_3CN)_4][BF_4]$ and $[Cu(CH_3CN)_2(PPh_3)_2][BF_4]$ were synthesized based on literature procedures.[15, 16] The ligands, 1,4-bis[2-(2'-pyridyl)benzimidazolyl]benzene (1,4-bmb), 4,4'-bis[2-(2'-pyridyl)benzimidazolyl]biphenyl (bmbp) , 1,3,5-tris[2-(2'-pyridyl)benzimidazolyl]benzene (tmb) and 1,3-bis[2-(2'-pyridyl)benzimidazolyl]benzene (1,3-bmb) were synthesized using the methods reported previously by our group.[12]

3.2.2 Synthesis of $[Cu_2(1,4\text{-bmb})(PPh_3)_4][BF_4]_2$ (3.1)

A CH_2Cl_2 (8 mL) solution of $[Cu(CH_3CN)_2(PPh_3)_2]BF_4$ (0.222 g, 0.29 mmol) was mixed with a CH_2Cl_2 (5 mL) solution of 1,4-bmb (0.068 g, 0.15 mmol). The mixture was stirred for 2 h at room temperature. Then 2 mL of toluene was successfully layered upon

the solution. Slow evaporation of the solvents and diffusion of toluene into the CH_2Cl_2 layer afforded complex **3.1** as a yellow solid after 2 days (0.201 g, 74% yield). $^{31}P\{^1H\}$ NMR in CD_2Cl_2 (δ, ppm, 298 K): 3.14. ^1H NMR in CD_2Cl_2, 300 MHz (δ, ppm, 298 K): 8.42 (d, J = 5.0 Hz, 2H), 8.05 (br s, 2H), 7.77 (br s, 4H), 7.55 (br s, 4H), 7.48-7.39 (m, 20 H), 7.28-7.21 (m, 48H). Anal. Calcd. for $C_{102}H_{80}Cu_2B_2F_8N_6P_4 \cdot 0.5CH_2Cl_2$: C, 66.29; H, 4.37; N, 4.53. Found: C, 66.56; H, 4.42; N, 4.80.

3.2.3 Synthesis of $[Cu_2(1,3\text{-bmb})(PPh_3)_4][BF_4]_2$ (3.2)

A solution of 1,3-bmb (0.026 g, 0.055 mmol) in CH_2Cl_2 (5 mL) was mixed with a solution of $[Cu(CH_3CN)_2(PPh_3)_2]BF_4$ (0.082 g, 0.110 mol) in CH_2Cl_2 (5 mL) to produce a yellow solution that was layered with toluene and hexanes. Yellow crystals were obtained after 3 days (0.077 g, 76%). $^{31}P\{^1H\}$ NMR (CD_2Cl_2, δ, ppm, 298 K): 3.36. ^1H NMR in CD_2Cl_2, 300 MHz (δ, ppm, 298 K): 8.40 (br s, 2H), 8.26 (t, J = 8.0 Hz, 2H), 8.06 (br s, 2H), 7.83 (d, 8.0 Hz, 2H), 7.53-7.17 (m, 72H). Anal. Calcd for $C_{102}H_{80}B_2Cu_2F_8N_6P_4$: C, 67.52; H, 4.44; N, 4.63. Found: C, 67.84; H, 4.38; N, 4.84.

3.2.4 Synthesis of $[Cu_3(tmb)(PPh_3)_6][BF_4]_3$ (3.3)

A solution of tmb (0.025 g, 0.038 mmol) in CH_2Cl_2 (5 mL) was mixed with $[Cu(CH_3CN)_2(PPh_3)_2]BF_4$ (0.086 g, 0.114 mmol) dissolved in CH_2Cl_2 (5 mL) to produce a yellow solution. The solution was layered with toluene and hexanes. Yellow and orange crystals were obtained after 4 days (0.065 g, 62%). $^{31}P\{^1H\}$ NMR (CD_2Cl_2, δ, ppm, 298 K): 3.33. ^1H NMR in CD_2Cl_2, 300 MHz (δ, ppm, 298 K): 8.40 (br s, 3H), 7.92-7.7.76 (m, 3H), 7.73-7.58 (m, 6H), 7.53-7.39 (m, 6H), 7.30-7.10 (m, 99H). Anal. Calcd

for $C_{150}H_{117}B_3Cu_3F_{12}N_9P_6 \bullet CH_2Cl_2$: 65.54; H 4.30; N, 4.56. Found: C 65.15; H 4.57; N 4.82.

3.2.5 Synthesis of $[Cu_2(bmbp)(PPh_3)_4][BF_4]_2$ (3.4)

A CH_2Cl_2 (8 mL) solution of $[Cu(CH_3CN)_2(PPh_3)_2]BF_4$ (0.300 g, 0.40 mmol) was mixed with a $CHCl_3$ (10 mL) solution of bmbp (0.108 g, 0.20 mmol). Toluene was added. Slow evaporation of the solvents afforded complex **3.4** as yellow crystals after 3 days (0.103 g, 89% yield). $^{31}P\{^1H\}$ NMR (CD_2Cl_2, δ, ppm, 298 K): 3.18. ^1H NMR in CD_2Cl_2 (δ, ppm, 298 K): 8.38 (d, J = 4.8 Hz, 2H), 8.18 (d, J = 8.4 Hz, 4H), 7.83 (td, J = 8.0 Hz, J = 1.6 Hz, 2H), 7.56 (d, J = 8.4 Hz, 4H), 7.47-7.20 (m, 72H). Anal. Calcd for $C_{108}H_{84}B_2Cu_2F_8N_6P_4$: C, 68.61; H, 4.45; N, 4.45. Found: C, 68.35; H, 4.44; N, 4.48.

3.2.6 X-ray Crystallographic Analysis

Single crystals of compounds **3.2–3.4** were obtained from the mixed solvent solution of either toluene/CH_2Cl_2 or toluene/CH_2Cl_2/$CHCl_3$. Attempts to grow single crystals of compound **3.1** were unsuccessful. Crystals were mounted on glass fibres for data collection. Data were collected on a Siemens P4 single-crystal X-ray diffractometer with a Smart CCD-1000 detector and graphite-monochromated Mo Kα radiation, operating at 50 kV and 30 mA at 23 °C for **3.2** and at -93 ºC for **3.3** and **3.4**. No significant decay was observed for all samples. Data were processed on a PC using the Bruker SHELXTL software package (version 5.10)[17] and were corrected for Lorentz and polarization effects. Compound **3.2** belongs to the monoclinic space group *P2/c* while compounds **3.3** and **3.4** belong to the triclinic space group *P-1*. Solvent molecules were located in the crystal

lattice for all three compounds. For **3.2**, each molecule co-crystallizes with two toluene solvent molecules. For **3.3**, 2.5 CH_2Cl_2 and 0.5 toluene solvent molecules per molecule of **3.3** were located. For **3.4**, one toluene, four $CHCl_3$ and two CH_2Cl_2 solvent molecules co-crystallized with each molecule of **3.4**. All toluene solvent molecules in **3.2**–**3.4** are disordered and could not be fully modeled. The BF_4 anions in all compounds were also found to display disordering and were refined successfully. One of the phenyl groups on the PPh_3 ligands in **3.2** and **3.3** displays rotational disorder. One of the 2-(2'-pyridyl)benzimidazolyl units in **3.3** (the one that is bound to the Cu(3) atom) is disordered over two sites with 50% occupancy for each site. The disordering of this unit was modeled successfully. However, due to the disordering the Cu(3)–N bond lengths are not accurate. The biphenyl unit in **3.4** also displays disordering over two sites with 50% occupancy factor for each site. Most non-hydrogen atoms except the disordered ones in **3.2**–**3.4** were refined anisotropically. All hydrogen atoms except those on disordered carbon atoms were calculated, and their contributions in structural factor calculations were included. The crystallographic data are given in Table 3.1. Selected bond lengths and angles for complexes **3.2**–**3.4** are listed in Table 3.2.

3.2.7 Quantum Yield Measurements

The absolute photoluminescent quantum yields of all Cu(I) complexes doped in PMMA films (20% complex : 80% PMMA by weight) were measured at ambient temperature using a commercial fluorimeter in combination with an integration sphere according to the literature procedure.[18, 19]

3.2.8 Fabrication of Electroluminescent Devices

The EL device using compound **3.4** as the emitter was fabricated on an indium-tin-oxide (ITO) substrate, which was cleaned by an ultraviolet ozone cleaner immediately before use. The solution for spin-coating was made up of the $CHCl_3$ solution of PVK and compound **3.4** (80:20 wt%). This solution was spin-cast onto an ITO glass at 1500 rpm. The hole blocking layer F-TBB (1,3,5-tris(4'-fluorobiphenyl-4-yl)benzene) and the electron transport layer Alq_3 were deposited by vacuum. The cathode composed of LiF and Al was deposited on the substrate by conventional vapour vacuum deposition. The triple-layer device with the structure of ITO/PKV+ **3.4** (~60 nm)/F-TBB (15 nm)/Alq_3 (15 nm)/LiF (1.0 nm)/Al (15 nm) was fabricated. The active device area is 1.0 x 5.0 mm^2. The current/voltage characteristics were measured using a Keithley 238 current/voltage unit. The EL spectra and the luminance for the devices were measured by using a Photo Research-650 Spectra Colourimeter.

Table 3.1 Crystallographic Data for Compounds **3.2–3.4.**

	3.2	**3.3**	**3.4**
formula	$C_{116}H_{96}N_6P_4F_8B_2Cu_2$	$C_{156}H_{126}N_9F_{12}P_6B_3Cl_5Cu_3$	$C_{117}H_{100}N_6F_8B_2Cl_{16}P_4Cu_2$
fw	1998.57	2940.77	2629.77
space group	P2/c	P-1	P-1
a, Å	15.941(7)	13.444(4)	10.753(4)
b, Å	10.920(5)	17.235(6)	12.997(5)
c, Å	29.012(13)	30.922(10)	21.737(9)
α, deg	90.00	92.044	96.050(7)
β, deg	98.577(8)	101.857(6)	92.137(8)
γ, deg	90.00	96.359	100.115(7)
V, Å^3	4994(4)	6972(4)	2969(2)
Z	2	2	1
D_{calc}, gcm^{-3}	1.329	1.401	1.471
μ, cm^{-1}	5.58	6.91	8.37
$2\theta_{max}$, deg	56.86	56.72	56.68
no. of reflns measd	34315	42390	17180
no. of reflns used	11660	28402	11686
(R_{int})	(0.1080)	(0.0606)	(0.0335)
no. of params	604	1705	699
final *R* [I > 2σ(I)]			
R1[a]	0.0721	0.0991	0.0684
*w*R2[b]	0.1660	0.2168	0.1659
R (all data)			
R1[a]	0.2471	0.2400	0.1367
*w*R2[b]	0.2124	0.2692	0.1894
GOF on F^2	0.769	1.014	0.756

[a] $R1 = \Sigma[|F_o| - |F_c|]/\Sigma|F_o|$. [b] $wR2 = \{\Sigma[w(F_o^2 - F_c^2)]/ \Sigma(wF_o^2)\}^{1/2}$.
$\omega = 1/[\sigma^2(F_o^2) + (0.075P)^2]$, where $P = [\max.(F_o^2,0) + 2F_c^2]/3$.

Table 3.2 Selected bond lengths (Å) and angles (º) of **3.2-3.4**.

		3.2	
Cu(1)-N(2)	2.063(5)	N(2)-Cu(1)-N(1)	78.3(2)
Cu(1)-N(1)	2.176(5)	N(2)-Cu(1)-P(1)	106.70(14)
Cu(1)-P(1)	2.2505(18)	N(1)-Cu(1)-P(1)	116.36(14)
Cu(1)-P(2)	2.2564(19)	N(2)-Cu(1)-P(2)	115.86(13)
		N(1)-Cu(1)-P(2)	105.85(14)
		P(1)-Cu(1)-P(2)	124.66(7)
		3.3	
Cu(1)-N(1)	2.063(6)	N(1)-Cu(1)-N(2)	79.4(2)
Cu(1)-N(2)	2.155(6)	N(1)-Cu(1)-P(3)	112.46(17)
Cu(1)-P(3)	2.234(2)	N(2)-Cu(1)-P(3)	114.34(16)
Cu(1)-P(5)	2.256(2)	N(1)-Cu(1)-P(5)	105.14(17)
Cu(2)-N(4)	2.073(6)	N(2)-Cu(1)-P(5)	105.69(17)
Cu(2)-N(5)	2.124(6)	P(3)-Cu(1)-P(5)	128.68(8)
Cu(2)-P(6)	2.237(3)	N(4)-Cu(2)-N(5)	80.2(2)
Cu(2)-P(4)	2.252(2)	N(4)-Cu(2)-P(6)	116.85(19)
Cu(3)-N(7)	1.951(12)	N(5)-Cu(2)-P(6)	110.94(18)
Cu(3)-P(1)	2.238(3)	N(4)-Cu(2)-P(4)	102.99(18)
Cu(3)-P(2)	2.246(3)	N(5)-Cu(2)-P(4)	108.55(18)
Cu(3)-N(9A)	2.293(13)	P(6)-Cu(2)-P(4)	127.28(9)
P(2)-Cu(3)-N(9A)	101.7(3)	N(7A)-Cu(3)-P(1)	119.1(4)
P(1)-Cu(3)-P(2)	132.93(10)	N(7)-Cu(3)-P(1)	110.0(4)
N(7)-Cu(3)-N(9A)	76.7(5)	N(7A)-Cu(3)-P(2)	103.5(4)
P(1)-Cu(3)-N(9A)	104.5(3)	N(7)-Cu(3)-P(2)	113.7(4)
		3.4	
Cu(1)-N(1)	2.062(4)	N(1)-Cu(1)-P(1)	110.56(12)
Cu(1)-N(2)	2.104(5)	N(2)-Cu(1)-P(1)	110.75(12)
Cu(1)-P(1)	2.2466(15)	N(1)-Cu(1)-P(2)	112.86(12)
Cu(1)-P(2)	2.2530(17)	N(2)-Cu(1)-P(2)	106.81(12)
		P(1)-Cu(1)-P(2)	126.32(5)
		N(1)-Cu(1)-N(2)	79.55(17)

3.3 Results and discussion

3.3.1 Syntheses and Structures

The organic ligands used in this study are 1,4-bis[2-(2'-pyridyl)benzimidazolyl]benzene (1,4-bmb), 1,3-bis[2-(2'-pyridyl)benzimidazolyl]benzene (1,3-bmb), 1,3,5-tris[2-(2'-pyridyl)benzimidazolyl]benzene (tmb), and 4,4'-bis[2-(2'-pyridyl)benzimidazolyl]-benzenebiphenyl (bmbp), which were synthesized using an Ullmann condensation procedure reported recently by our group.[12] The structures of these four ligands are shown in Figure 3.2. These molecules have been found to be excellent chelate ligands for binding to Cu(I) ions. The reactions of these ligands with the stoichiometric amount of $[Cu(CH_3CN)_2(PPh_3)_2][BF_4]$ resulted in the isolation of the corresponding yellow crystalline Cu(I) complexes, $[Cu_2(1,4\text{-bmb})(PPh_3)_4][BF_4]_2$ (**3.1**), $[Cu_2(1,3\text{-bmb})(PPh_3)_4][BF_4]_2$ (**3.2**), $[Cu_3(tmb)(PPh_3)_6][BF_4]_3$ (**3.3**), and $[Cu_2(bmbp)(PPh_3)_4][BF_4]_2$ (**3.4**), respectively in good yields. Compounds **3.1** – **3.4** are stable in solution under air. For compounds **3.2** – **3.4**, single crystals that are suitable for X-ray experiments were obtained and their structures were therefore determined by single-crystal X-ray diffraction analysis.

3.3.2 Crystal Structures

3.3.2.1 Structure of **3.2**

The structure of **3.2** is shown in Figure 3.3 and Figure 3.4 with the BF^- removed for clarity. The Cu(I) ion has an approximately tetrahedral geometry with two terminal PPh_3 ligands and one 2-(2'-pyridyl)benzimidazolyl chelate. There is a distinct difference

between the two Cu–N bond lengths: the Cu(1)–N(1) (pyridyl) bond length (2.176(5) Å) is much longer than that of Cu(1)–N(2) (imidazolyl, 2.063(5) Å), indicating that the imidazolyl nitrogen atom is a stronger donor than that of the pyridyl as was reported for the pbb complexes **2.1-2.4** presented in Chapter 2.[11] The same trend was also observed for the structures of **3.3** and **3.4** (see Table 3.2). The 2-(2'-pyridyl)benzimidazolyl chelate plane is approximately perpendicular to the central benzene plane, due to steric interactions between the pyridyl *ortho* hydrogen atom and those of the central benzene ring. The Cu(1)–Cu(1A) separation distance is 9.82(1) Å.

Complex **3.2** possesses a crystallographically imposed C_2 symmetry. The C_2 symmetry is the consequence of the relative orientation of the two 2-(2'-pyridyl)benzimidazolyl groups with respect to the central benzene plane. In the crystal structure, these two units are oriented *anti* to each other (structure **B**, Figure 3.5). The other possible orientation is **A** where the two 2-(2'- pyridyl)benzimidazolyl groups have a *syn* arrangement and are related by a mirror plane symmetry. Although the crystal structure of **3.1** was not determined, similar *syn* and *anti* isomers as depicted in Figure 3.5 are also possible. In fact our group has observed that for Pt(II) complexes, $[(PtPh_2)_2$(1,3-bmb)] and $[(PtPh_2)_2$(1,4-bmb)], both *syn* and *anti* isomers coexist in solution at ambient temperature and they only interconvert at high temperature, which was attributed to the hindered rotation of the 2-(2'-pyridyl)benzimidazolyl chelate unit.[12]

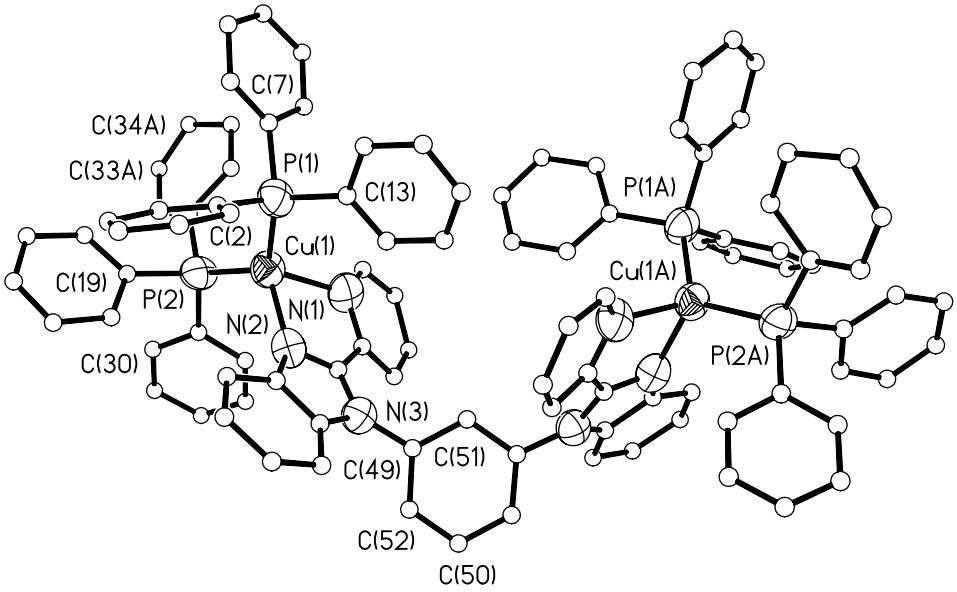

Figure 3.3 A diagram showing the structure of **3.2.** For clarity, all carbon atoms are shown as ideal spheres and all hydrogen atoms are removed**.** The BF_4^- anion is not shown.

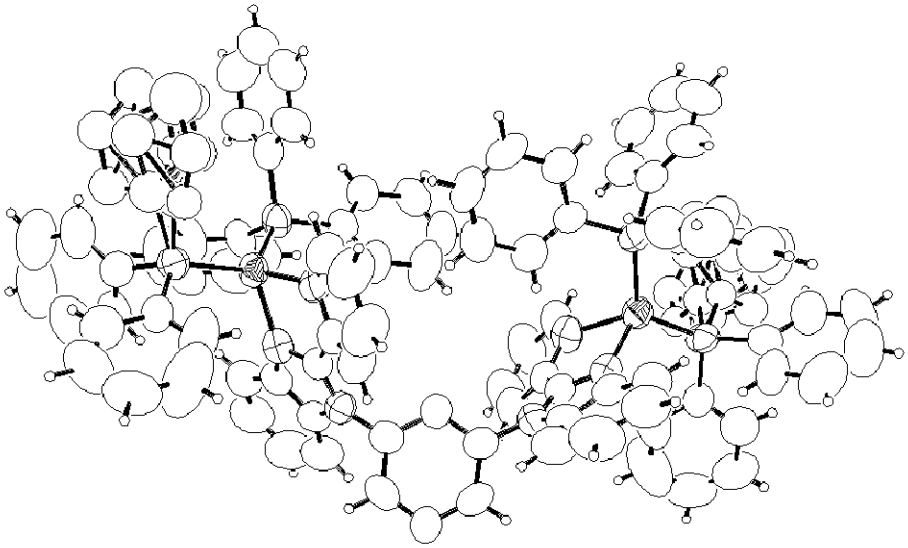

Figure 3.4 Structure of **3.2** shown with disordered ligands and all non-hydrogen atoms shown as thermal ellipsoids.

3.3.2.2 Structure of **3.3**

Compound **3.3** contains three Cu(I) centres each of which is chelated by a 2-(2'-pyridyl)benzimidazolyl unit, and further coordinated by two PPh_3 ligands, in the same manner as in **3.2** (Figure 3.6 and Figure 3.7). The Cu–Cu separation distances are Cu(1)–Cu(2) 12.75(1) Å, Cu(2)–Cu(3) 10.27(1) Å, Cu(1)–Cu(3) 10.25(1) Å, respectively, which are in average much longer than that in **3.2**, clearly caused by the increased congestion of ligands in **3.3**. One important feature is that the 2-(2'-pyridyl)benzimidazolyl unit chelated to the Cu(3) centre has two different orientations – **A** where it orients in the same direction as the other two 2-(2'-pyridyl)benzimidazolyl units and **B** where it orients in the opposite orientation with respect to the other two 2-(2'-pyridyl)benzimidazolyl units (see Figure 3.8). Crystallographically this is manifested as a two-site disordering. Based on the crystal structural data, it is believed that compound **3.3** exists as a 1:1 mixture of the isomers **A** and **B** in the solid state.

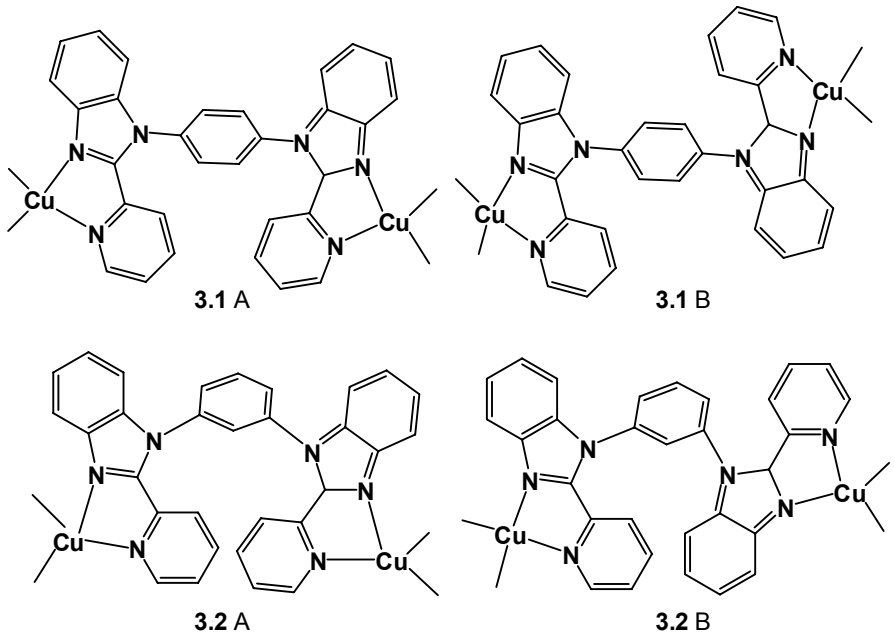

Figure 3.5 The two different orientations of **3.1** and **3.2**.

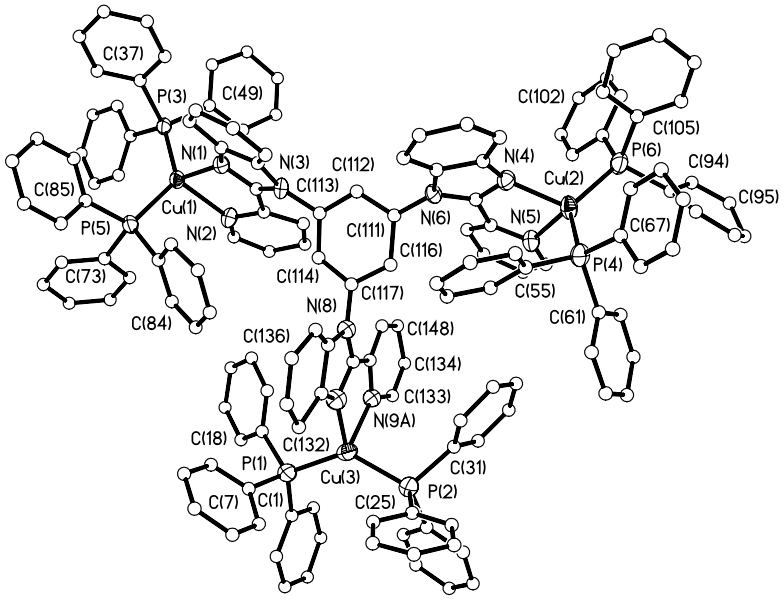

Figure 3.6 A diagram showing the structure of **3.3**. For clarity, only one orientation of the disordered groups is shown, hydrogen atoms are omitted, all carbon atoms are shown as ideal spheres. Anions are not shown.

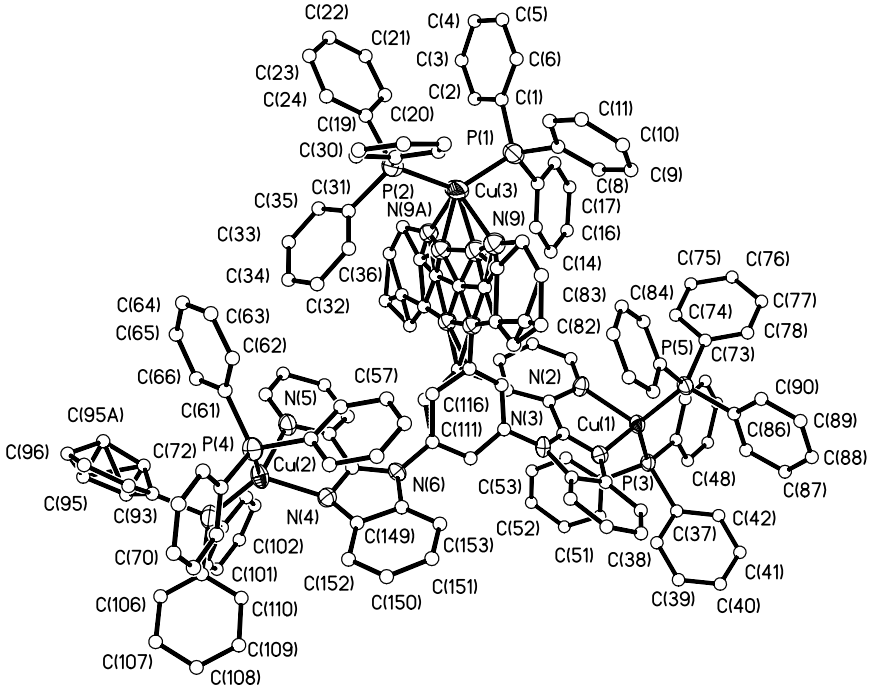

Figure 3.7 A diagram shown the disordering of the N(9a) 2-Py-benzimidazolyl ring bound to Cu(3), and the C(94) phenyl ring in **3.3.**

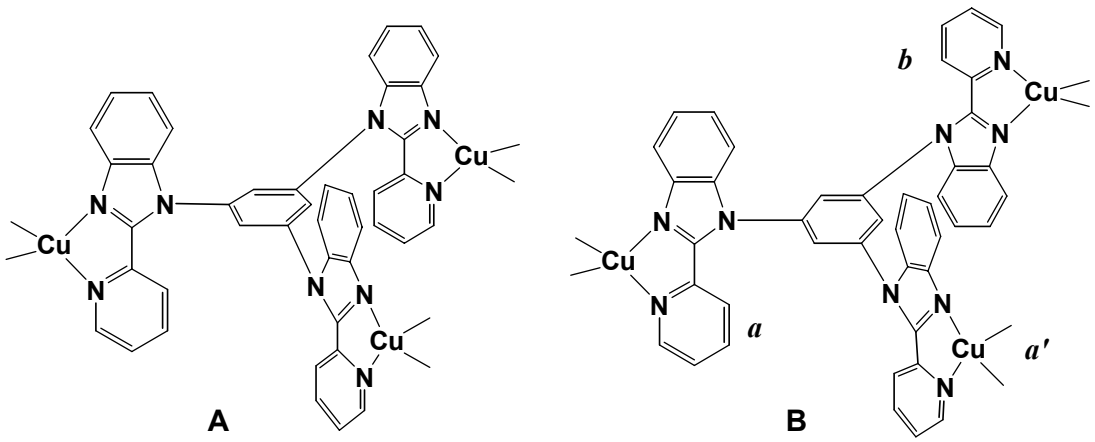

Figure 3.8 The isomers of **3.3.**

3.3.2.3 Structure of **3.4**

The structure of compound **3.4** is shown in Figure 3.9 and Figure 3.10. Complex **3.4** possesses a crystallographically imposed inversion centre symmetry that relates the two Cu(1) units. The coordination environment around the Cu(I) centre is similar to that observed in **3.2** and **3.3**. The Cu(1)–Cu(1A) separation distance, 17.32(2) Å, is much longer than those in **3.2** and **3.3**, due to the increased length of the biphenyl linker in the ligand. Because of the free rotation around the C–C bond in the biphenyl unit, no structural isomerism similar to those observed in **3.2** and **3.3** is present for **3.4**.

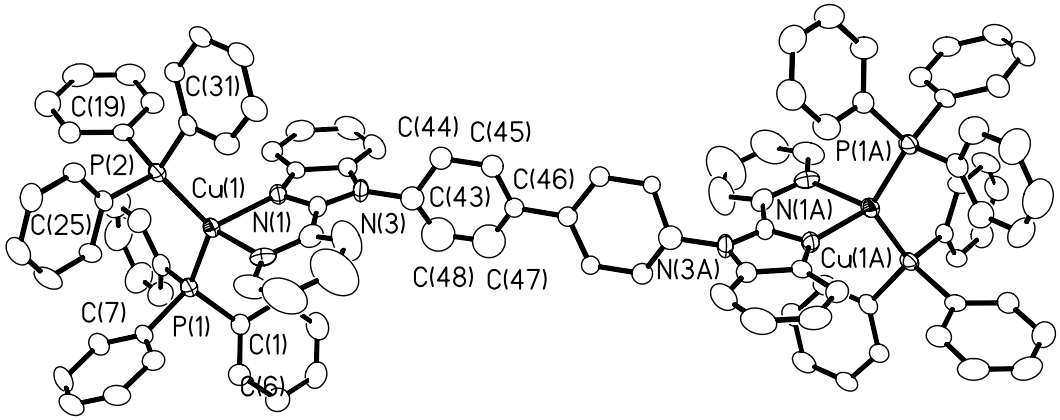

Figure 3.9 A diagram showing the structure of **3.4** with 50% thermal ellipsoids. For clarity, only one orientation of the disordered biphenyl group is shown and all hydrogen atoms are omitted. Anions are not shown.

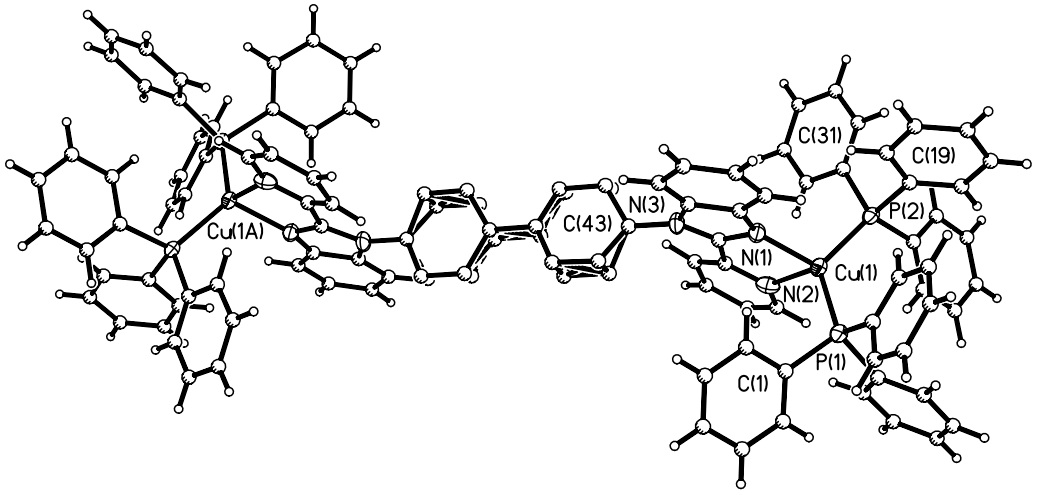

Figure 3.10 A diagram showing the disordered biphenyl linker of 3.4.

The N–Cu–N bite angles in compounds **3.2**–**3.4** range from 76.7(5) to 80.2(2)º and the P–Cu–P bond angles from 124.66(7) to 132.93(10)º these are similar to the values observed for the mononuclear triphenylphosphine complex **2.1** reported in Chapter 2. The average (78.8º) of the N–Cu–N angles is a few degrees smaller than that of $[Cu(phen)(PPh_3)_2]^+$ (80.90(9)º) and the average (127.9º) of the P–Cu–P bond angles is much larger than that of $[Cu(phen)(PPh_3)_2]^+$ (115.44(4)º),[20] which can be explained by the increased steric congestion in **3.2**–**3.4**. The torsion angles between the phenyl ring and the 2-(2`-pyridyl)benzimidazolyl moiety are 57.10° and 55.51° for **3.2** and **3.3** respectively, caused by the interactions of the ortho hydrogen atoms, analogous to the interactions reported in Chapter 2 for complexes **2.1-2.4**. Due to the disorder in the phenyl groups in **3.4** the torsion angle between the phenyl and 2-(2'-pyridyl)-

benzimidazolyl group could not be reliably calculated. No π-π interactions in the crystal lattice were observed for **3.2-3.4**.

3.3.3 Variable Temperature NMR

To determine if the *syn* and *anti* isomers **A** and **B** coexist in solution for **3.1** and **3.2**, variable temperature $^{31}P\{^{1}H\}$ NMR for both compounds were carried out (Figure 3.5). In the temperature range of 298 – 183 K, only one ^{31}P chemical shift was observed for both compounds (no free PPh_3 peak was observed), which could be explained by the existence of one isomer. It is also possible that the single ^{31}P chemical shifts is caused by the chemical shifts for the **A** and **B** isomers being very similar, hence indistinguishable. This ^{31}P peak appeared at near 3.0 ppm for all four complexes, similar to the chemical shift seen for complex **2.1.**[11] Variable temperature ^{1}H NMR experiments confirmed that both isomers exist in solution but are not distinguishable by ^{31}P NMR.

The variable ^{1}H NMR spectra for **3.1** are shown in Figure 3.11. At 298 K, one set of broad chemical shifts were observed for the 2-(2'-pyridyl)benzimidazolyl unit of the complex. As the temperature was lowered, two distinct sets of chemical shifts with ~1:1 ratio were observed, which supports the coexistence of the **A** and **B** isomers in solution. The **A** and **B** isomers undergo a dynamic exchange at temperatures above 203 K. The activation energy of this exchange process for **3.1** was estimated[21] to be ~61 kJ mol^{-1} by using the two chemical shifts at the 7.9-8.1 ppm region and the coalescence temperature of 298 K. Below this temperature the exchange between these isomers is greatly hindered. However, above 298 K rotation of the 2-(2'-pyridyl)benzimidazolyl group

with respect to the central phenyl linker causes slow exchange of the isomers and broad peaks in the NMR. Variable temperature ^{1}H NMR experiments also confirmed the coexistence of isomers **A** and **B** in solution for **3.2** with a similar activation energy barrier, ~62 kJ mol^{-1} (Figure 3.12).

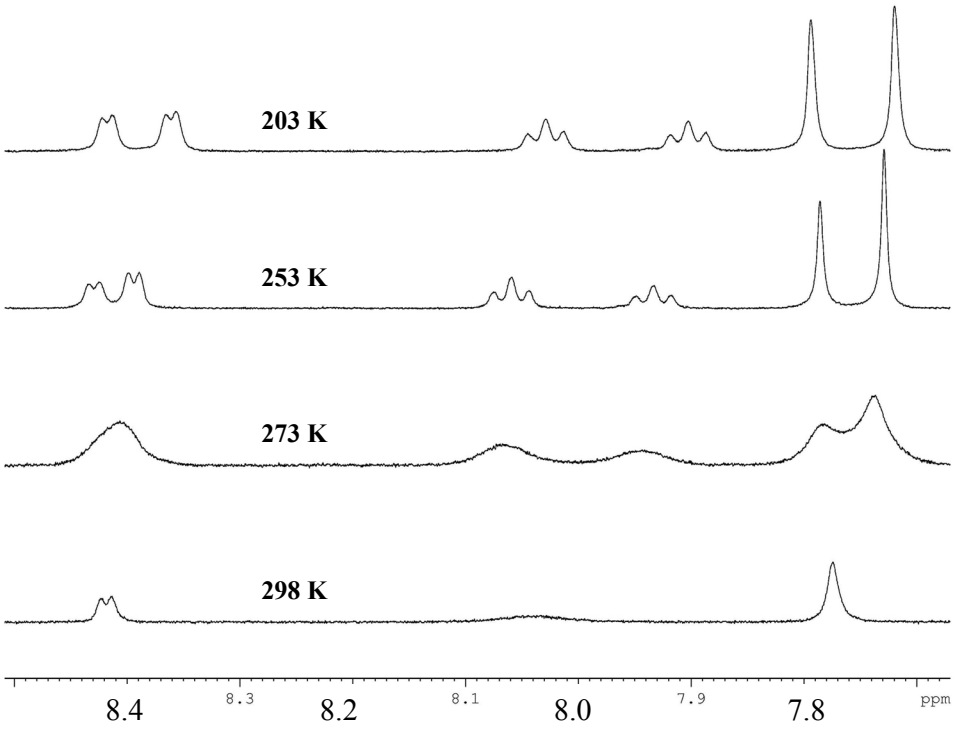

Figure 3.11 Variable temperature ^{1}H NMR spectra for **3.1** showing part of the aromatic region.

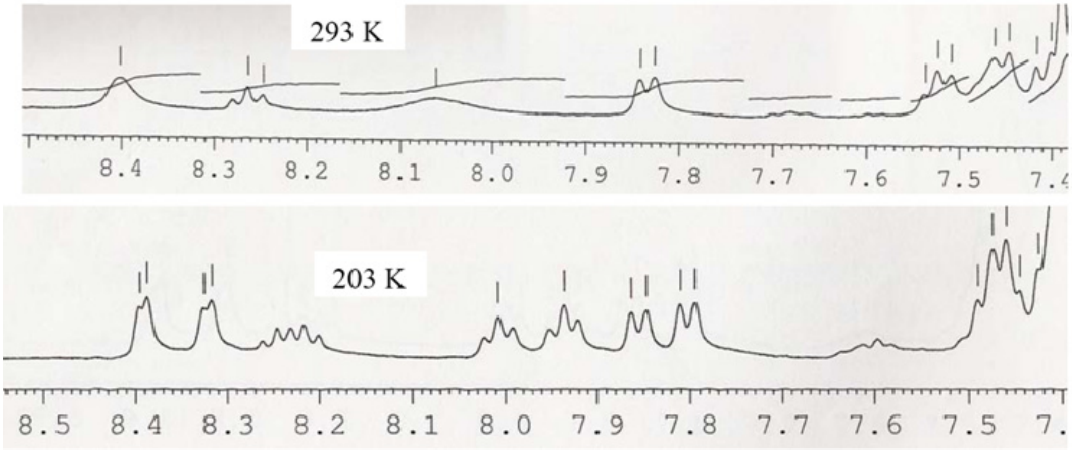

Figure 3.12 ^{1}H NMR spectra of compound **3.2** in CD_2Cl_2 showing part of the aromatic region at 293 K and 203 K.

^{1}H NMR study indicated that the two isomers of **3.3** coexist in solution and undergo inter-conversion at ambient temperature, which is consistent with the behaviour of **3.1** and **3.2**. Due to the complexity of the ^{1}H NMR spectra of **3.3**, it was not possible to estimate the activation energy (Figure 3.13). Similar isomerisation was also reported for the analogous Pt(II) compound $(PtPh_2)_3$(tmb).[12]

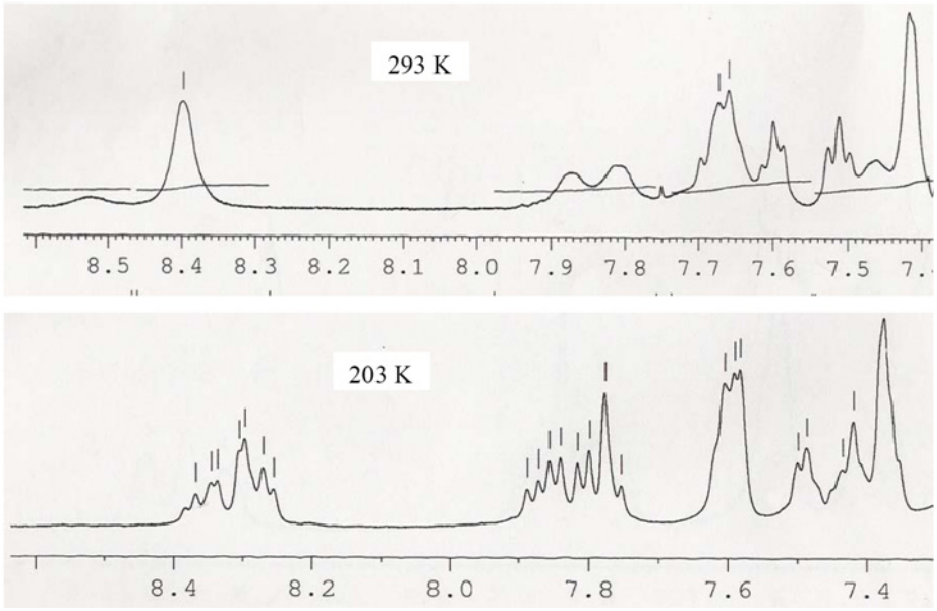

Figure 3.13 ^{1}H NMR spectra of **3.3** in CD_2Cl_2 showing part of the aromatic region at 293 K and 203 K.

3.3.4 UV-Vis Absorption Spectra

The UV-Vis absorption spectra of the free ligands 1,4-bmb, bmbp, 1,3-bmb, and tmb are similar with two absorption bands with $\lambda_{max} \approx 230$ and 300 nm, attributed to the $\pi \rightarrow \pi^*$ transition centered on the 2-(2'-pyridyl)benzimidazolyl units.[12] An overlay of the absorption of the ligand bmp and complex **3.1** is shown in Figure 3.14. In CH_2Cl_2, the absorption spectra of complexes **3.1 –3.4** have similar features as the ligands (Figure 3.16). However, in addition to the high energy absorption bands, all complexes have a weak and broad low energy shoulder band in the 350 – 450 nm region, which accounts for the yellow colour of the complexes. This low energy transition band resembles the MLCT band observed in $[Cu(phen)(PPh_3)_2]BF_4$[2] and more closely, the absorption spectra

seen from complex **2.1**. It is therefore attributed to MLCT transfer transitions involving the *N*, *N*-chelate ligand and the Cu(I) ion. The MLCT band of **3.1** – **3.4** shifts toward a shorter wavelength in the polar solvent CH_3CN as shown by Figure 3.15, which is consistent with the behaviour of complexes **2.1-2.4** as well as reported Cu(I) phenanthroline complexes.[1, 2] supporting the assignment of this transition to a charge transfer.

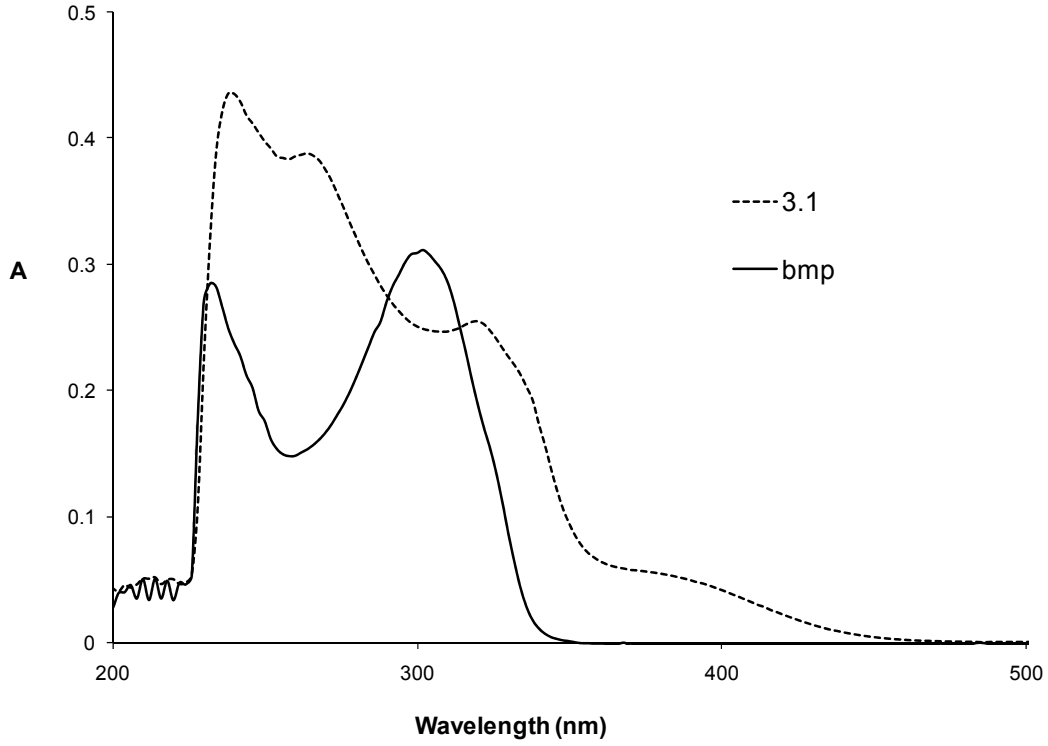

Figure 3.14 UV-Vis spectra of the ligand bmp its Cu(I) complex **3.1** in CH_2Cl_2 at rt.

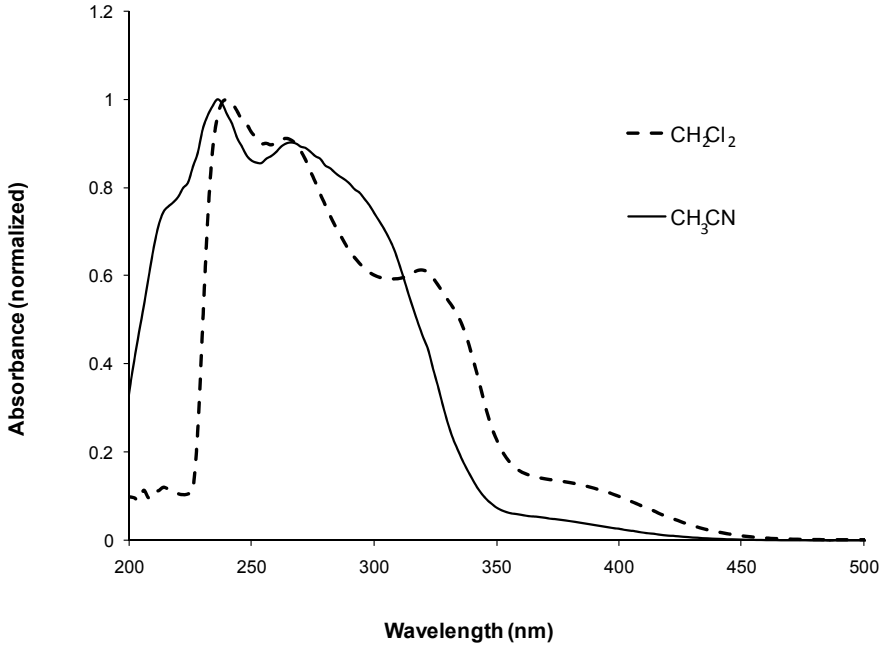

Figure 3.15 The UV-Vis spectra of **3.1** in CH_2Cl_2 and CH_3CN recorded at the same concentration at rt.

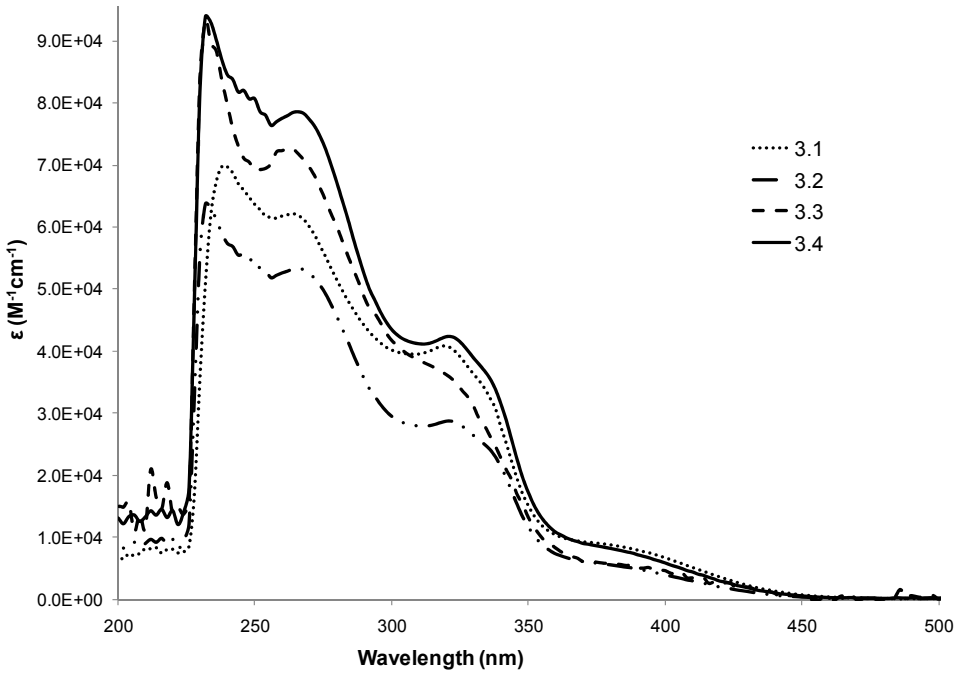

Figure 3.16 Absorption spectra of **3.1-3.4** in CH_2Cl_2.

3.3.5 Electrochemical Properties

The redox properties of the complexes were examined by cyclic voltammetry in CH_3CN solution. Complexes **3.1**–**3.4** display a broad and irreversible oxidation peak with the peak height at 1.63 V (**3.1**), 1.67 V (**3.2**), 1.79 (**3.3**), and 1.71 V (**3.4**), respectively, as an example, the scan of **3.3** is shown in Figure 3.17. A poorly resolved shoulder peak is also observed for **3.1** (at ~1.35 V) and for **3.4** (at ~1.45 V). The broad oxidation peak of the complex likely involves multiple electron transfer originating from the chelate ligand and the Cu(I) centre. The electrochemical behaviour of **3.1**–**3.4** resembles that of $[Cu(phen)(PPh_3)_2]BF_4$ reported by McMillin and coworkers as irreversible oxidation peak was observed.[1, 2] However, the oxidation potential of the $[Cu(phen)(PPh_3)_2][BF_4]$ complex (+1.35 V) is much lower than those observed for **3.1**–**3.4**, which indicates that the HOMO level of complexes **3.1–3.4** is much deeper than that of $[Cu(phen)(PPh_3)_2]BF_4$.[2] Furthermore, the electrochemical data appears to support that the HOMO level of the complexes has contributions from both ligand and the Cu(I) centre. A reversible reduction peak at ~ -2.0 V was observed for all four complexes which can be attributed to the reduction of the chelate ligand.

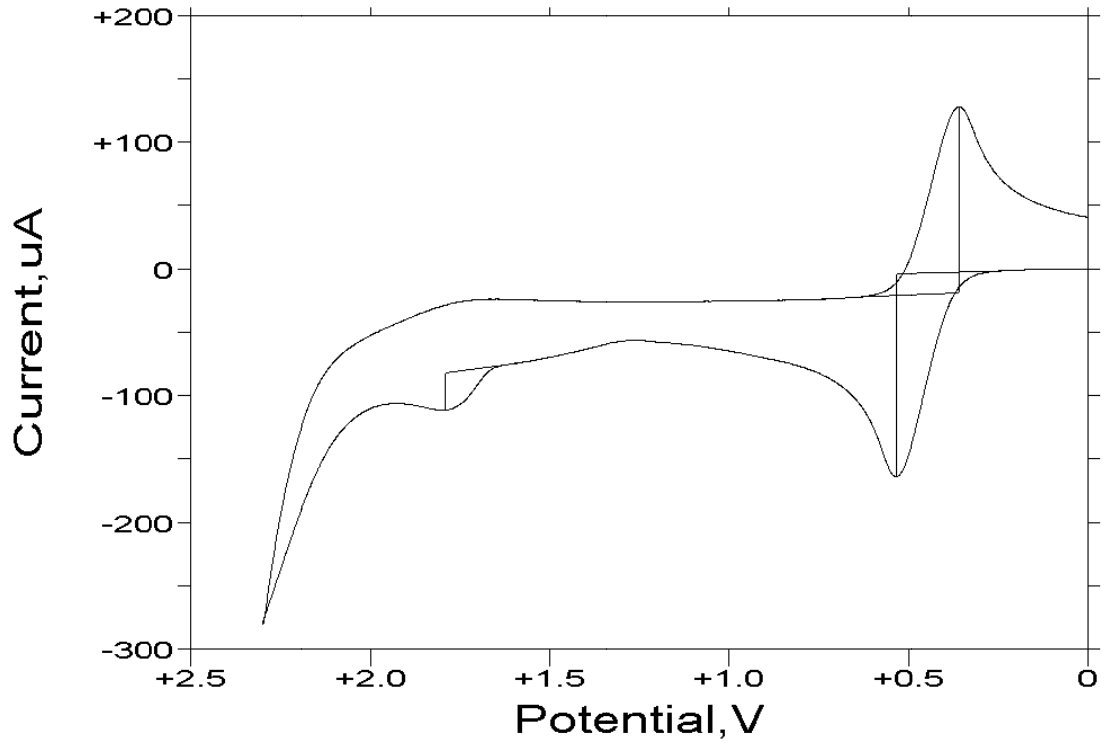

Figure 3.17 CV scan of **3.3** showing the oxidation curve, measured in CH_3CN with a ferrocene standard.

3.3.6 Luminescence

The luminescent properties of the complexes were examined. When irradiated by UV light, the free ligands emit a weak purple/blue colour with $\lambda_{max} \approx 365–415$ nm in CH_2Cl_2 solution at ambient temperature, which were assigned to fluorescent emissions originating from a ligand centered $\pi \rightarrow \pi^*$ transition.[12] These are similar to the emission of the free ligand from Chapter 2 (pbb) with $\lambda_{max}= 380$ nm. At 77 K, a broad phosphorescent emission band for all free ligands in the 400–650 nm region with $\lambda_{max} \approx 500$ nm in CH_2Cl_2 was observed. The decay lifetime of the phosphorescent emission of

the free ligands was found to be in the range of 7.0(1) to 13.2(1) μs. In contrast to the behaviour of the free ligands, complexes **3.1** and **3.4** display a weak yellow-orange emission in solution such as THF and CH_2Cl_2 while **3.2** and **3.3** do not have any detectable emission in solution at ambient temperature. The spectrum of **3.4** in CH_2Cl_2 is shown (Figure 3.18). When doped into a polymer matrix such as PVK (polyvinyl carbazole) or PMMA(Poly(methyl methacrylate)), these compounds display fairly bright yellow orange luminescence when irradiated by UV light at ambient temperature. The PMMA film emission energy of **3.1** – **3.4** at ambient temperature is similar with the λ_{max} at 535 – 550 nm as shown in Figure 3.19. At 77 K, there is a 10–20 nm red shift in emission energy for the PMMA film (Figure 3.19). The emission spectra of **3.1**–**3.4** in CH_2Cl_2 at 77 K resemble those of the PMMA film (Figure 3.20). Using an integration sphere, the absolute emission quantum yield of complexes **3.1**–**3.4** (doped in PMMA, 20:80% by weight) was measured to be 11%, 17%, 12%, and 15%, respectively, which are comparable to that of $[Cu(phen)(PPh_3)_2][BF_4]$ (14%).[6] One thing that was observed is that the phosphorescent emission band of the free ligands only partially overlaps with the MLCT absorption band of the metal complexes, which may explain the relatively low quantum efficiency of complexes **3.1**–**3.4**. The decay lifetimes of complexes **3.1**–**3.4** at 77 K in CH_2Cl_2 and in PMMA were determined by using a time-resolved phosphorescent spectrometer. Most the decay curves are fitted well with a single component (~200 μs). For those that displayed a small deviation from the single component fit, two components were used, which generated a long decay lifetime (the dominating one) and a relatively

fast decay lifetime. The long decay lifetime displayed by the Cu(I) complexes, characteristic of triplet state emission, is much longer than that of $[Cu(phen)(PPh_3)_2][BF_4]$,[1, 2, 10] which may hinder their use as emitters in EL devices. The UV-Vis absorption and luminescent data are given in Table 3.3.

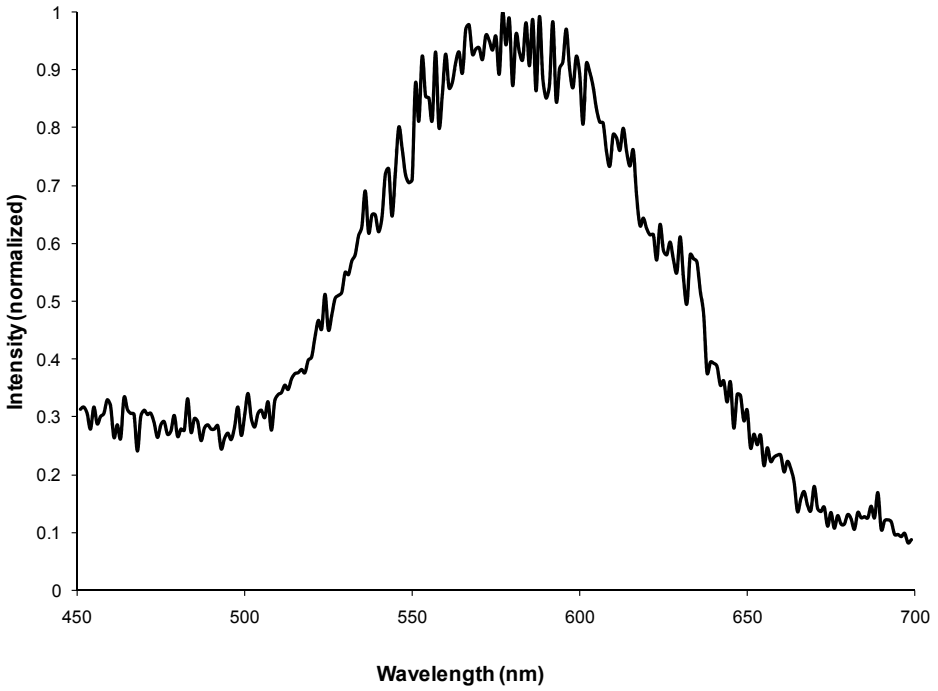

Figure 3.18 Solution emission of **3.4** in CH_2Cl_2 at rt.

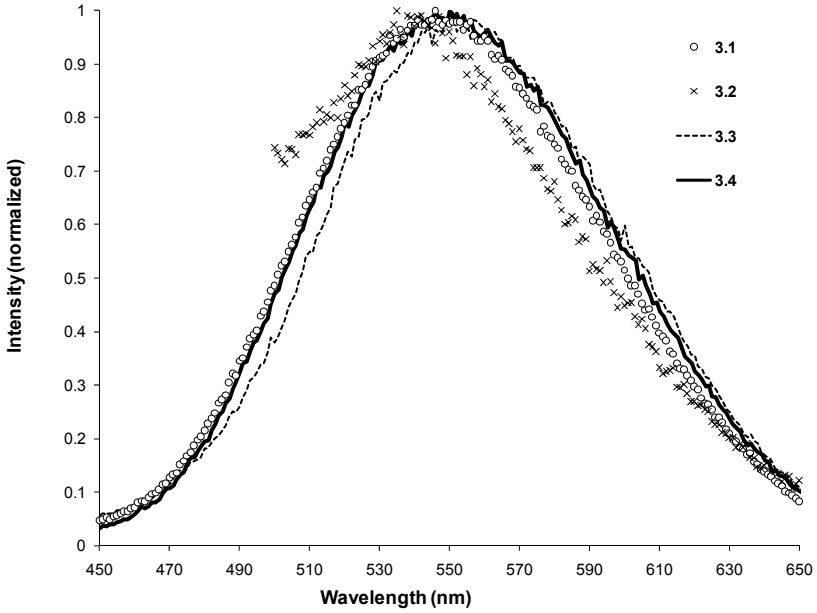

Figure 3.19 Emission spectra of **3.1-3.4** doped 20% wt in PMMA measured at rt.

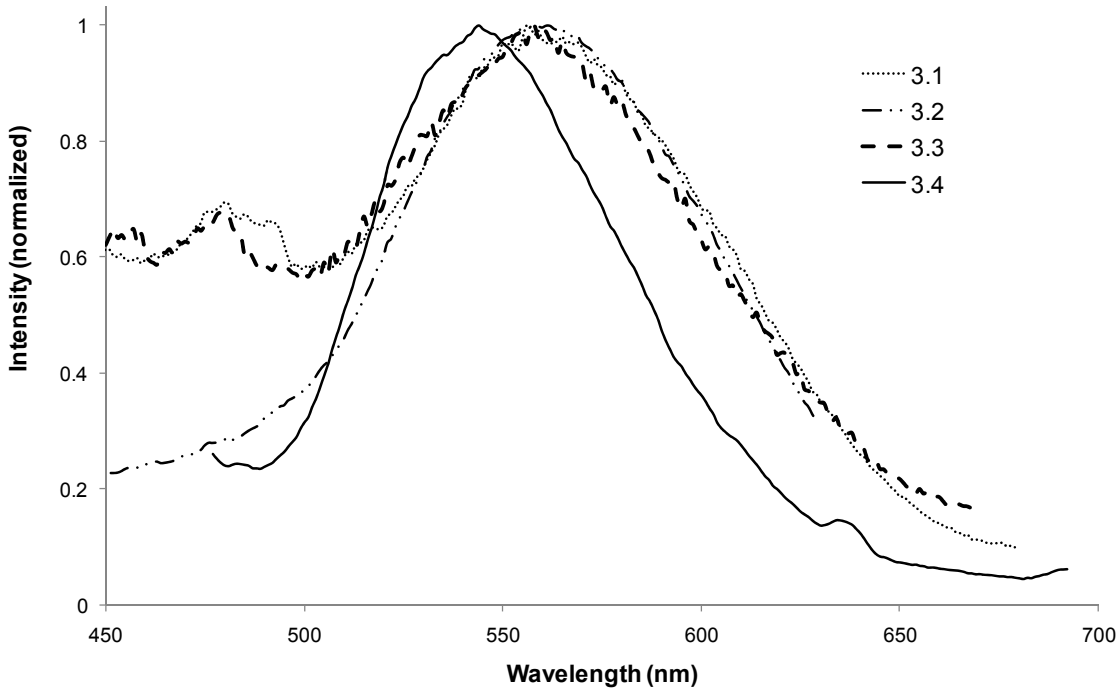

Figure 3.20 Emission of complex **3.1-3.4** in frozen CH_2Cl_2 at 77 K.

3.3.7 Electroluminescent device of 3.4

Compound **3.4** was selected as a representative example for the investigation of electroluminescent properties of the Cu(I) complexes because of its relatively high solubility, good film forming properties with PMMA, and its relatively short decay lifetime and high quantum efficiency in PMMA, compared to compounds **3.1**–**3.3**. The electroluminescent device was fabricated by spin-coating the compound **3.4**:PVK blend (20:80% by weight) in CH_2Cl_2 on the ITO substrate. The choice of PVK as the host material is based on the fact that PVK is an excellent hole transport molecule and its emission band is near 400 nm, that overlaps with the MLCT absorption band of complex **3.4**.[21] A hole blocking layer F-TBB to prevent the exciton formation within the Alq_3 layer (F-TBB = 1,3,5-tris(4'-fluorobiphenyl-4-yl)benzene, 15 nm) was deposited on top of the **3.4**:PVK layer by vacuum deposition. The electron transport layer Alq_3 (15 nm) was also deposited on top of the F-TBB layer by vacuum. Finally the cathode layer LiF (1 nm) and Al (15 nm) was deposited on top of the organic layers by thermal evaporation. The device produced an orange emission which matches very well with the PL spectrum of the **3.4**:PVK blend film (λ_{max} = 580 nm), as shown in Figure 3.21. No PVK or Alq_3 emission was observed. However, as shown by the luminance vs voltage (*L*–*V*) and the current efficiency–*V* data in Figure 3.22, the EL device of **3.4** is not bright and the efficiency is low. The long decay lifetime of the triplet state emission and the relatively low photoluminescent quantum efficiency of compound **3.4** may be partially responsible for the low EL efficiency of the device. Devices fabricated with $[Cu(dnpb)(DPEphos)]^+$

(dnpb = 2,9-di-*n*-butyl=1,10-phenanthroline and DPEphos = bis[2-(diphenylphosphino)phenyl]ether) as the emitting layer had a current efficiency of 10.5 cd/A and a peak brightness of 1663 cd/m^2.[10] This is almost thirty times brighter and substantially more efficient. The exceptionally long decay lifetime of complexes **3.1**–**3.4** is clearly associated with the 2-(2'-pyridyl)benzimidazolyl unit. Therefore, in order to dramatically improve the performance of the EL devices, further chemical modifications on the chelate ligands are necessary.

Table 3.3 Absorption and luminescent data for **3.1-3.4.**

Compd	Absorp.,[a] nm λ_{max} (ε, $M^{-1}cm^{-1}$)	Em., $\lambda_{max,}$ nm			Φ^b	τ (μs)	
		In CH_2Cl_2[a] 77K	In PMMA 77K[b]	In PMMA rt[b]		In CH_2Cl_2 77K	In PMMA 77K
3.1	240 (69,694), 264 (61,156), 320 (40,851), 380 (8,394)	557	556	546	11	211(1)	196(2)
3.2	234 (63,104), 264 (43,878), 320 (27,730), 386 (4,668)	561	556	535	17	99(4), 279(5)	112(10), 349(17)
3.3	232 (93,029), 262 (72,418), 312 (38,016), 388 (5,567)	558	570	547	12	241(1)	263.4(7)
3.4	232 (93,813), 266 (78,507), 322 (42,322), 380 (8,271)	561	563	550	15	74(5), 220(7)	188(1)

[a] [c] = 10^{-5} M [b] 20 wt % in PMMA.

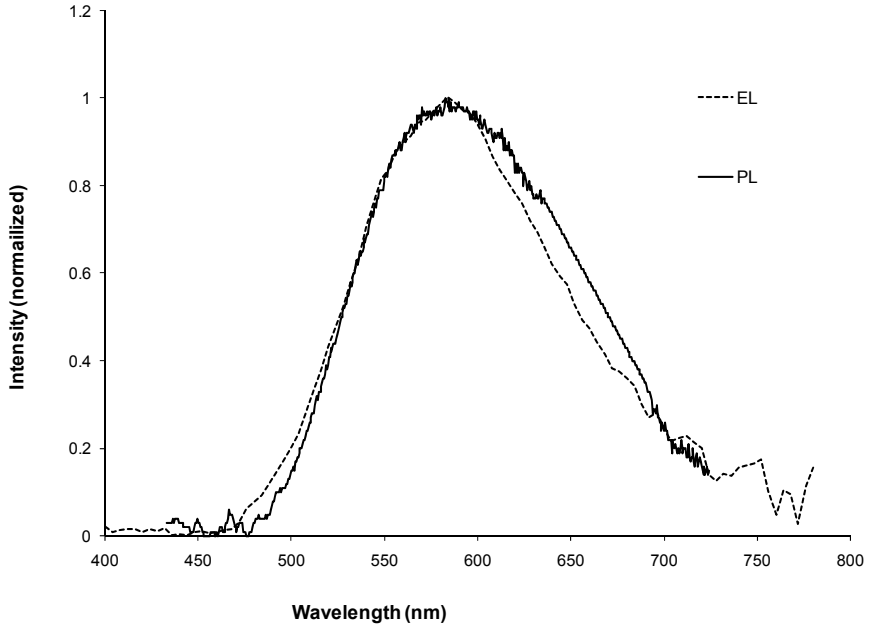

Figure 3.21 The photoluminescence spectrum of **3.4** in PVK and the electroluminescent spectrum of the device.

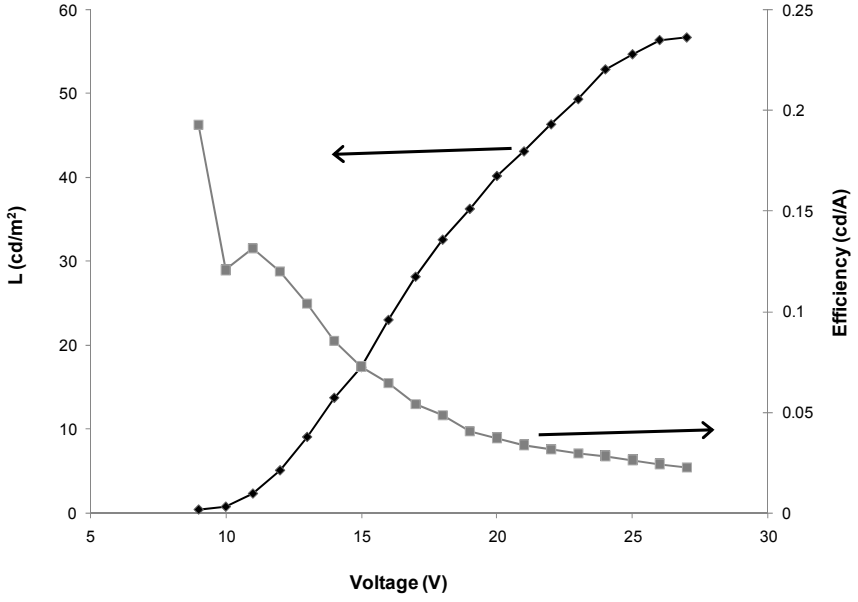

Figure 3.22 The luminance and current efficiency vs. voltage characteristics of the EL device for **3.4**.

3.3.8 Mononuclear Complex versus Dinuclear Complex

The coordination environment of complex **3.4** is essentially identical to that of the mononuclear complex **2.1** from Chapter 2. In fact, compound **2.1** can be considered as one-half of the dinuclear Cu(I) compound **3.4**. Hence, compound **2.1** and the dinuclear compound **3.4** provide an opportunity to compare the difference between mononuclear copper(I) complexes and the corresponding dinuclear copper(I) complexes. In terms of emission energy, there is very little difference between the mononuclear complex **2.1** and the dinuclear compound **3.4**. In addition, the two compounds have similar emission quantum efficiencies (13% for **2.1** and 15% for **3.4**) in PMMA. This is not entirely surprising, as there is no evidence for electronic communication between the two Cu(I) centres in **3.4**, which is mostly due to the orthogonal arrangement between the central biphenyl unit and the 2-(2'-pyridyl)benzimidazolyl chelating groups. The major difference between **2.1** and **3.4** is the decay lifetime: at 77 K, the mononuclear compound **2.1** has a decay lifetime (the dominant slow component) about 80 μs longer in CH_2Cl_2 and about 160 μs longer in PMMA than those of **3.4**. Clearly, the presence of the extra copper(I) centre in the dinuclear complex does appear to shorten the decay lifetime considerably, despite the fact that the two Cu(I) centres are far from each other (17.32 Å), which may be attributed to more degrees of freedom in the molecule. Hence, the dinuclear complexes may be more suitable for OLED applications.

3.4 Conclusions

In summary, four dinuclear and trinuclear Cu(I) complexes based on bmb, tmb and bmbp ligands that either display a linear shape or a star shape have been synthesized and fully characterized. These complexes have a good stability in solution and in the solid state. Except complex **3.4** that has a 4,4'-biphenyl linker in the chelate ligand, these complexes display syn and anti structural isomerism caused by the hindered rotation of the 2-(2'-pyridyl)benzimidazolyl chelate unit. Isomer inter-conversion occurs in solution at ambient temperature. Yellow-orange luminescence due to MLCT transitions has been observed for all complexes. These new complexes display exceptionally long decay lifetimes which may hinder their uses as emitters in EL devices as demonstrated by the poor performance of the EL device based on complex **3.4**. On the other hand, the long decay lifetime of **3.1**–**3.4** may render them as good candidates for photochemistry. The absorption and emission properties of **3.1-3.4** are similar to those found for **2.1** but they have shorter decay lifetimes making better candidates for OLED applications.

3.5 References

(1) Cuttell, D. G.; Kuang, S. M.; Fanwick, P. E.; McMillin, D. R.; Walton, R. A. *J. Am. Chem. Soc.* **2002**, *124*, 6.

(2) Kuang, S. M.; Cuttell, D. G.; McMillin, D. R.; Fanwick, P. E.; Walton, R. A. *Inorg. Chem.* **2002**, *41*, 3313.

(3) Yao, Y.; Perkovic, M. W.; Rillema, D. P.; Woods, C. *Inorg. Chem.* **1992**, *31*, 3956.

(4) Armaroli, N.; Balzani, V.; Barigelletti, F.; De Cola, L.; Flamigni, L.; Sauvage, J. P.; Hemmert, C. *J. Am. Chem. Soc* **1994**, *116*, 5211.

(5) Dietrich-Buchecker, C. O.; Nierengarten, J. F.; Sauvage, J. P.; Armaroli, N.; Balzani, V.; De Cola, L. *J. Am. Chem. Soc* **1993**, *115*, 11237.

(6) Yam, V. W. W.; Lo, K. K. W. J. *Chem. Soc. Dalton. Trans.* **1995**, 499.

(7) Juris, A.; Ziessel, R. *Inorg. Chim. Acta.* . **1991**, *30*, 2144.

(8) Balzani, V.; Juris, A.; Venturi, M. *Chem. Rev.* **1996**, *96*, 759.

(9) Youinou, M. T.; Ziessel, R.; Lehn, J. M. *Inorg. Chem.* **1991**, *30*, 2144.

(10) Zhang, Q.; Zhou, Q.; Cheng, Y.; Wang, L.; Ma, D.; Jing, X.; Wang, F. *Adv. Mater.* **2004**, *16*, 432.

(11) McCormick, T.; Jia, W.; Wang, S. *Inorg. Chem.* **2006**, *45*, 147.

(12) Liu, Q. D.; Jia, W. L.; Wang, S. *Inorg. Chem.* **2005**, *44*, 1332.

(13) Adachi, C.; Tsutsui, T.; Saito, S. *Appl. Phys. Lett.* **1990**, *56*, 799.

(14) Shirota, Y. *J. Mater. Chem.* **2000**, *10*, 1.

(15) Kubas, G. J. *Inorg. Synth.* **1979**, *19*, 90.

(16) Diez, J.; Falagan, S.; Gamasa, P.; Gimeno, J. *Polyhedron* **1988**, *7*, 37.

(17) Bruker Analytical X-ray Systems **1999**, *version 5.10*.

(18) Palsson, L.; Monk, A. P. *Adv. Mater.* **2002**, *14*, 757.

(19) Mello, J. C.; Wittmann, H. F.; Friend, R. H. *Adv. Mater.* **1997**, *9*, 230.

(20) Kirchhoff, J. R.; McMillin, D. R.; Robinson, W. R.; Powell, D. R.; McKenzie, A. T.; Chen, S. *Inorg. Chem.* **1985**, *24*, 3928.

(21) Williams, D. H.; Fleming, I. In *Spectroscopic Methods in Organic Chemistry;* McGraw-Hill: London, 1987.

(22) Zhang, Y.; Hu, Y.; Chen, J.; Zhou, Q.; Ma, D. *J. Phys. D: Appl. Phys.* **2003**, *36*, 2006.

Chapter 4
Synthesis of 2-(2'-Pyridyl)indole Based Ligands

4.1 Introduction

The group 2-(2'-(pyridyl)indole differs from the 2-(2'-pyridyl)benzimidazole group discussed in Chapters 2 and 3 in that 2-(2'-pyridyl)indole has a carbon in the three position of the indole rather than the nitrogen in the benzimidazole, as shown in Figure 4.1. It has been shown that 2-(2'-pyridyl)indole can act as a blue emitter when deprotonated. Our group has previously made zinc, boron and aluminum complexes using this class of ligands, where the indole is deprotonated to give an anionic ligand that binds to the metal or boron atom through N,N' chelation.[1, 2] Complexes of the 2-(2'-pyridyl)indole anion with Pt(II) and Pd(II) have resulted in similar N,N' chelation rather than cyclometallated C,N chelated complexes.[3, 4] It was found that a substituent on the nitrogen atom of the indole ring protects it from chelation, but does not deactivate the indole towards the electrophilic attack by the metal, thus allowing the formation of C,N chelated metal complexes.[3] In previously reported complexes, a methyl group is used to protect the nitrogen.[3, 5-7] In this chapter, it is demonstrated that by using phenyl substituents on the nitrogen of the indole ring, a series of ligands similar to those presented in Chapter 3 can be made. These ligands have a 2-(2'-pyridyl)indole in place of the 2-(2'-pyridyl)benzimidazole, as shown in Figure 4.2. This group of ligands should allow for C,N chelation, or binding to a metal through just the nitrogen of the pyridyl, thus achieving new fluorescent or phosphorescent metal complexes.

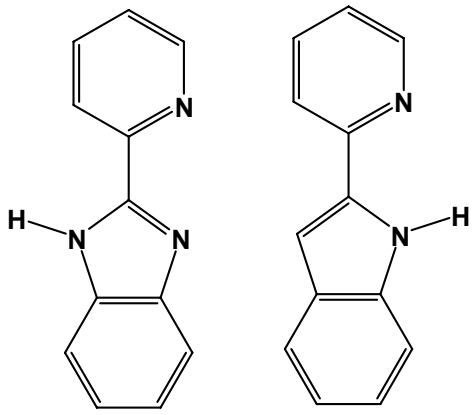

Figure 4.1 Structure of 2-(2'-pyridyl)benzimidazole and 2-(2'-pyridyl)indole.

During the course of synthesizing 2-(2'-pyridyl)indolyl benzene (pib), 1,4-bis[2-(2'-pyridyl)indolyl]benzene (bib) and 1,3,5-tris[2-(2'-pyridyl)indolyl]benzene) (tib) (shown in Figure 4.2), a new class of atropisomeric ligands was discovered, shown in Figure 4.3. Structurally, the new atropisomeric ligands, bis[3,3'(2-(2'-pyridyl)indolyl benzene)] (bpib), bis[3,3'(1,4-bis[2-(2'-pyridyl)indolyl]benzene (bbip) and bis[3,3'(1,3,5-tris[2-(2'-pyridyl)indolyl]benzene)] (btib) can be considered as the corresponding 3,3'-C-C coupled dimer of pib, bib and tib, respectively. Hindered rotation around the formed C-C bond results in axial chirality making the dimers atropisomeric.

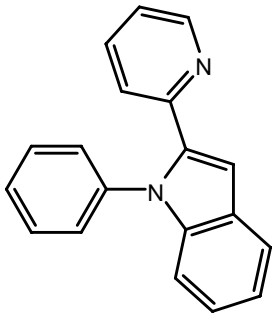

2-(2'-pyridyl)indolyl benzene (pib)

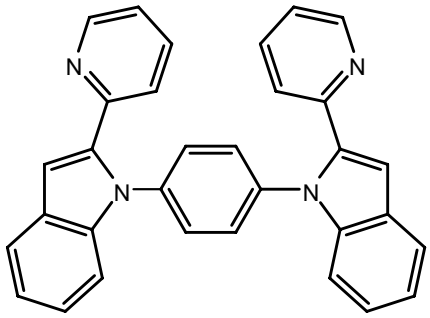

1,4 - bis[2-(2'-pyridyl)indolyl]benzene (bib)

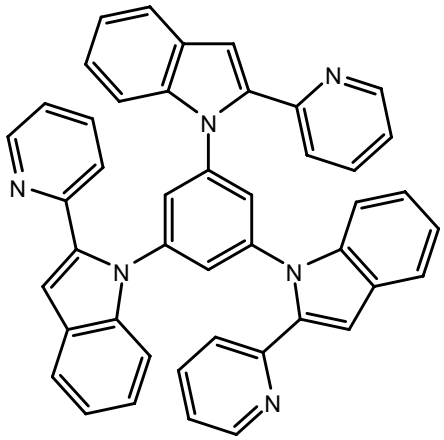

1,3,5 - tris[2-(2'-pyridyl)indolyl]benzene (tib)

Figure 4.2 Structures of the monomer 2-(2'-pyridyl)indolyl based ligands pib, bib and tib.

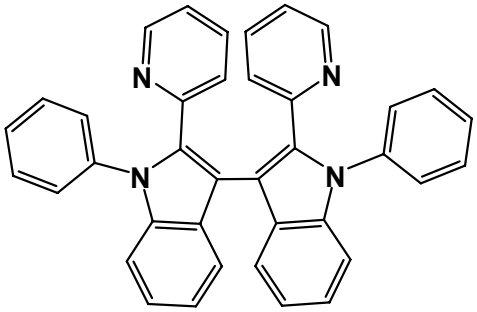

bis[3,3'(2-(2'-pyridyl)indolyl benzene)] (bpib)

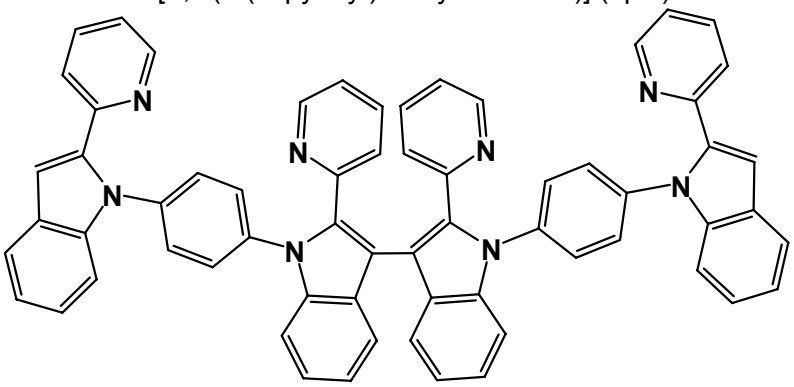

bis[3,3'(1,4 - bis[2-(2'-pyridyl)indolyl]benzene)] (bbib)

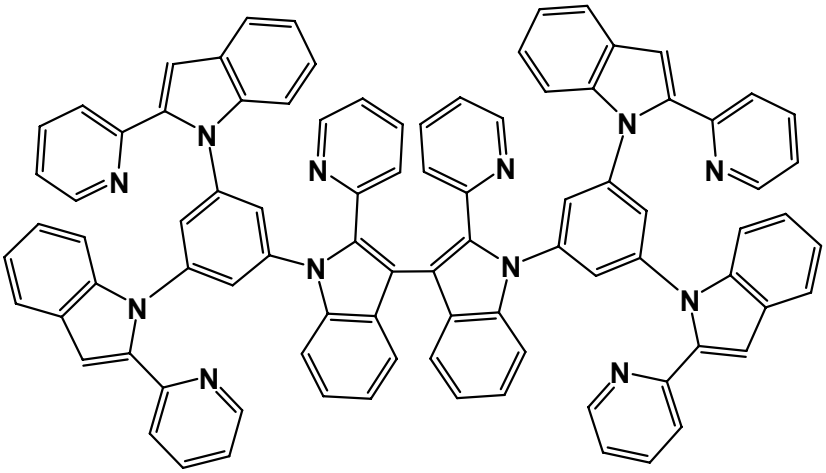

bis[3,3'(1,3,5 - tris[2-(2'-pyridyl)indolyl]benzene)] (btib)

Figure 4.3 Structures of dimers 2-(2'-pyridyl)indolyl based ligands – bpib, bbib and btib.

Atropisomeric chelate ligands such as BINAP (2,2'-bis(diphenylphosphino)-1,1'-binaphthyl) are well known for their important roles in asymmetric catalysis involving transition metals.[8-12] The majority of previously known atropisomeric ligands are based on 1,1'-binaphthyl with phosphine binding sites.[8-12] Atropisomeric ligands based on 3,3'-bi-indolyl are rare but some examples with phosphine donors have been reported.[13] Compared to phosphine ligands, pyridyl and polypyridyl ligands are in general harder donors, more stable toward oxidation, and can have rich photophysical/photochemical properties when bound to metal ions. Hence, atropisomeric chelate ligands based on pyridine or polypyridine are attractive not only for their potential use in certain asymmetric reactions, but also for their applications in chiral supramolecular assembly and chiral recognition.[8-12, 14] In spite of these, examples of atropisomeric ligands involving pyridyls as donors are scarce and only a few examples are known in literature.[15]

Copper catalyzed Ullmann condensation reactions are commonly known for C-N bond formation but not direct C-C bond coupling.[16, 17] Examples of one-pot or tandem reactions to form both C-C and C-N in the product are known previously (with Pd catalysts in most instances).[18, 19] However, simultaneous aryl C-C coupling and the formation of multiple aryl C-N bonds catalyzed by copper as shown in Figure 4.4, Figure 4.5 and Figure 4.6 are rare. This chapter will examine the synthesis and characterization of this class of atropisomeric ligands.

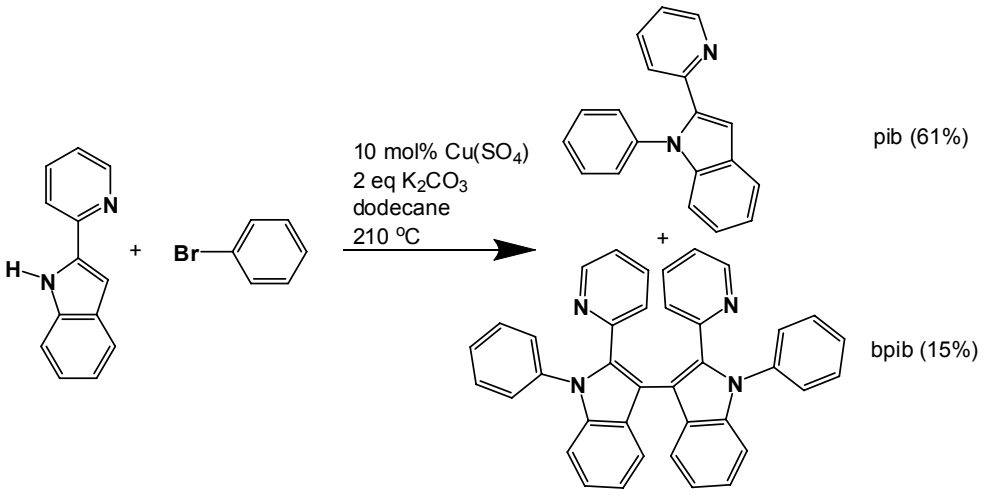

Figure 4.4 Reaction scheme for the synthesis of pib and bpib.

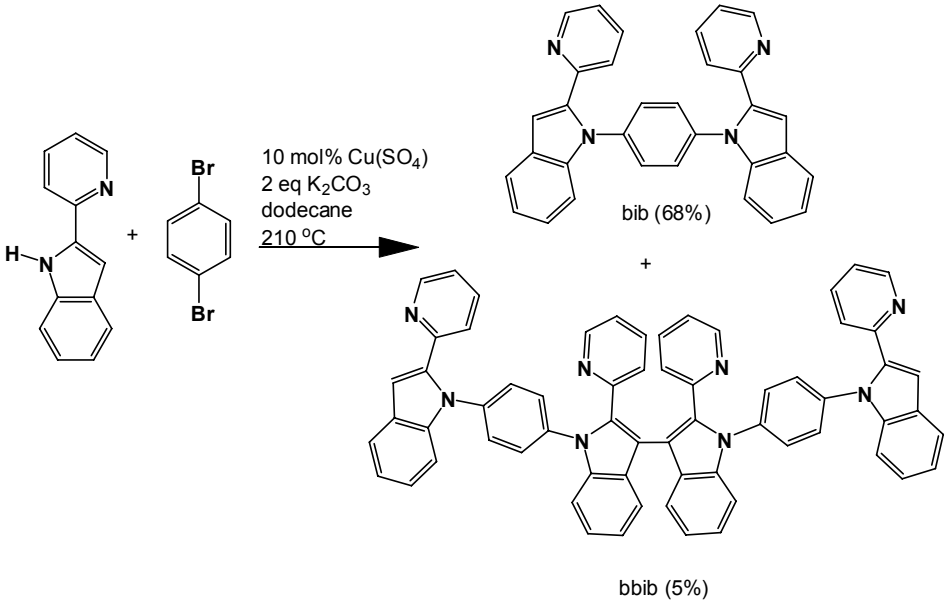

Figure 4.5 Reaction scheme for the synthesis of bib and bbib.

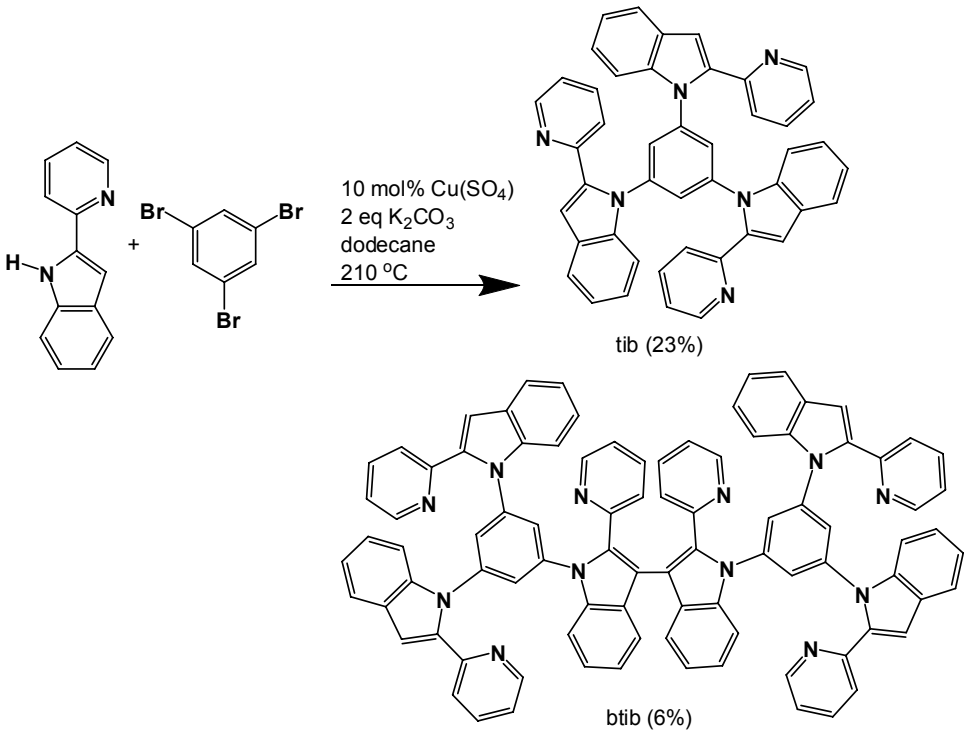

Figure 4.6 Reaction scheme for the synthesis of tib and btib.

4.2 Experimental

4.2.1 General Considerations

All starting materials were purchased from Aldrich Chemical Company and used without further purification. Solvents were freshly distilled over appropriate drying reagents under N_2 atmosphere. All experiments were conducted under a nitrogen atmosphere using standard Schlenk techniques unless otherwise stated. TLC was carried out on silica gel. Flash chromatography was carried out on silica (silica gel 60, 70-230 mesh). ^{1}H, ^{13}C NMR spectra were recorded on a Bruker Avance 400 MHz or 500 MHz spectrometer as stated. Excitation and emission spectra were recorded on a Photon Technologies

International QuantaMaster Model C-60 spectrometer. Elemental analyses were performed by Canadian Microanalytical Service Ltd., Delta, British Columbia, Canada or at the University of Toronto, Canada. The 2-(2'-pyridyl)indole was prepared using Fisher cyclization, based on literature procedures.[20, 21]

4.2.2 DFT Calculations

The *ab initio* molecular orbital calculations were performed for pib and bpib. The geometric parameters from X-ray diffraction analysis were used as the starting point for the geometry optimization by the Gaussian suit of programs (Gaussian 03).[22] Restricted density functional theory calculations at the B3LYP/6-311+G(d) level of theory were used for the energy calculations. The rotation barrier calculation for bpib was done first with the B3LYP/STO-3G level of theory with 18 steps of 20 degree rotations around the 3,3' C-C bond dihedral. The geometry was optimized at each step. After determining the high energy geometry using the simple basis set, the rotational barrier calculation was repeated at the B3LYP/6-311+G(d) level of theory with only 6 steps and a 60 degree rotation around the 3,3' C-C bond dihedral between each step.

4.2.3 Synthesis of 2-(2'-pyridyl)indolyl benzene (pib)

A mixture of 2-(2'-pyridyl)indole (2.67 g, 140 mmol), bromobenzene (4 mL), copper(II) sulphate (34 mg, 14 mmol), potassium carbonate (3.78 g, 280 mmol) in 2 mL of dodecane was refluxed for 24 hours. A 10% solution of NaOH in water was used to neutralize the brown reaction mixture after cooling to room temperature. This was washed three times with CH_2Cl_2. The extract was dried with magnesium sulphate. The

product was purified by column chromatography (tetrahydrofuran/hexanes/toluene 1:1:0.1 on silica) and subsequent recrystallization from ethylacetate and hexanes to afford a clear colourless crystal. 61% yield. ^{1}H NMR in CD_2Cl_2, 400 MHz (δ, ppm, 298 K): 8.51 (d, *J* = 4.0 Hz, 1H), 7.75 (dd, *J* = 8.0 Hz, *J* = 4.0 Hz, 1H), 7.58 (ddd, *J* = 4.0 Hz, *J* = 8.0, *J* = 8.0 Hz, 1H), 7.45-7.41 (m, 1H), 7.51-7.47 (m, 2H), 7.34-7.30 (m, 3H), 7.27-7.19 (m, 3H), 7.17-7.13 (m, 2H). ^{13}C NMR in CD_2Cl_2, 100 MHz (δ, ppm, 298 K): 106.1, 110.0, 111.2, 121.2, 121.4, 122.1, 123.5, 123.6, 127.6, 128.3, 128.4, 129.6, 136.2, 139.5, 140.2, 149.8, 151.7. Anal calcd for $C_{19}H_{12}N_2$: C, 84.42; H, 5.22; N, 10.36. Found: C, 83.92; H, 5.20; N, 10.36. MP 124-126 °C.

4.2.4 Synthesis of bis[3,3'-(2-(2'-pyridyl)indolyl benzene)] (bpib)

This compound was isolated as a by-product from the reaction mixture for pib in 15% yield after recrystallization from CH_2Cl_2 and hexanes. ^{1}H NMR in CD_2Cl_2, 500 MHz(δ, ppm, 298 K): 8.13 (d, *J* = 4.0 Hz, 1H), 7.57 (d, *J* = 8.0 Hz, 1H), 7.44-7.37 (m, 3H), 7.33-7.26 (m, 5H), 7.16 (dd, *J* = 8 Hz, *J* = 8 Hz, 1H), 6.97 (d, *J* =12.5 Hz, 1H), 6.89 (ddd, *J* = 7.0 Hz, *J* =5.0 Hz, J=1.0 Hz, 1H),. ^{13}C NMR in CD_2Cl_2 125 MHz (δ, ppm, 298 K): 100.4, 111.1, 120.9, 121.2, 121.5, 123.5, 126.1, 127.0, 128.1, 129.2, 135.6, 137.7, 138.8, 139.3, 139.3, 149.1, 151.6. Anal calcd for $C_{38}H_{26}N_4$: C, 84.73; H, 4.87; N, 10.40. Found: C, 84.44, H 4.88, N 10.34. MP: 248-251 °C.

4.2.5 Synthesis of 1,4-bis[2-(2'-pyridyl)indolyl] benzene (bib)

A mixture of 2-(2'-pyridyl)indole (212 mg, 1.09 mmol), 1,4-dibromobenzene (104 mg, 0.44 mmol), copper(II) sulfate (20 mg, 0.08 mmol) and potassium carbonate (150 mg,

1.10 mmol) was refluxed in 2 mL of dodecane for 8 hours. A 10% solution of NaOH in water was used to neutralize the brown reaction mixture after cooling to room temperature. This was washed three times with CH_2Cl_2, the extract was dried with magnesium sulphate. The product was purified by column chromatography (ethyl acetate/hexanes 1:1 on silica) and subsequent recrystallization from ethyl acetate and hexanes. 68% yield. ^{1}H NMR in CD_2Cl_2, 500 MHz (δ, ppm, 298 K): 8.55 (d, *J* = 5.0 Hz, 1H), 7.77 (d, *J* = 8.0 Hz, 1H), 7.67 (ddd, *J* = 1.8 Hz, *J* = 7.8 Hz, *J* = 7.8 Hz, 1H), 7.43-7.38 (m, 4H), 7.19 (s, 1H), 7.30 (ddd, *J* = 1.0 Hz, *J* = 8.25 Hz, *J* = 8.25 Hz, 1H), 7.26-7.24 (m, 1H), 7.23-7.20 (m, 1H). ^{13}C NMR in CD_2Cl_2 125 MHz (δ, ppm, 298 K):100.4, 106.2, 111.1, 121.4, 121.5, 122.2, 123.6, 128.5, 129.0, 136.3, 138.38, 140.1, 140.1, 149.7, 151.6. Anal calcd for $C_{32}H_{22}N_4$: C, 83.09; H, 4.79; N, 12.11. Found: C, 82.54; H, 5.09; N, 11.91.

4.2.6 Synthesis of bis[3,3'-(1,4-bis[2-(2'-pyridyl)indolyl] benzene)] (bbib)

This product was isolated from the reaction mixture for the synthesis of bib in 5% yield (35mg) after recrystallization from ethyl acetate. ^{1}H NMR in CD_2Cl_2, 500 MHz (δ, ppm, 298 K): 8.52 (d, *J* = 4.0 Hz, 1H), 8.24 (d, *J* = 4.0 Hz, 1H), 7.76 (d, *J* = 8.0 Hz, 1H), 7.65-7.61 (m, 2H), 7.54 (d, *J* = 8.0 Hz, 1H), 7.38-7.28 (m, 10H), 7.26-7.21 (m 3H), 7.18 (s, 1H), 7.10 (d, *J* = 8.0 Hz, 1H), 6.99 (ddd, *J* = 7.5 Hz, *J* = 5.0 Hz, *J* = 0.8 Hz, 1H). ^{13}C NMR in CD_2Cl_2 125 MHz (δ, ppm, 298 K): 106.2, 110.9, 111.1, 111.1, 121.2, 121.3, 121.5, 121.7, 122.1, 123.6, 123.7, 126.1, 128.4, 128.7, 128.8, 129.3, 135.8, 136.2, 137.7,

138.2, 128.8, 140.1, 149.2, 149.7, 151.5, 151.6. High res mass spec calcd for $C_{64}H_{42}N_8$ (m/z): 923.3532. Found: 923.3580.

4.2.7 Synthesis of 1,3,5-tris[2-(2'-pyridyl)indolyl] benzene (tib)

A mixture of 1,3,5-tribromobenzene (160 mg 0.5 mmol), 2-(2'-pyridyl)indole (300 mg, 1.5 mmol), copper(II) sulphate (40 mg, 0.15 mmol) and potassium carbonate (430 mg, 3.0 mmol) was refluxed in 2 mL of dodecane for 24 hours. A 10% solution of NaOH in water was used to neutralize the brown reaction mixture after cooling to room temperature. This was washed three times with CH_2Cl_2, the extract was dried with magnesium sulphate. The product was purified by column chromatography (THF/hexanes 1:1 on silica) and subsequent recrystallization from ethyl acetate and hexanes gave 23% yield of tib. ^{1}H NMR in CD_2Cl_2, 500 MHz (δ, ppm, 298 K): 8.61 (d, *J* = 4.0 Hz, 1H), 7.76-7.72 (m, 1H), 7.70 (d, *J* = 7.5 Hz, 1H), 7.51 (d, *J* = 8.0 Hz, 1H), 7.29-7.26 (m, 1H), 7.30 (s, 1H), 7.21-7.18 (m, 1H), 7.15-7.11 (m, 1H), 7.11 (s, 1H), 6.91 (d, *J* = 6.5 Hz, 1H),. ^{13}C NMR in CD_2Cl_2 125 MHz (δ, ppm, 298 K): 106.7, 110.9, 121.4, 121.5, 122.25, 123.7, 123.8, 126.5, 136.6, 139.8, 140.0, 140.9, 149.9, 151.5. Anal calcd for $C_{45}H_{30}N_6$: C, 82.55; H, 4.62; N, 12.84. Found: C, 82.45, H 4.82, N12.66.

4.2.8 Synthesis of bis[3,3'-(1,3,5-tris[2-(2'-pyridyl)indolyl] benzene)] (btib)

This product was isolated from the reaction mixture for the synthesis of tib in 6% yield (35mg) after recrystallization from THF. ^{1}H NMR in CD_2Cl_2, 500 MHz (δ, ppm, 310 K): 8.60 (d, *J* = 5.0 Hz, 2H), 8.29 (d, *J* = 5.0 Hz, 1H), 7.72 (dd, *J* = 7.5 Hz, *J* = 7.5 Hz, 2H), 7.68 (d, *J* = 10 Hz, 2H),7.51 (d, *J* = 8.0 Hz, 1H), 7.46 (d, *J* = 5 Hz, 2H), 7.39 (d, *J* = 5 Hz,

1H), 7.32-7.27 (m, 5H), 7.30 (s, 1H), 7.29-7.26 (m, 1H), 7.21 (s, 1H), 7.21-7.18 (m, 1H), 7.18-7.15 (m, 2H),7.15-7.11 (m, 1H), 7.13-7.07 (m, 6H), 7.03-6.99 (m, 2H), 6.93 (br, 1H), 6.78 (br, 2H). Anal calcd for $C_{90}H_{58}N_{12}$: C, 82.67; H, 4.47; N, 12.86. Found: C, 81.65; H, 4.42; N, 12.55. (note ¼ CH_2Cl_2 calc. C 81.5936, H 4.41, N 12.66).

4.2.9 X-ray Diffraction Analyses

Single crystals of tib, bpib and bbib were mounted on glass fibres for data collection. Data was collected on a Bruker Apex II single-crystal X-ray diffractometer with graphite monochromated Mo Kα radiation, operating at 50 kV and 30 mA at 180 K. No significant decay was observed in any samples. Data were processed on a PC with the aid of the Bruker SHELXTL software package (version 5.10)[23] and are corrected for absorption effects. All structures were solved by direct methods. The crystals of tib belong to the triclinic space group *P-1*. The crystals of bpib and bbib belong to the monoclinic space group $P2_1/n$ and the orthorhombic space group *Pbcn*, respectively. Molecules of bpib possess a crystallographically imposed C2 axis. All hydrogen atoms are calculated and their contributions are included in structural factor calculations. A disordered CH_2Cl_2 was found in the lattice of tib (0.5 CH_2Cl_2 per molecule) which was refined successfully. The X-ray crystallographic data are presented in Table 4.1. Selected bond lengths, bond angles and torsion angles are shown in Table 4.2.

Table 4.1 Crystallographic data for tib, bpib and bbib.

	tib	**bpib**	**bbib**
formula	$C_{45.50}H_{31}ClN_6$	$C_{38}H_{26}N_4$	$C_{64}H_{42}N_8$
fw	697.21	538.63	923.06
space group	P-1	$P2_1/n$	Pbcn
a, Å	10.831(11)	8.8041(10)	14.4704(12)
b, Å	13.157(13)	16.7489(18)	15.2828(13)
c, Å	13.558(13)	18.758(2)	21.9590(18)
α, deg	96.213(18)	90.00	90.00
β, deg	92.03(2)	97.126(2)	90.00
γ, deg	113.041(15)	90.00	90.00
V, Å^3	1761(3)	2744.7(5)	4856.2(7)
Z	2	4	4
D_{calc}, gcm^{-3}	1.315	1.303	1.263
μ, cm^{-1}	0.152	0.77	0.76
$2\theta_{max}$, deg	56.90	56.70	34.93
no. of reflns measd	11764	15773	47826
no. of reflns used (R_{int})	7845 (0.1030)	4833 (0.0279)	4962 (0.0941)
no. of params	488	379	325
final *R* [I > 2σ(I)]			
R1[a]	0.0789	0.0326	0.0534
*w*R2[b]	0.1262	0.0735	0.1285
R (all data)			
R1[a]	0.3391	0.0524	0.1145
*w*R2[b]	0.1700	0.0804	0.1572
GOF on F^2	0.722	0.813	1.014

[a] $R1 = \Sigma[|F_o| - |F_c|]/\Sigma|F_o|$. [b] $wR2 = \{\Sigma[w(F_o^2 - F_c^2)]/ \Sigma(wF_o^2)\}^{1/2}$.
$\omega = 1/[\sigma^2(F_o^2) + (0.075P)^2]$, where $P = [\max.(F_o^2,0) + 2F_c^2]/3$.

Table 4.2 Selected bond length (Å), angles (°), and torsion angles (°) for tib, bpib and bbib.

		tib	
C(5)-N(3)	1.428(5)	N(1)-C(1)-C(6)	120.2(5)
C(1)-N(1)	1.446(5)	N(2)-C(3)-C(2)	121.1(5)
C(3)-N(2)	1.422(5)	N(3)-C(5)-C(4)	118.2(5)
		C(14)-N(1)-C(1)-C(2)	-121.94
		C(27)-N(2)-C(3)-C(4)	136.62
		C(40)-N(3)-C(5)-C(6)	126.07
		bpib	
Cu(8)-C(8A)	1.4685(18)	C(7)-C(8)-C(8A))	127.09(11)
C(6)-N(1)	1.4322(16)	C(6)-N(1)-C(7)	127.93(11)
C(7)-C(19)	2.2505(18)	C(7)-C(8)-C(8A)-C(7A)	48.60
		N(2)-C(19)-C(7)-N(1)	-130.98
		C(1)-C(6)-N(1)-C(7)	59.79
		bbib	
C(7)-C(7A)	1.471(4)	C(8)-C(7)-C(7A)	125.88(16)
N(1)-C(27)	1.430(3)	C(1)-N(1)-C(27)	126.20(18)
N(3)-C(30)	1.437(4)	C(7)-C(8)-C(9)	128.4(2)
C(21)-C(22)	1.464(4)	C(25)-C(26)-C(26A)-C(25A)	48.87
C(8)-C(9)	1.476(3)	C(25)-N(4)-C(17)-C(17)	122.60
		C(15)-C(14)-N(2)-C(6)	-52.38
		N(2)-C(6)-C(5)-N(1)	-40.14

4.3 Results and Discussion

4.3.1 Synthesis

The ligands pib, bib and tib were synthesized using the Ullmann condensation reaction of 2-(2'-pyridyl)indole with bromobenzene, 1,4-bromobenzene, and 1,3,5-tribromobenzene, respectively, using $CuSO_4$ as the catalyst and K_2CO_3 as the base, as shown in Figure 4.4-Figure 4.6. The structures of these three ligands are shown in Figure 4.2. The ligands were obtained in reasonable yields of 61%, 68% and 23% for pib, bib and tib respectively. The low yield for tib can be explained by the formation of the 1,3 substituted and mono-substituted benzene as by-products. The loss of bromine under Ullmann condensation conditions has previously been reported for poly substituted benzene reactions.[24]

The ligands bpib, bbib and btib were isolated as a side product from the reactions with the intended targets being pib, bib and tib respectively as shown in Figure 4.4, Figure 4.5 and Figure 4.6. In a one pot reaction both C-N and C-C bonds were formed. Copper catalyzed Ullmann condensation reactions are commonly known for C-N bond formation but not for direct arylation. The isolation of the 3,3'-bi-indolyl products from these reactions is therefore surprising. The isolated yield of the small dimer bpib is modest with only 15%. However, NMR of the crude reaction mixture indicates a 2:1 ratio of pib to bpib. The isolated yields of the larger dimers bbib and btib are low (5% and 6% respectively), which are caused mainly by their poor solubility (slightly soluble in CH_2Cl_2) and the formation of mono-and di-substituted (in case of 1,3,5-tribromobenzene)

C-N coupling side products. Also, C-C homo-coupling at the 3 position of the terminal 2-(2'-pyridyl)indolyl in bpib and btib is also possible, which can result in the formation of larger oligomeric species, such as those shown in Figure 4.7, and contribute to the low yield of the dimer. Indeed, insoluble organic products were observed from the reaction mixtures for bbib and btib synthesis. A mass spectrum of the crude reaction mixture of bbib showed mass peaks for oligomers up to seven (pyridyl)indolyl-phenyl-(pyridyl)indolyl units (up to 3290.4064 mass units). However, the insolubility has prevented full characterization of these high molecular weight species.

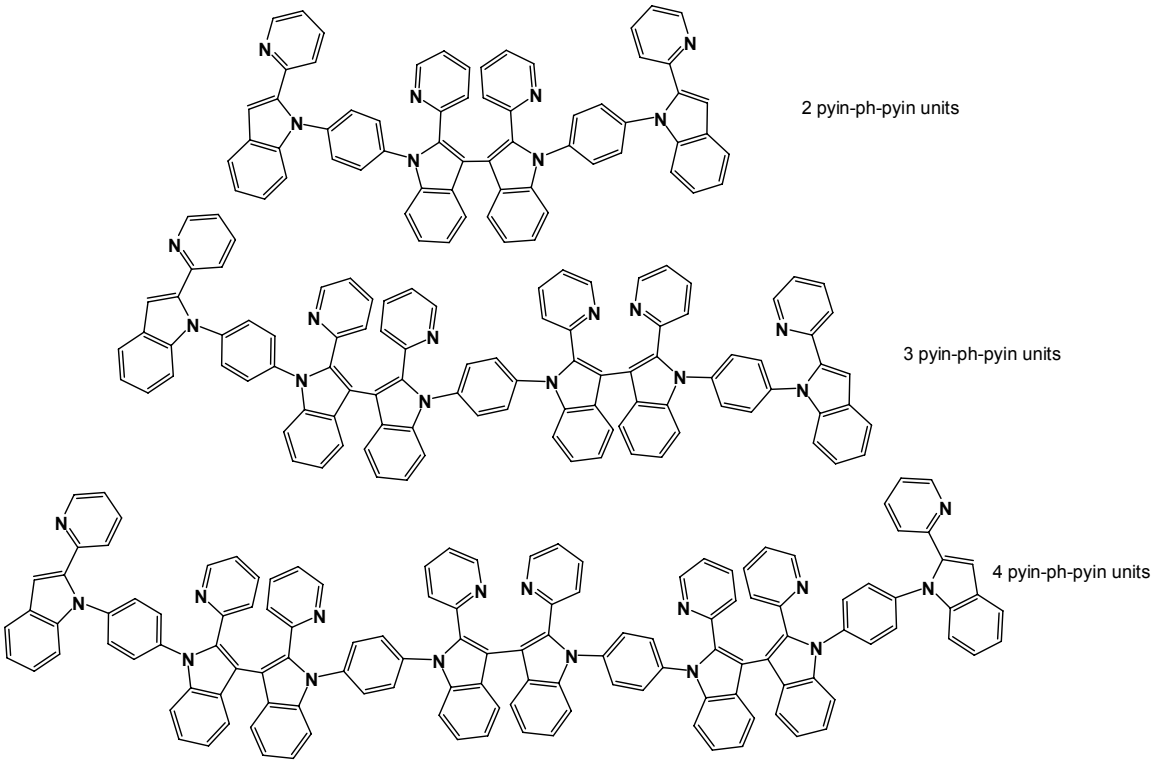

Figure 4.7 Structures for the oligomers of bib up to four units long.

The apparent monomer-dimer structural relationship between pib and bpib suggests that one possible explanation for the formation of bpib is that pib is the precursor which undergoes direct C-C coupling at the three position of indolyl to form the dimer. To verify this, direct coupling of pib to form bpib was attempted using a base and a copper catalyst at elevated temperatures, as in the original reaction, but no reaction was observed. It has been demonstrated that copper catalyzed C-C coupling reactions at unfunctionalized sp^2 carbon centres can be obtained with the aid of an oxidant.[25-28] Unfunctionalized C-C bond formation for biaryl and bipyrroles has also been reported using a hypervalent iodine radical source such as phenyliodine bis(trifluoroacetate) (PIFA).[29] Attempts to use PIFA and other oxidants with or without copper using the reaction conditions reported in literature failed to convert pib to bpib. However, if the reaction was carried out at high temperature (210^{o}C) in the presence of PIFA (with or without copper), some conversion of pib to bpib (~15% by NMR) along with a large amount of decomposition products was observed. The original one-pot reaction is therefore still the simplest and the best way to produce bpib.

Direct C-C coupling of indole via either a potassium salt or a lithium salt intermediate and the subsequent oxidation by oxidants such as I_2 was known to produce 3,3'-bi-indole in low yield.[30-32] In the reactions, brominated benzenes are likely the source of radical oxidants generated under the high temperature reaction conditions. The 2-pyridyl group on the indole ring likely functions as a directing group that binds to the Cu ion initially, facilitating the activation of the C-H bond and the subsequent 3,3'-C-C

coupling. Similar *ortho*-assisted 1,1'-C-C coupling of naphthalene[8, 16, 17] and C-C coupling in other molecules are well documented.[33] In fact, a crystal structure of a Cu(I) complex with pib (discussed further in Chapter 5) shows the proximity of the coordinated Cu(I) centre to the proton on the three position of the indole ring with a distance of 2.58 Å. To verify this hypothesis, the 2'-(2-pyridyl)indole was replaced with (2-phenyl)indole as shown in Figure 4.8 (reaction carried out by Julian Morey). No dimer product was observed in the reaction mixture, supporting the theory that the C-C bond forming reaction is a consequence of the pyridyl group directing the copper catalyst to the 3 position on the indole.

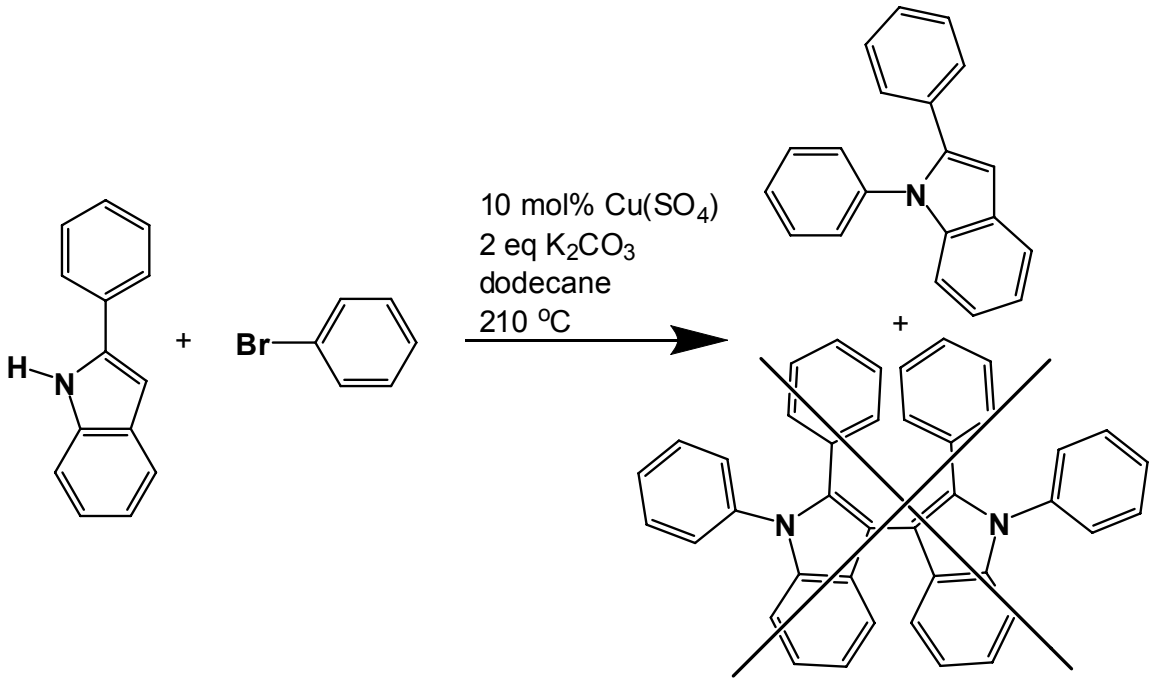

Figure 4.8 Reaction scheme for the coupling of 2-phenylindole where no dimer product was observed.

4.3.2 Structures in Solution

4.3.2.1 Structure of bib and tib in Solution

Ligands bib and tib are sterically crowded molecules and it is expected that the 2-(2'-pyridyl)indolyl groups are restricted and do not rotate freely around the phenyl-indolyl bond. This was confirmed by variable temperature ^{1}H NMR experiments. The *syn* and *anti* isomers **A** and **B** for bib and **C** and **D** for tib coexist in solution as shown in Figure 4.9. These are similar to the stereoisomers for complexes **3.1-3.3** discussed in Chapter 3. In the *syn* (**A** and **C**) configuration all pyridyl rings are on the same side of the central phenyl ring. This results in a C_2 symmetry for bib and C_3 symmetry for tib that should only have one set of chemical shifts for the 2-(2'pyridyl)indole groups in solution. In the *anti* geometry (**B** and **D**) one of the 2-(2'pyridyl)indolyl groups orients in the opposite direction. For bib this should result in two sets of chemical shifts for the 2-(2'pyridyl)indolyl groups appearing in a 1:1 ratio because the *syn* geometry has a C2 axis making the groups equivalent, and the *anti* has a mirror plan, thus there should be one set of peaks per isomer. For tib there should be two sets of peaks for the 2-(2'pyridyl)indolyl groups but in a 2:1 ratio for the *syn* isomer because of the mirror plan that lies on the 2-(2'pyridyl)indolyl group oriented in the opposite direction. The *anti* should only exhibit one set of peaks and statistically there should be a 2:1 ratio between *anti* and *syn*. The variable ^{1}H NMR spectra for bib are shown in Figure 4.10. At 298 K, one set of chemical shifts were observed. As the temperature was lowered some of the signals split into two distinct sets of chemical shifts with ~2:1, which supports the coexistence of the

A and **B** isomers in solution, however the ratio is not as expected which may support one isomer is preferred over the other. The **A** and **B** isomers undergo a dynamic exchange at temperatures above 223 K. The activation energy of this exchange process for bib was estimated to be 46 kJ mol^{-1} by using the two chemical shifts at the 7.13 and 7.11 ppm region and the coalescence temperature of 213 K.

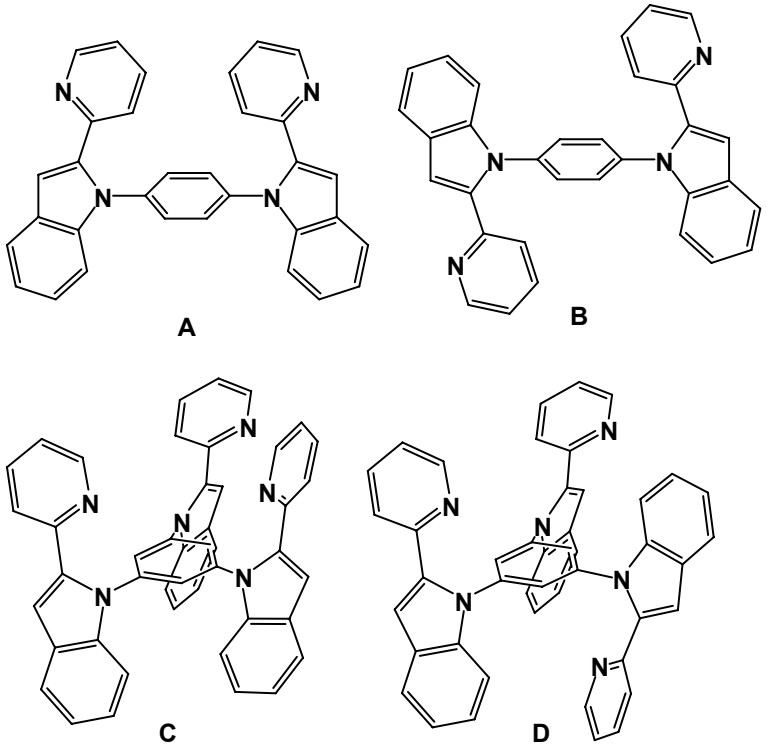

Figure 4.9 Structure of stereoisomers of bib, *syn*-**A** and *anti*-**B** for bib, and for tib, *syn*-**C** and *anti*-**D.**

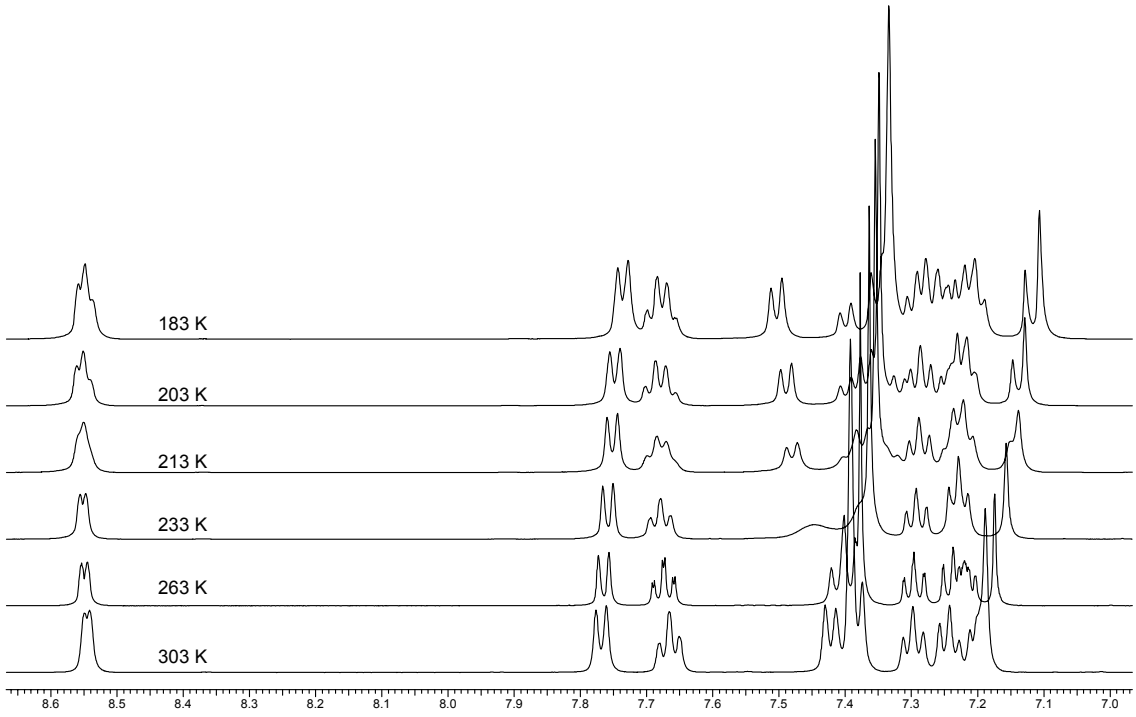

Figure 4.10 Variable temperature ^{1}H NMR of bib in CD_2Cl_2.

Similar variable temperature NMR response was observed for tib as shown in Figure 4.11. The small peak near 8.6 ppm that is visible at low temperatures is from an impurity. The coexistence of isomers **C** and **D** shown in Figure 4.9 undergo dynamic exchange in solution above 263 K. The exchange energy could not be calculated due to the 2:1 ratio of the site exchange. The 2:1 ratio is verified by looking at the H_1-pyridy peak at 8.7 ppm at room temperature that splits into two peaks with a ~2:1 ratio upon cooling although this could be caused by just the *anti* isomer, but from comparing to the other experiments it is likely that both isomers are present.

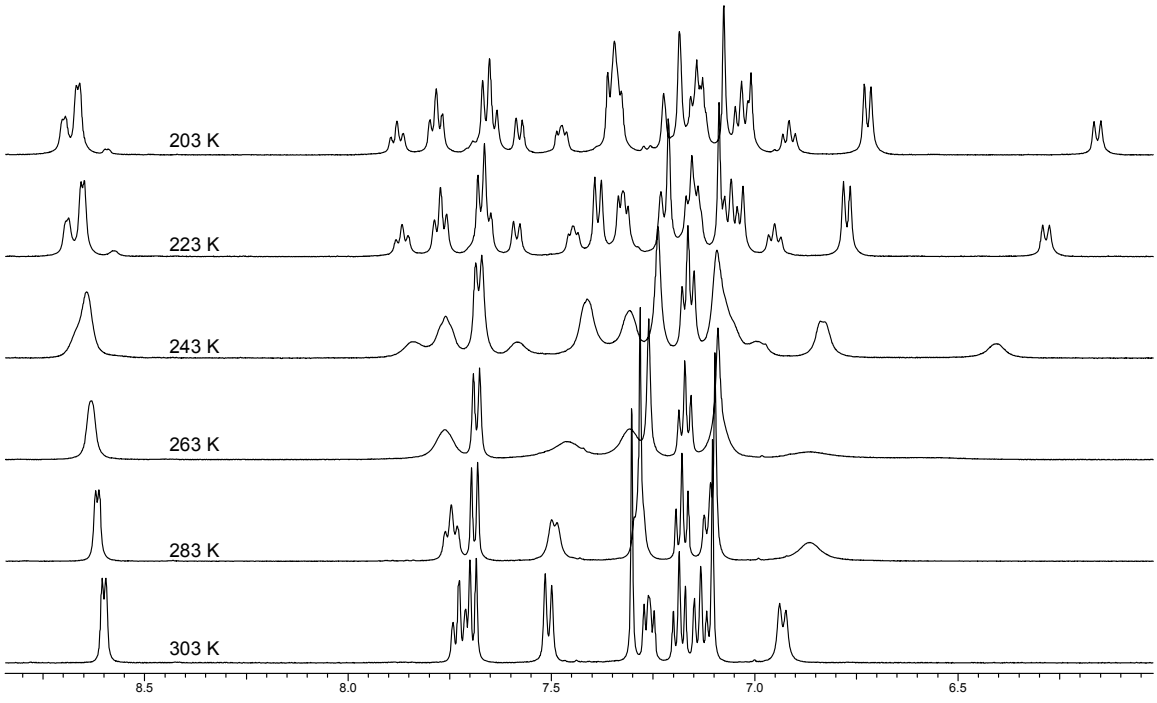

Figure 4.11 Variable temperature ^{1}H NMR of tib in CD_2Cl_2.

4.3.2.2 Structure of bpib, bbib and btib in Solution

The ^{1}H NMR spectrum of bpib shows that both halves of the molecule are chemically equivalent and low temperature does not resolve the halves of the molecule. The H_1-pyridyl proton (the proton on the carbon next to the nitrogen) for the dimer is shifted up-field compared to the monomer (8.13 ppm for dimer bpib compared to to 8.51 ppm for the monomer pib), this is likely due to π-π interactions between the pyridyl rings. The singlet at 7.17 ppm that is seen for pib from the proton at the three position on indole is not seen in bpib due to the C-C coupling in that position, both spectra of pib and bpib are shown in Figure 4.12.

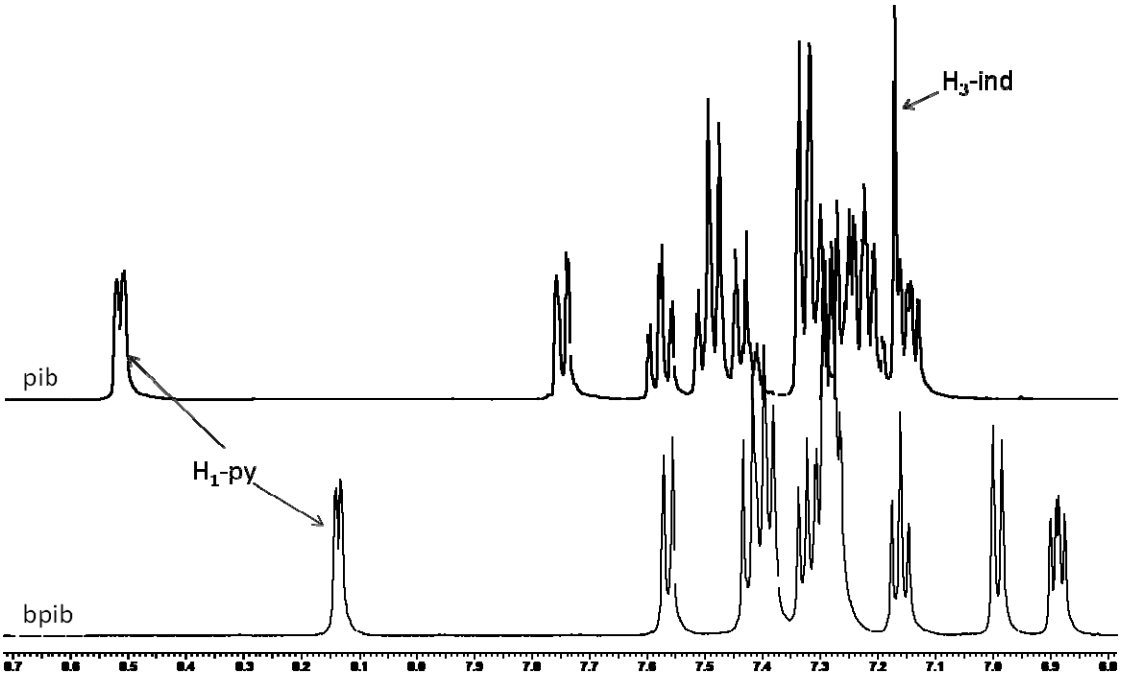

Figure 4.12 ^{1}H NMR of the monomer pib and the corresponding dimer bpib at 298 K in CD_2Cl_2.

The larger dimer bbib shows a 1:1 ratio for the two H_1-py peaks, one from the central pyridyl groups (8.24 ppm) and one from the distal pyridyl groups (8.52 ppm) as shown in Figure 4.13. Likewise, btib has a 2:1 ratio for the distal to central pyridyl peaks as shown in Figure 4.14. The impurity peaks seen in the btib spectrum may be caused by bi-substituted byproducts.

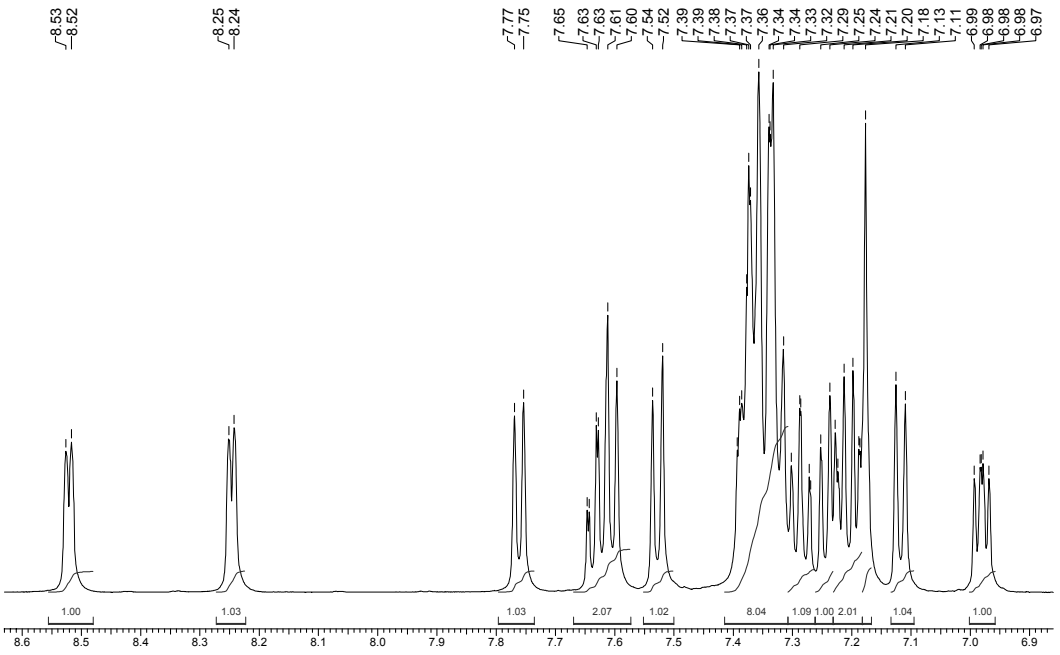

Figure 4.13 ^{1}H NMR spectra of bbib at 303 K in CD_2Cl_2.

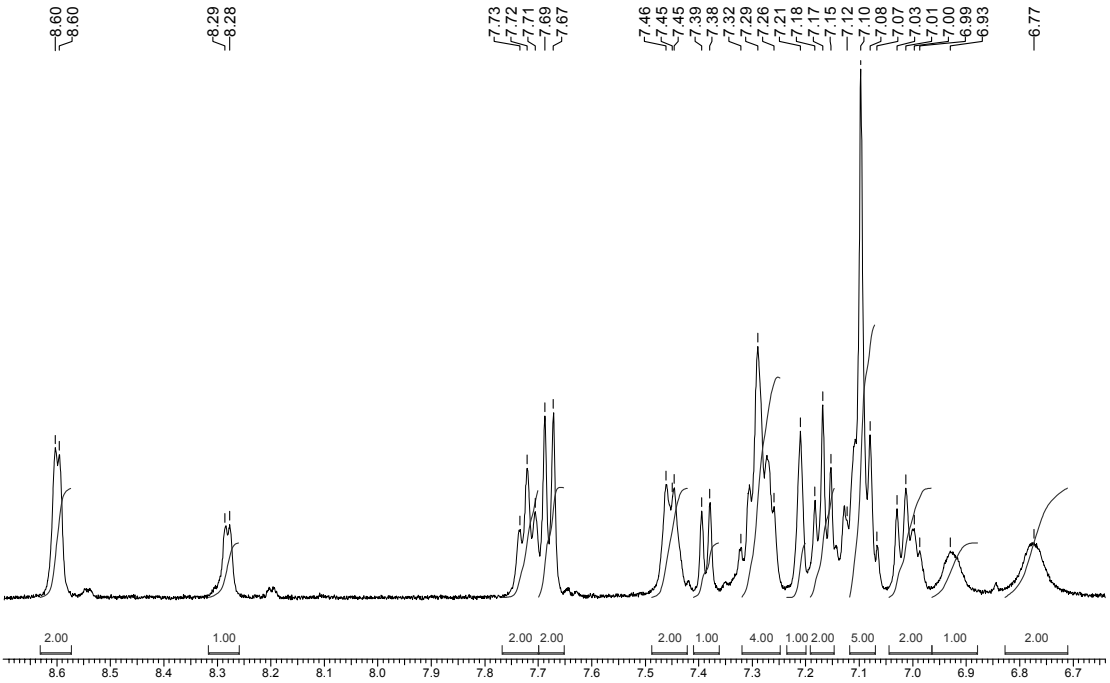

Figure 4.14 ^{1}H NMR spectra of btib in 303 K in CD_2Cl_2.

Broad peaks are observed at room temperature for the larger dimers bpib and btib due to isomerisation similar to **A** and **B**, but more 2-(2'-pyridyl)indolyl groups result in more combinations of orientations. This makes the low temperature spectrum more complicated as shown for bbib in Figure 4.15. Problems with insolubility prevented low temperature NMR of btib.

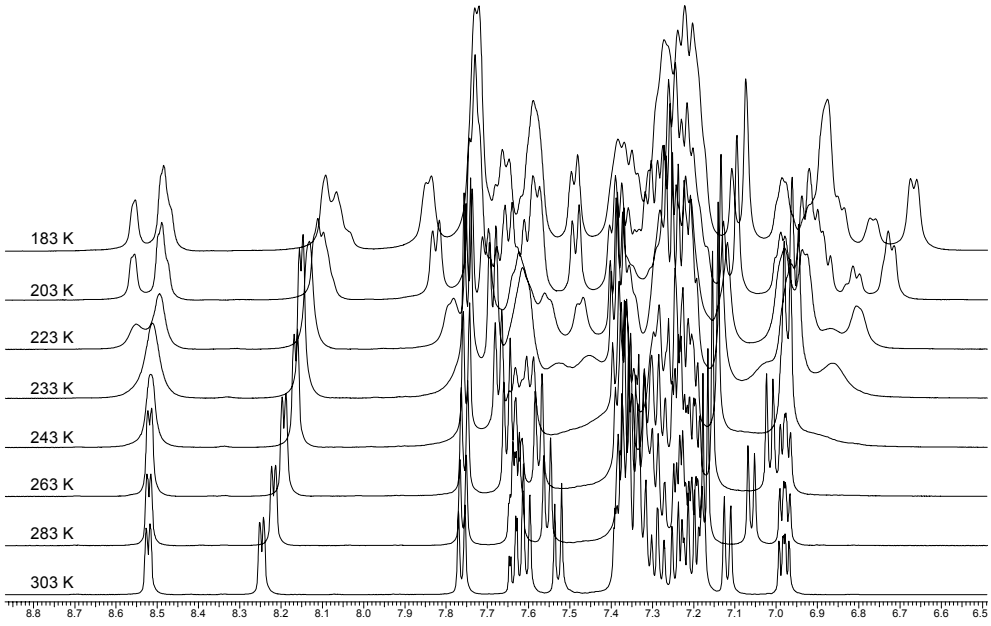

Figure 4.15 Variable temperature ^{1}H NMR of bbib in CD_2Cl_2.

4.3.3 Crystal structures

4.3.3.1 Structure of tib

The crystal structure of tib was determined by Qinde Liu and is shown in Figure 4.16. It was found that tib crystallized in the triclinic space group *P-1* with 0.5 CH_2Cl_2 solvent molecule. The N-C bond lengths between the indolyl and central benzene are on average

1.432 Å. The structure indicates the 2-(2'-pyridyl)inolyl groups are oriented in the *anti* geometry, with two of the pyridyl groups above the plane of the central phenyl ring, and one below. The N(3)-C(5)-C(4) and N(2)-C(3)-C(2) bond angles are 120.2(5)° and 120.1(5)° respectively. The (2'-pyridyl)indolyl that is pointed down has an N(1)-C(1)-C(6) angle that is slightly distorted at 118.2(5)°. The crystal packing structure diagram shows that two protons on the central phenyl ring are 2.807 Å from the pyridyl rings on neighbouring molecules.

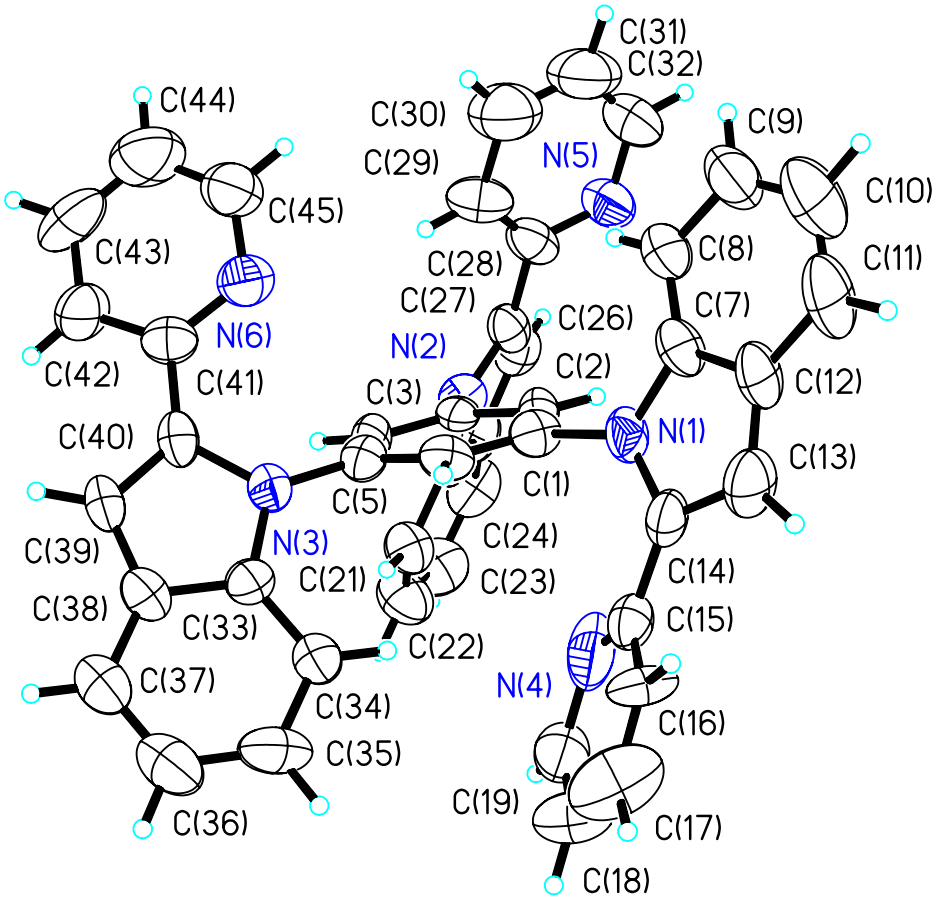

Figure 4.16 Structure of tib with labelling scheme and 50% thermal ellipsoids.

4.3.3.2 Structure of bpib and bbib

The crystal structures of the dimers bpib and bbib have been determined by X-ray diffraction analyses and are shown in Figure 4.17 and Figure 4.18 respectively. Both bpib and bbib have an approximate C_2 symmetry. The dihedral angle between the indolyl rings is 125.1° for bpib and 128.5° for bbib. There are significant π–π interactions between the two central pyridyl rings with the atomic separation distances being 3.57 Å – 4.00 Å for bpib, and 3.50 – 3.90 Å for bbib. Consistent with the π–π interactions between the two py rings in solution is the distinct up-field shift (~0.4 ppm) by the $C_{(6)}$-H proton of py in the ^{1}H NMR spectra, from monomer to dimer.

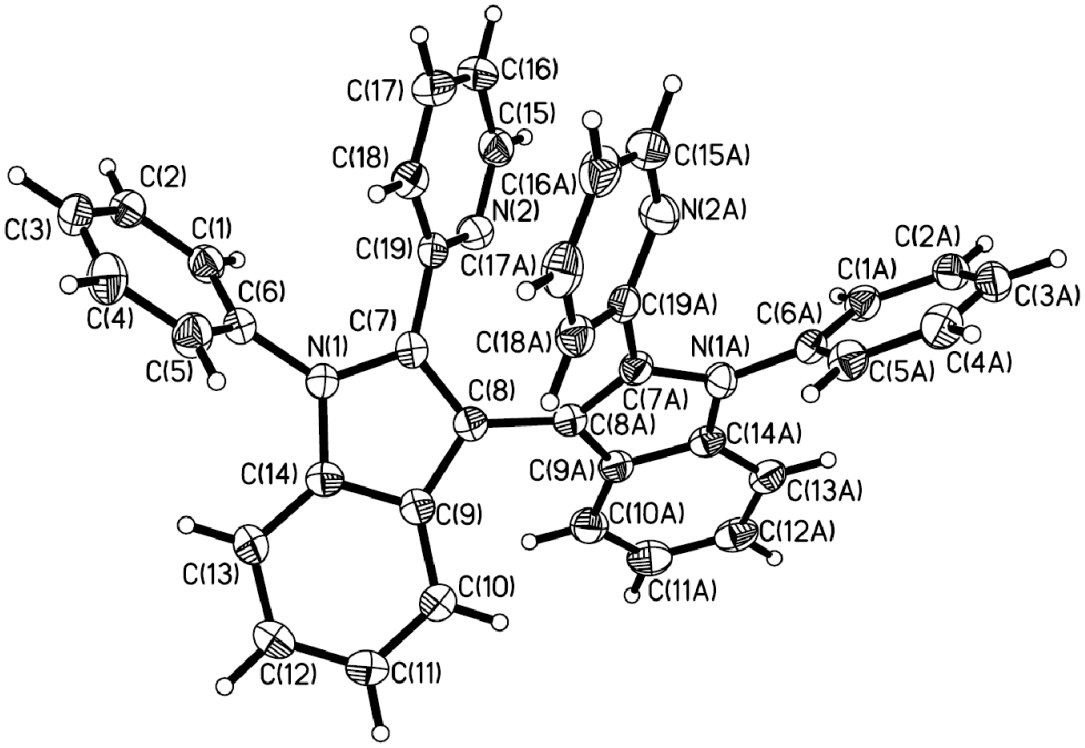

Figure 4.17 Crystal structure of bpib with labelling scheme and 50% thermal ellipsoids.

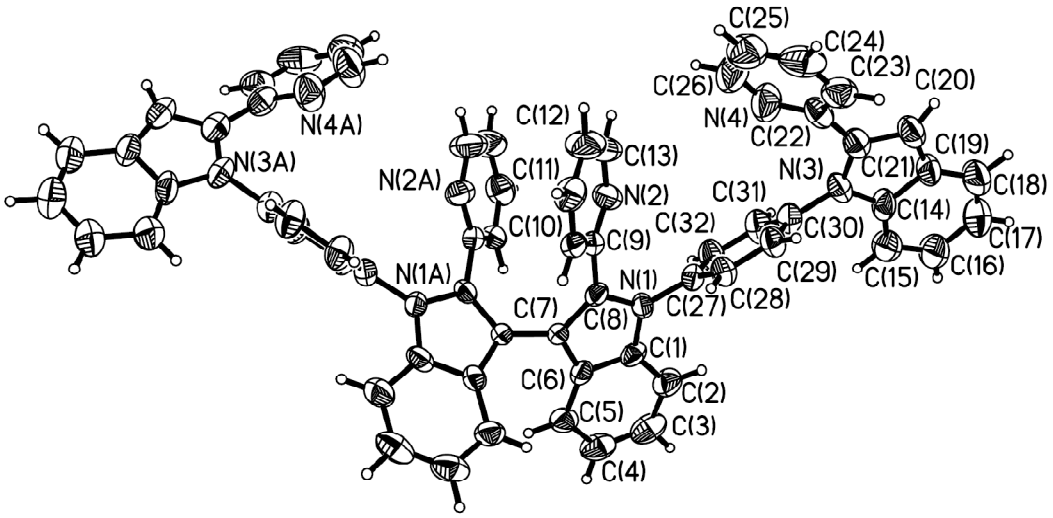

Figure 4.18 Crystal structure of bbib with labelling scheme and 50% thermal ellipsoids.

4.3.4 UV-Vis Absorption Spectra

The UV-Vis absorption spectrum of pib, bib and tib are all similar in shape, with the molar absorptivity increasing with the number of 2-(2'-pyridyl)indole chromophores as shown in Figure 4.19 and summarized in Table 4.3. The peaks at 230-308 nm are assigned to π-π* transitions.

Compared to their corresponding monomers, the bi-indolyl molecules have a shoulder peak at ~350 nm in the UV-Vis spectra, which most likely originates from π–π interactions of the two central pyridyl rings in the dimer, as revealed by the crystal structures of bpib and bbib. The molar absorptivities of the dimers also increase with the number of chromophores per molecule. All UV-Vis absorption spectra are shown in Figure 4.19.

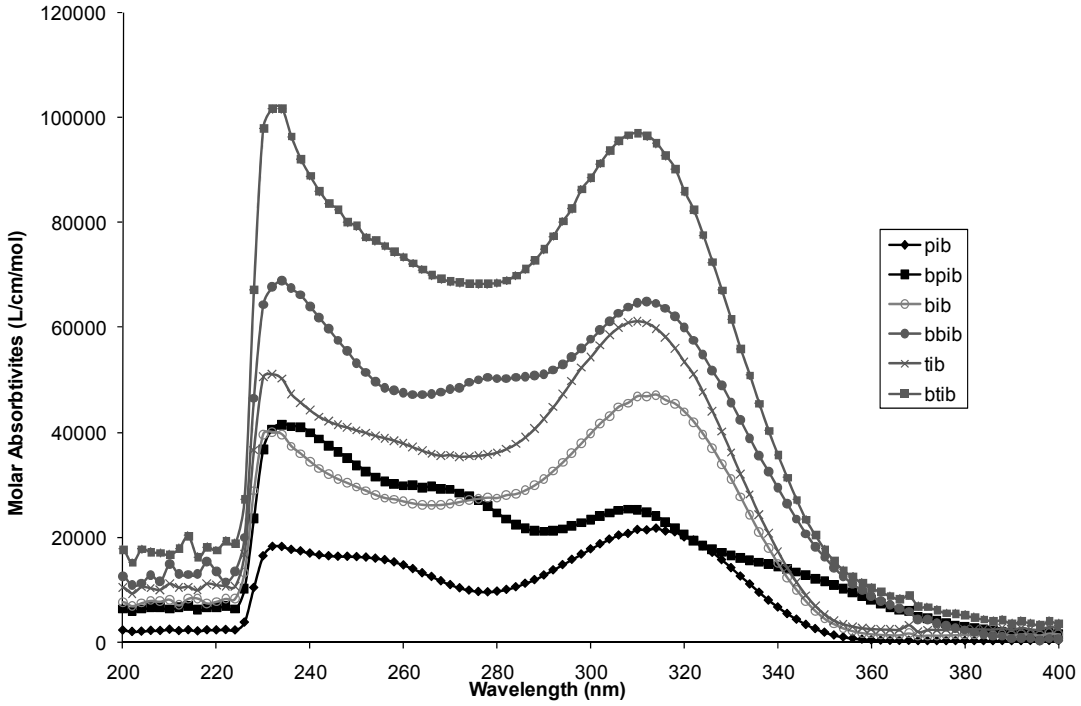

Figure 4.19 UV-Vis absorption spectra in CH_2Cl_2 for pib, bib, tib, bpib, bbib and btib.

4.3.5 Emission

The most significant difference between the monomer and the dimer is observed in the fluorescence spectra, as summarized in Table 4.3. As shown in Figure 4.20, all monomers emit in the UV region with λ_{max} = 385-389 nm (Φ = 0.45 for pib). In contrast, all dimers emit in the visible region with λ_{max} = ~445 nm (Φ = 0.22 for bpib). This dramatic spectral red shift and the identical emission spectra by all dimers are consistent with intramolecular excimer formation between the two central pyridyl rings in the dimer, a phenomenon similar to the recently reported intramolecular excimer emission involving

two carbazole rings[34] or two pyrene rings in a sterically constrained environment.[35, 36] The restricted rotation around the 3,3'-C-C bond in the dimer molecules is believed to facilitate the intramolecular py-py interaction and the excimer formation.

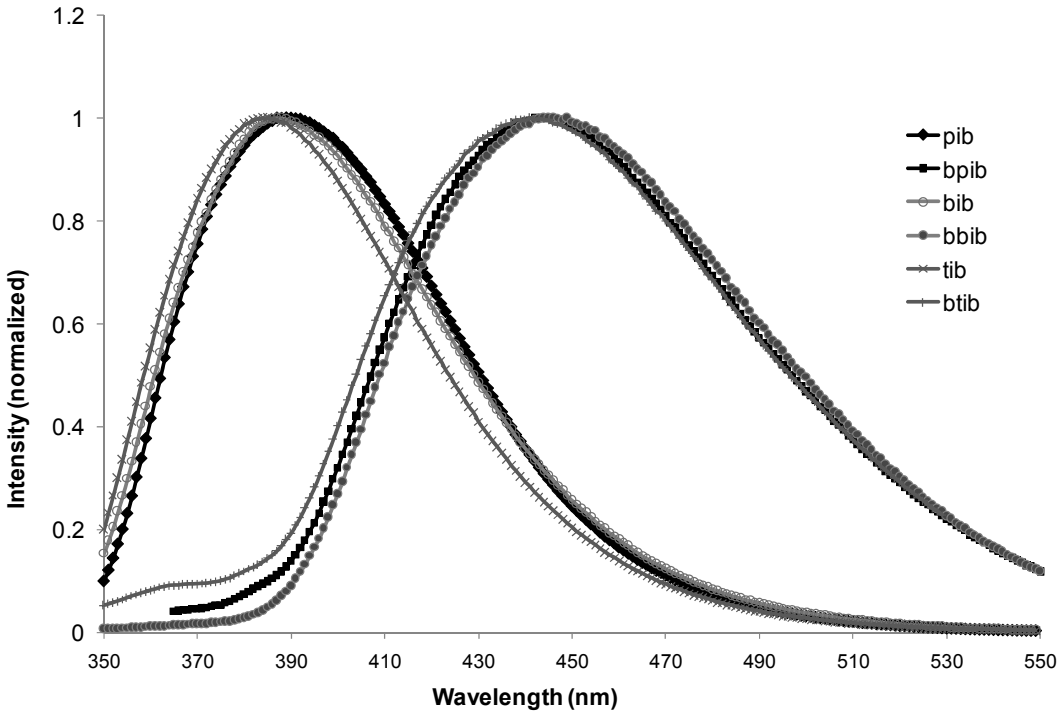

Figure 4.20 Emission spectra of pib, bib, tib, bpib, bbib and btib in CH_2Cl_2 at rt, ~$1x10^{-5}$ M.

Table 4.3 Absorption and emission data for pib, bib, tib, bpib, bbib and btib.

Compound	Absorption		Emission
	λ_{max} (nm)	ε x10^4 ($M^{-1}cm^{-1}$)	λ_{max}(nm)
pib	232	1.82	389
	256 s	1.57	
	312	2.14	
bib	232	4.00	387
	312	1.37	
tib	230	5.06	385
	258 s	3.84	
	310	6.12	
bpib	234	4.16	441
	270 s	2.92	
	308	2.54	
	344 s	1.34	
bbib	234	6.89	446
	278 s	5.04	
	312	6.49	
btib	232	10.2	441
	308	9.44	

4.3.6 DFT Calculations

4.3.6.1 Rotation Barrier of bpib

DFT calculations performed on bpib indicate that the rotation barrier around the 3,3' C-C bond is ~92 kJ/mol. By comparison with the rotation barriers reported for previously known axially chiral molecules,[15, 37, 38] it is concluded that the enantiomers of bpib may be resolvable at ambient temperature. Two peaks were observed in the energy profile when the energy of the complex was plotted against the dihedral angle between the indole rings, one peak was 92 kJ/mol above the most stable structure and the other was 110 kJ/mol above the most stable structure as shown in Figure 4.21. The calculation was first done using a lower basis set (STO-3G). The dihedral around the C-C bond connecting

the two indole rings was rotated 20°, doing a total of 18 geometry optimizations in a full rotation around the bond. Using the information from the first calculation it was repeated using a higher basis set (6-311+G(d)) ensuring the calculation covered with most stable and unstable structures. This time the dihedral was rotated 60° between each optimization, with a total of six geometry optimizations being performed.

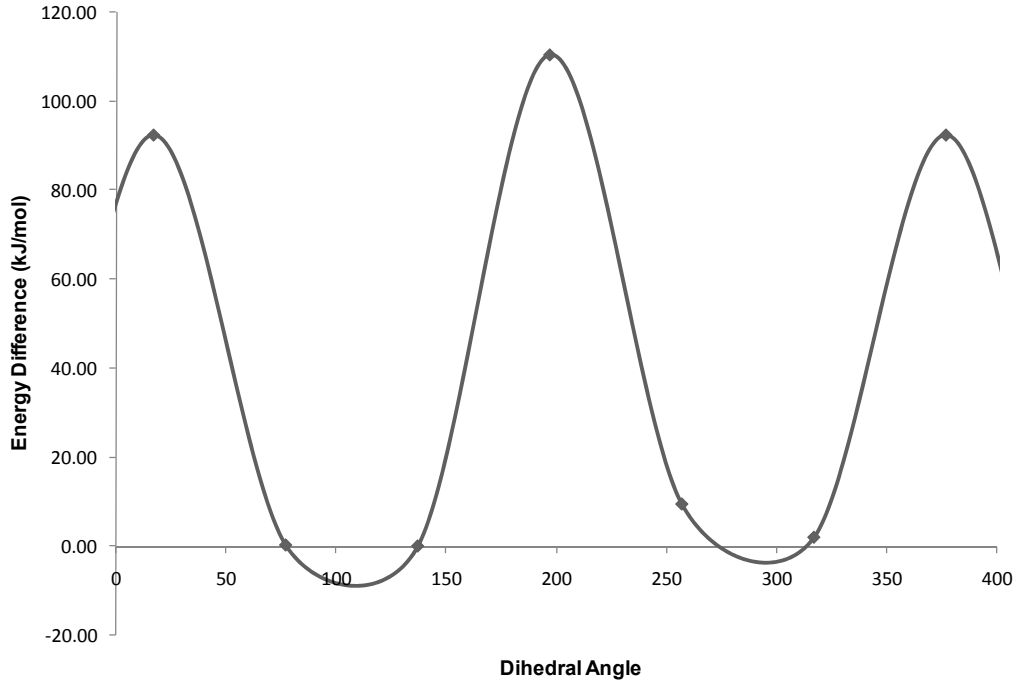

Figure 4.21 Plot of the calculated energy difference between the most stable structure and those at various dihedral angles around the C(8)-C(8A) bond of bpib.

4.3.6.2 Molecular Orbitals of pib and bpib

The molecular orbitals of pib and bpib were also calculated, and the HOMO and LUMO diagrams are shown in Figure 4.22. The calculated band gaps (4.12 eV for pib and 3.94

eV for bpib) are consistent with the absorption and emission data. The HOMO of pib is mainly π character on the pyridyl-indole, with a small contribution from the phenyl ring. The LUMO is mainly π* character. The HOMO and LUMO of bpib are also π and π* in character respectively, however there is considerable overlap between the neighbouring 2-(2'-pyridyl)indolyl groups. This supports that the lowest absorption and emission band is a result of exciplex emission in bpib. The dihedral angle between the indoles in the optimized structure is 148°, compared to 131° in the crystal structure the change could be due to intramolecular π- π interactions in the crystal structure.

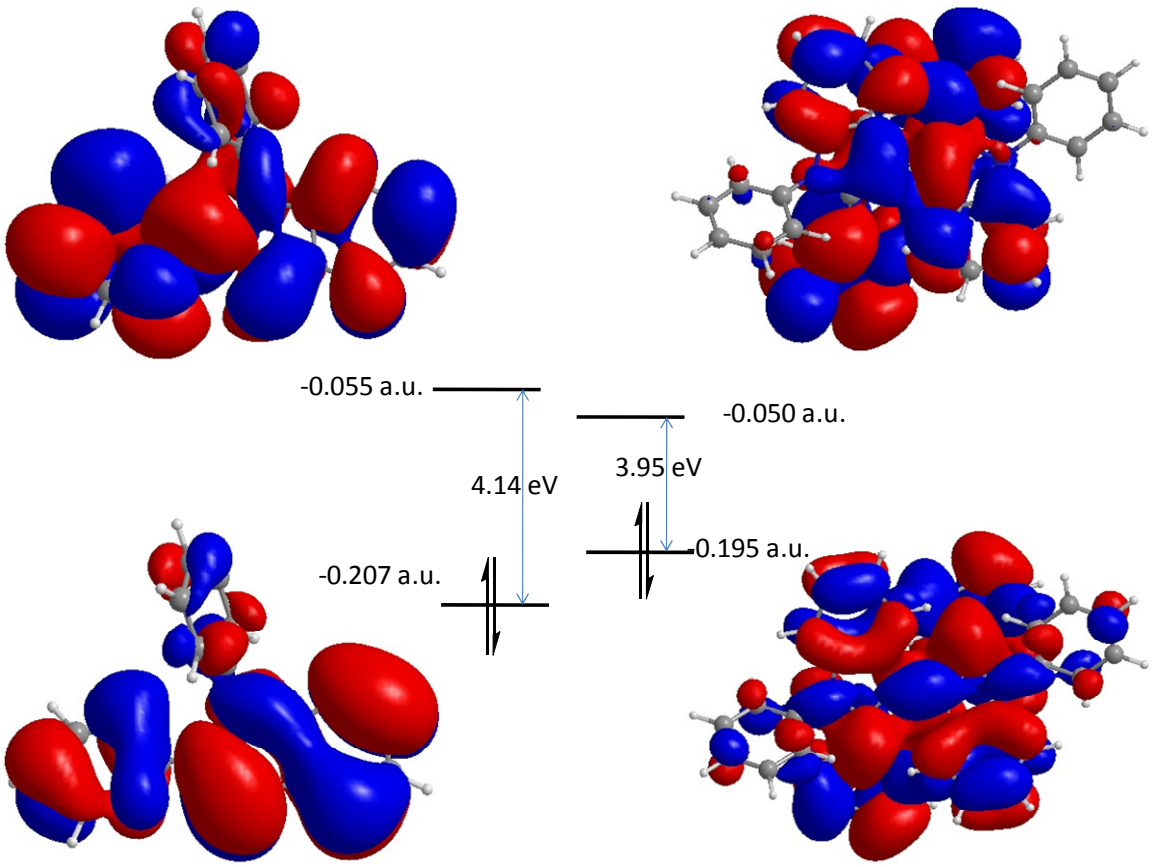

Figure 4.22 HOMO and LUMO diagrams for pib (left) and bpib (right) and the energies of the HOMO and LUMO levels are shown.

4.3.7 Separation of Enantiomers

Despite numerous attempts, efforts to resolve the enantiomers of the new atropisomeric ligands by repeated co-crystallization with optically pure tartaric acid using procedures[15] reported for 1,1'-bis(2-py-naphthyl) resolution have not been successful, possibly due to similar solubilities of the diastereomer salts. Chiral HPLC was also attempted to separate the enantiomers, but problems with solubility and limited access to HPLC and a variety

of stationary phases prevented success in this technique. Separation was tried using a Whelk-O stationary phase (based on 1-(3,5-dinitrobenzamido)-1,2,3,4-tetrahydro-phenanthrene, a π–electron acceptor/π-electron donor phase), however, no separation was achieved.

4.4 Conclusions

New 2-(2'-pyridyl)indolyl ligands with a benzene core have been achieved. This class of molecules are blue emitters with similar luminescent properties. A new class of atropisomeric ligands based on bis-indolyl have been discovered and synthesized by one-pot reactions catalyzed by copper ions. These reactions involve the formation of multiple C-N and C-C bonds and likely complex mechanisms that have not been fully understood. In addition, the new dimer ligands display intramolecular excimer emission and may be used to form chiral N,N chelate metal complexes, which may find applications in asymmetric catalysis and chiral sensing.

4.5 References

(1) Liu, S.; Wu, Q.; Schmider, H. L.; Aziz, H.; Hu, N.; Popovic, Z.; Wang, S. *J. Am. Chem. Soc.* **2000**, *122*, 3671.

(2) Liu, Q.; Mudadu, M. S.; Schmider, H.; Thummel, R.; Tao, Y.; Wang, S. *Organometallics* **2002**, *21*, 4743.

(3) Cravotto, G.; Demartin, F.; Palmisano, G.; Penoni, Andrea Radice, Tiziano; Tollari, S. *J. Organomet. Chem.* **2005**, *690*, 2017.

(4) Karshtedt, D.; McBee, J. L.; Bell, A. T.; Tilley, T. D. *Organometallics* **2006**, *25*, 1801.

(5) Tollari, S.; Cenini, S.; Penoni, A.; Granata, G.; Palmisano, G.; Demartin, F. *J. Organomet. Chem.* **2000**, *608*, 34.

(6) Wu, F.; Hardesty, J.; Thummel, R. P. *J. Org. Chem.* **1998**, *63*, 4055.

(7) Wu, F.; Chamchoumis, C. M.; Thummel, R. P. *Inorg. Chem.* **2000**, *39*, 584.

(8) Bringmann, G.; Price Mortimer, A. J.; Keller, P. A.; Gresser, M. J.; Garner, J.; Breuning, M. *Angew. Chem. Int. Ed.* **2005**, *44*, 5384.

(9) Wu, C. D.; Lin, W. *Angew. Chem. Int. Ed.* **2007**, *46*, 1076.

(10) Wu, C. D.; Zhang, L.; Lin, W. *Inorg. Chem.* **2006**, *45*, 7278.

(11) Shimizu, H.; Nagasaki, I.; Saito, T. *Tetrahedron* **2005**, *61*, 5404.

(12) McCarthy, M.; Guiry, P. J. *Tetrahedron* **2001**, *57*, 3809.

(13) Berens, U.; Brown, J. M.; Long, J.; Seike, R. *Tetrahedron: Asymmetry* **1996**, *7*, 285.

(14) Lehn, J. M. *Proc. Natl. Acad. Sci. U.S.A.* **2002**, *99*, 4763.

(15) Charmant, J. P. H.; Fallis, I. A.; Hunt, N. J.; Lloyd-Jones, G. C.; Murray, M.; Nowak, T. J. *J. Chem Soc. , Dalton Trans.* **2000**, 1723.

(16) Hassan, J.; Sévignon, M.; Gozzi, C.; Schulz, E.; Lemaire, M. *Chem. Rev.* **2002**, *102*, 1359.

(17) Antilla, J. C.; Klapars, A.; Buchwald, S. L. *J. Am. Chem. Soc.* **2002**, *124*, 11684.

(18) Lira, R.; Wolfe, J. P. *J. Am. Chem. Soc.* **2004**, *126*, 13906.

(19) Nandakumar, M. V.; Verkade, J. G. *Angew. Chem. Int. Ed.* **2005**, *44*, 3115.

(20) AI-Azawe, S.; Sarkis, G. Y. *J. Chem. Eng. Data* **1973**, *18*, 109.

(21) Caixach, J.; Capell, R.; Galvez, C.; Gonzalez, A.; Roca, N. J. *Heterocycl. Chem.* **1979**, *16*, 1631.

(22) Gaussian 03, Revision C.02, Frisch, M. J.; Trucks, G. W.; Schlegel, H. B.; Scuseria, G. E.; Robb, M. A.; Cheeseman, J. R.; Montgomery, Jr., J. A.; Vreven, T.; Kudin, K. N.; Burant, J. C.; Millam, J. M.; Iyengar, S. S.; Tomasi, J.; Barone, V.; Mennucci, B.; Cossi, M.; Scalmani, G.; Rega, N.; Petersson, G. A.; Nakatsuji, H.; Hada, M.; Ehara, M.; Toyota, K.; Fukuda, R.; Hasegawa, J.; Ishida, M.; Nakajima, T.; Honda, Y.; Kitao, O.; Nakai, H.; Klene, M.; Li, X.; Knox, J. E.; Hratchian, H. P.; Cross, J. B.; Bakken, V.; Adamo, C.; Jaramillo, J.; Gomperts, R.; Stratmann, R. E.; Yazyev, O.; Austin, A. J.; Cammi, R.; Pomelli, C.; Ochterski, J. W.; Ayala, P. Y.; Morokuma, K.; Voth, G. A.; Salvador, P.; Dannenberg, J. J.; Zakrzewski, V. G.; Dapprich, S.; Daniels, A. D.; Strain, M. C.; Farkas, O.; Malick, D. K.; Rabuck, A. D.; Raghavachari, K.; Foresman, J. B.; Ortiz, J. V.; Cui, Q.; Baboul, A. G.; Clifford, S.; Cioslowski, J.; Stefanov, B. B.; Liu, G.; Liashenko, A.; Piskorz, P.; Komaromi, I.; Martin, R. L.; Fox, D. J.; Keith, T.; Al-Laham, M. A.; Peng, C. Y.; Nanayakkara, A.; Challacombe, M.; Gill, P. M. W.; Johnson, B.; Chen, W.; Wong, M. W.; Gonzalez, C.; and Pople, J. A.; Gaussian, Inc., Wallingford CT, 2004.

(23) Bruker Analytical X-ray Systems **1999**, *version 5.10*.

(24)Liu, Q. D.; Jia, W. L.; Wang, S. *Inorg. Chem.* **2005**, *44*, 1332.

(25) Li, Z.; Bohle, D. S.; Li, C. J. *Proc. Natl. Acad. Sci. U.S.A.* **2006**, *103*, 8928.

(26) Li, Z.; Li, C. J. *Eur. J. Org. Chem.* **2005**, *127*, 3173.

(27) Li, Z.; Li, C. J. *J. Am. Chem. Soc.* **2005**, *127*, 3672.

(28) Li, Z.; Li, C. J. *J. Am. Chem. Soc.* **2004**, *126*, 11810.

(29) Dohi, T.; Morimoto, K.; Maruyama, A.; Kita, Y. *Org. Lett.* **2006**, *8*, 2007.

(30) Witkop, B.; Patrick, J. B. *J. Am. Chem. Soc.* **1951**, *73*, 713.

(31) Abramovitch, R. A.; Berkeley, W. Cue, Jr. *J. Org. Chem.* **1980**, *45*, 5316.

(32) Johnson, D. A.; Gribble, G. W. *Heterocycles* **1986**, *24*, 2127.

(33) Itami, K.; Kamei, T.; Yoshida, J. *J. Am. Chem. Soc.* **2003**, *125*, 14670.

(34) Benten, H.; Ohkita, H.; Ito, S.; Yamamoto, M.; Sakumoto, N.; Hori, K.; Tohda, Y.; Tani, K.; Nakamura, Y.; Nishimura, J. *J. Phys. Chem. B* **2005**, *109*, 19681.

(35) Benniston, A. C.; Harriman, A.; Howell, S. L.; Sams, C. A.; Zhi, Y. G. *Chem. Eur. J.* **2007**, *13*, 4665.

(36) Lodeiro, C.; Lima, J. C.; Parola, A. J.; Seixas de Melo, J. S.; Capelo, J. L.; Covelo, B.; Tamayo, A.; Pedra, B. *Sensors and Actuators B* **2006**, *115*, 276.

(37) Spivey, A. C.; Charbonneau, P.; Fekner, T.; Hochmuth, D. H.; Maddaford, A.; Malardier-Jugroot, C.; Redgrave, A. J.; Whitehead, M. A. *J. Org. Chem.* **2001**, *66*, 7394.

(38) Spivey, A. C.; Maddaford, A.; Leese, D. P.; Redgrave, A. J. *J. Chem. Soc. , Perkin Trans. 1* **2001**, 1785.

Chapter 5
Cu(I), Pd(II) and Pt(II) Complexes of 2-(2'-pyridyl)indolyl Based Ligands

5.1 Introduction

The ligands pib and bpib, discussed in Chapter 4, although both 2-(2'-pyridyl)indolyl based, have different coordination geometries. The ligand pib only has one nitrogen available to bind to a metal centre, and can also act as a C,N chelate if the C-H bond in the three position of the indole is activated. The ligand bpib is a chiral N,N chelate. Chiral ligands are essential to asymmetric catalysis. Most of the chiral ligands available are phosphine ligands that often contain either a 1,1-binaphthyl core such as BINAP (2,2'-bis(diphenylphosphino)-1,1'-binaphthyl),[1-7] or a biferrocene core such as 2,2'-bis[(diethylphosphino)methyl]-1,1'-biferrocene (EtTrap-H)[8, 9] shown in Figure 5.1. A review by Chelucci and Thummel outlined the importance of chiral nitrogen donor ligands in asymmetric homogeneous catalysis highlighting the ability to use pyridine based ligands in reactions where phosphines are incompatible with the reaction conditions.[10] Atropisomeric ligands involving pyridyl donors are scarce and only a few examples are known in literature.[11] As a result, metal complexes containing atropisomeric N,N-chelate ligands have not been adequately explored. In Chapter 4, a new class of pyridyl based atropisomeric ligands was introduced. This chapter examines the coordination chemistry and photophysical properties of the 2-(2'-pyridyl)indolyl

based ligands pib shown in Figure 5.2 and bpib shown in Figure 5.3 with the metal ions Cu(I), Pd(II) and Pt(II).

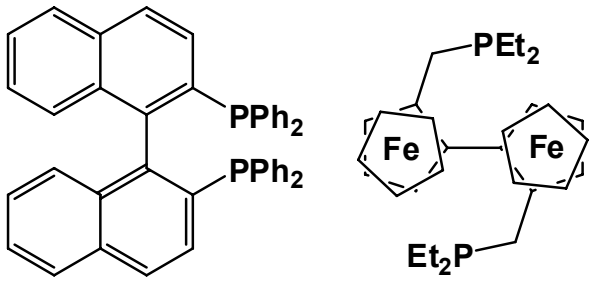

Figure 5.1 Structure of two common atropisomeric ligands BINAP and EtTrap-H.

The $[Cu(pib)(PPh_3)_2]BF_4$ (**5.1**) complex was made to compare the photophysical properties of a three coordinate Cu(I) complex to the four coordinate Cu(I) complexes discussed in Chapters 2 and 3. Use of Pt(II) and Pd(II) complexes as emitters has attracted attention because the strong spin-orbit coupling promotes efficient intersystem crossing from the singlet to the triplet excited-state allowing for efficient phosphorescent emitters.[12, 13] Unlike the Cu(I) pib complex, Pd(II) and Pt(II) metal ions can adopt a square-planar, cyclometallated geometry where the pib is a C,N chelate to the metal centre. Similar structures have been obtained for 2-(2'-pyridyl)indolyl based ligands where the nitrogen on the indole ring is protected with a methyl group.[14] Also cycloplatinated phenyl-pyridine complexes have shown MLCT based absorption bands.[15] C-N chelates with Pt(II) have been shown to form emissive aggregates that can be used in

white OLED complexes[16] Syntheses of the Pd(II) complex **5.2** and Pt(II) complex **5.3** have been accomplished – their structures and photophysical properties will be discussed.

Unlike pib, bpib has two pyridyl nitrogens available for binding metal ions. The investigation has shown that it acts as an N,N chelate for Cu(I), Pd(II) and Pt(II), with distinct geometries. The crystal structure of the Cu(I) complex was found be homo-chiral, having two bpib ligands, of the same chirality, coordinated to each Cu(I) centre. Homochiral crystallization from a racemic mixture is a rare event,[17-20] and in this case the enantiomers of the complex could be separated by selecting individual crystals. This was verified by measuring the circular dichroism spectrum of the crystals in solution. Homo-chiral crystallization was not observed for other metal complexes of bpib although the structures of the Pd(II) and Pt(II) complexes of bpib display unusual geometries. The details will be presented in this chapter.

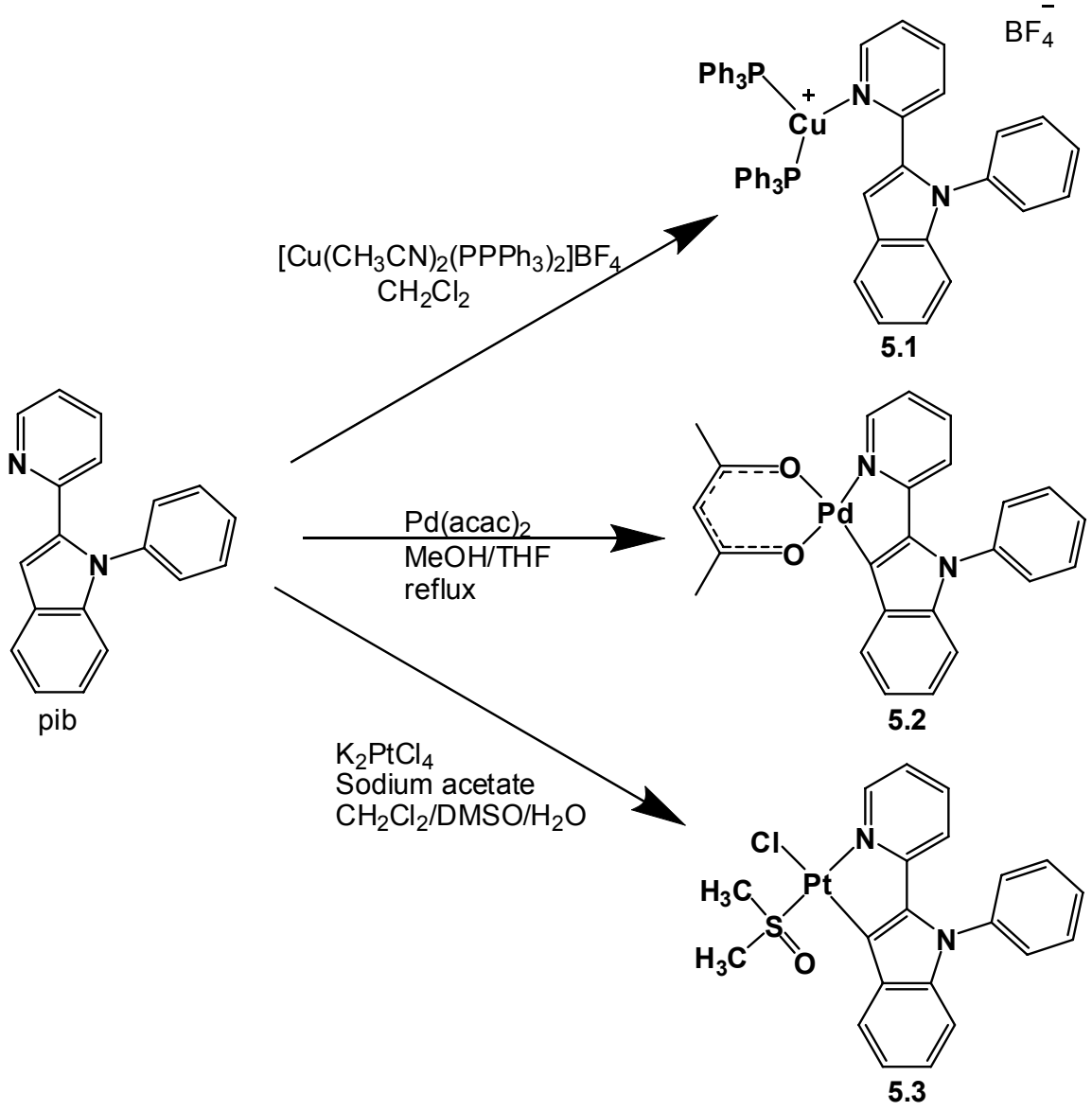

Figure 5.2 Syntheses of complexes **5.1-5.3**.

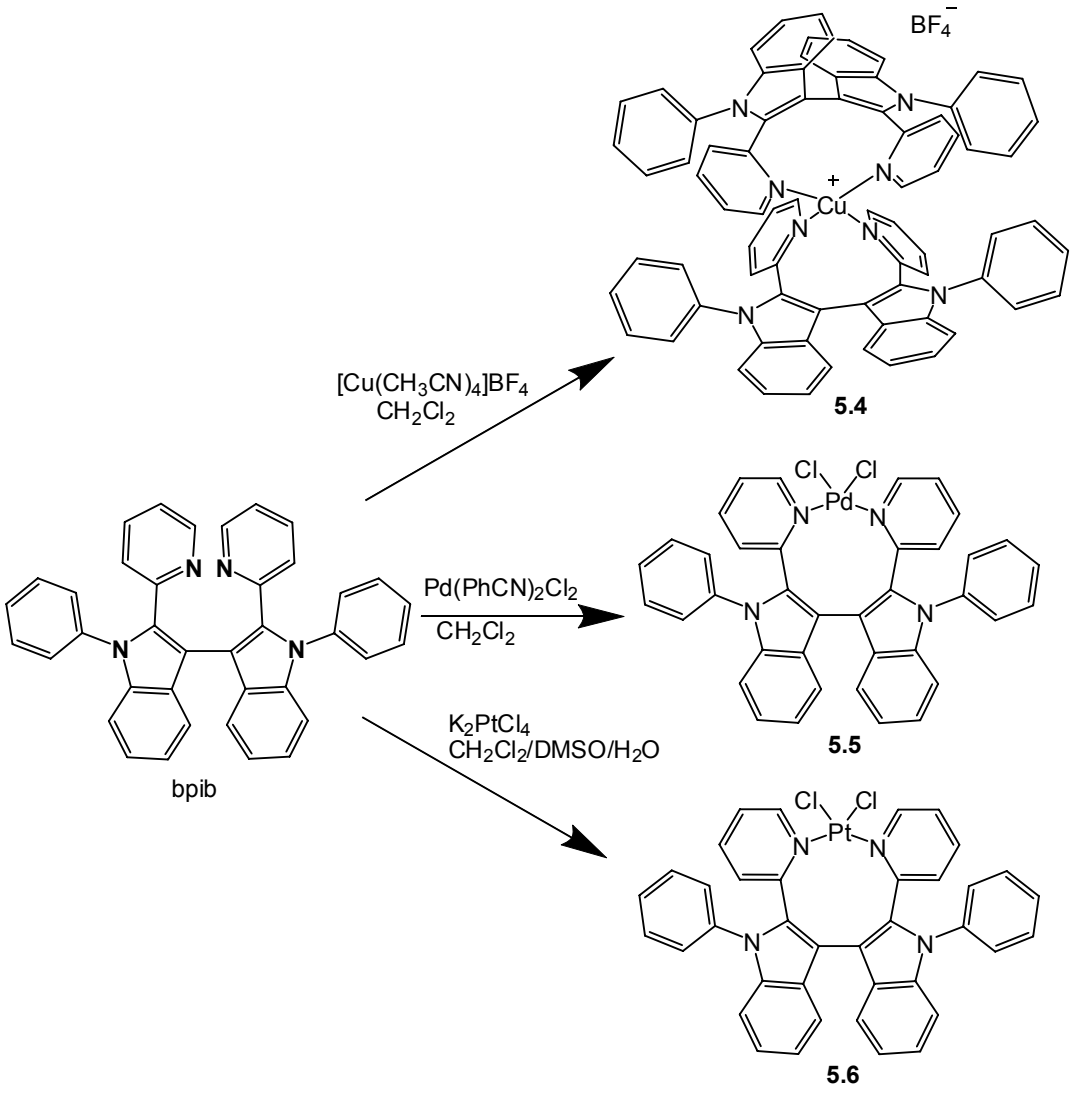

Figure 5.3 Syntheses of complexes **5.4-5.6.**

5.2 Experimental

5.2.1 General Considerations

All starting materials were purchased from Aldrich Chemical Company and used without further purification. Solvents were freshly distilled over appropriate drying reagents

under N_2 atmosphere. TLC was carried out on silica gel. Flash chromatography was carried out on silica (silica gel 60, 70-230 mesh). ^{1}H NMR spectra were recorded on a Bruker Avance 500 MHz spectrometer as stated. Excitation and emission spectra were recorded on a Photon Technologies International QuantaMaster Model C-60 spectrometer. Elemental analyses were performed by Canadian Microanalytical Service Ltd., Delta, British Columbia, Canada or at the University of Toronto, Canada. Circular dichroism (CD) spectra were recorded on a Jasco 715 spectrometer with a 1 cm path length. Copper(I) complexes, $[Cu(CH_3CN)_4][BF_4]$ and $[Cu(CH_3CN)_2(PPh_3)_2][BF_4]$,[21] and 2-(2'-pyridyl)indole[22, 23] were prepared based on literature procedures.

5.2.2 Synthesis of $[Cu(pib)(PPh_3)]BF_4$ (5.1)

In a dry box a solution of 42 mg (0.16 mmol) of pib in CH_2Cl_2 was stirred for 0.5 h with a solution of 120 mg (0.16 mmol) of $[Cu(CNCH_3)_2(PPh_3)_2]BF_4$ also in CH_2Cl_2. The clear colourless solution was layered with toluene. Clear, colourless crystals were obtained through slow diffusion after 5 days in a 73% yield. ^{1}H NMR in CD_2Cl_2, 500 MHz (δ, ppm, 253 K): 8.60 (d, J = 5 Hz, 1H), 7.75 (dd, J = 7.5 Hz, J = 7.5 Hz, 1H), 7.53 (dd, J = 5Hz, J = 5 Hz, 1H), 7.45-7.42 (m, 7H), 7.39 (d, J = 5 Hz, 1H), 7.35-7.32 (m, 2H), 7.29-7.26 (m, 2H), 7.17-7.14 (m, 14H), 6.96-6.92 (m, 12H), 6.87 (d, J = 10 Hz, 1H), 6.46 (d, J = 5 Hz, 2H). Anal calcd for $C_{55}H_{44}BCuF_4N_2P_2$: C, 69.89; H, 4.69; N, 2.96. Found: C, 69.89; H, 4.81; N, 2.93.

5.2.3 Synthesis of Pd(pib)(acac) (5.2)

The ligand pib (270 mg, 1.0 mmol) was dissolved in THF and mixed with 276 mg (0.99 mmol) of $Pd(acac)_2$ dissolved in MeOH. The mixture was stirred and refluxed for 12 h. The solvent was removed under reduced pressure. The orange coloured residue was dissolved in CH_2Cl_2 to give a yellow solution. By slow evaporation of the solvent three types of crystals were obtained, a colourless crystal identified as pib, an orange crystal identified as $Pd(acac)_2$ and a yellow crystal of the desired product in 25% yield. The crystals were manually separated and **5.2** was recrystallized from CH_2Cl_2 and hexanes. ^{1}H NMR in CD_2Cl_2, 500 MHz (δ, ppm, 298 K): 8.76 (d, *J* = 5.0 Hz, 1H), 8.25 (d, *J* = 7.5 Hz, 1H), 7.64-7.61 (m, 2H), 7.56 (dd, *J* = 7.5 Hz, *J* = 7.5 Hz, 1H), 7.50-7.45 (m, 3H), 7.19 (dd, *J* = 7.5 Hz, *J* = 7.5 Hz, 1H), 7.10 (dd, *J* = 7.5 Hz, *J* = 7.5 Hz, 1H), 7.03 (d, *J* = 8.3 Hz, 1H), 6.95 (dd, *J* = 7.5 Hz, *J* = 7.5 Hz, 1H), 5.36 (s, 1H), 6.45 (d, *J* = 8.2 Hz, 1H), 2.22 (s, 3H), 2.13 (s, 3H),. Anal calcd for $C_{24}H_{23}N_2O_2Pd$: C, 60.32; H, 4.85; N, 5.86. Found: C, 60.66; H, 4.21; N, 5.80.

5.2.4 Synthesis of Pt(pib)Cl(dmso) (5.3)

A solution of pib (100 mg, 0.37 mmol) in 5 mL of CH_2Cl_2 was added to a solution of K_2PtCl_4 (140 mg, 0.37 mmol) in 5 mL of water and 1 mL of DMSO. The biphasic mixture was stirred for 1h until the organic layer turned yellow. The base sodium acetate (31 mg, 0.37 mmol) was added and the solution was allowed to stir overnight. The CH_2Cl_2 organic layer was extracted and washed 3 times with water. The organic layer was dried with $MgSO_4$ and the solvent was removed under vacuum. The red residue was

then dissolved in a minimum of CH_2Cl_2 to give a yellow solution that was layered with THF and hexanes. Slow diffusion afforded deep red crystals after 7 days in 57 % yield. ^{1}H NMR in CD_2Cl_2, 500 MHz (δ, ppm, 298 K): 9.57(d, satellites, J = 5 Hz, J_{Pt-H} = 20 Hz, 1H), 8.50 (d, J = 5 Hz, 1H), 7.66-7.61 (m, 3H), J = 7.5 Hz, 1H), 7.19 (dd, J = 7.5 Hz), 7.11 (dd, J = 5 Hz, J = 5 Hz, 1H), 7.03 (dd, J = 5 Hz, J = 5 Hz, 1H), 6.98 (d, J = 10 Hz, 1H), 6.43 (d, J = 10 hz, 1H), 7.48-7.43 (m, 3H), 3.73 (s, satellites, J_{Pt-H} = 11.75 Hz, 6H). Anal calcd for $C_{21}H_{19}ClN_2OPtS$: Calc: C, 43.64; H, 3.31; N, 4.85. Found: C, 43.65; H, 3.30; N, 5.14.

5.2.5 Synthesis of $[Cu(bpib)_2]BF_4$ (5.4)

A solution of 3 mg (9 μmol) of $[Cu(CH_3CN)_4]BF_4$ in *ca*. 3 mL of CH_2Cl_2 was added drop wise to a stirred solution of 10 mg (18 μmol) of bpib in ca 3 mL of CH_2Cl_2 in the dry box. The solution turned from clear colorless to a clear orange solution. The solution was stirred for 15 minutes and then layered with toluene. Red-orange crystals were obtained through slow diffusion and evaporation of solvents after one week in 88% yield. ^{1}H NMR in CD_2Cl_2, 500 MHz (δ, ppm, 233 K): 7.76 (d, J = 10 Hz, 1H), 7.68 (dd, J = 7.5 Hz, J = 7.5 Hz, 1H), 7.59-7.56 (m, 1H), 7.47 (dd, J = 7.5 Hz, J=7.5 Hz, 1H), 7.27 (d, J = 10 Hz, 1H), 7.20 (d, J = 10 Hz, 1H), 7.15 (dd, J = 7.5 Hz, J = 7.5 Hz, 1H), 6.98 (d, J = 10 Hz, 1), 6.88 (dd, J = 5.0 Hz, J = 5.0 Hz,1H), 6.79 (dd, J = 7.5, J = 7.5 Hz, 1H), 6.57 (m, 2H), 4.78 (d, J = 10 Hz, 1H). Anal calcd for $C_{76}H_{52}BCuF_4N_8 \cdot 1.5CH_2Cl_2$: C, 68.70; H, 4.06; N, 8.27. Found: C, 69.22; H, 4.11; N 8.39.

5.2.6 Synthesis of Pd(bpib)Cl_2 (5.5)

A solution of 150 mg (280 μmol) of bpib in THF was layered with a solution of 108 mg of palladium bis-(phenylacetonitrile) dichloride (280 μmol) in ethyl acetate to give a red powder. The residue was re-dissolved in CH_2Cl_2, slow evaporation of solvent resulted in red crystals in ca. 3 days (62% yield). ^{1}H NMR in CD_2Cl_2, 500 MHz (δ, ppm, 263 K): 8.43 (d, *J* = 5 Hz, 1H), 7.83 (d, *J* = 10 Hz, 1H), 7.62 (dd, *J* = 7.5 Hz, *J* = 7.5 Hz, 1H), 7.54 (dd, *J* = 7.5 Hz, *J* = 7.5 Hz, 1H), 7.41 (d, *J* = 5 Hz, 2H), 7.38 (d, *J* = 5 Hz, 1H), 7.30 (d, *J* = 10 Hz, 1H), 7.26-7.18 (m, 4H), 7.10 (dd, *J* = 7.5 Hz, *J* = 7.5 Hz, 1H). Anal calcd for $C_{38}H_{26}N_4PdCl_2$: C, 63.75; H, 3.66; N, 7.83. Exp: C, 62.32; H, 3.47; N, 7.51.

5.2.7 Synthesis of Pt(bpib)Cl_2 (5.6)

A mixture of 1 mL DMSO, 5 mL H_2O and 5 mL CH_2Cl_2 was used to dissolve K_2PtCl_4 (85 mg, 206 μmol). The mixture was stirred for 30 minutes until the organic layer became yellow. A solution of bpib (100mg, 187 μmol) in 3 mL of CH_2Cl_2 was slowly added. The mixture was refluxed for 6 h. The organic layer was extracted and washed three times with water. The solvent was removed under vacuum to leave a yellow film. After CH_2Cl_2 was added, the mixture was filtered to remove the white powder. The white powder was identified as $Pt(DMSO)_2Cl_2$. The yellow solution was allowed to slowly evaporate to afford orange crystals of **5.6** in 13% yield. ^{1}H NMR in CD_2Cl_2, 500 MHz (δ, ppm, 263 K): 8.77 (d, *J* = 5.6 Hz, 1H), 8.14 (d, *J* = 7.7 Hz, 1H), 7.87 (d, *J* = 7.6 Hz, 1H), 7.52-7.49 (m, 2H), 7.47 (d, *J* = 8 Hz, 1H), 7.39 (dd, *J* = 7.5, *J* = 7.5, 1H), 7.35 (dd, *J* = 7 Hz, J= 7 Hz, 1H), 7.27 (dd, *J* = 7.5 Hz, 1H), 7.12 (dd, *J* = 7.5 Hz, *J* = 7.5 Hz,

1H), 6.98-6.95 (m, 2H), 6.73 (d, J = 9 Hz, 1H). Anal calcd for $C_{38}H_{26}Cl_2N_4Pt \cdot CH_2Cl_2$: C, 52.66; H, 3.17; N, 6.30. Exp: C, 52.03; H, 3.24; N, 6.33.

5.2.8 X-ray Diffraction

Single crystals of compounds **5.1**-**5.6** were obtained. Crystals were mounted on glass fibres for data collection. Data were collected on a Bruker Apex II single-crystal X-ray diffractometer with monochromated Mo Kα radiation, operating at 50 kV and 30 mA at 180 K. No significant decay was observed for any sample. Data were processed on a PC using the Bruker SHELXTL software package10 (version 5.10)[24] and were corrected for Lorentz and polarization effects. Compound **5.1** belongs to the triclinic space group *P*-1. Compound **5.2** belongs to the orthorhombic space group $P2_12_12_1$. Compounds **5.3, 5.5** and **5.6** belong to the monoclinic space groups $P2_1$, *C*2/*c*, and *C2/c*, respectively. Compound **5.4** belongs to the chiral tetragonal space group *I422*. These were determined by the systematic absences and the successful solution and refinements of the structures. Solvent molecules were located in the crystal lattices for **5.4 - 5.6**. For **5.4**, each molecule co-crystallizes with four CH_2Cl_2 solvent molecules and for **5.5** and **5.6**, there are two CH_2Cl_2 per molecule. The BF_4^- anions in compounds **5.1** and **5.4** were also found to display some degree of disordering and were refined successfully. Most non-hydrogen atoms except the disordered ones in **5.1** and **5.4** were refined anisotropically. All hydrogen atoms were calculated, and their contributions were included in structural factor calculations. The crystallographic data are reported in Table 5.1 for **5.1-5.3** and in Table 5.2 for **5.4-5.6**. Selected bond lengths and angles are reported in Table 5.3.

Table 5.1 Crystal structure data for complexes **5.1-5.3**.

	5.1	**5.2**	**5.3**
formula	$C_{55}H_{44}B_1Cu_1F_4N_2P_2$	$C_{24}H_{20}N_2O_2Pd_1$	$C_{21}H_{19}Cl_1N_2O_1Pt_1S_1$
fw	945.21	474.82	577.98
space group	P-1	$P2_12_12_1$	$P2_1$
a, Å	11.1351(10)	12.1096(18)	9.5841(2)
b, Å	12.2860(11)	12.2832(18)	18.7723(3)
c, Å	17.1702(16)	12.777(2)	11.4484(2)
α, deg	84.859(2)	90.00	90.00
β, deg	87.411(2)	90.00	107.6690(10)
γ, deg	74.293(2)	90.00	90.00
V, Å^3	2251.6(4)	2049.2(4)	1962.58(6)
Z	2	4	4
D_{calc}, gcm^{-3}	1.394	1.539	1.956
μ, cm^{-1}	6.14	9.28	74.06
$2\theta_{max}$, deg	56.31	52.00	54.26
no. of reflns measd	15767	10916	15172
no. of reflns used (R_{int})	10297 (0.0280)	4022	7612 (0.0190
no. of params	595	265	492
final *R* [I > 2σ(I)]			
R1[a]	0.0453	0.0497	0.0182
*w*R2[b]	0.0743	0.1159	0.0370
R (all data)			
R1[a]	0.1051	0.0720	0.0191
*w*R2[b]	0.0855	0.1316	0.0372
GOF on F^2	0.816	1.074	1.086

[a] $R1 = \Sigma[|F_o| - |F_c|]/\Sigma|F_o|$. [b] $wR2 = \{\Sigma[w(F_o^2 - F_c^2)]/ \Sigma(wF_o^2)\}^{1/2}$.

$\omega = 1/[\sigma^2(F_o^2) + (0.075P)^2]$, where $P = [\max.(F_o^2,0) + 2F_c^2]/3$.

Table 5.2 Crystal structure data for **5.4-5.6.**

	5.4	**5.5**	**5.6**
formula	$C_{80}H_{60}B_1Cl_8Cu_1F_4N_8$	$C_{40}H_{30}Cl_6N_4Pd_1$	$C_{40}H_{30}Cl_6N_4Pt_1$
fw	1567.30	885.78	974.47
space group	I422	C2/c	C2/c
a, Å	20.783(2)	17.8880(11)	17.8594(2)
b, Å	20.783(2)	12.3483(8)	12.3237(2)
c, Å	17.347(2)	17.3962(11)	17.4634(2)
α, deg	90.00	90.00	90.00
β, deg	90.00	102.9640(10)	103.1340(10)
γ, deg	90.00	90.00	90.00
V, Å3	7492.4(13)	3744.6(4)	3743.04(9)
Z	4	4	4
Dcalc, gcm-3	1.389	1.571	1.729
μ, cm-1	6.37	9.60	42.13
2θmax, deg	56.66	56.48	54.2
no. of reflns measd	23223	20627	12925
no. of reflns used (Rint)	4570 (0.1416)	4378 (0.0184)	7366 (0.0175)
no. of params	236	231	231
final R [I > 2σ(I)]			
R1a	0.0702	0.0258	0.0206
wR2b	0.1553	0.0654	0.0468
R (all data)			
R1a	0.1745	0.0271	0.0230
wR2b	0.1761	0.0662	0.0468
GOF on F2	0.706	1.068	1.061

[a] $R1 = \Sigma[|F_o| - |F_c|]/\Sigma|F_o|$. [b] $wR2 = \{\Sigma[w(F_o^2 - F_c^2)]/ \Sigma(wF_o^2)\}^{1/2}$.

$\omega = 1/[\sigma^2(F_o^2) + (0.075P)^2]$, where $P = [\max.(F_o^2,0) + 2F_c^2]/3$.

Table 5.3 Selected bond lengths (Å) and angles (°) for complexes **5.1-5.6.**

		5.1	
Cu(1)-P(2)	2.2134(8)	N(1)-Cu(1)-P(2)	127.14(6)
Cu(1)-P(1)	2.2640(7)	N(1)-Cu(1)-P(1)	105.22(6)
Cu(1)-N(1)	2.003(2)	P(2)-Cu(1)-P(1)	126.36(3)
		5.2	
Pd(1)-C(2)	1.968(7)	C(2)-Pd(1)-O(2)	93.2(2)
Pd(1)-O(2)	1.997(5)	C(2)-Pd(1)-N(2)	80.8(3)
Pd(1)-N(2)	2.045(6)	O(2)-Pd(1)-N(2)	173.7(2)
Pd(1)-O(1)	2.066(5)	C(2)-Pd(1)-O(1)	173.3(2)
O(2)-Pd(1)-O(1)	93.2(2)	C(10)-C(9)-C(1)	130.5(7)
N(2)-Pd(1)-O(1)	92.8(2)	N(2)-C(9)-C(1)	109.7(6)
		5.3	
Pt(1)-C(2)	2.000(3)	C(2)-Pt(1)-N(1)	80.38(16)
Pt(1)-N(1)	2.078(4)	C(2)-Pt(1)-S(1)	95.14(14)
Pt(1)-S(1)	2.2043(11)	N(1)-Pt(1)-S(1)	173.95(10)
Pt(1)-Cl(1)	2.3678(10)	C(2)-Pt(1)-Cl(1)	172.19(13)
S(1)-Pt(1)-Cl(1)	92.51(4)	N(1)-Pt(1)-Cl(1)	91.88(10)
N(1)-C(9)-C(1)	111.5(4)		
		5.4	
N-Cu	2.076(5)	N(1)-Cu(1)-N(1A)	137.1(3)
		N(1)-Cu(1)-(N1B)	98.3(3)
		5.6	
Pd(1)-N(2)	2.0206(14)	Cl(1A)-Pd(1)-Cl(1)	65.22(3)
Pd(1)-Cl(1)	2.3092(4)	C(7)-C(8)-C(9)	106.54(15)
N(2)-Pd(1)-Cl(1A)	88.70(4)	C(7)-C(8)-C(8A)	29.71(18)
C(9)-C(8)-C(8A)	23.03(16)	N(2)-Pd(1)-Cl(1)	93.22(4)
C(8)-C(7)-C(19)	31.48(15)		
		5.6	
Pt(1)-N(3)	1.982(11)	N(3)-Pt(1)-N(1)	164.62(14)
Pt(1)-N(1)	2.054(9)	N(3)-Pt(1)-Cl(2)	93.7(3)
Pt(1)-Cl(2)	2.301(4)	N(1)-Pt(1)-Cl(2)	89.3(3)
Pt(1)-Cl(1)	2.312(4)	N(3)-Pt(1)-Cl(1)	87.0(3)
N(1)-Pt(1)-Cl(1)	92.8(3)	Cl(2)-Pt(1)-Cl(1)	169.80(3)

5.3 Results and Discussion

5.3.1 Synthesis

The ligands were synthesized as described in Chapter 4. The syntheses of the pib based complexes **5.1-5.3** are shown in Figure 5.2. The syntheses of bpib based complexes **5.4-5.6** are shown in Figure 5.3. Complex **5.1** was synthesized under a nitrogen atmosphere by stirring pib with $Cu(CNCH_3)_2(PPh_3)_2$ in CH_2Cl_2. Slow evaporation of the solvent resulted in clear colourless crystals in 73% yield. The solid was stable under air.

Pib acts as a C,N chelate ligand with Pd(II) and Pt(II) with the deprotonation of the indole ring. The cyclometallated complex **5.2** was prepared by heating pib with one equivalent of $Pd(acac)_2$. The generally accepted mechanism of this cyclometallation involves the coordination of the pyridyl nitrogen to the Pd(II), followed by electrophilic substitution by the Pd(II) at the three position of the indole ring.[15] The acac acts as a base to aid the deprotonation of the indole ring in the three position for cyclometallation. This reaction gave a low yield and some of the starting materials were recovered. A stronger base may allow for better conversion of the reactants to the desired product. The crystals of **5.2** were manually separated from the crystals of the starting material under a microscope, and subsequently recrystallized to give stable orange crystals.

Both of the Pt(II) complexes **5.3** and **5.6** were prepared using K_2PtCl_4 and the corresponding ligand refluxed in water:DMSO:CH_2Cl_2 5:1:5 mixture for six hours. The K_2PtCl_4 is dissolved in the water, and then reacts with DMSO to give $Pt(DMSO)_2Cl_2$ in the organic layer that then reacts with the ligand. However, for **5.3** a base was added to

the reaction mixture after one hour to facilitate deprotonation of pib and subsequent cyclometallation. Complex **5.3** crystallized in large stable red block crystals in reasonable yield. Conversely, for **5.6** the yield was low, but orange crystals could be isolated through slow evaporation of the solvent. $Pt(DMSO)_2Cl_2$, as well as un-coordinated bpib was also isolated from the reaction mixture of **5.6**.

The complex **5.4** was made under a nitrogen atmosphere. Using either $[Cu(CH_3CN)_2(PPh_3)_2]BF_4$ or $[Cu(CH_3CN)_4]BF_4$ as the starting material yielded the same 2:1 bpib:Cu complex. Unexpectedly bpib displaces the triphenylphosphine ligands, and no $[Cu(bpib)(PPh_3)_2]^+$ was observed. This is likely due to stabilization of the 2:1 complex by both the chelation effect and interligand π-π interactions on the complex. Stable red crystals were isolated through slow evaporation of solvents.

Complex **5.5** was produced when bpib was dissolved in THF and mixed with a stoichiometric amount palladium bis-(phenylnitrile) dichloride dissolved in CH_2Cl_2. A red powder came out of the solution that produced red crystals through slow evaporation after the power was re-dissolved CH_2Cl_2. The chelating bpib ligand displaces the labile phenylnitrile ligands. All complexes were characterized by x-ray diffraction analyses.

5.3.2 Crystal Structures

5.3.2.1 Structure of **5.1**

Complex **5.1** crystallizes in the triclinic space group *P-1* with the BF_4 anion showing three site disordering. The Cu(1) centre has a distorted trigonal planar geometry with a P(2)-Cu(1)-P(1) bond angle of 126.36(3)°, shown in Figure 5.4. The P-Cu-N angles are

127.14(6)° and 105.22(6)° for N(1)-Cu(1)-P(2) and N(1)-Cu(1)-P(1) respectively. The difference in bond angles is caused by the indolyl moiety being twisted with respect to the pyridyl ring (torsion of 135.68° for N(2)-C(6)-C(5)-N(1)). This results in the phenyl ring being closer to P(2) increasing the steric strain on that side of the molecule. The Cu(1)-N(1) bong length is 2.003(2) Å. This is only slightly shorter than the bond length found for the tetrahedral triphenylphosphine complex **2.1** previously reported that has Cu-N bond length of 2.092(4) Å. It is noteworthy that the H(7A)-Cu(1) (where H(7A) is the proton on the C3 of the indole) distance is 2.585 Å. This proximity may be responsible for the Cu(I) activated homo-coupling of the bpib discussed in Chapter 4 as shown Figure 5.4. The packing structure of **5.1** shows edge to face π interactions between the phenyl ring on the pib ligand of one molecule with the phenyl ring on one of the triphenylphosphines of another with a C-C separation of 3.523Å.

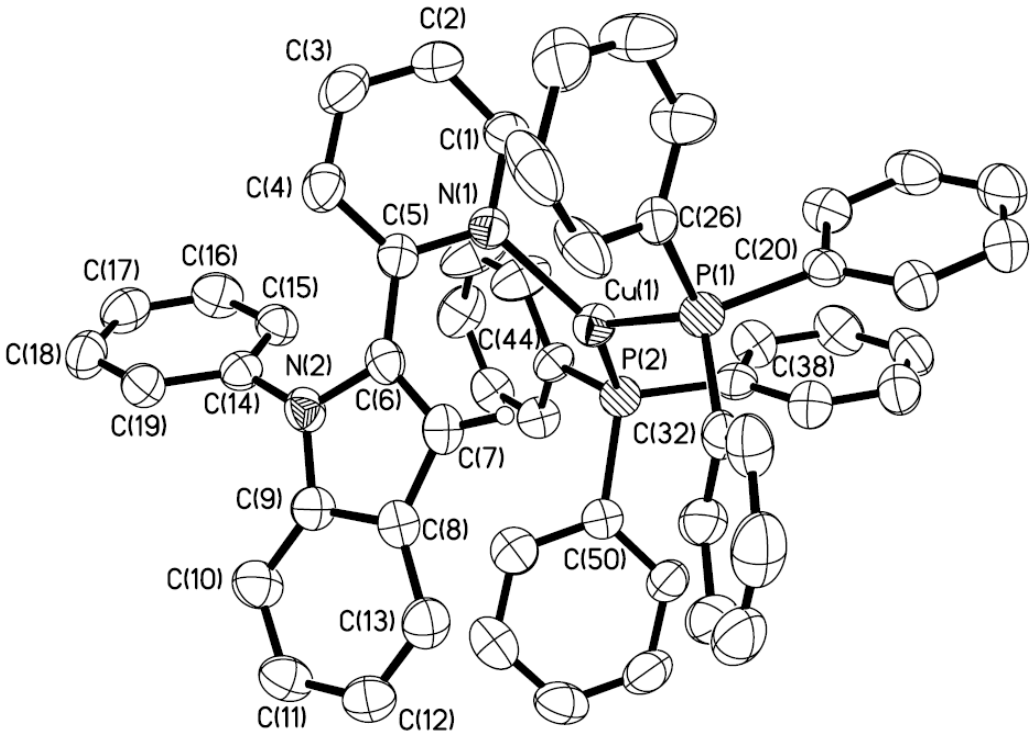

Figure 5.4 Structure of **5.1** with 50% thermal ellipsoids where hydrogen atoms (expect H(7A)) and the disordered BF_4^- were removed for clarity.

5.3.2.2 Structures of **5.2** and **5.3**

Complexes **5.2** and **5.3** have the same cyclometallated N,C-chelate structures around the metal centres for the pib ligand, but the ancillary ligands are different. The structure of **5.2** is shown in Figure 5.5. Complex **5.2** has an acetylacetonate (acac) ancillary ligand with Pd(1)-O(1) and Pd(1)-O(2) distances of 2.066(5) Å and 1.997(5) Å respectively. The Pd(1)-N(2) bond length is 1.968(7) Å which is comparable to the Pd-N bond length reported for a similar cyclopalladated complex with the ligand 2-(2-pyridyl)benzo[b]-

furan that has a Pd-N bond length of 1.996(2) Å.[25] This same complex has a C-Pd bond length of 1.972(2) Å which is also similar to the Pd(1)-C(2) bond length found for complex **5.2** of 1.968(7) Å. The Pd atom is in a slightly distorted square planar geometry with the O(1)-Pd(1)-O(2) angle being 93.2(2)° and the N(2)-Pd(1)-C(2) angle being more constrained at 80.8(3)° due to the formation of a five membered ring (the 2-(2-pyridyl)-benzo[b]furan complex has a N-Pd-C bond angle of 81.36(9)°). The C-N chelation forces the pyridyl ring to be in the same plane as the indolyl. The C(1)-C(9)-N(2) bond angle is only 109.7(6)°, an obvious ring strain caused by the formation of the five membered cyclometallated ring. There are no apparent Pd-Pd or π-π interactions in the crystal structure; the closest Pd-Pd distance is 7.409Å.

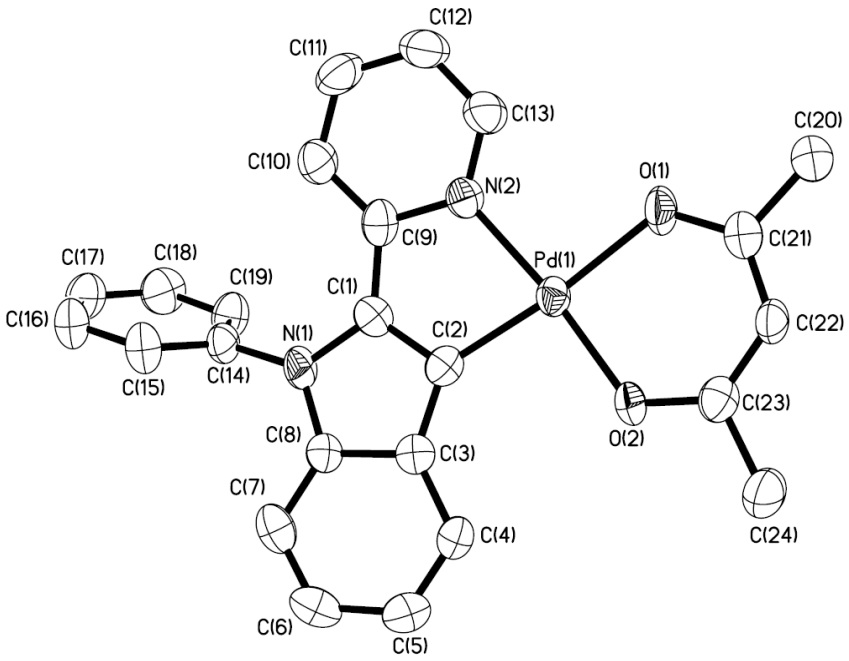

Figure 5.5 Crystal structure of **5.2** with 50% thermal ellipsoids, the hydrogen atoms have been removed for clarity.

The structure of **5.3** is shown in Figure 5.6. The geometry around the Pt(1) centre in **5.3** is quite similar to Pd(1) in **5.2**. However, the Pt coordination sphere in **5.3** is completed with one Cl and a DMSO solvent molecule. The C(2)-Pt(1)-N(1) bond angle is 80.38(16)°. The N(1)-C(9)-C(1) bond angle is slightly more relaxed than **5.2** with an angle of 111.5(4)°. The Pt(1)-C(2) bond length is 2.000(3) Å, only slightly longer than Pd-C bond length in **5.2**. The Pt(1)-N(1) is also slightly longer than that of the Pd-N with a bond length of 2.078(4) Å. There are two independent molecules in the asymmetric unit with a Pt-Pt distance of 5.519 Å. For **5.3** the pyridyl ring of one molecule interacts with the indole of the other with a distance of 3.321Å. The crystal structure of the Pt(II) complex of 1-methyl-2-(2'-pyridyl)-1*H*-indole has been reported in literature and shows similar geometry around the Pt(II) centre with the Pt-N and Pt-C bond lengths being 2.063(16) Å and 2.038(14) Å respectively, and a C-Pt-N bond angle of 79.7(6)°.[14]

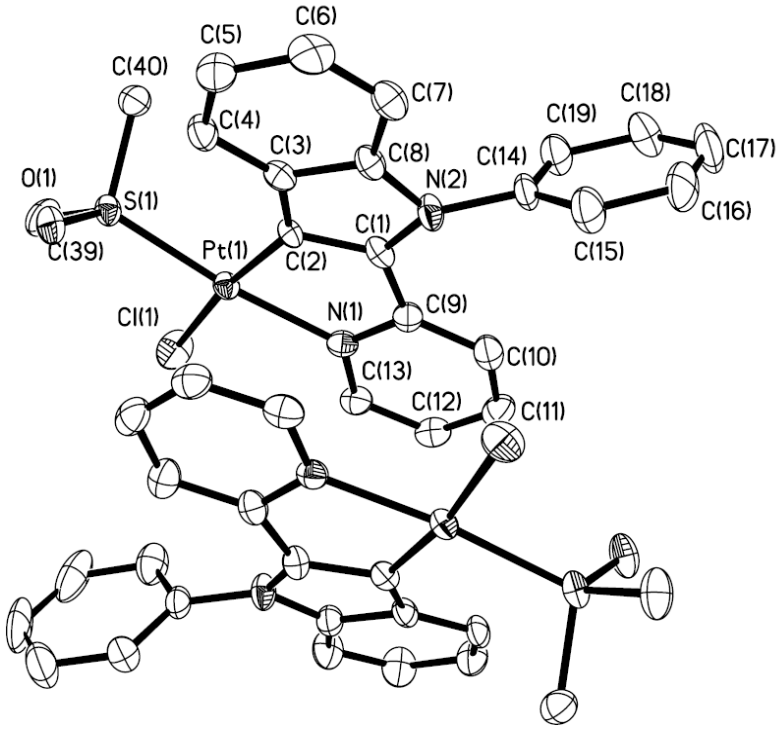

Figure 5.6 Crystal structure of **5.3** with 50% thermal ellipsoids showing the two molecules in the asymmetric unit; the hydrogen atoms have been removed for clarity.

5.3.2.3 Structure of **5.4**

The crystal structure of **5.4** belongs to the tetragonal chiral space group *I422* and is shown in Figure 5.7. The Cu(I) centre is chelated to two bpib ligands, each with the same chirality. This results in each crystal containing only one enantiomer of ligand, as well as only one enantiomer of the **5.4** complex. The Cu(I) centre in **5.4** has a distorted tetrahedral geometry with the N-Cu-N chelate bite angle being 137.1(3)°. The Cu-N bond lengths are all 2.076(5) Å. The $[Cu(bpib)_2]^+$ cation has a crystallographically imposed D_2 symmetry, which is a consequence of chelation by two identical enantiomers

of bpib to the Cu(I) centre. The crystal structure also shows both intra- and inter-ligand π-π interactions. The preferential coordination of the same enantiomer of bpib to the Cu(I) ion is likely due to the favourable intra-ligand interactions and multiple π-π interactions. A proton on the phenyl ring of one bpib ligand points into the pyridyl ring of the other bpib, and has a H-C distance of 2.845 Å. The same crystal structure was obtained with $[Cu(CH_3CN)_4]BF_4$ or $[Cu(PPh_3)_2(CH_3CN)_2]BF_4$ as the starting material for the reaction. Despite the formation of the large 9-membered chelate ring, the fact that the bpib ligand can replace PPh_3 ligands on the Cu(I) centre is an indication that the bpib ligand can act as a very effective chelate.

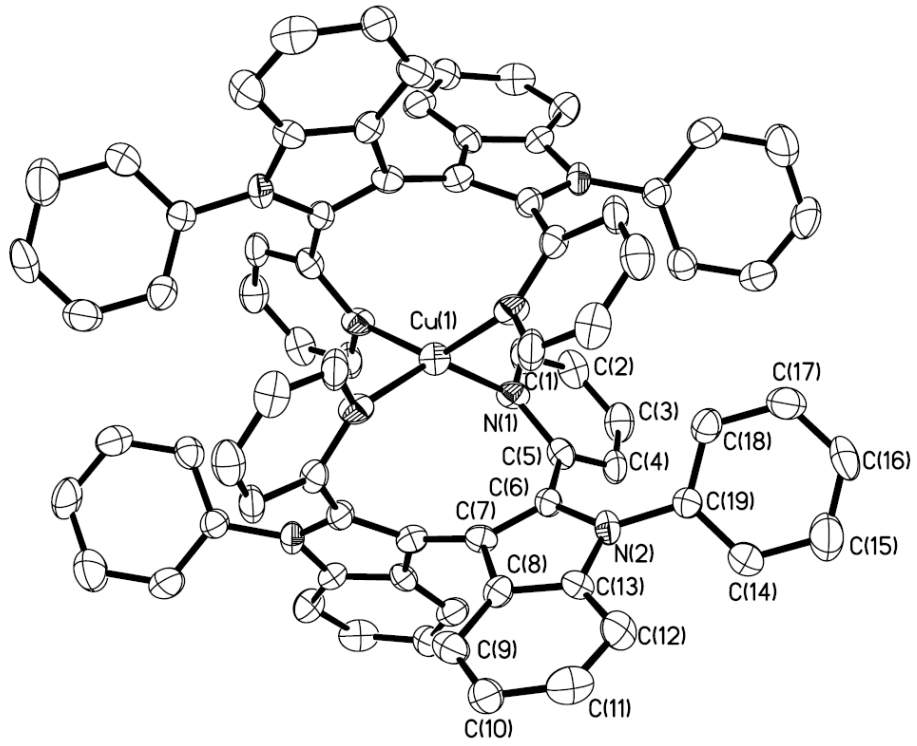

Figure 5.7 Crystal structure of complex **5.4** with 50% thermal ellipsoids. Hydrogen atoms, solvent molecules and the anion have been removed for clarity.

Most interestingly, in the crystal lattice (Figure 5.8) **5.4** stacks along the *c* axis to form homo-chiral columns. The resulting chiral channels are occupied by the BF_4^- anions and CH_2Cl_2 solvent molecules. The homochiral crystallization of **5.4** from a racemic solution mixture is interesting due to the relatively rare occurrence of such an event.[17-20] More importantly it allows us to separate the enantiomers by the Pasteur method, namely hand-picking the crystals. Homochiral crystallization was verified by circular dichroism (CD) spectroscopy on single crystals of complex **5.4**.

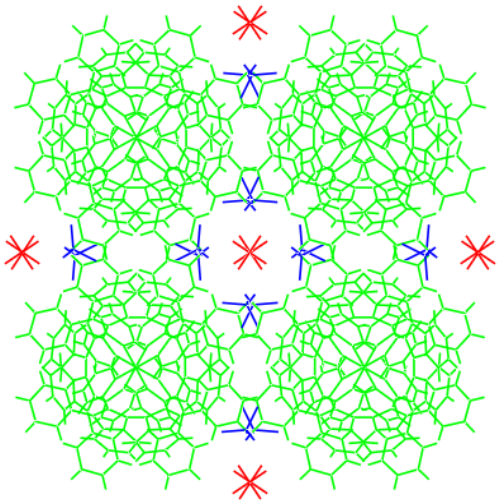

Figure 5.8 Packing structure of **5.4** down the c axis showing the chiral channels, the molecules of **5.4** are green, BF_4^- are red and CH_2Cl_2 solvent molecules are blue.

5.3.2.4 Structures of **5.5** and **5.6**

Most chelating ligands coordinate to square planar metal centres in a *cis* geometry. However, the crystal structure of Pd(II) (**5.5**) and Pt(II) (**5.6**) complexes revealed a trans-chelating geometry. Biferrocene trans-chelating diphenyl phoshino Pt(II) and Pd(II) complexes have been reported[8, 26] and some of these trans-chelating chiral bisphosphines have been demonstrated to be useful in asymmetric catalysis.[9, 27, 28] Although N,N trans-chelating ligands are scarce, a trans-chelating Pd(II) complex with a bipyridine ligand has been reported where the trans geometry is achieved by using a rigid backbone 1,2-bis-(2-pyridylethynyl)benzene that holds the pyridyl groups in position to chelate in a 180° geometry to the Pd(II) centre.[29, 30] This Pd complex was reported to be a highly active catalyst for the Heck reaction.[31] However, chiral N,N trans-chelating complexes have not been reported previously, which could be useful in asymmetric catalysis. The structure and properties of the novel trans-chelated Pd(bpib) and Pt(bpib) complexes formed with the chiral N,N chelate bpib will be discussed.

Complexes **5.5** and **5.6** were found to have bpib trans-chelated to the metal centre as shown in Figure 5.9 and Figure 5.10 respectively. Both crystallized in the *C2/c* space groups and possess a C2 axis. Trans-chelated Pt(II) and Pd(II) complexes are rare, and ones with pyridyl ligands are even more so. Both complexes show a distorted square planar geometry around the metal centre. The nine-membered chelate ring is clearly responsible for the distortion of the square planar geometry. The Pd(1)-N(2) bond length in 5.5 is 2.0206(14) Å, similar to that of **5.2**. The 1,2-bis-(2-pyridylethynyl)benzene

trans-chelated pyridyl complex reported in literature has a similar Pd-N bond length of 2.0113(19) Å.29 The N(2A)-Pd(1)-N(2) bond angle is 165.09(8)°. Most trans-chelated complexes show strain in the chelate ring, with the L-M-L bond angle (L is the donor atom, usually phosphine or occasionally nitrogen) ranging from28 150.7° to8 ,32 179°. The torsion angle between the two indole rings in **5.5** is 118.23°. Complex **5.5** crystallizes with two CH_2Cl_2 solvent molecules.

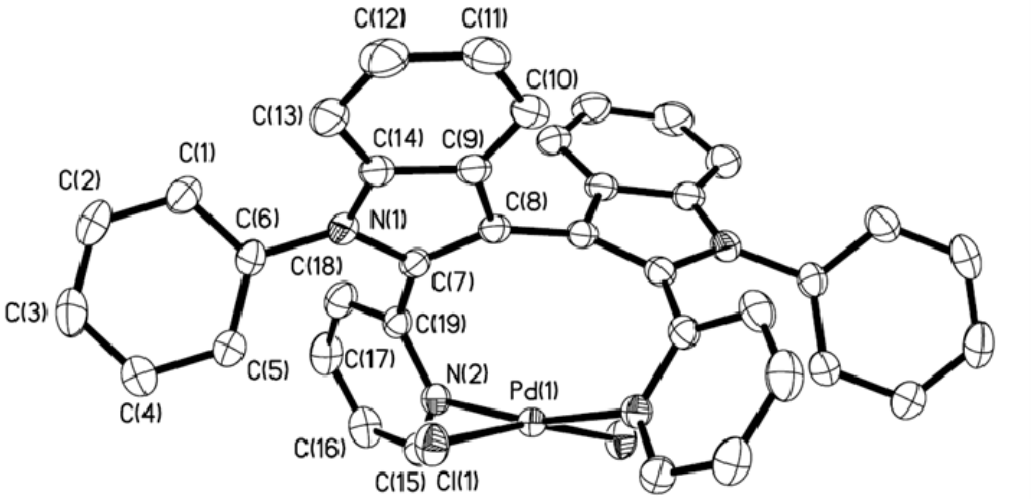

Figure 5.9 Structure of **5.5** with 50% thermal ellipsoids. The hydrogen atoms and solvent molecules are removed for clarity.

Complex **5.6** is isostructural with **5.5**. The structure is very similar to **5.5** but the nine-membered chelation ring is more strained, with a smaller N(3)-Pt(1)-N(1) bond angle of 164.62(14)°. The ring strain in the Pt complex could be a cause of the low yield. The Pt-N bond length is 2.054(9) Å (from literature Pt-N bonds in cis chelate complexes

are 1.997-2.056 Å).[12] The torsion angle between the indole rings is 115.76°, which is smaller than to that found for complex **5.5**.

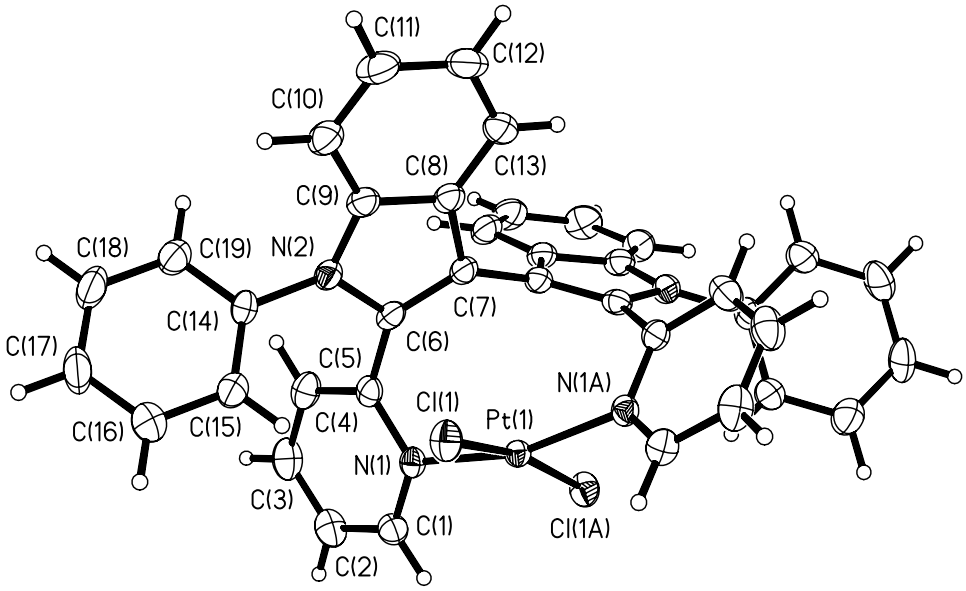

Figure 5.10 Structure of **5.6** with 50% thermal ellipsoids. The solvent molecules are removed for clarity.

The pyridyl based trans-chelating ligand reported in literature is very rigid, where the two pyridyl groups are held at ~180° with a 1,2-bis-(2-pyridylethynyl)benzene trans-chelated backbone.[29, 33] A report by Marty and Werner in 1987 looked at the necessity of a rigid backbone for forming trans-chelating complexes and found that it was not necessary for phosphine trans-chelating ligands.[34] Complexes **5.5** and **5.6** show that a rigid ligand is not necessary for pyridyl based ligands to form a trans-chelating structure. In this case the trans-chelating structure is preferred because a cis-chelation would be

very sterically constrained due to the large N-M-N bite angle. The trans-chelate structures of **5.5** and **5.6** were found to exist in solution as well as in the solid state.

5.3.3 Structure in Solution

5.3.3.1 Structures of **5.1-5.3** in solution

The behaviour of **5.1-5.3** in solution was examined by ^{1}H NMR CD_2Cl_2. For complex **5.1,** the most downfield peak at 8.5 ppm is very broad at room temperature, and sharpens into a doublet as the temperature is lowered to 253 K as shown in Figure 5.11. Although full assignment of the peaks was not possible due to a large amount of peak overlap in the aromatic region of the spectrum from the protons from the triphenylphosphines, this peak is attributed to the H_1 on the pyridyl group by comparison to the other complexes. The broad signal at room temperature is likely due to the pyridyl group exchanging between coordinated and non-coordinated states. The low temperature spectrum presumably represents the coordinated state of the ligand, as many peaks are shifted when compared to the free ligand. The exchange may be attributed to the non-chelating nature of the pib ligand which makes it a relatively weak donor. The dynamic exchange was not observed for **5.2** and **5.3** and sharp peaks were observed for these two complexes at room temperature, as shown in Figure 5.12 and Figure 5.13. Complex **5.2** and complex **5.3** have a similar ^{1}H NMR spectrum. However for complex **5.3,** the H_1-pyridyl peak is shifted down-field at 9.57 ppm, compared to the Pd(II) complex, and displays satellite peaks characteristic of Pt-H coupling.

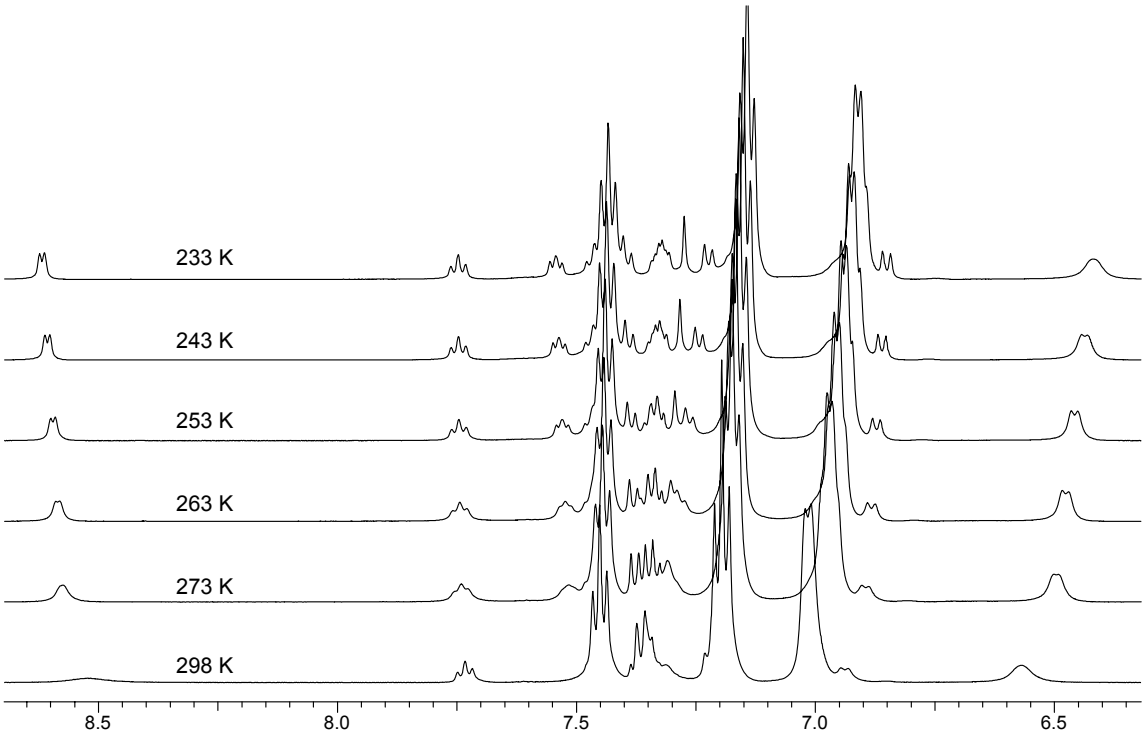

Figure 5.11 Variable temperature ^{1}H NMR of **5.1** in CD_2Cl_2 displaying broad H_1-pyridyl peak at ambient temperature that sharpens as the temperature is lowered.

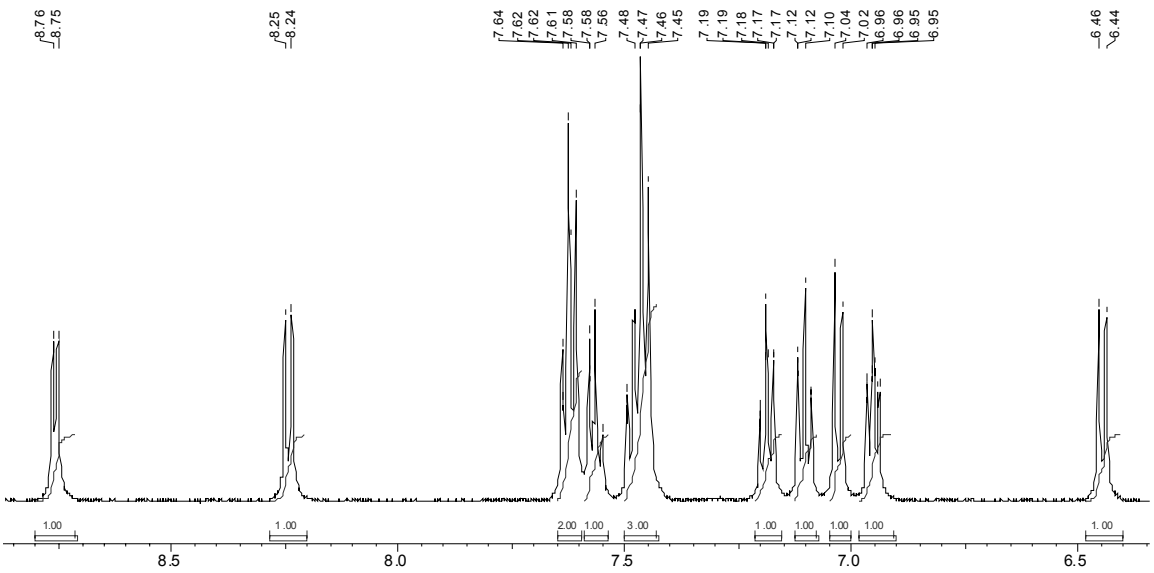

Figure 5.12 The aromatic region of the ^{1}H NMR of **5.2** in CD_2Cl_2 at ambient temperature.

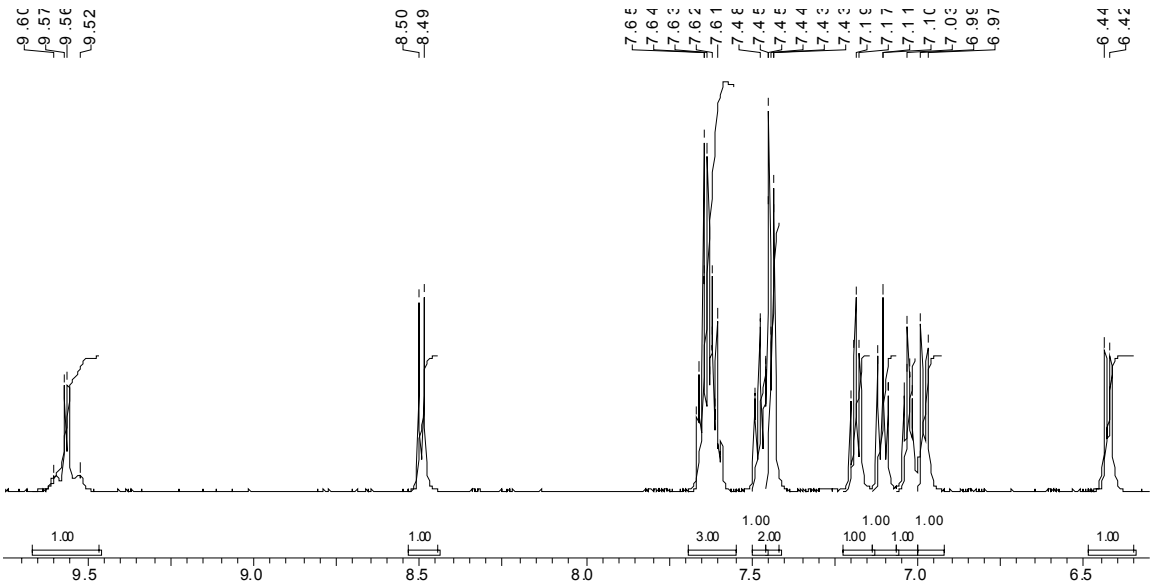

Figure 5.13 The aromatic region of the ^{1}H NMR of **5.3** in CD_2Cl_2 at ambient temperature where the H_1-peak shows Pt-H coupling.

5.3.3.2 Structure of **5.4-5.6** in solution

The ^{1}H NMR spectrum of complexes **5.4-5.6** show some broad peaks at room temperature. These broad peaks were assigned by COSY and found to be from the protons on the phenyl rings. As the temperature was lowered the peaks sharpened indicating hindered rotation of the phenyl ring. This hindered rotation is caused by the forced twist between the pyridyl and indolyl rings upon coordination of the bpib ligand to a metal centre causing increased ortho hydrogen interactions between the phenyl ring and the pyridyl ring as can be seen in Figure 5.7, Figure 5.9 and Figure 5.10.

Complex **5.4** shows broad phenyl peaks that sharpen when cooled to 253K. One of the broad peaks, not noticeable at room temperature, appears at 4.78 ppm in the variable temperature ^{1}H NMR shown in Figure 5.14. This doublet peak is assigned to the phenyl proton H9 in Figure 5.15. This up-field shift is caused by the interaction of the phenyl ring on one of the ligands with the pyridine "π-cloud" on the second ligand as can been seen in the crystal structure in Figure 5.7. The up-field shift of an aromatic proton in the "π-cloud" of a neighbouring π system has been previously reported.[35] The H_1-pyridyl peak in **5.4** is also shifted up-field to 7.19 ppm, also likely due to steric congestion and π-π interactions. The H_1-pyridyl peak is found at 8.1 ppm in the free ligand, and is shifted down-field for other metal complexes. These shifts support that π-π interactions are present in solution as well as in the crystal structure, which likely led to the homo-chiral crystallization as well as displacement of the PPh_3 ligands observed for complex **5.4**.

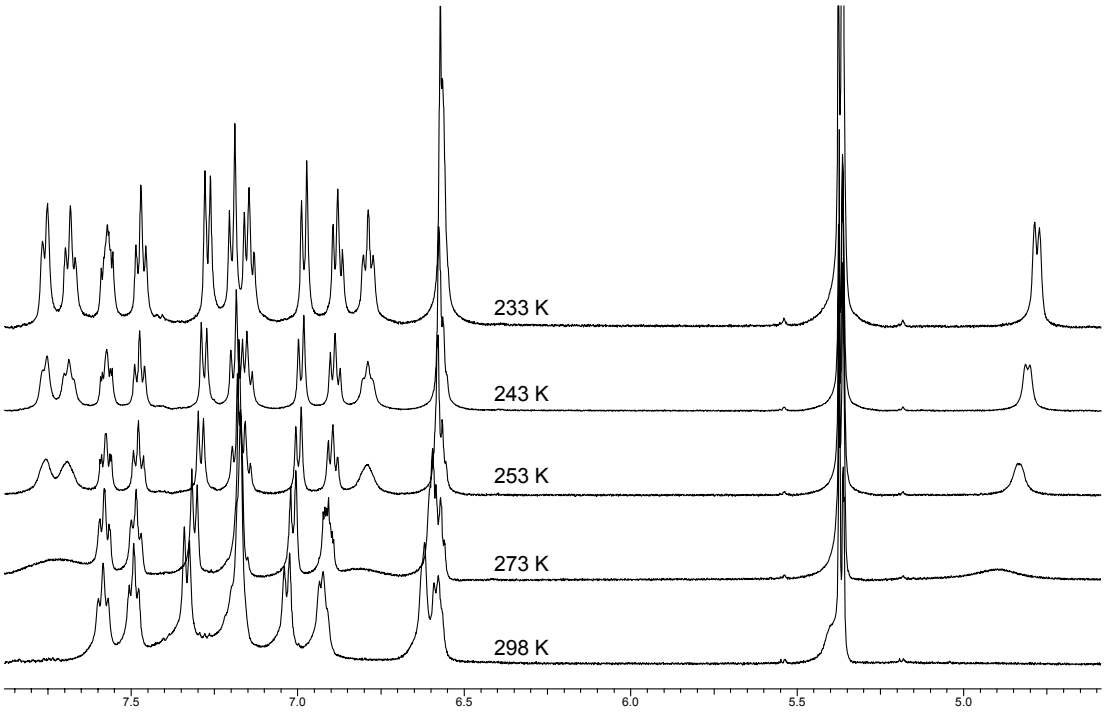

Figure 5.14 Variable temperature ^{1}H NMR spectra of **5.4** in CD_2Cl_2.

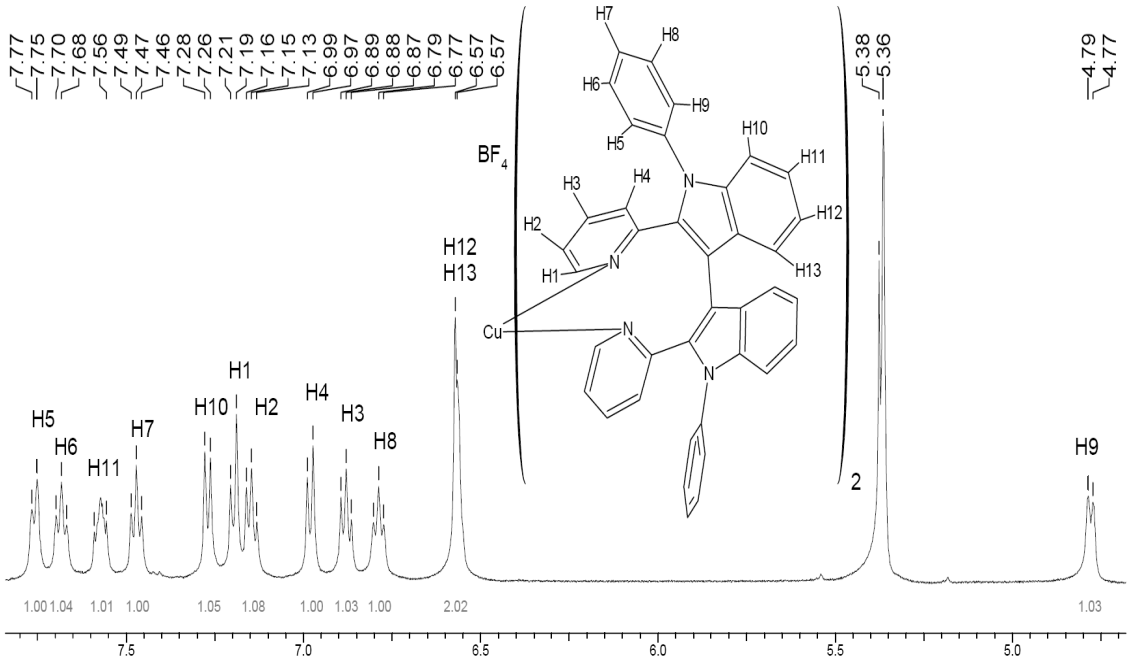

Figure 5.15 ^{1}H NMR spectrum of **5.4** at 233 K with peaks assignments by COSY.

Because complex **5.5** and **5.6** only have one bpib ligand per metal centre they do not show the same up field shift as observed in **5.4** due to the lack of inter-ligand π-π interactions. However, both complexes still display broad phenyl peaks that are resolved at low temperatures as shown in Figure 5.16 and Figure 5.17. This, again, is caused by the hindered rotation of the phenyl ring due to interactions of the ortho-hydrogen atoms in the bpib ligand after coordinated to the metal centre. **5.5** also shows evidence of dissociation, the H_1-pyridyl proton of bpib at 8.1 ppm appears over several days. After several days ~12% ligand dissociation was observed for **5.5**. The same dissociation was not observed for complex **5.6,** although a small amount of impurity is observed in the spectrum with a peak appearing at 8.5 ppm.

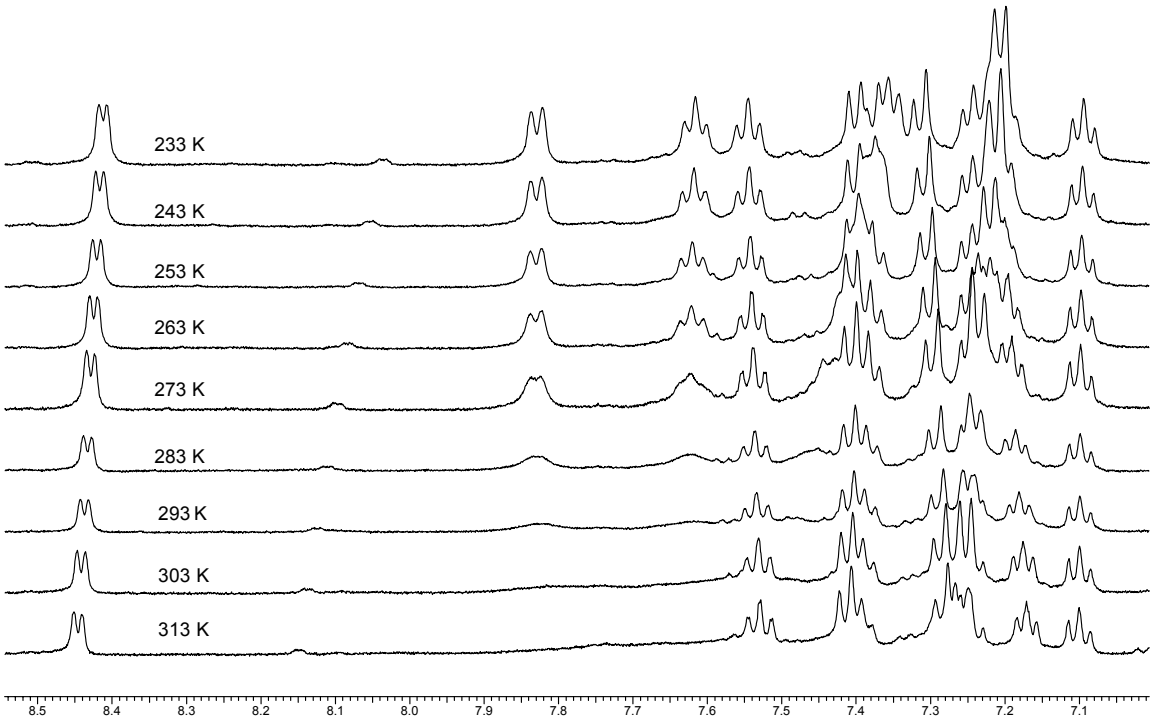

Figure 5.16 Variable temperature ^{1}H NMR of **5.5** in CD_2Cl_2.

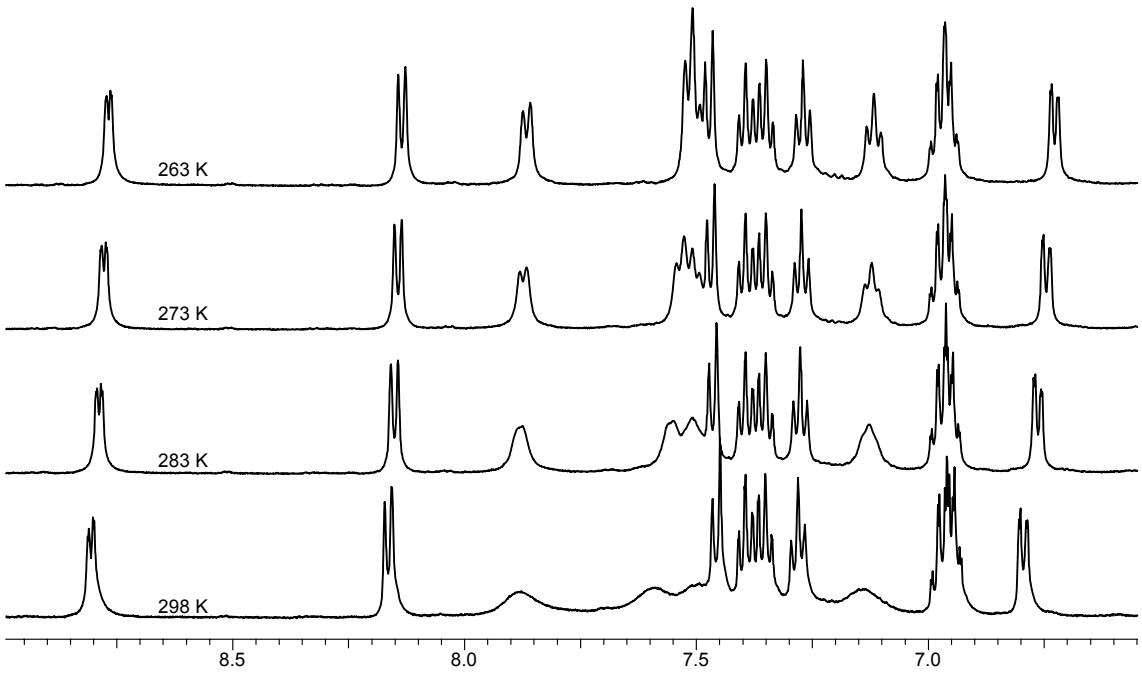

Figure 5.17 Variable temperature ^{1}H NMR of **5.6** in CD_2Cl_2.

5.3.4 UV-Vis Absorption Spectra

The high energy region of the absorption spectra (230-350 nm) of the complexes closely matches that of the free ligands and is assigned to π-π* transitions as shown in Figure 5.18 and Figure 5.19. Compared to the pib based complexes **5.1-5.3**, the bpib based complexes **5.5** and **5.6** have approximately double the molar absorptivity in this region because each molecule has two 2-pyridyl(indolyl) units and **5.4** has four, which accounts for the higher molar absorptivity of this complex.

The UV-Vis absorption spectrum of complex **5.1** only shows slight change from the free ligand. No apparent low energy MLCT is observed. It is believed that because

the Cu(I) is in a three-coordinate trigonal planar geometry, charge transfer from the metal centre is not possible. In four coordinate complexes the Cu(I) centre distorts from tetrahedral to square planar upon excitation. This is not possible for the three-coordinate Cu(I) and as such no MLCT is observed.

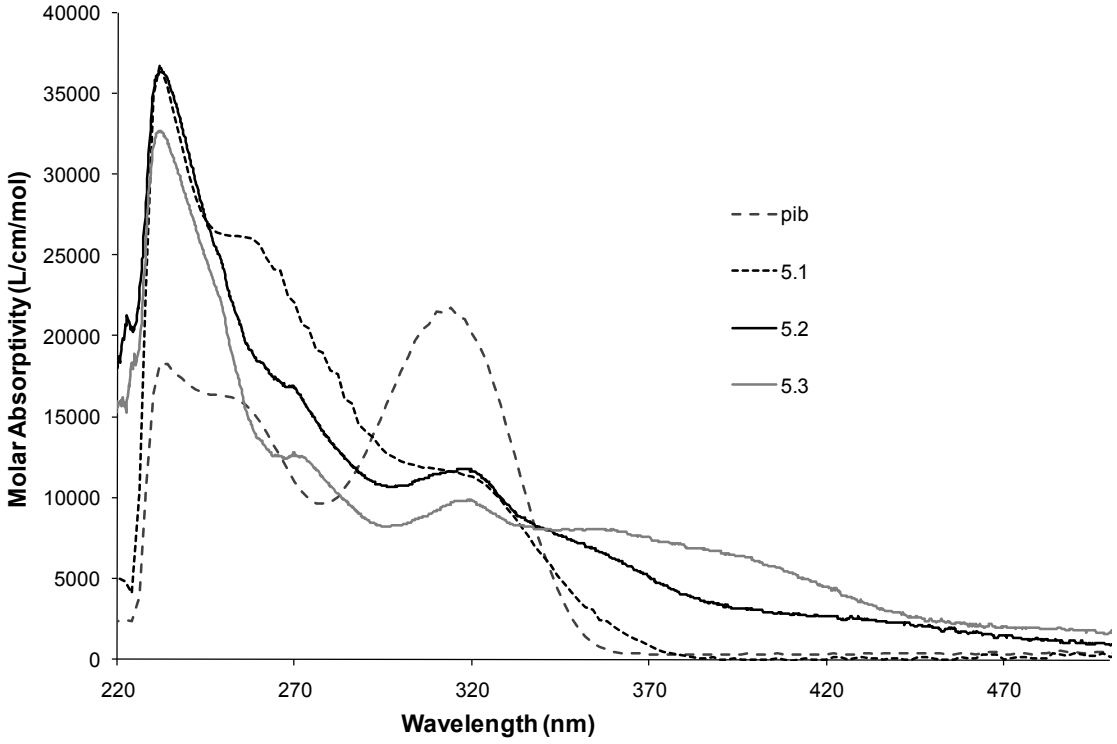

Figure 5.18 UV-Vis absorption spectrum of pib based complexes **5.1-5.3** as well as the free ligand pib for comparison.

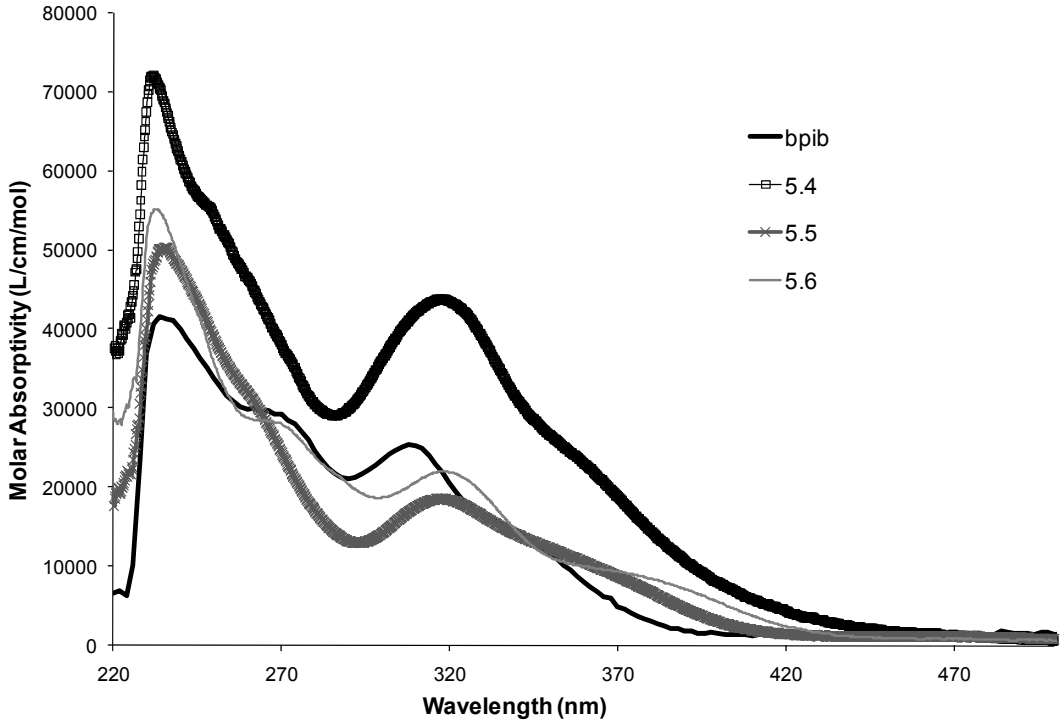

Figure 5.19 UV-Vis absorption spectrum of bpib based complexes **5.4-5.6** as well as the free ligand bpib for comparison.

MLCT absorption bands are observed for complexes **5.2-5.6**. The cyclometallated complexes **5.2** and **5.3** have shoulders in the absorption spectrum at 352 nm and 404 nm respectively, and both have tails that extend past 500 nm. Similar absorptions have been reported for cyclometallated Pd(II) and Pt(II) complexes in literature that are assigned to MLCT absorptions.[15] The N,N-chelating bpib complexes of Pt(II) and Pd(II) also display MLCT absorptions as shown in Figure 5.19. Complex **5.5** shows a low energy shoulder band at ~360 nm attributed to a MLCT. Complex **5.6,** shows a low energy absorption band at ~380 nm, which is also assigned to a MLCT transition similar to MLCT bands in other pyridyl Pt(II) complexes.[12]

The Cu(I) complex **5.4** appears red coloured, compared to the colourless three-coordinated complex **5.1**. This is because this complex also shows a lower energy transition band at ~360 nm with the tail extending to 470 nm, again assigned to MLCT transitions. It should also be noted that the high molar absorptivities seen for complex **5.4** in the 230-350 nm region of the spectrum can be attributed to four 2-(2'-pyridyl)indolyl units in the molecule.

5.3.5 CD Spectra

Because complex **5.4** crystallizes in the chiral space group *I422,* each crystal contains only one enantiomer of $[Cu(bpib)_2]^+$. The solution made with a single crystal of complex **5.4** is enantiomerically pure. To verify this, the circular dichroism (CD) spectrum of **5.4** was examined. The CD spectra of hand-picked single crystals of **5.4** with opposite chirality recorded in CH_2Cl_2 are shown in Figure 5.20. They indeed display mirror image spectra indicating that the selected crystals are in fact enantiomers of each other. The spectra were monitored over time to determine the stability of **5.4** to racemization in solution at ambient temperature. In the absence of air, the CD spectrum does not change for weeks, indicating that **5.4** retains its chiral structure in solution and does not undergo racemization. It was thought that the homo-chiral crystallization could be utilized to separate the enantiomers of the ligand bpib since both ligands on the Cu(I) centre are of the same chirality. However, attempts to free the ligand from the copper centre by the addition of $[N(C_2H_5)_4]CN$ were unsuccessful.

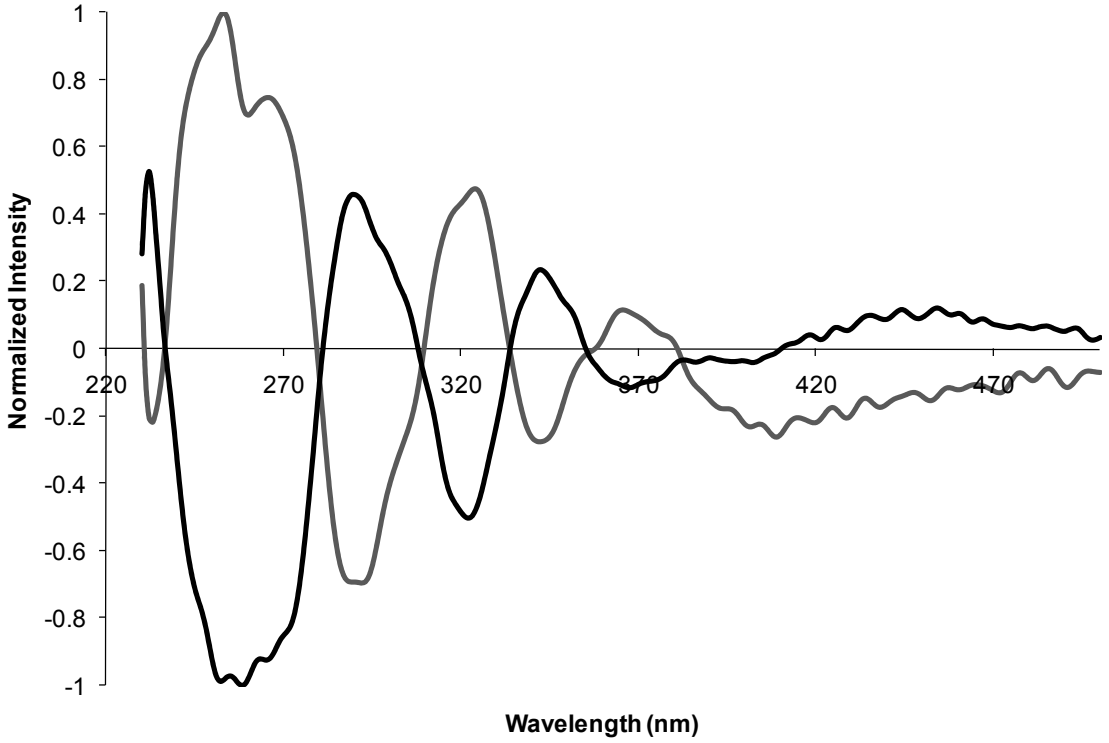

Figure 5.20 CD spectrum of two separate crystals of **5.4.** Mirror image spectra indicate the two crystals were enantiomers.

5.3.6 Luminescent Spectra

Solution luminescence was not observed for any of the complexes. However, a frozen solution of CH_2Cl_2 at 77 K displayed MLCT emission for complexes **5.2-5.4** and **5.6**, as shown in Figure 5.21 and are summarized in Table 5.4. For complex **5.1,** green emission (λ_{max} = 540 nm) was also observed when doped 20%wt into PMMA (Poly(methyl methacrylate)) polymer, in a neat film or in a frozen CH_2Cl_2 solution at 77 K. A MLCT absorption band is not observed in the UV-Vis spectrum for this compound so the origin

of this emission is uncertain. The decay lifetime of this emission is 14(3) μs, indicating that it is phosphorescent emission. Previous reports in literature attribute the emission of three coordinate Cu(I) complexes to $^3\pi$-$^1\pi$ ligand based transitions.[36, 37]

The cyclometallated complexes **5.2** and **5.3** display long lived red emission in a glassy solution at 77 K (λ_{max} = 616 nm for **5.2** and λ_{max} = 635 nm for **5.3**). These complexes do display MLCT absorption bands. Therefore, the observed red emission is likely ^{3}MLCT phosphorescence. The decay lifetime of both complexes was determined to be 50 μs and 9.4 μs respectively. Previously reported cyclometallated Pt and Pd complexes often display similar MLCT based emission in frozen solution or in the solid state.[38] Often emission in solution for these complexes is not observed due to solvent quenching of the long lived excited state.

For complex **5.4** emission in frozen solution is observed at λ_{max} = 540 nm. This complex is a four coordinate Cu(I) complex and shows a low energy MLCT absorption band. The emission was therefore attributed to phosphorescence from this MLCT state with a lifetime of 6.1 μs.

Complex **5.5** does not show any emission in solution, at 77 K or in the solid state. Lack of emission from Pd complexes is common. At ambient temperature, in solution, the quenching can be caused by collisions with the solvent molecules.[39, 40] In the solid state the quenching can be attributed to intermolecular interactions in the crystal lattice.[41]

Complex **5.6** shows emission with λ_{max} = 595 nm at 77 K in CH_2Cl_2 with a lifetime of 231(2) μs. It is also MLCT based phosphorescence as observed for many

Pt(II) complexes. Our group has reported Pt(II) 2-(2'-pyridyl)benzimidazolyl based complexes that displays phosphorescent emission at 588 nm in the solid state.[41] Similarly, emission is seen in the solid state for the Pt(II) complexes **5.3** and **5.6** and Pd(II) complex **5.2**, but problems making adequate films prevented measurement of this emission; however, it appeared similar in colour to the frozen solution emission.

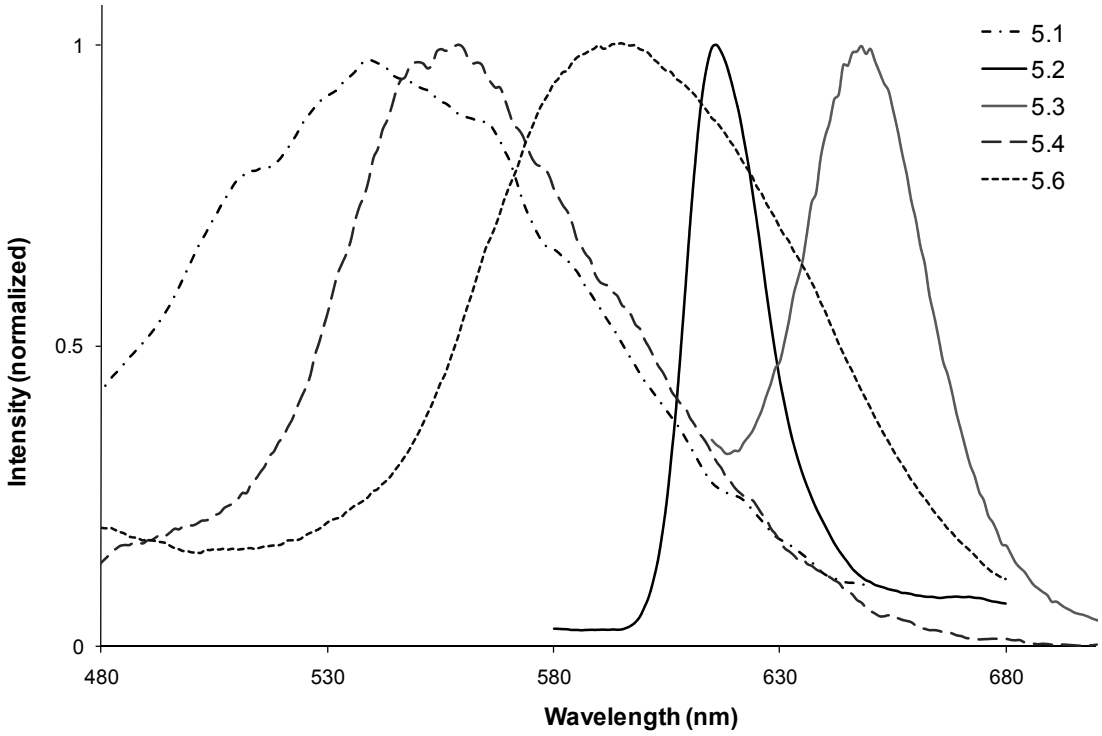

Figure 5.21 The emission spectra of complexes **5.1-5.4** and **5.6** in frozen CH_2Cl_2 at 77 K. The spectra were recorded after a 150 μs delay to ensure only the phosphorescence was observed.

Table 5.4 Absorption and phosphorescence data for complexes **5.1-5.6.**

Complex	Absorption		Em λ_{max} (nm)	τ (μs)
	λ_{max} (nm)	ε ($M^{-1}cm^{-1}$)		
Pib	234	18233	389	
	254 s	16000		
	314	21726		
5.1	233	36800	540[b]	14.4 ± 3.2
	258 s	26000		
	314 s	11700		
5.2	233	36100	616[b]	50.74 ± 0.37
	318	11800		
	352	7000		
5.3	233	32200	648[b]	9.448 ± 0.049
	272 s	12400		
	329	9900		
	404 b	5800		
Bpib	234	41600	445	
	268 s	29200		
	310	25200		
	340 s	11400		
5.4	232	72100	560[b]	6.156 ± 0.348
	249 s	55100		
	319	43600		
	361	22600		
5.5	237	49500		
	320	18400		
	362	10100		
5.6	233	54600	595[b]	231.8 ± 2.14
	270 s	27800		
	319	21900		
	383	7920		

[a] $1x10^{-5}$ M solution in CH_2Cl_2 [b] 77 K in CH_2Cl_2 with 150 μs delay

5.4 Conclusions

New Cu(I), Pd(II) and Pt(II) complexes of the 2-(2'-pyridyl)indoly based ligands pib and bpib were synthesized and characterized. The photophysical properties, crystal structures and solution behaviour were investigated. The three coordinate Cu(I) complex **5.1** has a distorted trigonal planar geometry and emits yellow colour in the solid state and the frozen solution. The origin of the emission is attributed to $^{3}\pi$-$^{1}\pi$ ligand transitions, since no MLCT absorption band is observed. The cyclometallated Pd(II) and Pt(II) pib complexes **5.2** and **5.3** display MLCT absorption in solution and red coloured emission in a frozen CH_2Cl_2 solution.

The complexes made with the atropisomeric ligand bpib display interesting and unusual crystal structures. The Cu(I) complex **5.4** crystallizes homochirally with two bpib ligands per Cu(I) centre. The crystal structures of the Pd(II) and Pt(II) complexes contain the bpib ligand that chelates to the metal centre with the pyridyl groups being trans to one another. The trans-chelating geometry reveals that it is not necessary to use a rigid ligand to obtain a trans-chelated complex. All complexes of bpib display MLCT based emission when frozen in CH_2Cl_2 except the Pd(II) complex, **5.5**. Solid state emission is observed for the cyclometallated complexes **5.2** and **5.3** as well as for **5.6**. These complexes could potentially be used as red phosphorescent emitters for OLEDs but further investigations would be necessary.

5.5 References

(1) Tominaga, H.; Sakai, K.; Tsubomura, T. *J. Chem. Soc., Chem. Commun.* **1995**, 2273.

(2) Bringmann, G.; Price Mortimer, A. J.; Keller, P. A.; Gresser, M. J.; Garner, J.; Breuning, M. *Angew. Chem. Int. Ed.* **2005**, *44*, 5384.

(3) Wu, C. D.; Lin, W. *Angew. Chem. Int. Ed.* **2007**, *46*, 1076.

(4) Wu, C. D.; Zhang, L.; Lin, W. *Inorg. Chem.* **2006**, *45*, 7278.

(5) Shimizu, H.; Nagasaki, I.; Saito, T. *Tetrahedron* **2005**, *61*, 5404.

(6) McCarthy, M.; Guiry, P. J. *Tetrahedron* **2001**, *57*, 3809.

(7) Berens, U.; Brown, J. M.; Long, J.; Seike, R. *Tetrahedron: Asymmetry,* **1996**, *7*, 285.

(8) Kuwano, R.; Uemura, T.; Saitoh, M.; Ito, Y. *Bull. Chem. Soc. Jpn.* **1997**, *70*, 2807.

(9) Kuwano, R.; Uemura, T.; Saitoh, M.; Ito, Y. *Tetrahedron: Asymmetry* **2004**, *15*, 2263.

(10) Chelucci, G.; Thummel, R. P. *Chem. Rev.* **2002**, *102*, 3129.

(11) Charmant, J. P. H.; Fallis, I. A.; Hunt, N. J.; Lloyd-Jones, G. C.; Murray, M.; Nowak, T. J. *J. Chem Soc., Dalton Trans.* **2000**, 1723.

(12) Chang, S.; Kavitha, J.; Li, S.; Hsu, C.; Chi, Y.; Yeh, Y.; Chou, P.; Lee, H.; Carty, A., J; Tao, Y.; Chien, C. *Inorg. Chem.* **2006**, 137.

(13) Chang, S.; Li, E. Y.; Chou, P.; Chi, Y. *Inorg. Chem.* **2007**, *46*, 7064.

(14) Tollari, S.; Cenini, S.; Penoni, A.; Granata, G.; Palmisano, G.; Demartin, F. *J. Organomet. Chem.* **2000**, *608*, 34.

(15) Thummel, R. P.; Jahng, Y. *J. Org. Chem.* **1987**, *52*, 73.

(16) Ma, B.; Djurovich, P. I.; Garon, S.; Alleyne, B.; Thompson, M. E. *Adv. Funct. Mater.* **2006**, *16*, 2438.

(17) Tamura, R.; Takahashi, H.; Fugimoto, D.; Ushio, T. *Top. Curr. Chem.* **2007**, *269*, 53.

(18) Li, M.; Sun, Q.; Bai, Y.; Duan, C. Zhang, B.; Meng, Q. *Dalton Trans.* **2006**, 2572.

(19) Gu, X.; Xue, D. *Inorg. Chem.* **2006**, *45*, 9257.

(20) Motsumoto, T.; Kasai, T.; Tatsumi, K. *Chem. Lett.* **2002**, *31*, 346.

(21) Kubas, G. J. *Inorg. Synth.* **1979**, *19*, 90.

(22) AI-Azawe, S.; Sarkis, G. Y. *J. Chem.Eng. Data* **1973**, *18*, 109.

(23) Caixach, J.; Capell, R.; Galvez, C.; Gonzalez, A.; Roca, N. J. *Heterocycl. Chem.* **1979**, *16*, 1631.

(24) Bruker Analytical X-ray Systems **1999**, version *5.10*.

(25) Nonoyama, M.; Nakajimab, K. *Polyhedron* **1998**, *6*, 1.

(26) Sawamura, M.; Hamashima, H.; Ito, Y. *Tetrahedron: Asymmetry* **1991**, *2*, 593.

(27) Petocz, G.; Berente, Z.; Kegl, T.; Kollar, L. *J. Organomet. Chem.* **2004**, *689*, 1188.

(28) Yin, J.; Buchwald, S. L. *J. Am. Chem. Soc.* **2002**, *124,* 6043.

(29) Bosch, E.; Barnes, C. L. *Inorg. Chem.* **2001**, *40*, 3097.

(30) Hu, Y.; Chamchoumis, C.; Grebowicz, J. S.; Thummel, R. P. *Inorg. Chem.* **2002**, *41*, 2296.

(31) Kawano, T.; Shinomauru, T.; Ikuo, U. *Org. Lett.* **2002**, *4*, 2545.

(32) Eberhard, M. R.; Heslop, K. M.; Orpen, A. G.; Pringle, P. G. *Organometallics* **2005**, *24*, 335.

(33) Bosch, E.; Barnes, C. L. *J. Coord. Chem.* **2003**, *56*, 329.

(34) Martyt, W.; Kapoor, P. N.; Biirgi, H.; Fischer, E. *Helv. Chim. Acta* **1987**, *70*, 158.

(35) Ting, Y.; Lai, Y. *J. Am. Chem. Soc.* **2004**, *126*, 909.

(36) Omary, M. A.; Rawashdeh-Omary, M. A.; Diyabalanage, H. V. K.; Dias, H. V. R. *Inorg. Chem.* **2003**, *42*, 8612.

(37) Zhao, S.; Wang, R.; Wang, S. *Inorg. Chem.* **2006**, *45*, 5830.

(38) Li, J.; Djurovich, P. I.; Alleyne, B. D.; Yousufuddin, M.; Ho, N. N.; Thomas, J. C.; Peters, J. C.; Bau, R.; Thompson, M. E. *Inorg. Chem.* **2005**, *44*, 1713.

(39) Ingle, J. D.; Crouch, S. R. In *Ch 12;* Spectrochemical Analysis; Premtoce Hall: New Jersey, 1988.

(40) Lakowicz, J. R. In *Principles of Fluorescence Spectroscopy, 2nd edn;* Kluwer Academic: New York, 1999.

(41) Liu, Q. D.; Thorn, L.; Kozin, I.; Song, D.; Seward, C. *J. Chem. Soc. Dalton. Trans.* **2002**, 3234.

Chapter 6
Interaction of bpib and bbib With Group 12 Metal Ions and Chiral Sensing of Zn(II) Carboxylates.

6.1 Introduction

Chiral sensing is an important and intensive research field due to its broad applications in probing and understanding chiral recognition events in biological systems, the development of chiral catalytic systems and the syntheses of new chiral drugs.[1-8] Among the various physical methods for fast and sensitive chiral sensing and the determination of enantiomeric excess (ee), circular dichroism (CD) is commonly used. In order for CD to work effectively, however, either the chiral host or the chiral guest must have a strong absorption in the UV-Vis region and the resulting host-guest complexes must have distinct CD spectra.[9, 10]

Many examples of using enantiomerically pure host molecules for chiral sensing by CD detection methods are known in the literature.[11-16] Using an enantiomerically pure host has several drawbacks, the first of which is that asymmetric synthesis or chiral purification must be employed in obtaining the host, and this purification may not always be possible, limiting the hosts available. Second, as will be shown, a racemic host can have a more sensitive CD response, than an enantiomerically pure host. Supramolecular hosts that produce a CD signal when interacting with a chiral guest have been shown to be viable chiral sensors.[17-22] Some of the benefits of using a racemic host are also seen for achiral hosts that react with a chiral guest to give a CD response. Many achiral

supramolecular hosts such as porphyrin derivatives have also been shown to be able to act as chiral sensors via induced chirality upon binding with chiral guest molecules.[13, 23-25] In contrast, chiral sensing based on racemic substrates/hosts using CD methods[26] has hardly been explored despite the apparent advantage of not needing to resolve the racemic substrate. Furthermore, examples of chiral sensing of organic molecules mediated by metal-ligand interactions remain rare.[23, 27-32]

The new class of N,N-chelate atropisomeric ligands reported in Chapter 4 including bpib and bbib are shown in Figure 6.1. Although the enantiomers of these ligands have not been resolved, it has been shown in Chapter 5 that the racemate bpib can bind to a Cu(I) ion to form homochiral complexes that upon resolution by hand-picking the crystals display distinct CD spectra.[33] Further investigation on this system has led to the discovery that the racemic atropisomers bpib and bbib can be used directly for sensing of certain chiral zinc(II) carboxylates such as (*S*)-2-Br-3-Me-butyrate (*S*-BrMeBu) and (*R*)-2-Br-3-Me-butyrate (*R*-BrMeBu) and determining the ee by CD methods. The Zn(II) binding to the chelate ligands bpib and bbib, shown in Figure 6.1, is inevitably affected by the carboxylate binding ability to the Zn(II) centre, which has been found to play a key role in the CD response. The details of the investigation are presented in this chapter. The fluorescent response of ligand bpib and bbib toward other group 12 metal salts, namely Cd(II) and Hg(II) were also examined for comparison.

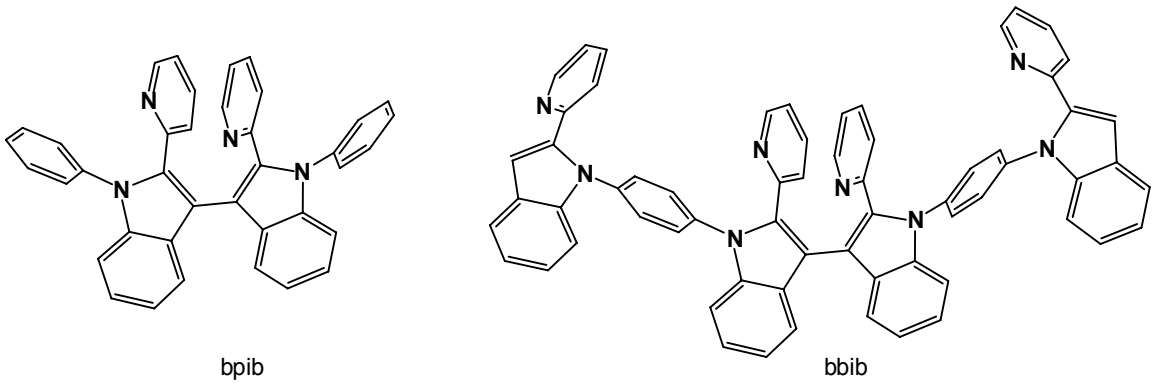

Figure 6.1 Structure of ligands bpib and bbib used for chiral sensing.

6.1.1 Experimental

6.1.2 General Considerations

All starting materials were purchased from Aldrich Chemical Company and used without further purification. Solvents were freshly distilled over appropriate drying reagents under N_2 atmosphere. Thin layer chromatography was carried out on silica gel. Flash chromatography was carried out on silica (silica gel 60, 70-230 mesh). All UV-Vis spectra were collected by using Ocean Optics Inc. spectrometer and Spectra Suite software. ^{1}H NMR spectra were recorded on a Bruker Avance 500 MHz spectrometer. Excitation and emission spectra were recorded on a Photon Technologies International QuantaMaster Model C-60 spectrometer. The CD spectra were recorded on a Jasco 715 circular dichroism spectrometer with a 1 cm path length. Elemental analyses were performed by Canadian Microanalytical Service Ltd., Delta, British Columbia, Canada or at the University of Toronto, Canada. Ligands bpib and bbib were prepared using the procedures presented in Chapter 4.[33]

6.1.3 Synthesis of $Zn(BrMeBu)_2$

1 mmol of ZnO and 2 mmol of (*R*) or (*S*)-2-bromo-3-methylbutyric acid were added to 10 mL of degassed toluene. The mixture was stirred under N_2 overnight and the solvent was removed under vacuum. The residue was dissolved in THF. After the removal of the insoluble solid, the solvent was evaporated to give the product. The racemic salt can be made in the same manner by using racemic 2-bromo-3-methylbutyric acid.

6.1.4 Synthesis of $Zn(bpib)(tfa)_2$ (6.1)

A solution of 82 mg (0.280 mmol) of $Zn(tfa)_2$ in ~5 mL of THF was layered on top of a solution of 150 mg (0.280 mmol) of bpib in ~5 mL of CH_2Cl_2. Slow diffusion of the layers resulted in light yellow crystals of the complex in 44% yield in ca. 5 days. ^{1}H NMR in CD_2Cl_2, 500 MHz, (δ, ppm, 223 K): 6.97-7.00 (m, 3H), 7.22-7.25 (m, 1H), 7.29 (dd, J = 7.5 Hz, J = 7.5Hz, 1H), 7.36 (d, J = 5.0 Hz, 1H), 7.39-7.41 (m, 2H), 7.47 (dd, J = 7.5 Hz, J = 7.5 Hz, 1H), 7.70 (dd, J = 7.5 Hz, J = 7.5 Hz, 1H), 7.87 (dd, J = 7.5 Hz, J = 7.5 Hz, 1H), 7.92 (d, J = 5.0 Hz, 1H), 8.68 (d, J = 5.0 Hz, 1H). Anal. calcd for $C_{42}H_{26}F_6N_4O_4Zn$: C 60.77, H 3.15, N 6.75. Found: C 60.65, H 3.16, N 6.60.

6.1.5 Synthesis of $Zn(bbib)(tfa)_2$ (6.2)

A solution 75 mg (0.081mmol) of bbib in ca. 10 mL of CH_2Cl_2 was layered with a solution of 24 mg (0.081 mmol) of $Zn(tfa)_2$ in THF. The layers were allowed to slowly mix. As the solvents evaporated, yellow power precipitated. The solution was decanted and the powder was re-crystallized from CH_2Cl_2 and hexanes to afford light yellow crystals (48% yield). ^{1}H NMR in CD_2Cl_2 500 MHz, (δ, ppm, 298 K): 8.76 (d, J = 5 Hz,

1H), 8.48 (d, J = 5 Hz, 1H), 7.95 (dd, J = 7.5, 7.5 Hz, 1H), 7.78 (d, J = 5 Hz, 1H), 7.69 (dd, J = 7.5, 7.5 Hz, 1H), 7.62 (br s, 2H), 7.51-7.44 (m, 6H), 7.38 (d, J = 10 Hz, 1H), 7.34-7.30 (m, 2H), 7.26 (dd, J = 7.5, 7.5 Hz, 1H), 7.21 (dd, J =5, 5 Hz, 1H), 7.17 (s, 1H), 7.04 (s, 2H). Anal calcd for $C_{68}H_{42}F_6N_4O_4Zn \cdot 3.5\ CH_2Cl_2$: C 56.81, H 3.27, N 7.41. C, 56.43, H, 3.14, N, 7.59

6.1.6 Syntheses of Zn(bpib)(*S*-BrMeBu)$_2$ and Zn(bbib)(*S*-BrMeBu)$_2$ (6.3 and 6.4)

These two compounds were synthesized on NMR scale, by combining 4.7 mg (8.8 μmol) of bpib with 3.8 mg (9.1 μmol) of Zn(*S*-BrMeBu)$_2$, or 5.8 mg (6.3 μmol) of bbib with 2.8 mg (6.5 μmol) of Zn(*S*-BrMeBu)$_2$ in the same manner as for the Zn(tfa)$_2$ complexes. ^{1}H NMR for **6.3** in CD_2Cl_2, 500 MHz, (δ, ppm, 203 K): 8.73 (d, *J* = 5 Hz, 0.35H, *o*-H, py, minor diastereomer), 8.70 (d *J* = 5 Hz, 0.65H, *o*-H, py, major diastereomer), 7.88 (d, *J* = 10, 1H), 7.77 (dd, *J* = 7.5 Hz, *J* = 7.5 Hz, 1H), 7.67 (dd, *J* = 7.5 Hz, *J* = 7.5 Hz 1H), 7.45-7.41 (m, 3H), 7.37 (dd, *J* = 7.5 Hz, *J* = 7.5 Hz, 1H), 7.34-7.31 (m, 2H), 7.27-7.18 (m, 2H), 6.97 (d, *J* = 5 Hz, 1H) 6.92 (d, *J* = 10, 1H), 4.12 (d, *J* = 5 Hz, 0.65H, α-H, BrMeBu, major diastereomer), 3.91 (d, *J* = 5 Hz, 0.35H, α-H, BrMeBu, minor diastereomer), 1.93 (m, 1H), 0.61 (s, 6H). ^{1}H NMR **6.4** in CD_2Cl_2 (500 MHz, δ, ppm, 298 K): 8.86 (d, *J*=5 Hz, 1 H), 8.52 (s, 1H), 7.88-7.77 (m, 3H), 7.68 (dd, *J*=7.5 Hz, *J* = 7.5 Hz, 1H), 7.51 (d, *J* = 10 Hz, 1H), 7.46-7.39 (m, 6H), 7.33-7.24 (m, 4H), 7.21 (dd, *J* = 5 Hz, J=5 Hz, 1H), 7.18 (s, 1H), 7.05 (d, *J* = 10 Hz, 1H), 7.01 (dd, *J* = 5 Hz, *J* = 5 Hz, 1H), 3.99 (s, 1H), 1.71 (m, 1H), 0.32 (s, 6H).

6.1.7 Molecular Orbital Calculations

The ground state molecular geometry optimizations were performed for (S_a,*R*)-**6.3** and (S_a,*S*)-**6.3** (where the S_a denotes the enantiomer of the ligand and the second denotes the enantiomer of the BrMeBu). The geometric parameters from X-ray diffraction analysis of **6.1** were modified using GaussView and used as the starting point for the geometry optimization. The Gaussian suite of programs (Gaussian 03)[34] was used for the restricted density functional theory calculations at the B3LYP/6-311G(d) level of theory. CD spectra for both diastereomers were computed by TD-DFT calculations using the optimized geometrical parameters and the same basis set. The first 25 singlet states were calculated.

6.1.8 Titration Experiments

For the typical CD and fluorescent titration experiments, a 1 x 10^{-5} M solution of bpib or bbib in CH_2Cl_2 was prepared. 0.1 molar equivalents of a 1 x 10^{-2} M solution of metal salt in THF were added with a micro-pipette. The solution was mixed for 2 minutes before recording the spectrum. The NMR titration experiment was carried out with ~5 mg of bpib or bbib in CD_2Cl_2 in an NMR tube and 1.0 M solution of Zn(*R*- BrMeBu)$_2$ in CD_3OD was added incrementally with a micro-pipette.

6.1.9 X-ray Crystallographic Analysis

Single crystals of **6.1** and **6.2** were mounted on glass fibres for data collection. Data were collected at ambient temperature for **6.1** and at 77 K for **6.2** on a Bruker Apex II single-crystal X-ray diffractometer with graphite-monochromated Mo Kα radiation, operating at

50 kV and 30 mA. The crystals of **6.1** belong to the triclinic space group *P-1* while the crystals of **6.2** belong to the monoclinic space group *C2/c*. No significant decay was observed for both samples. Data were processed on a PC using the Bruker SHELXTL software package (version 5.10)[35] and are corrected for absorption effects. The structures were solved by direct methods. One of the CF_3 groups in **6.1** displays rotational disordering that was modeled and refined successfully. All non-hydrogen atoms were refined anisotropically. The crystal data and selected bond lengths and angles are provided in Table 6.1 and Table 6.2, respectively.

Table 6.1 Crystallographic data for **6.1** and **6.2**.

	6.1	**6.2**
formula	$C_{42}H_{26}N_4O_4F_6Zn$	$C_{68}H_{42}N_8F_6O_4Zn$
fw	830.04	1214.47
space group	*P-1*	*C2/c*
a, Å	10.6357(8)	35.7829(7)
b, Å	12.5165(9)	10.303(2)
c, Å	13.8985(10)	16.481(3)
α, deg	95.1930(10)	90.00
β, deg	100.6520(10)	114.325(1)
γ, deg	99.6660(10)	90.00
V, Å^3	1778.3(2)	5536.74(18)
Z	2	4
D_{calc}, gcm^{-3}	1.550	1.457
μ, cm^{-1}	7.73	5.25
$2\theta_{max}$, deg	56.46	54.28
no. of reflections measured	19981	26959
no. of reflections used (R_{int})	7966 (0.0228)	6118 (0.0733)
no. of paramters	568	393
final *R* [I > 2σ(I)] R_1[a], wR_2[b]	0.0343, 0.0822	0.0460, 0.0882
R (all data) R_1[a], wR_2[b]	0.0459, 0.0879	0.0906, 0.1038
GOF on F^2	1.034	1.015

[a] $R1 = \Sigma[|F_o| - |F_c|]/\Sigma|F_o|$. [b] $wR2 = \{\Sigma[w(F_o^2 - F_c^2)]/ \Sigma(wF_o^2)\}^{1/2}$.

$\omega = 1/[\sigma^2(F_o^2) + (0.075P)^2]$, where $P = [\max.(F_o^2,0) + 2F_c^2]/3$.

Table 6.2 Selected bond lengths of complexes **6.1** and **6.2.**

		6.1	
Zn(1)-O(1)	1.9890(13)	O(4)-Zn(1)-O(1)	106.11(6)
Zn1(1)-O(4)	1.9872(14)	O(4)-Zn(1)-N(1)	102.53(6)
Zn(1)-N(1)	2.0557(15)	O(1)-Zn(1)-N(1)	95.57(6)
Zn(1)-N(4)	2.0655(15)	O(4)-Zn(1)-N(4)	105.34(6)
		O(1)-Zn(1)-N(4)	105.34(6)
		N(1)-Zn(1)-N(4)	140.81(6)
		6.2	
Zn(1)-O(2)	1.9716(17)	O(2)-Zn(1)-O(2')	119.57(11)
Zn1(1)-N(1)	2.061(2)	O(2)-Zn(1)-N(1)	102.60(7)
		O(2)-Zn(1)-N(1')	98.20(7)
		N(1)-Zn(1)-N(1')	137.99(11)

6.2 Results and Discussion

6.2.1 Synthesis of Zn(II) Carboxylates with Ligands bpib and bbib

The chiral sensing study focused on the Zn(II) chiral carboxylates: (*S*)-2-bromo-3-methyl-butyrate (*S*-BrMeBu) and (*R*)-2-bromo-3-methyl-butyrate (*R*-BrMeBu). To synthesize (*S*)-Zn(BrMeBu) and (*R*)-Zn(BrMeBu) the chiral acids ((*S*)-2-bromo-3-methyl-butyric acid or (*R*)-2-bromo-3-methyl-butyric acid) were mixed with ZnO in toluene and bubbled with N_2 overnight. To get racemic Zn(BrMeBu) equal parts of pre-synthesized (*S*)-Zn(BrMeBu)$_2$ and (*R*)-Zn(BrMeBu)$_2$ were mixed.

To establish the binding mode of the chiral Zn(II) carboxylate with the chelate ligands bpib and bbib, attempts were made to obtain single crystals of Zn(bpib)(BrMeBu)$_2$ (**6.3**) and Zn(bpib)(BrMeBu)$_2$ (**6.4**) for X-ray diffraction analysis.

Attempts to synthesize these complexes involved dissolving the ligand in CH_2Cl_2 and layering it with a solution of Zn(BrMeBu) in THF. Slow evaporation of solvents led to a yellowish powder. However, no crystals suitable for X-ray diffraction were obtained for the complexes of $Zn(BrMeBu)_2$. Use of both racemic and enantiomerically pure Zn(BrMeBu) did not result in crystals. Therefore, attention was focused on obtaining single crystals of the non-chiral Zn(II) carboxylate, $Zn(tfa)_2$, tfa = $CF_3CO_2^-$ with ligands bpib and bbib. Again the ligands bpib or bbib were dissolved in CH_2Cl_2 and layered with a solution of $Zn(tfa)_2$ in THF. Fortunately, slow evaporation of solvents led to the isolation of single crystals of both complexes $Zn(bpib)(tfa)_2$ (**6.1**) and $Zn(bbib)(tfa)_2$ (**6.2**). Their structures were successfully determined by X-ray diffraction. Both complexes were found to be 1:1 adducts of the ligand with $Zn(tfa)_2$

6.2.2 Structures of 6.1 and 6.2

As shown in Figure 6.2, the molecule of **6.1** has an approximate C_2 symmetry with the Zn centre being chelated by two pyridyl groups of the bpib ligand. The dihedral angle between the two indolyl rings is 118.1°, that is considerably smaller than that of the free ligand (125.1°) (Chapter 4), indicating a greater twist between the two rings due to Zn(II) coordination. The two tfa anions are bound to the Zn centre as terminal ligands. The Zn–N (2.056(1)–2.065(1) Å) and the Zn–O (1.987(1)–1.989 (1) Å) bond lengths are normal;[3, 8, 36-40] however, the geometry around the Zn(II) ion is a highly distorted tetrahedron with a very large N–Zn–N angle, 140.81(6)°, resembling that observed in the structure of $[Cu(bpib)_2]^+$ discussed in Chapter 5.[33]

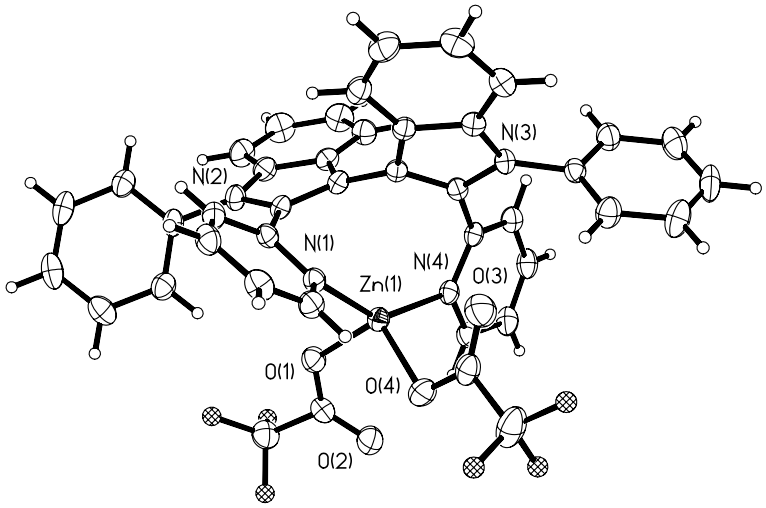

Figure 6.2 The structure of **6.1** with 50% thermal ellipsoids and labelling schemes for the key atoms. Only one set of the disordered F atoms are shown for clarity.

Consistent with the behaviour of the complexes **5.4-5.6** presented in Chapter 5, the phenyl group on ligand bpib in **6.1** displays a hindered rotation around the C-N bond in solution due to non-bonding hydrogen interactions between the phenyl, the indolyl and the pyridyl groups, as confirmed by variable temperature ^{1}H NMR spectra of **6.1** shown in Figure 6.3.

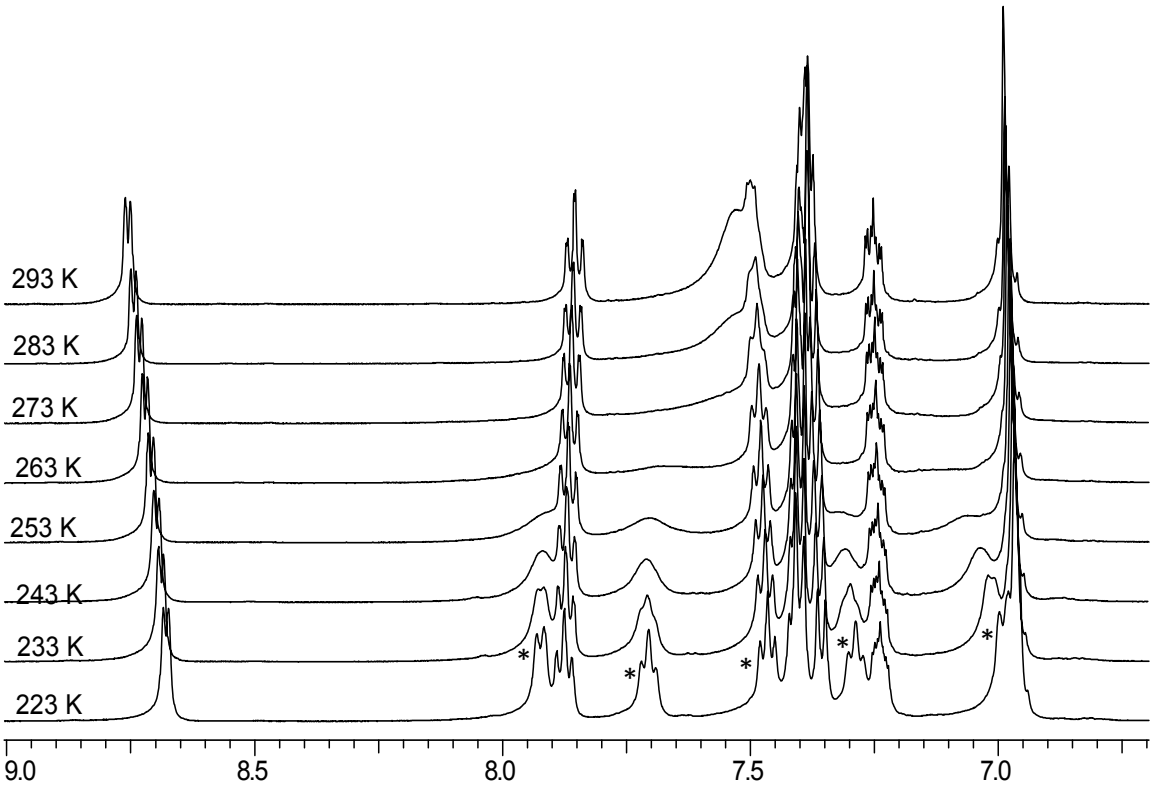

Figure 6.3 Variable temperature ^{1}H NMR of **6.1** in CD_2Cl_2 with * indicating the phenyl peaks.

The structure of **6.2** is shown in Figure 6.4. This molecule has a crystallographically imposed C_2 symmetry. The Zn(II) ion is bound to the two central pyridyl rings of the bbib ligand in the same manner as that in **6.1** with similar Zn–O and Zn–N bond lengths. One notable difference is the bond angles of O–Zn–O (106.11(6)° for **6.1**, 119.57(11)° for **6.2** and N–Zn–N, 140.81(6)° for **6.1**, 139.99(11)° for **6.2**). The much smaller O–Zn–O bond angle in **6.1** is likely caused by the relatively short separation distance between the non-coordinating O(3) atom and the Zn(II) ion (2.836(1) Å), which is much shorter than that between O(2) and Zn(1) (3.003(1) Å) in (106.11(6)°)

in **6.2**. The dihedral angle between the two central indolyl rings in **6.2** is 128.8°, much greater than that in **6.1** but nearly identical with that of the free ligand bbib (128.5°). The inner indolyl ring and the outer indolyl ring are not co-planar with the phenyl linker with a dihedral angle of 122.7° and 126.1°, respectively, with respect to the phenyl plane, which is again caused by non-bonding interactions of hydrogen atoms between the 2-(2-pyridyl)indolyl group and the phenyl. Significantly, in the crystal structure of **6.2**, the two neighbouring inner and outer 2-(2-pyridyl)indolyl groups are on the same side with respect to the phenyl plane, i.e. having the *syn-syn* geometry, **A**, shown in Figure 6.5. The coordination of the two central pyridyl rings to the Zn(II) ion forces the two central 2-(2-pyridyl)indolyls to orient to opposite directions (dihedral angle, 128.8°). As a result, the other possible geometric isomers are *anti-anti* and *syn-anti* shown as **B** and **C**, respectively, in Figure 6.5. Variable temperature ^{1}H NMR data of **6.2** appear to indicate that there are two dominating isomers in solution with about a 1:1 ratio (Figure 6.6), based on the appearance of two distinct H_1-pyridyl chemical shifts at low temperature. However, it is possible that the chemical shifts of isomer **C** overlap with those of **A** and **B**, making it difficult to determine the precise distributions of the three isomers in solution. Nonetheless, the structural isomerism observed in **6.2** is not surprising due to their similarity with that observed in Pt(II) and Cu(I) complexes based on 1,3- and 1,4-bis[2-(2-py)benzimidazolyl]-benzene ligands as discussed in previous work in our group as well as in Chapter 3.[41, 42] Since only one nitrogen is available to bind on the distal 2-

(2'-pyridyl)indolyl group it does not bind to the Zn(II) ions; it is not a strong enough donor without the chelate effect.

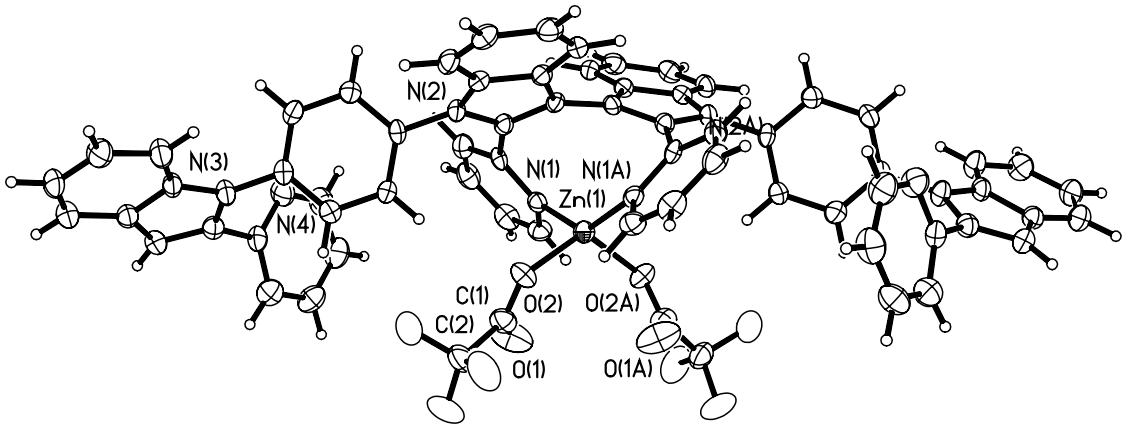

Figure 6.4 The structure of **6.2** with 50% thermal ellipsoids and labeling schemes for the key atoms.

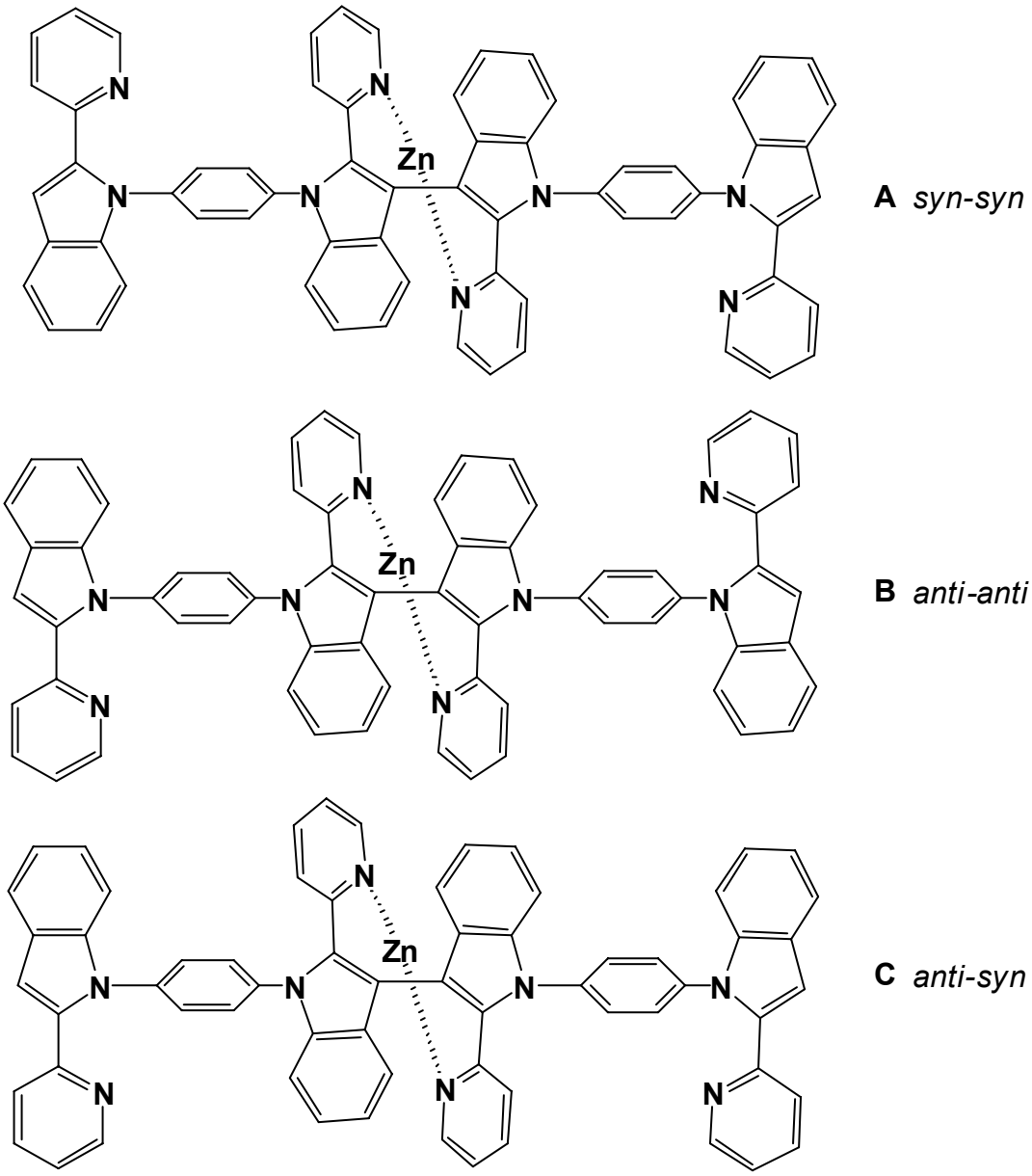

Figure 6.5 Structure of geometric isomers of **6.2.**

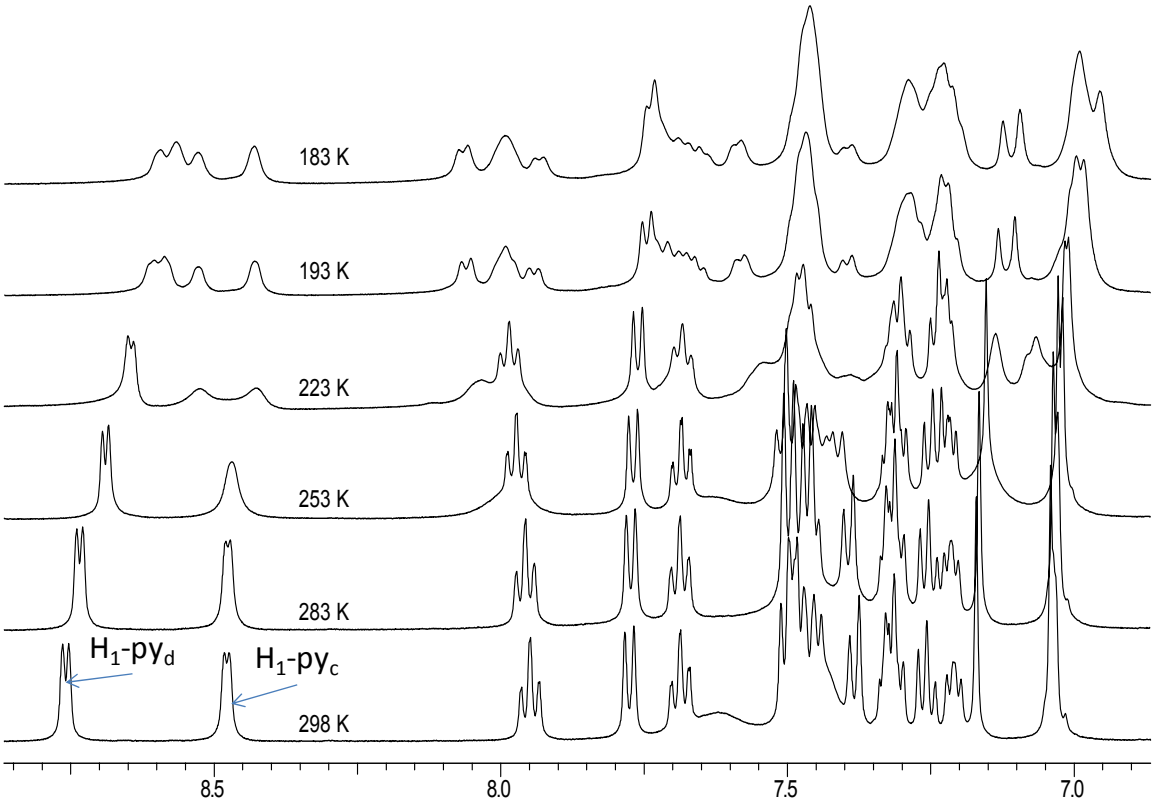

Figure 6.6 Variable temperature ^{1}H NMR of **6.2** in CD_2Cl_2 where H_1-py_d is the proton in the H_1 position on the distal pyridyl group and H_1-py_c is the proton on the central pyridyl group.

6.2.3 Structures of (*S*)-6.3 and (*S*)-6.4 in solution

The chiral Zn(II) salt, Zn(*S*-BrMeBu)$_2$ or Zn(*R*-BrMeBu)$_2$ was found to bind to bpib and bbib in the same manner as Zn(tfa)$_2$, based on the similarity of the ^{1}H NMR data of **6.3** and **6.4** with those of **6.1** and **6.2** respectively. However, the presence of the chiral centre on the BrMeBu ligand can lead to the formation of diastereomers. For example,

diastereomers (R_a,*S*)-**6.3** and (S_a,*S*)-**6.3** are expected when Zn(*S*-BrMeBu)$_2$ is reacted with racemic bpib as shown in Figure 6.7. ^{1}H NMR titration experiments indeed showed that when < 1 eq. of Zn(*S*-BrMeBu)$_2$ was added to the solution of bpib in CD_2Cl_2, two sets of well resolved chemical shifts for both the H_1-pyridly and H_α-BrMeBu protons with ~2:1 ratio were observed (Figure 6.9 and Figure 6.10), which can be attributed to the two diastereomers. ^{1}H NMR titration experiments also confirmed that Zn(BrMeBu)$_2$ binds to bpib fairly strongly due to the fact that the free ligand and the bound ligand have distinct and well resolved signals when the Zn(II):bpib ratio is less than 1 (Figure 6.9 and Figure 6.10). When > 1 eq. of Zn(*R*-BrMeBu)$_2$ was added, the diastereomer peaks were no longer resolved at ambient temperature, which can be attributed to the dynamic exchange between bound and non-bound Zn(*R*-BrMeBu)$_2$. With a 1:1 ratio of Zn(*S*-BrMeBu):bpib, the diastereomer peaks can be resolved at ~203 K with the same 2:1 integrated intensity ratio, as observed in the NMR titration experiments (Figure 6.10 and Figure 6.8).

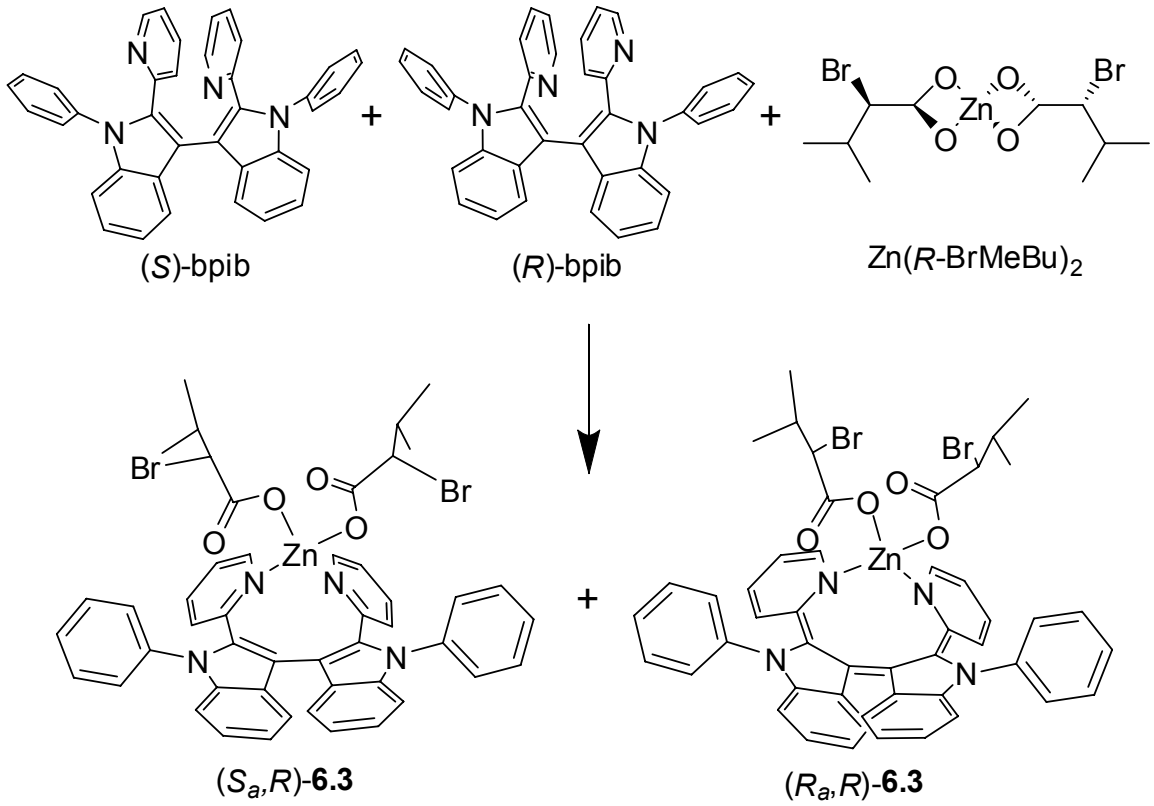

Figure 6.7 A Scheme showing the formation of diastereomers from the reaction of racemic bpib with (R)-$Zn(BrMeBu)_2$.

The variable temperature ^1H NMR spectra of (*R)*-**6.4** is complex due to the presence of geometric isomers and diastereomers associated with each geometric isomers. Similar geometric isomer peaks are observed in **6.2,** which complicate the diastereomer peak assignments in the H_1-py region. However, the two H_α-BrMeBu diastereomer peaks in the spectrum of (*R)*-**6.4** are well resolved at ~223 K with ~2:1 ratio, similar to that of (*R*)-**6.3** (Figure 6.11 and Figure 6.12). Hence, NMR experiments

established that for both ligands bpib and bbib there is a preferential formation for one of the diastereomers with Zn(*R*-BrMeBu)$_2$ (or Zn(*S*-BrMeBu)$_2$).

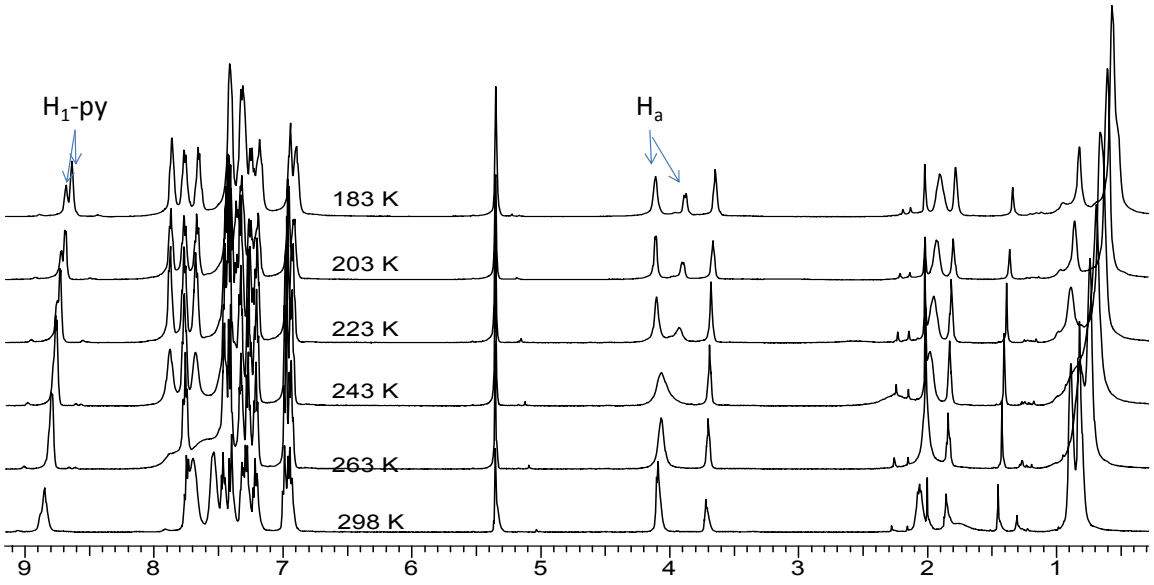

Figure 6.8 The full variable temperature ^{1}H NMR spectrum of **6.3** with one eq. of Zn(*S*-BrMeBu)$_2$ in CD_2Cl_2 with the chemical shifts of H_1 on the pyridyl group, and H_a from Zn(BrMeBu)$_2$ are indicated.

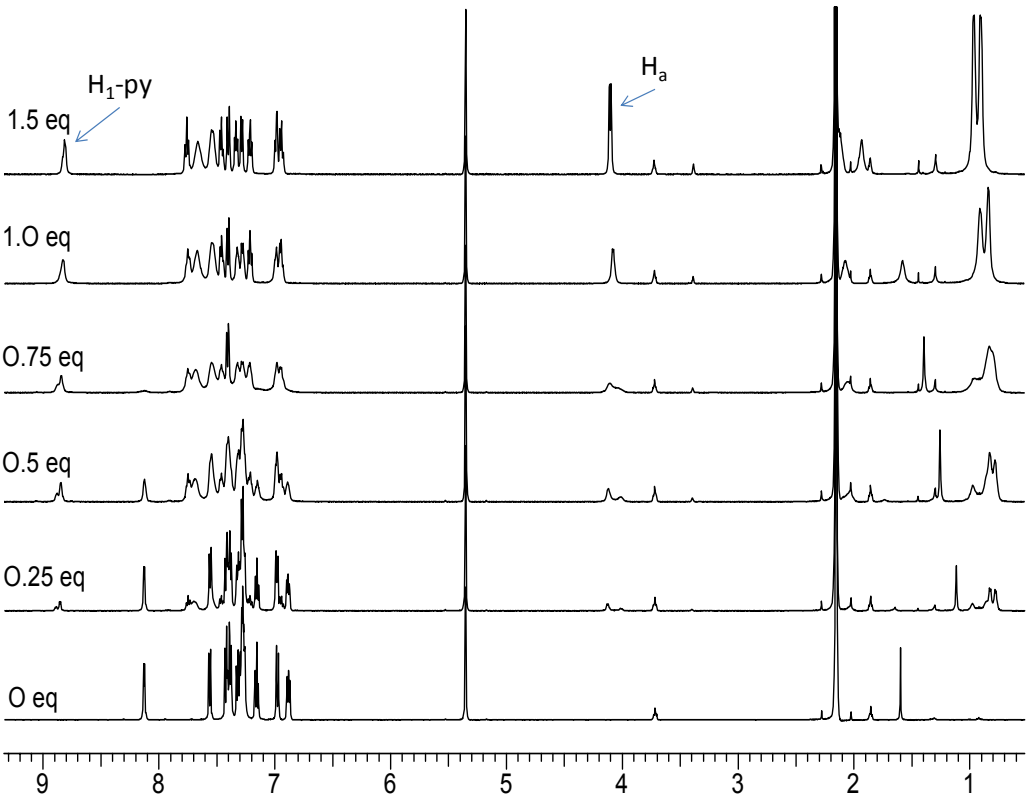

Figure 6.9 ^{1}H NMR spectrum of bpib in CD_2Cl_2 at 298 K with the addition of (*R*)-Zn(BrMeBu)$_2$; the chemical shifts of H_1 on the pyridyl group, and H_a from Zn(BrMeBu)$_2$ are indicated.

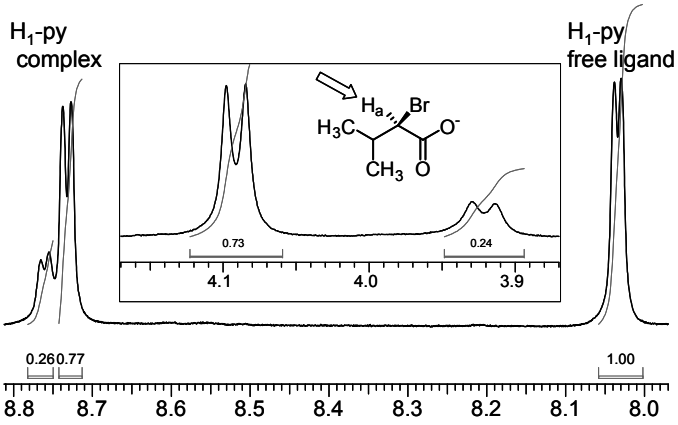

Figure 6.10 The partial ^{1}H NMR spectrum of **6.3** with 0.5 eq. Zn(*S*-BrMeBu)$_2$ in CD_2Cl_2 at 298 K showing the H_1-py peaks and the H_a–BrMeBu peaks of the two diastereomers.

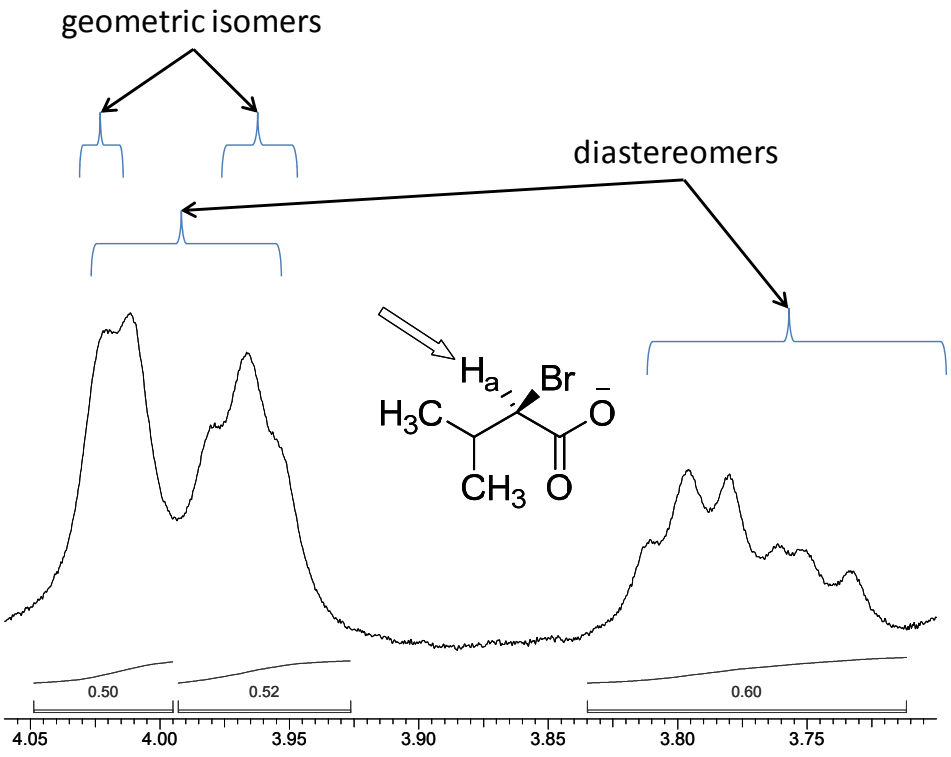

Figure 6.11 The partial ^{1}H NMR spectrum of **6.4** in CD_2Cl_2 at 203 K showing the H_a-BrMeBu peaks of diastereomers (the two sets of peaks at 4.00-3.93 ppm, 3.83-3.72 ppm) and geometrical isomers (the multiple peaks within each set of the diastereomer peaks).

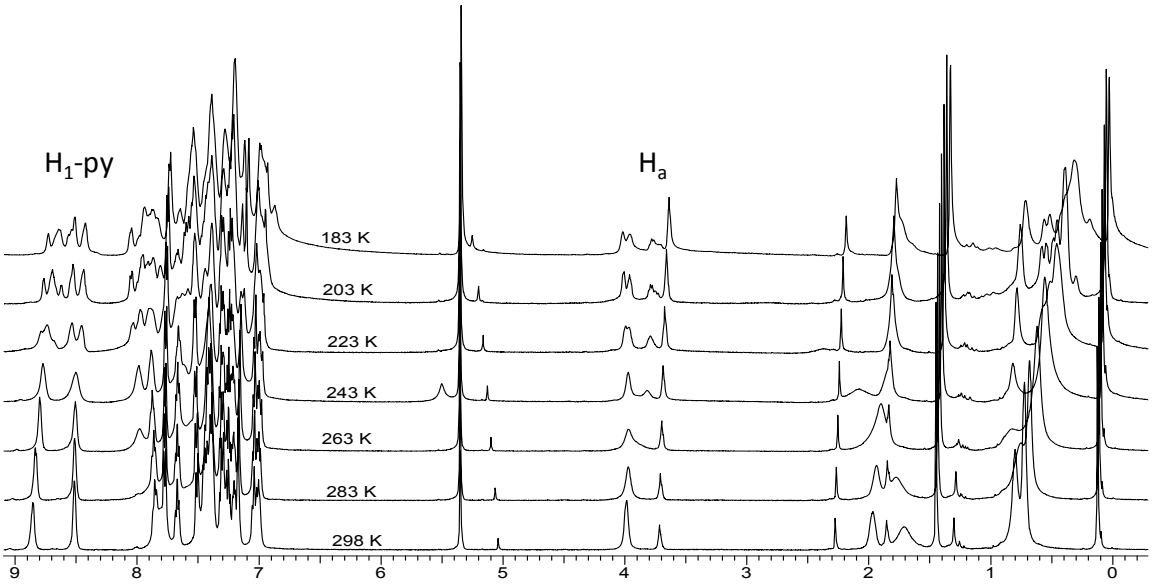

Figure 6.12 The full variable temperature ^{1}H NMR spectra of **6.4** in CD_2Cl_2**.**

6.2.4 Calculated Structures of 6.3

To determine which diastereomer of **6.3** is favoured, DFT calculations were performed using the Gaussian 03 suite of programs at the B3LYP level of theory with 6-311G(d) basis set[34] for the diastereomers (S_a,*R*)-**6.3** and (S_a,*S*)-**6.3**, assuming that a similar binding mode as that of $Zn(tfa)_2$ is adopted by the chiral zinc salt. The crystal structure geometry of **6.1** was modified and used as a starting geometry. Geometry optimization was performed for both diastereomers and the calculated structures for both diastereomers are shown in Figure 6.13. Indeed, the structures of the two diastereomers resemble that of **6.1**. The computational results indicated an energy difference of ~8.50 kJ/mol between (S_a,*R)*-**6.3** and (S_a,*S)*-**6.3** with the(S_a,*S)*-**6.3** complex (or (R_a,*R)*-**6.3**) being the more stable diastereomer.

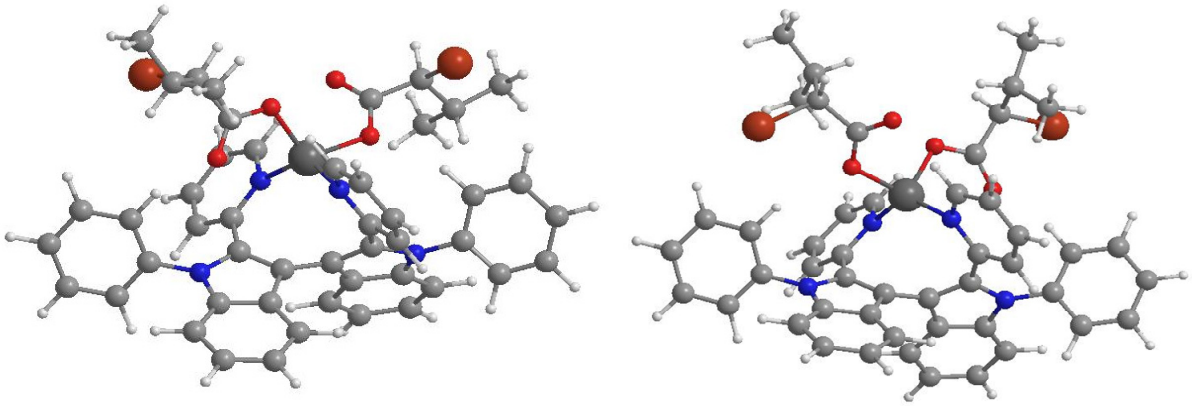

Figure 6.13 Calculated structures of (S_a,*R*)-**6.3** (left) and (S_a,*R*)-**6.3** right**.** C: grey, H: white, N: blue, O: red, Br: orange, Zn: dark grey.

6.2.5 CD Spectral Response of bpib and bbib Toward Zn(*R*-BrMeBu)$_2$ and Zn(*S*-BrMeBu)$_2$

6.2.5.1 Response of bpib

To establish whether or not the racemic ligands bpib and bbib are capable of distinguishing chiral Zn(II) carboxylates, the CD spectral change of bpib and bbib toward Zn(*R*-BrMeBu)$_2$ and Zn(*S*-BrMeBu)$_2$ was examined. As shown in Figure 6.14 and Figure 6.15, the addition of either Zn(*S*-BrMeBu)$_2$ or Zn(*R*-BrMeBu)$_2$ to the solution of the racemic bpib in CH_2Cl_2 (1.0×10^{-5} M) causes the appearance of a distinct CD spectrum in the 225–400 nm region which increases intensity with the amount of Zn(II) added until the addition of 1 eq of Zn(*S*-BrMeBu) or Zn(*R*-BrMeBu). The CD spectrum of (*S)*-**6.3** is approximately the mirror image of that of (*R)*-**6.3** in the 250–400 nm region, supporting that the racemic bpib can indeed distinguish the enantiomers of Zn(BrMeBu)$_2$ by CD.

Because $Zn(BrMeBu)_2$ has no absorption or a CD signal at $\lambda > 250$ nm, the intense CD bands in 250–450 nm region are clearly the consequence of the electronic transitions of bpib, as supported by the UV-Vis spectra of bpib and its Zn(II) complex (Figure 6.16). The UV-Vis spectra of the Zn(II) complexes of bpib are very similar in shape to that of bpib alone. Significantly, at a fixed concentration of the ligand bpib and Zn(BrMeBu), the intensity of the CD band at $\lambda_{max} = 320$ nm is linearly dependent on the ee of the chiral Zn(II) carboxylate, as shown by Figure 6.14, supporting that the N,N'-chelate bpib may be used for the quantitative determination of ee of $Zn(BrMeBu)_2$. Plotting the intensity of the peak at 320 nm vs enantiomeric excess gives a line with the equation $y = 0.0408x - 0.1698$ with R^2 value of 0.9704.

Polarimetry measurements also displayed a chiral response. When one molar equivalent of racemic bpib was added to a 10 g/L solution of (*S*)-$Zn(BrMeBu)_2$ the specific rotation went from 7.0° to 225.3°. If the total mass of the complex is included in the specific rotation calculation a rotation of 100.1° is found. A racemic mixture of bpib alone did not display a specific rotation.

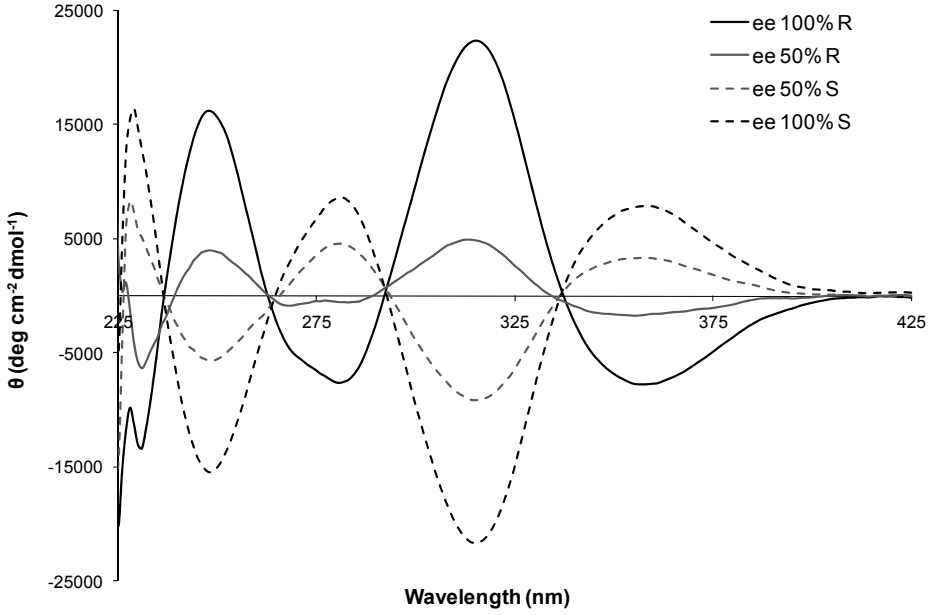

Figure 6.14 CD spectra of bpib (2.0 × 10-5 M) with one equivalent of $Zn(BrMeBu)_2$ of varying ee in CH_2Cl_2**.**

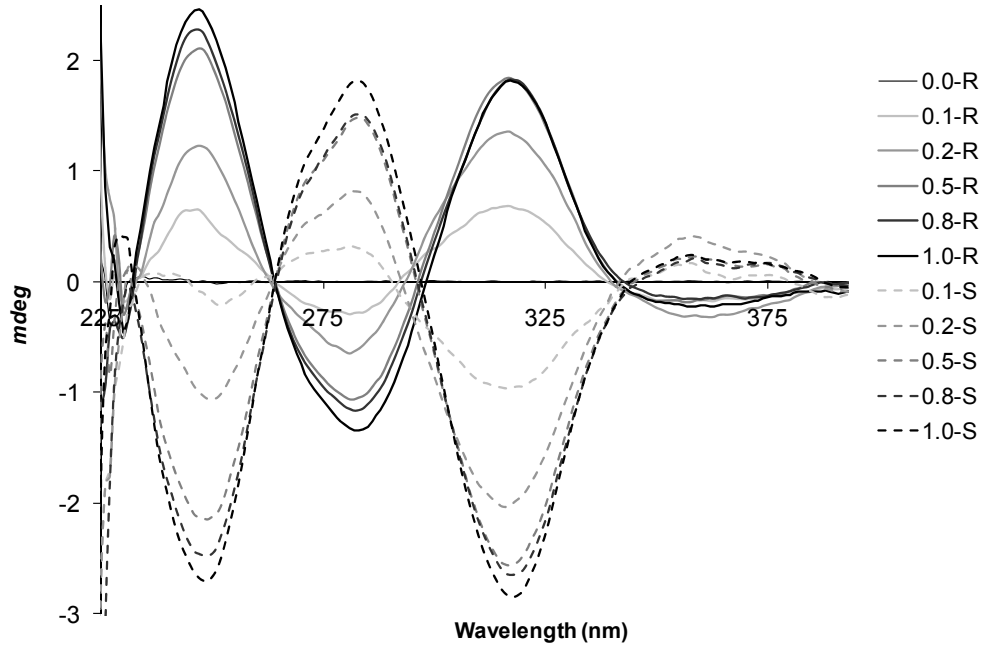

Figure 6.15 CD titration diagrams of bpib (1.0 x 10^{-5} M) in CH_2Cl_2 by various equivalents of Zn(*R*-BrMeBu)$_2$ and Zn(*S*-BrMeBu)$_2$, respectively.

6.2.5.2 CD Response of bbib

The larger racemic chelate ligands bbib and btib were found to display a similar CD spectral response upon the addition of the chiral $Zn(BrMeBu)_2$ except that the CD band at 320 nm is more intense and dominant, compared to that of bpib (Figure 6.16). Further examination of using btib as a chiral sensor was not done because of solubility problems with the ligand. However, the response of bbib is consistent with the fact that the Zn(II) binding site in **6.4** is similar to that of **6.3** as established by the crystal structures **6.1** and **6.2** and ^{1}H NMR data. It was anticipated that the larger ligands should have a larger response in the CD due to their greater absorbance. The CD spectra were measured at $1x10^{-5}$ M with one equivalent of $Zn(R\text{-}BrMeBu)_2$ added. The shape of the CD spectrum is similar to that of the bpib with chiral Zn(BrMeBu), but a larger magnitude. The UV-Vis spectrum of bbib with Zn(BrMeBu) has greater molar absorptivity due to the larger number of chromophores per molecule. When the molar absorptivity of the ligand was taken into consideration, the larger ligands, in fact, have a smaller response than that found for bpib. The relatively intense CD band at 320 nm in the spectrum of bbib with $Zn(BrMeBu)_2$ is consistent with the greater extinction coefficient of the corresponding absorption band, compared to that of bpib, as shown in Figure 6.16. Based on the NMR data and the calculated structures, the CD response of racemic bpib and bbib toward the chiral $Zn(BrMeBu)_2$ shown in Figure 6.16 is likely the consequence of the CD spectral difference of the diastereomers and the preferential formation of one diastereomer.

a)

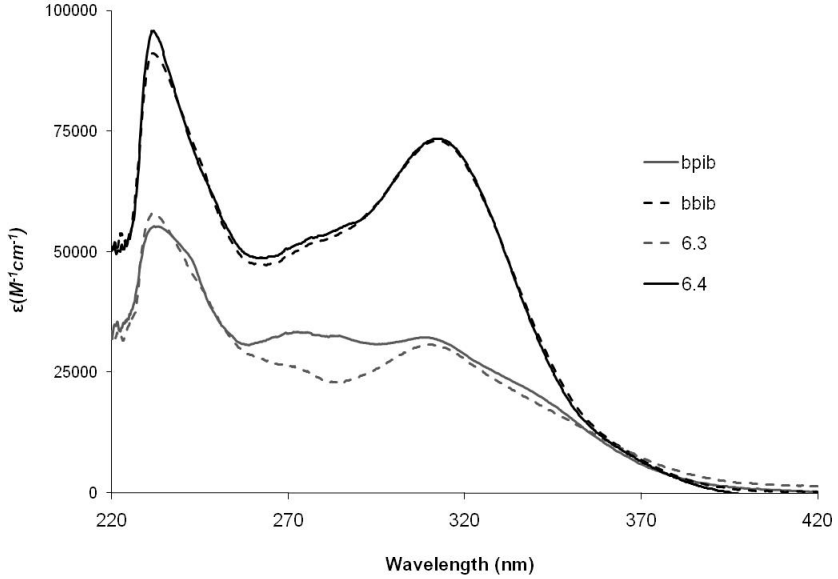

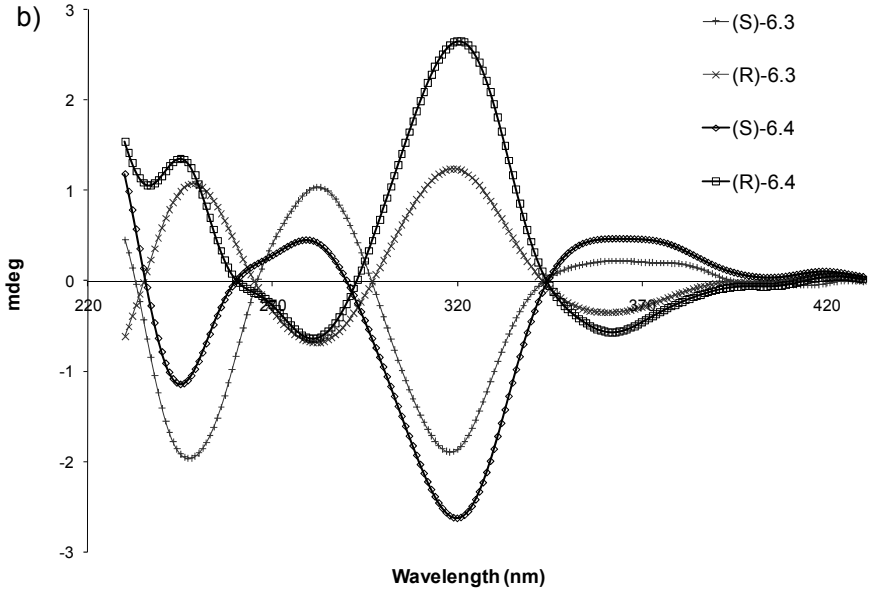

Figure 6.16 a) The UV-Vis spectra of bpib, bbib and their complexes with $Zn(BrMeBu)_2$ b) The CD spectra of bpib and bbib (1.0 x 10 -5 M) with one equivalent of (*R*) or (*S*) chiral $Zn(BrMeBu)_2$ in CH_2Cl_2.

6.2.5.3 Solvent Effect

During the course of our study it was also noted that the solvent molecules played a role in the interaction of the ligand with the metal ion. No CD spectrum was observed when THF was used as the solvent. Gradually changing the solvent from all CH_2Cl_2 to THF, the intensity of the CD spectrum decreased linearly with the amount of THF added. Furthermore, the ^1H NMR also shows broadening of some peaks in the presence of methanol. These are an indication of interactions of these solvents molecules with the Zn(II) ion – presumably coordinating to the metal centre, competing with the chelate ligand.

6.2.5.4 bpib With the Free Acid

The CD response of bpib with the chiral acid, *S* (or *R*)-2-bromo-3-methylbutyric acid was examined since the acid can interact with the atropisomeric ligand via hydrogen bonds. However, no significant CD spectral change was observed with the free acid. It is likely that the weak hydrogen bonds between the racemic host and the chiral guest are not sufficient to differentiate the diastereomers to produce significant CD signals. Therefore, the Zn(II) coordination to the atropisomeric ligand is clearly a key for distinguishing the two enantiomers of the 2-bromo-3methylbutyrate via CD spectra. In other words, the Zn(II) ion functions as a mediator to facilitate the recognition event between atropisomeric ligand and the chiral carboxylate. Similar metal mediated chiral sensing has been reported in Chapter 1.[11, 43]

6.2.6 Computational Study

To determine if the (S_a,*R*)-**6.3** and (S_a,*S*)-**6.3** (or (R_a,*S*)-**6.3** and (R_a,*R*)-**6.3**) diastereomers have different CD spectra, TD-DFT calculations on this pair of diastereomers were performed using the optimized geometry parameters.[44, 45] The first 25 singlet states were calculated and a σ = 0.2 eV line width was used where Gaussian distributions were attributed to each transition, using the oscillator strength as the intensity.[46, 47] The electronic transitions with the highest oscillator strengths are shown in Table 6.3. The computed CD spectra of (S_a,*R*)-**6.3** and (S_a,*S*)-**6.3** are shown in Figure 6.17. These CD spectra are similar and match well with the experimental data in the 300 – 450 nm region, but notable differences are evident in the short wavelength region, due to mostly the chiral carboxylate contributions (Figure 6.17). Population analysis for the first 25 singlet excited states further confirms that most of the transitions with high oscillator strengths are dominated by 2-(2-pyridyl)indolyl parts of the ligand, which is consistent with the UV-Vis data. The orbital diagrams for HOMO, 2nd HOMO and the lowest three unoccupied orbitals for (S_a,*S*)-**6.3** shown in Figure 6.18 further illustrate that the low energy electronic transitions in the complex involve the central part of ligand bpib with little contributions from Zn(II) or the carboxylate. The orbital diagrams for the (S_a,*R*)-**6.3** are essentially the same as those shown for (S_a,*S*)-**6.3.** The computational results also support that using the pure *R*-bpib or the pure *S*-bpib alone will not be able to effectively distinguish the enantiomers of Zn(BrMeBu)$_2$ due to the similarity of the CD spectra of diastereomers (S_a,*R*)-**6.3** and (S_a,*S*)-**6.3** (or (R_a,*S*)-**6.3** and (R_a,*R*)-**6.3**). If enantiomerically pure bpib was used mirror image CD spectra for the addition of Zn(*S*-

BrMeBu) and Zn(*R*-BrMeBu) would not have been seen. Based on the computational results and NMR data, it is concluded that the distinct CD spectral response of the racemic bpib toward Zn(*R*-BrMeBu)$_2$ and Zn(*S*-BrMeBu)$_2$ is due to the preferential formation of diastereomers (R_a,*R*)-**6.3** and (S_a,*S*)-**6.3**, versus (S_a,*R*)-**6.3** and (R_a,*S*)-**6.3**, respectively.

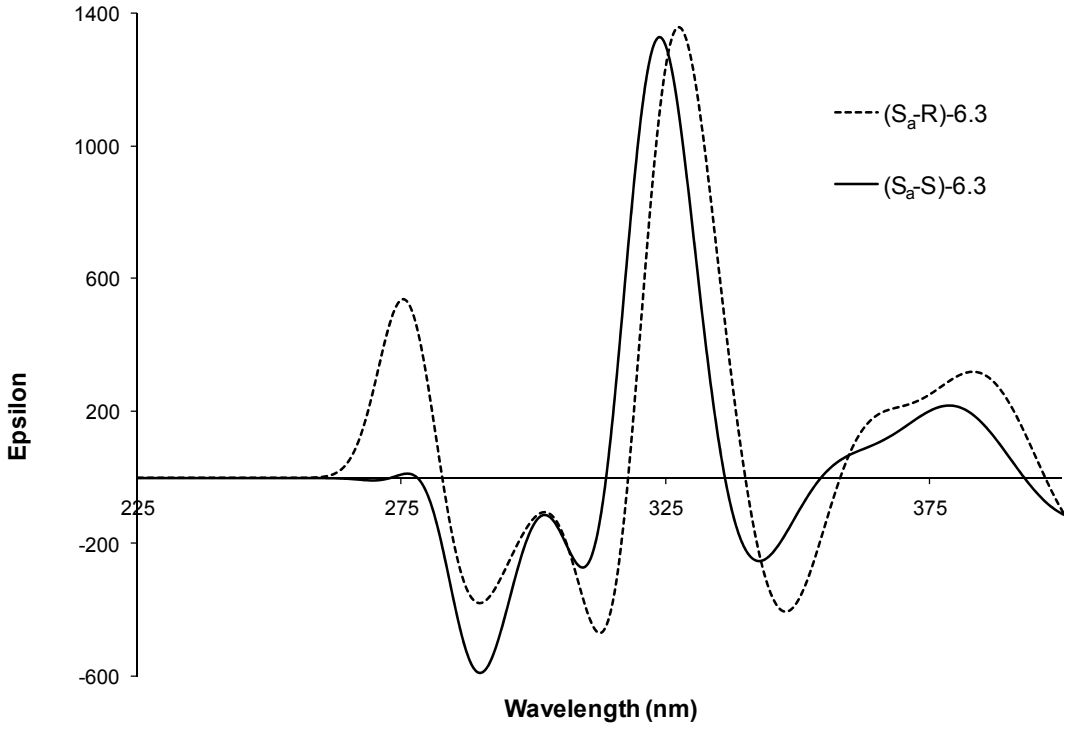

Figure 6.17 Computed CD spectra of (S_a,*R*)-**6.3** and (S_a,*R*)-**6.3**.

Table 6.3 The electronic transitions with the highest oscillator strengths for both (S_aS)-**6.3** and (S_aS)-**6.3; t**he HOMO level is 245 and the LUMO is 246.

State	Energy (nm)	Orbitals (coefficients)	Oscillator strength
(S_aS)-**6.3**			
2	380.21	245 -> 247 (0.6845)	0.0539
7	324.22	242 -> 246 (0.5668)	0.0837
8	323.03	242 -> 246 (0.2938)	0.1828
		243 -> 247 (0.5602)	
19	281.62	242 -> 248 (0.4727)	0.0533
		245 -> 250 (-0.4363)	
24	2.75.24	243 -> 249 (-0.3838)	0.0605
		245 -> 252 (-0.36190	
(S_aR)-**6.3**			
2	386.07	245 -> 247 (0.6833)	0.0499
7	327.62	243 -> 247 (0.5318)	0.0903
8	326.29	242 -> 246 (0.5460)	0.1837
		243 ->247 (0.3668)	
11	315.57	242 -> 247 (0.2625)	0.0812
		245 -> 249 (0.5975)	
25	275.83	243 -> 249 (0.2958)	0.0745
		245 -> 252 (0.5369)	

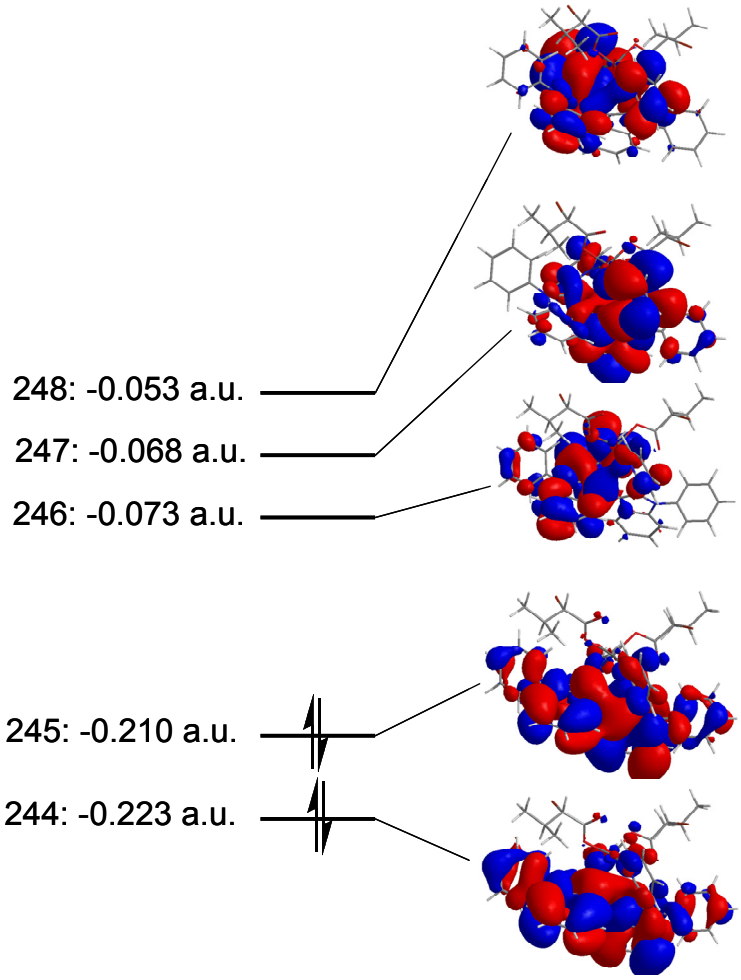

Figure 6.18 A diagram showing the frontier orbitals (orbital number and energy are shown on the left) of (S_a,*S*)-**6.3.** The corresponding orbitals for (S_a-*R*)-**6.3** are similar with slight difference in orbital energies (244: -0.223 a.u., 245: -0.211 a.u., 246: -0.076 a.u., 247: -0.071 a.u., 248: -0.055a.u.).

6.2.7 Selectivity and Fluorescent Response of bpib and bbib Toward Zn(II) Carboxylates

To find out if the atropisomeric *N*, *N*-chelate ligand bpib can discriminate other chiral Zn(II) acetate derivatives, the CD response of bpib toward Zn(*S*-MeBu)$_2$, MeBu = 2-methyl-butyrate was also examined.[36] Surprisingly, the addition of Zn(*S*-MeBu)$_2$ to the solution of the racemic bpib under the same conditions used for Zn(BrMeBu)$_2$ did not yield any significant CD signal in the 250 – 400 nm region. One possible explanation for the lack of CD response of bpib toward Zn(*S*-MeBu)$_2$ is that 2-methylbutyrate is a stronger donor due to the electron donating 2-methyl group, compared with 2-bromo-3-methylbutyrate, thus competing more effectively for the Zn(II) ion, and weakening the Zn(II) binding with the chelate ligand bpib. Because bpib and bbib are highly fluorescent molecules, the relative binding strength of Zn(II) acetate derivatives can be qualitatively compared by fluorescent titration experiments. Indeed, it was observed that the addition of Zn(BrMeBu)$_2$ and Zn(tfa)$_2$ to the solution of the racemic bpib in CH_2Cl_2 causes a red shift of the emission band of bpib. Under the same conditions, Zn(OAc)$_2$ and Zn(MeBu)$_2$ have little impact on the emission spectrum of bpib, unless a large excess of the Zn(II) salt (>15 eq.) is added. For comparison, fluorescent titration with Zn(ClO_4)$_2$ were also performed where the ClO_4^- anion is a well known poor donor and the Zn(II) ion is expected to bind strongly with the chelate ligand. The addition of Zn(ClO_4)$_2$ to the solution of bpib causes a strong fluorescent quenching and an emission peak red shift as well. As shown in Figure 6.19, the fluorescent response of Zn(BrMeBu)$_2$ toward bpib and bbib is between those of Zn(tfa)$_2$ and Zn(ClO_4)$_2$. One notable difference between the

chiral Zn(II) salt and the non-chiral Zn(II) salt is the absence of isosbestic points in the chiral Zn(II) salt titration diagrams, which is consistent with the presence of diastereomers of the chiral Zn(II) complexes. From the Stern-Volmer plots shown in Figure 6.25, it is evident that the binding of $Zn(BrMeBu)_2$ to ligand bpib is much stronger than that of $Zn(tfa)_2$, $Zn(MeBu)_2$ and $Zn(OAc)_2$ but much weaker than $Zn(ClO_4)_2$. Hence, the fluorescent data support that the lack of a CD response of ligand bpib toward the chiral Zn(*S*-MeBu)$_2$ is due to the weak binding of this particular Zn(II) salt. The fluorescent response of ligand bbib toward Zn(II) carboxylates follows the same pattern as that of ligand bpib, as shown by data in Figure 6.20 consistent with bbib having similar binding of Zn(II) as bpib.

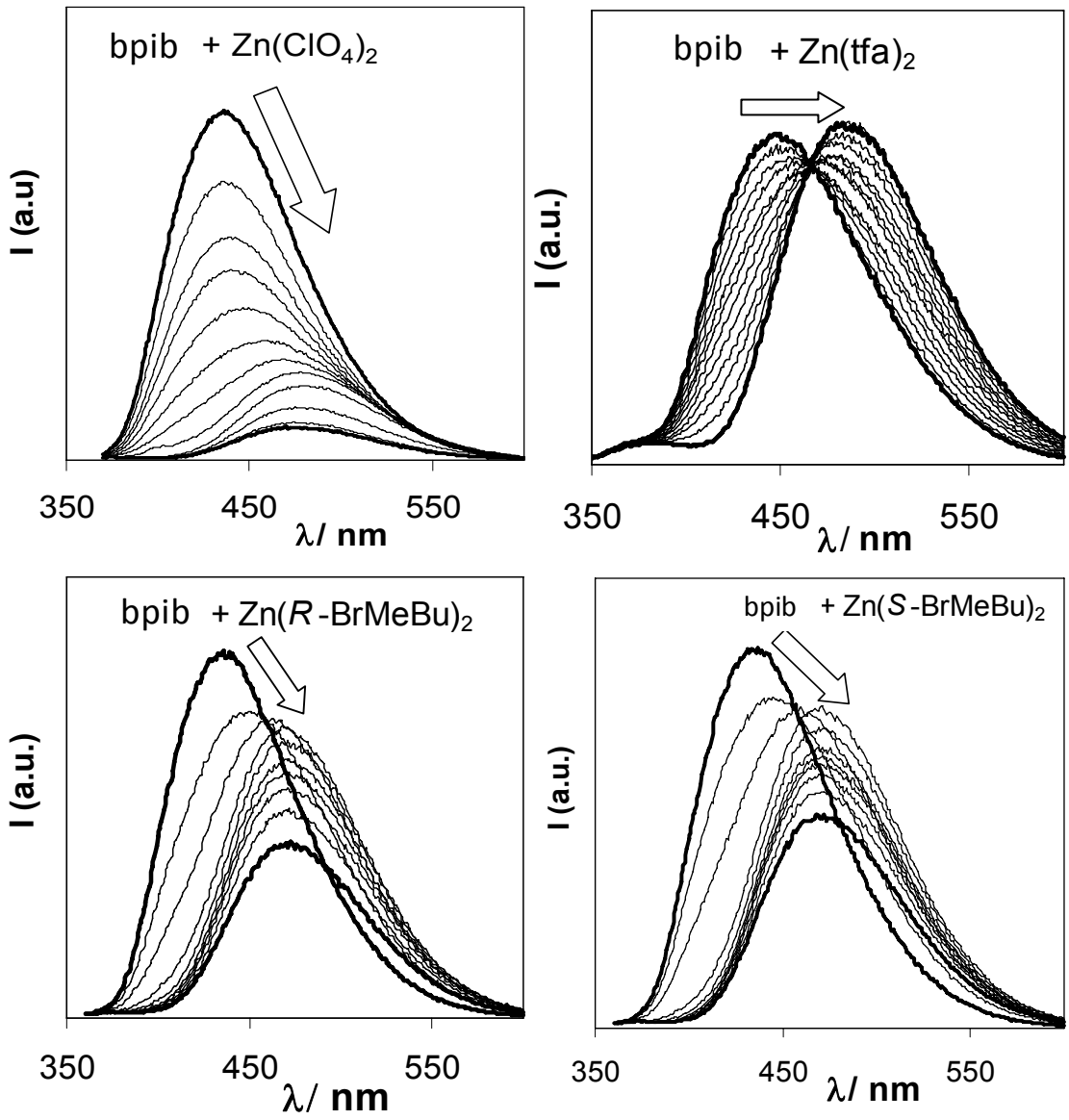

Figure 6.19 Fluorescent titration diagrams of the solution of bpib (1.0×10^{-5} M) in CH_2Cl_2 with $Zn(ClO_4)_2$ (0.0 – 2.0 eq.), $Zn(tfa)_2$ (0.0 – 5.0 eq.), and $Zn(BrMeBu)_2$ (0.0 – 5.0 eq.), respectively.

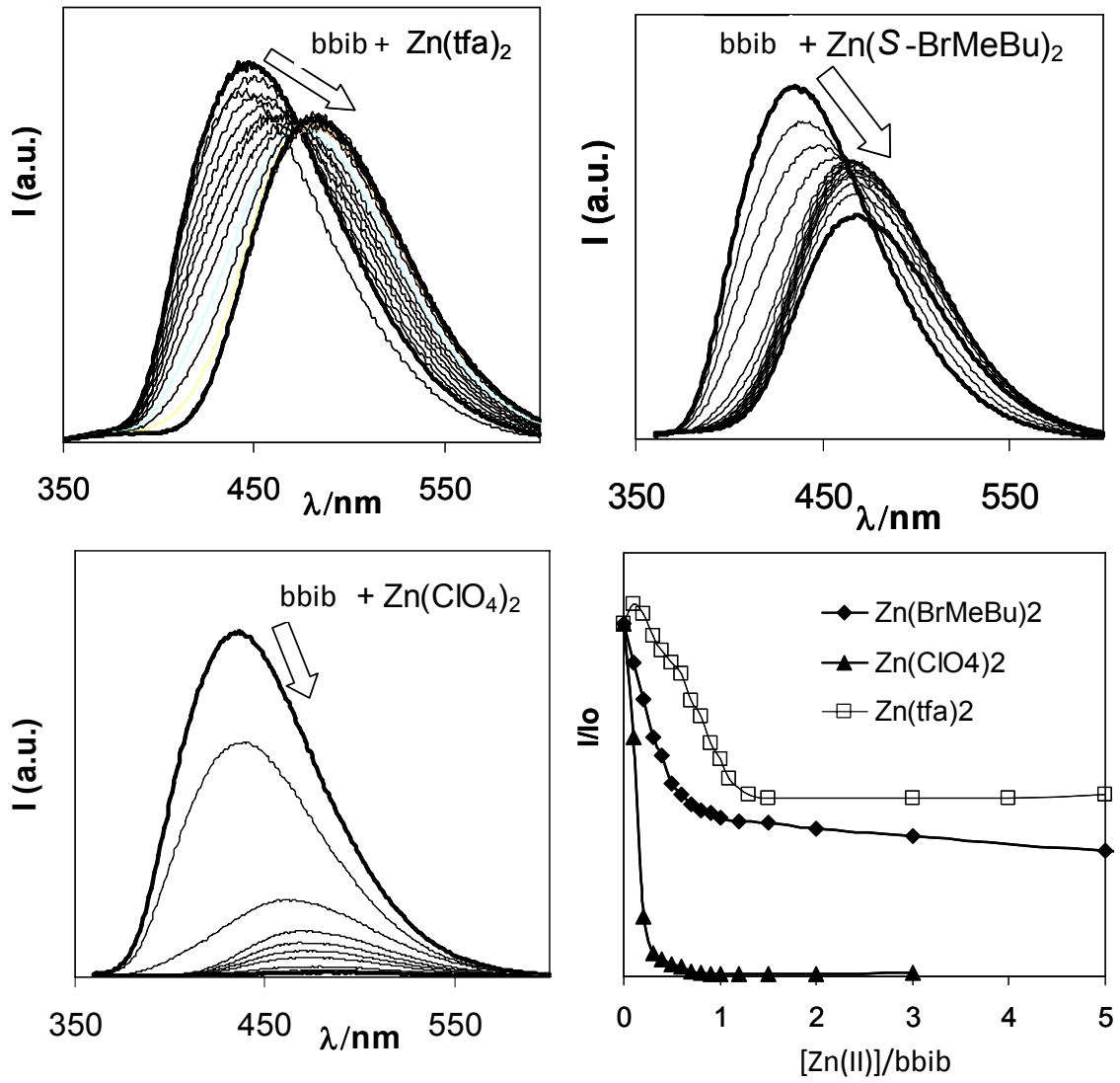

Figure 6.20 The fluorescent titration diagrams and Stern-Volmer plots of bbib (1.0×10^{-5} M) in CH_2Cl_2 by three different Zn(II) salts.

6.2.8 Selectivity and Fluorescent Response of bpib and bbib Toward Group 12 Salts

Fluorescent titrations with other group 12 metals ions Cd(II) and Hg(II) were also investigated. These metal ions were found to quench the emission of the ligand. As observed for Zn(II) salts, the anion was found to play a significant role in the extent of quenching observed for Cd(II) and Hg(II). Titrations with Cd(II) salts showed a red shift in the emission similar to those observed for the Zn(II) salts (Figure 6.21 and Figure 6.22). The largest decrease in emission was observed with the perchlorate anion, which is a poor donor. One equivalent of $Hg(ClO_4)_2$ resulted in complete quenching of the emission (Figure 6.23). While one equivalent of $Cd(ClO_4)_2$ dramatically quenched and red shifted the emission. However, no red shift was seen for either Hg(II) salt as shown in Figure 6.23 and Figure 6.24. The Stern-Volmer plots for Cd(II) and Hg(II) titrations are shown in Figure 6.25. The plateau of the curves indicates the formation of a one complex, which is similar to that of the Zn(II) complex. The titration experiments indicate that bpib could differentiate different group 12 metals since different emission quenching, and wavelength shifts are observed for the different metals and salts. From the observed interactions of Cd(II) and Hg(II) ions with bpib these metal centres could, in theory, also be used to facilitate chiral recognition if they contained a chiral carboxylate ion, however these are toxic metals.

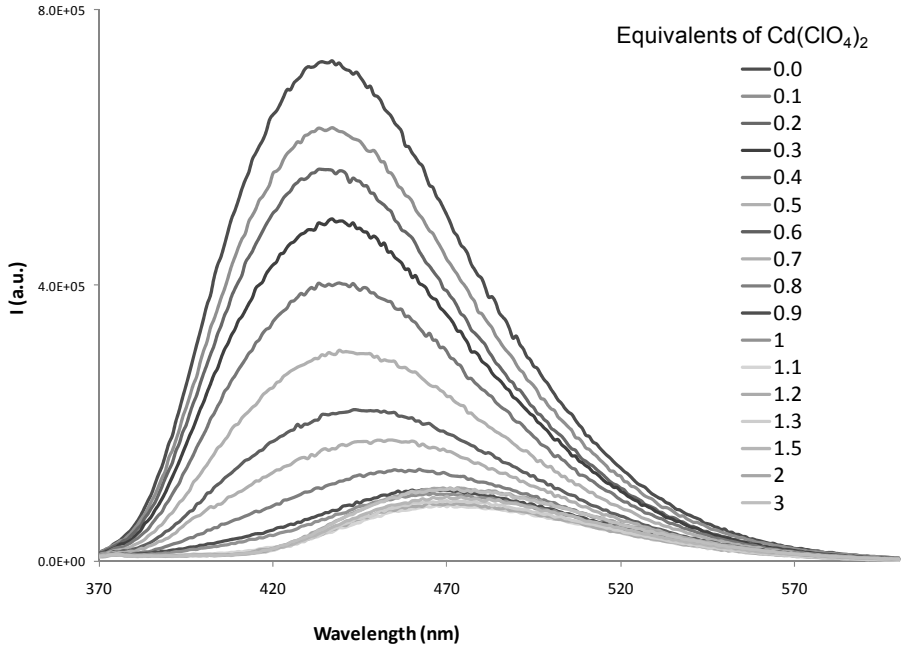

Figure 6.21 Fluorescent titration diagram of bpib with $Cd(ClO_4)_2$ in CH_2Cl_2 at a $1x10^{-5}$ M concentration.

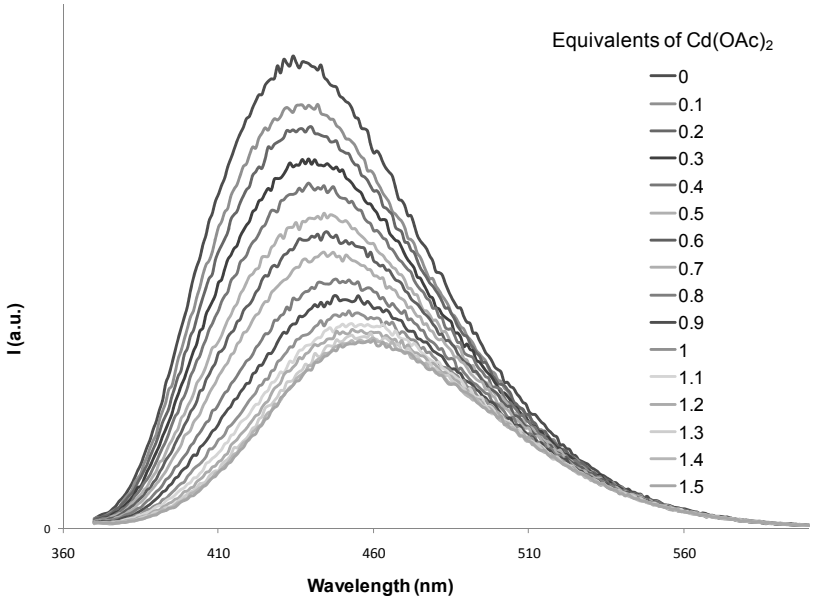

Figure 6.22 Fluorescent titration diagram of bpib with $Cd(OAc)_2$ in CH_2Cl_2 at a $1x10^{-5}$ M concentration.

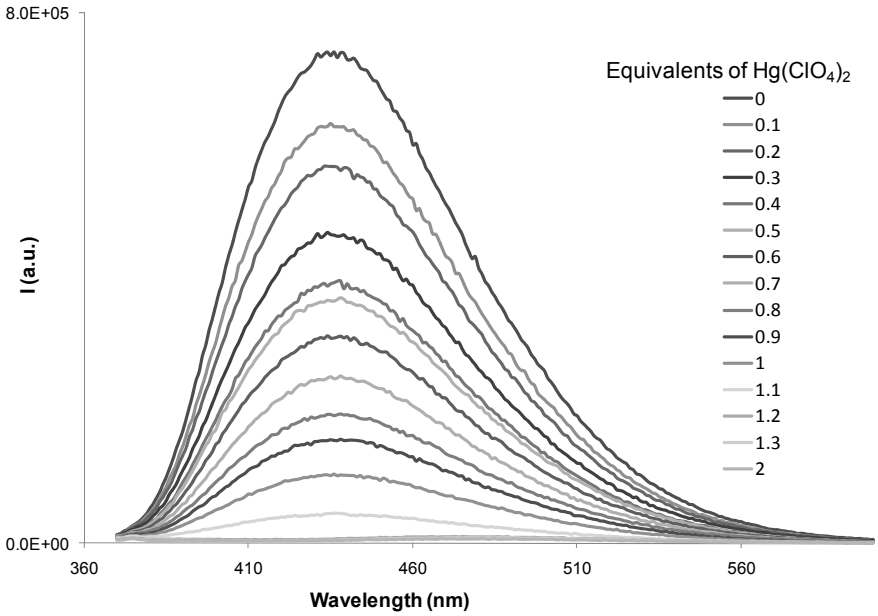

Figure 6.23 Fluorescent titration diagram of bpib with $Hg(ClO_4)_2$ in CH_2Cl_2 at a $1x10^{-5}$ M concentration.

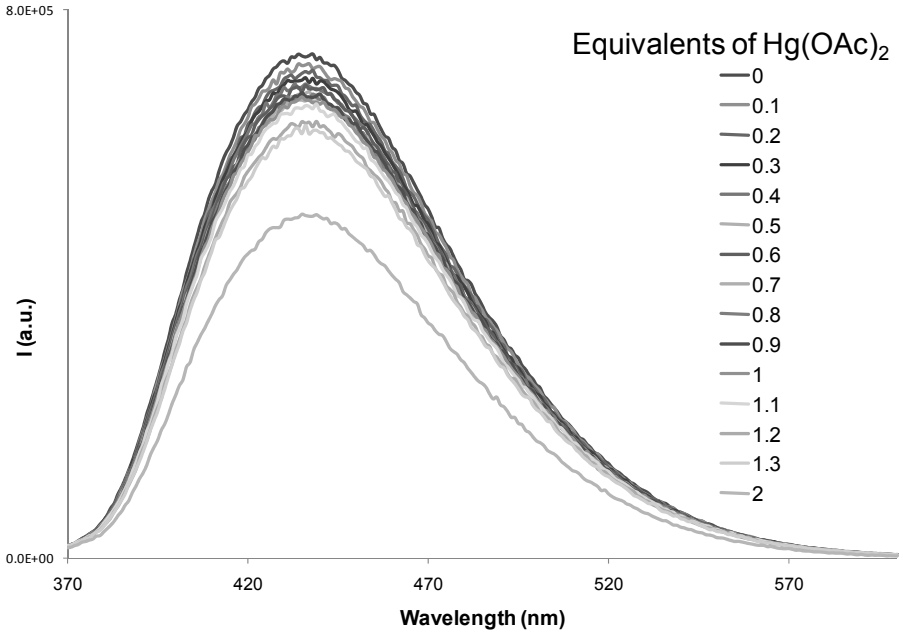

Figure 6.24 Fluorescent titration diagram of bpib with $Hg(OAc)_2$ in CH_2Cl_2 at a $1x10^{-5}$ M concentration.

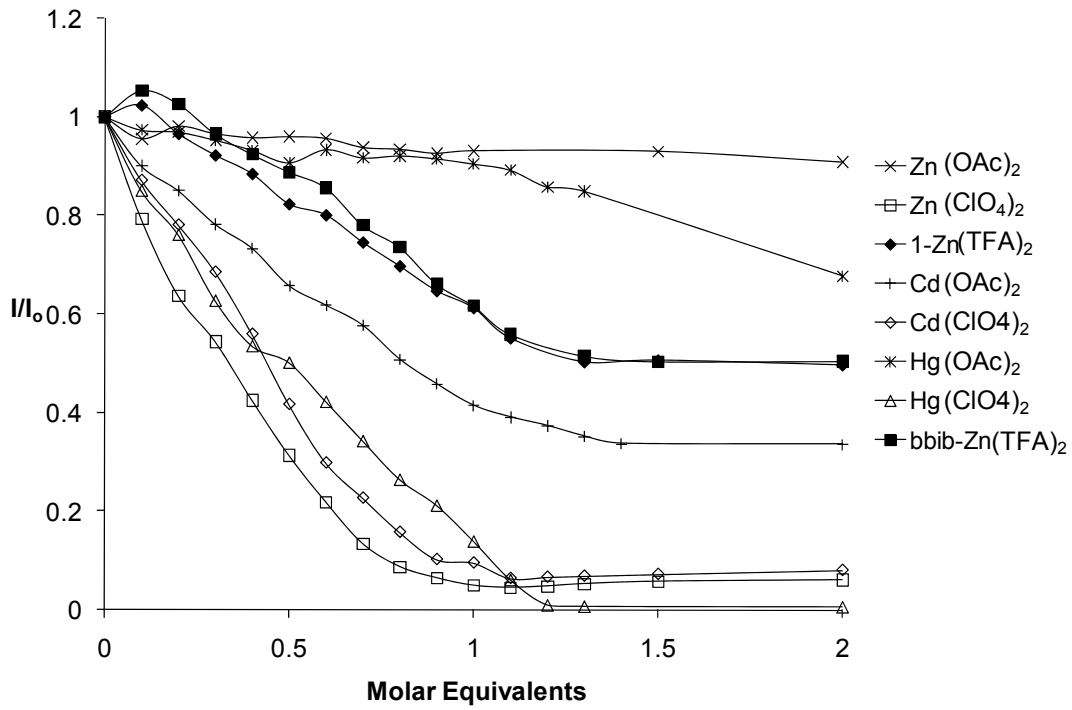

Figure 6.25 Stern-Volmer plots of bpib with group 12 metal salts and bbib with $Zn(TFA)_2$.

6.3 Conclusions

It has been demonstrated that the racemic atropisomeric ligands bpib and bbib are capable of distinguishing the enantiomers of $Zn(BrMeBu)_2$ and determining enantiomeric excess by using CD spectroscopy. Furthermore, it has been established that binding to the chelate site of ligands bpib and bbib by the chiral Zn(II) carboxylate is critical for achieving CD response. Strongly coordinating carboxylate salts produce weak or no CD response. The fluorescent quenching of bpib is dependent on both the metal and the salt used, with better donor ligands resulting in less quenching. The binding strength of the

carboxylate to the Zn(II) ion was also found to plays a key role in the CD response of bpib and bbib toward chiral Zinc carboxylates which may be used to discriminate different chiral acetates in conjunction with fluorescence spectra.

6.4 References

(1) Gottarelli, G.; Lena, S.; Masiero, S.; Pieraccini, S.; Spada, G. P. *Chirality* **2008**, *20*, 471.

(2) Matsushita, H.; Yamamoto, N.; Meijler, M. M.; Wirsching, P.; Lerner, R. A.; Matsushita, M.; Janda, K. D. *Mol. BioSyst.* **2005**, *1*, 303.

(3) Dybtsev, N. N.; Nuzhdin, A. L.; Chun, H.; Bryliakov, K. P.; Talsi, E. P.; Fedin, V. P.; Kim, K. *Angew. Chem., Int. Ed.* **2006**, *45*, 916.

(4) Takeuchi, M.; Mizuno, T.; Shinkai, S.; Shirakami, S.; Itoh, T. *Tetrahedron: Asymmetry* **2000**, *11*, 3311.

(5) Lee, S. J.; Lin, W. B. *J. Am. Chem. Soc.* **2002**, *124*, 4554.

(6) Ma, L.; White, P. S.; Lin, W. B. *J. Org. Chem.* **2002**, *67*, 7577.

(7) Mateos-Timoneda, M. A.; Crego-Calama, M.; Reinhoudt, D. N. *Chem. Soc. Rev.* **2004**, *33*, 363.

(8) Tan, H. Q.; Li, Y. G.; Zhang, Z. M.; Qin, C.; Wang, X. L.; Wang, E. B.; Su, Z. M. *J. Am. Chem. Soc.* **2007**, *129*, 10066.

(9) Fischbeck, A.; Bartke, N.; Humpf, H. U. *Monatshefte für Chem.* **2005**, *136*, 397, and references therein.

(10) Hayashi, T.; Aya, T.; Nonoguchi, M.; Mitzutani, T.; Hiseda, Y.; Kitagawa, S.; Ogoshi, H. *Tetrahedron* **2002**, *58*, 2803.

(11) Kim, W.; So, S. M.; Chagal, L.; Lough, A. J.; Kim, B. M.; Chin, J. *J. Org. Chem* **2006**, *71*, 8966.

(12) Maeda, K.; Morioka, K.; Yashima, E. *Macromolecules* **2007**, *40*, 1349.

(13) Li, W.; Jiang, D.; Suna, Y.; Aida, T. *J. Am. Chem. Soc.* **2005**, *127*, 7700.

(14) Lin, J.; Rajaram, A. R.; Pu, L. *Tetrahedron* **2004**, *60,* 11277.

(15) Chen, Z.; He, Y.; Hu, C.; Huang, X.; Hu, L. *Aust. J. Chem.* **2008**, *61*, 310.

(16) Pu, L. *Chem. Rev.* **2004**, *104*, 1687.

(17) Hembury, G. A.; Borovkov, V. V.; Inoue, Y. *Chem. Rev.* **2008**, *108*, 1.

(18) Bhyrappa, P.; Borokov, V. V.; Inoue, Y. *Org. Lett.* **2007**, *9*, 433.

(19) Ikeda, H.; Li, Q.; Ueno, A. *Bioorg. & Med. Chem. Lett.* **2006**, *16*, 5420.

(20) Ishi-I, T.; Crego-Calama, M.; Timmerman, P.; Reinhoudt, D. N.; Shinkai, S. *Angew. Chem. Int. Ed.* **2002**, *41*, 1924.

(21) Huang, X.; Nakanishi, K.; Berova, N. *Chirality* **2000**, *12*, 237.

(22) Piguet, C.; Bernardinelli, G.; Hopfgartner, G. *Chem. Rev.* **1997**, *97*, 2005.

(23) Kurtan, T.; Nasri, N.; Li, Y.; Huang, X.; Nakanishi, K.; Berova, N. *J. Am. Chem. Soc.* **2001**, *123*, 5962.

(24) Allenmark, S. *Chirality* **2003**, *15*, 409.

(25) Proni, G.; Pescitelli, G.; Huang, X.; Quraishi, N. Q.; Nakanishi, K.; Berova, N. *Chem. Commun.* **2002**, 1561.

(26) Maeda, K.; Yahima, E. *Top. Curr. Chem.* **2006**, *265*, 47.

(27) Gao, F.; Ruan, W.; Chen, J.; Zhang, Y.; Zhu, Z. *Spectrochim. Acta, Part A* **2005**, *62*, 886.

(28) Anderberg, P. I.; Turner, J. J.; Evans, K. J.; Hutchins, L. M.; Harding, M. M. *Dalton Trans.* **2004**, 1708.

(29) Dai, L.; Zhou, Z.; Zhang, Y.; Zhou, Y. *J. Chem. Soc., Chem. Commun.* **1987**, 1760.

(30) Meskers, S. C. J.; Dekkers, H. P. J. M. J. *Phys. Chem. A* **2001**, *105*, 4589.

(31) Tsukube, H.; Hosokubo, M.; Wada, M.; Shinoda, S.; Tamiaki, H. *Inorg. Chem.* **2001**, *40*, 740.

(32) Tsukube, H.; Shinoda, S.; Tamiaki, H. *Coord. Chem. Rev.* **2002**, 227.

(33) McCormick, T. M.; Liu, Q.; Wang, S. *Org. Lett.* **2007**, *9*, 4087.

(34) Gaussian 03, Revision C.02, Frisch, M. J.; Trucks, G. W.; Schlegel, H. B.; Scuseria, G. E.; Robb, M. A.; Cheeseman, J. R.; Montgomery, Jr., J. A.; Vreven, T.; Kudin, K. N.; Burant, J. C.; Millam, J. M.; Iyengar, S. S.; Tomasi, J.; Barone, V.; Mennucci, B.; Cossi, M.; Scalmani, G.; Rega, N.; Petersson, G. A.; Nakatsuji, H.; Hada, M.; Ehara, M.; Toyota, K.; Fukuda, R.; Hasegawa, J.; Ishida, M.; Nakajima, T.; Honda, Y.; Kitao, O.; Nakai, H.; Klene, M.; Li, X.; Knox, J. E.; Hratchian, H. P.; Cross, J. B.; Bakken, V.; Adamo, C.; Jaramillo, J.; Gomperts, R.; Stratmann, R. E.; Yazyev, O.; Austin, A. J.; Cammi, R.; Pomelli, C.; Ochterski, J. W.; Ayala, P. Y.; Morokuma, K.; Voth, G. A.; Salvador, P.; Dannenberg, J. J.; Zakrzewski, V. G.; Dapprich, S.; Daniels, A. D.; Strain, M. C.; Farkas, O.; Malick, D. K.; Rabuck, A. D.; Raghavachari, K.; Foresman, J. B.; Ortiz, J. V.; Cui, Q.; Baboul, A. G.; Clifford, S.; Cioslowski, J.; Stefanov, B. B.; Liu, G.; Liashenko, A.; Piskorz, P.; Komaromi, I.; Martin, R. L.; Fox, D. J.; Keith, T.; Al-Laham, M. A.; Peng, C. Y.; Nanayakkara, A.; Challacombe, M.; Gill, P. M. W.; Johnson, B.; Chen, W.; Wong, M. W.; Gonzalez, C.; and Pople, J. A.; Gaussian, Inc., Wallingford CT, 2004.

(35) Bruker Analytical X-ray Systems **1999**, version *5.10*.

(36) Wu, Q.; Lavinge, J. A.; Tao, Y.; D'Iorio, M.; Wang, S. *Inorg. Chem.* **2000**, *39*, 5248.

(37) Prince, R. H. In *chap. 56.1;* Wilkinson, G., Gillard, R. D. and McCleverty, J. A., Eds.; Comprehensive Coordination Chemistry; Pergamon Press: New York, 1987; Vol. 5.

(38) Kerr, M. C.; Preston, H. S.; Ammon, H. L.; Huheey, J. E.; Stewart, J. M. *J. Coord. Chem.* **1981**, *11*, 111.

(39) Pang, J.; Marcotte, E. J.; Seward, C.; Brown, R. S.; Wang, S. *Angew. Chem., Int. Ed.* **2001**, *40*, 4042.

(40) Liu, S.; Wu, Q.; Schmider, H. L.; Aziz, H.; Hu, N.; Popovic, Z.; Wang, S. *J. Am. Chem. Soc.* **2000**, *122*, 3671.

(41) Liu, Q. D.; Jia, W. L.; Wang, S. *Inorg. Chem.* **2005**, *44*, 1332.

(42) Jia, W. L.; McCormick, T.; Tao, Y.; Lu, J. P.; Wang, S. *Inorg. Chem.* **2005**, *44*, 5706.

(43) Ruan, W.; Zhao, X.; Wang, S.; Zhang, Y.; Zhang, Z.; Nan, J.; Zhu, Z.; Wang, J.; Ma, Y. *Chin. J. Chem.* **2005**, *23*, 1381.

(44) Crawford, T. D.; Tam, M. C.; Abrams, M. L. *J. Phys. Chem. A* **2007**, *111*, 12057.

(45) Autschbach, J.; Jorge, F. E.; Ziegler, T. *Inorg. Chem.* **42**, *2003*, 2867.

(46) Coughlin, F. J.; Oyler, K. D.; Pascal, R. A.; Bernhard, S. *Inorg. Chem.* **2008**, *47*, 974.

(47) O'Boyle, N. M.; Tenderholt, A. L.; Langner, K. M. *J. Comp. Chem.* **2007**, *29*, 839.

Chapter 7
Summary and Perspectives

7.1 Summary and Conclusions

This work started with the investigation of the effect of various phosphine ligands on the photophysical properties of Cu(I) complexes made with the N,N' chelating ligand 2-(2'-pyridyl)benzimazolyl benzene (pbb). Four phosphine ligands were chosen for their steric and electronic properties; PPh_3, DPPE, DPEphos and DPPMP. Previous reports had indicated that $[Cu(phen)(PP)]^+$ complexes made with DPEphos had shorter lifetimes and higher emission quantum yields than ones made with PPh_3 ancillary ligands This work set out to determine if this effect of the phosphine ligand on the photophysical properties was common among all Cu(I) N,N' chelated complexes. It was found that both electronic and steric factors of the phosphine ligand influenced the luminescent properties. However, the Cu(I) pbb complex made with DPEphos (**2.3**) appeared to dramatically decrease the emission quantum efficiency when compared with the PPh_3 complex (**2.1**). As such, further investigation was undertaken into 2-(2'-pyridyl)benzimidazolyl based Cu(I) complexes using PPh_3 as the ancillary ligands.

To determine whether (2'-pyridyl)benzimidazolyl based Cu(I) complexes could be used as the emitter in OLED devices, a series of linear and star-shaped (2'-pyridyl)benzimidazolyl ligands capable of binding two or three Cu(I) metal ions were developed. It was found that these complexes are stable and emit a yellow-orange colour from the MLCT band. However, the complexes display exceptionally long excited state

lifetimes, hindering their utility in OLEDs. A device was fabricated with complex **3.4** that displayed poor performance as predicted. Although (2'-pyridyl)benzimidazolyl based Cu(I) complexes were found not useful in OLED applications, it is clear that modification of both the N,N' ligand and phosphine ligands can have significant impact on the photophysical properties of Cu(I) complexes. This group of long lived phosphorescent Cu(I) complexes may find other applications in photochemistry.

To further explore the chemistry of Cu(I) complexes, a series of ligands based on 2-(2'-pyridyl)indole were synthesized that only contain one coordinating nitrogen and as such were expected to coordinate to Cu(I) as a monodentate ligand. In the course of the synthesis of pib, a new ligand bpib, that is a C-C coupled dimer of pib, was discovered. It was later determined that similar products could be isolated from the reactions of bib and tib. The dimers bpib, bbib and btib were the result of C-N and C-C coupling in a one-pot reaction. It was determined that the C-C bond forming reaction was a pyridyl directed homo-coupling of unfunctionalized arenes, catalyzed by copper. The luminescence and coordination chemistry of these ligands were examined. It was found that the ligand luminescence of the dimers was red shifted when compared to the monomers due to formation of an intramolecular exciplex. Hindered rotation around the C-C bond of the dimers results in the ligands being axially chiral. Although the enantiomers of bpib could not be separated, computations indicate that the C-C bond between the indoles does not rotate freely at room temperature, indicating that they are in fact atropisomers.

Cu(I), Pd(II) and Pt(II) complexes were made for both the monomer pib and the dimer bpib. The monomer Cu(I) complex **5.1** had the expected trigonal planar geometry; verified by the crystal structure. MLCT emission was not observed as indicated by UV-Vis spectrum and emission data. Thus, the emission is assigned to ligand centered $^3\pi$-$^1\pi$ phosphorescence. Complexes of pib with Pd(II) (**5.2**) and Pt(II) (**5.3**) were cyclometallated complexes, as verified by NMR and the X-ray crystallographic analysis. Both complexes were found to display red coloured phosphorescence in solid state and in frozen solution.

The Cu(I) complex **5.4** crystallized homo-chirally with two ligands per metal centre. Each crystal contains only one isomer of **5.4**, as verified by the CD spectrum taken for solutions of single crystals. This complex displayed MLCT absorption band in the visible region and emission was observed in frozen solution. The crystal structures of the Pd(II) and Pt(II) complexes **5.5** and **5.6** revealed that the bpib ligand coordinates to the metal centre in a 1:1 ratio. Although the crystals are not homo-chiral, they do display a rare trans-chelating geometry. Further investigation of these complexes could be into the use in catalytic applications. Emission was not seen for the Pd(II) complex, but the Pt(II) complex displayed red emission in frozen solution and in the solid state.

Due to the chiral discrimination that was seen in the crystallization of **5.4,** investigation into the ability of bpib and bbib to act as a chiral sensor was carried out. The CD spectral of racemic bpib to the chiral zinc carboxylate $Zn(BrMeBu)_2$ displayed chiral recognition, with a linear response to the ee of the target molecule. Through DFT

calculations it was determined that the observed CD response was caused by diasterieomeric excess. Chiral sensing with a racemic mixture of the chiral sensor is rare, but the benefits of this approach were discussed. One benefit is not having to purify the sensor molecule. In addition, the observed CD response to the enantiomers of the target molecule results in mirror image spectra. This work established a new class of atropisomeric ligands and their potential use in chiral sensing.

This research has established that careful selection of nitrogen donor ligands and ancillary phosphine ligands can influence the photophysical properties of Cu(I) complexes. Although MLCT based emission is observed for the four coordinate tetrahedral shaped Cu(I) complexes, the three coordinate complex only shows ligand based emission. The pib ligand formed emissive cyclometallated complexes with both Pd(II) and Pt(II). The chiral 2-(2'-pyridyl)indolyl ligand bpib acted as an N,N' chelate coordinated through the pyridines to make the homochiral complex **5.4** and the trans-chelated complexes **5.5** and **5.6**. It was also shown that a racemic mixture of bpib can act as a chiral sensor for Zn(II) carboxylates.

7.2 Future Directions

Future direction of this work should start with the transition metal complexes of bib and tib, especially the cyclometallated Pt(II) complex as shown in Figure 7.1. The monomer complex **5.3** displayed solid state red emission and as a result the polynuclear complexes may be a useful emitter for use in OLED devices, based on the observations of the lower

decay lifetimes and better layer forming ability seen for the Cu(I) 2-(2'-pyridyl)benzimidazolyl complexes. These ligands also provide an opportunity for making mixed metal complexes. If only one equivalent of K_2PtCl_4 is reacted with bib the other side of the ligand could be coordinated Cu(I) as shown in Figure 7.2. Mixed metal complexes have been of interested in catalytic water splitting reactions.

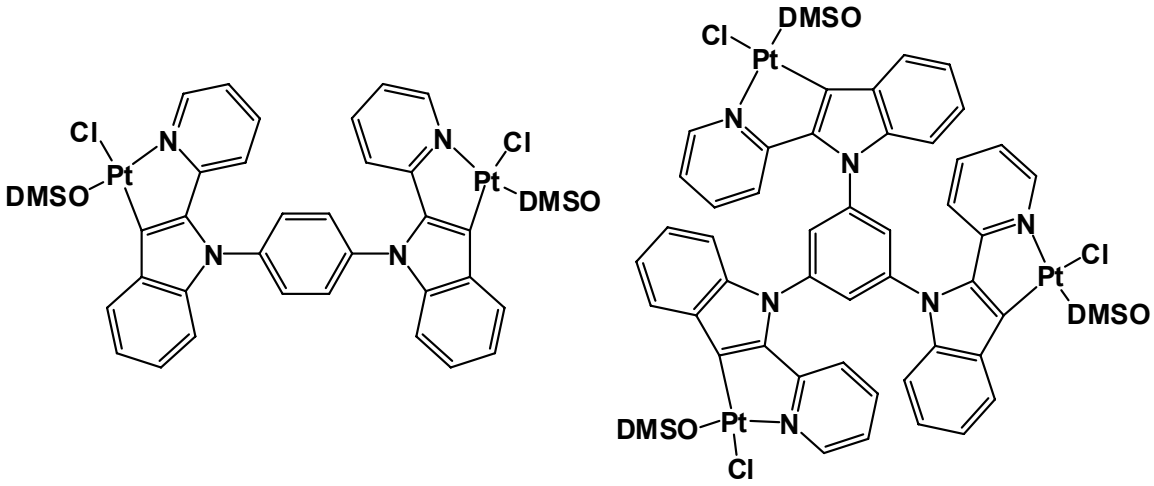

$Pt_2(bib)Cl_2(DMSO)_2$ $Pt_3(tib)Cl_3(DMSO)_3$

Figure 7.1 Proposed Pt(II) complexes with bib and btib.

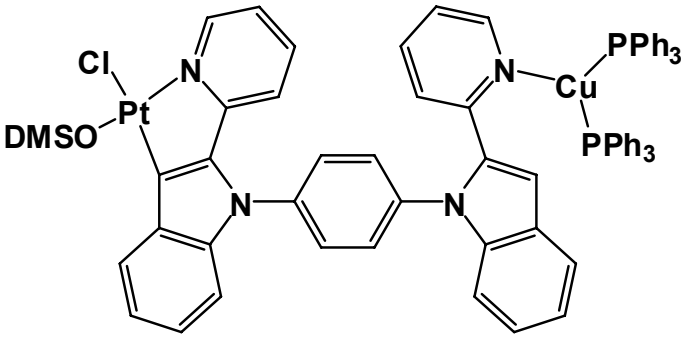

Figure 7.2 Bimetallic complex of bib with Pt(II) cyclometallated on one side and three coordinate copper on the other.

Another direction of the research is the development of ligands with two different binding sites such as the one shown in Figure 7.3. Synthesis of this ligand is currently underway. The two binding sites would have different coordination environments, leading to a wide variety of possible bimetallic complexes that could be made. Two examples are shown in Figure 7.4, but many combinations of Pt(II), Pd(II), Cu(I) and Ru(II) could be achieved with this ligand. They could be studied to determine the degree of interactions between the metal centres and if the photophysical properties of the complexes resemble one metal complex or the other, or if it is a mixture of the two.

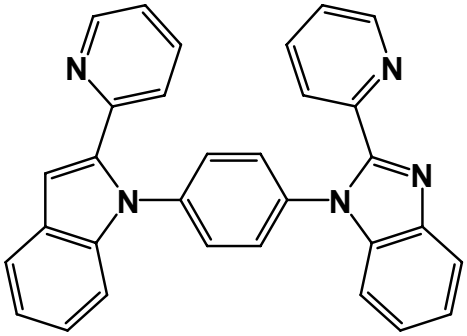

Figure 7.3 Structure of 1-(2-(2'-pyridyl)indolyl)-4-(2-(2'-pyridyl)benzaimidazolyl) benzene.

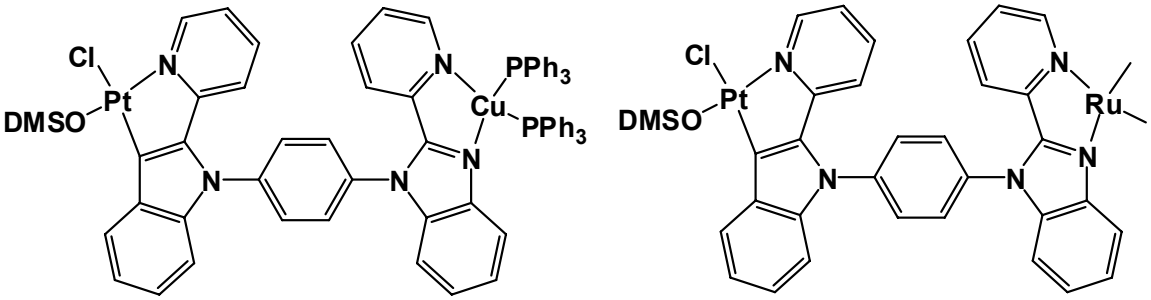

Figure 7.4 Structure of two possible bimetallic complexes.

The ligands bbib and btib discussed in Chapter 4 also have two different binding sites: the interior N,N chelate and the distal 2-(2'-pyridyl)indolyl groups that can act as N donors or as C,N chelates as has been shown. Complexes made from these could be quite interesting due to the unique geometries found for transition metal complexes of the bpib ligand. Preliminary results indicate that these molecules may have solubility problems.

Further investigation into Cu(I) trigonal planar complexes could also be rewarding. Investigations into the luminescent properties of three coordinate Cu(I) complexes are scarce, but preliminary reports seem to support the idea that the presence of the metal centre allows access to the triplet π state with very long excited state lifetimes. Although long excited state lifetimes are not desirable for OLED applications, they can be useful in other areas of photochemistry.